

UNIVERSITÀ DEGLI STUDI DI CATANIA
Dipartimento di Ingegneria Civile e Architettura
Dottorato in Valutazione e Mitigazione dei Rischi Urbani e Territoriali

IN JOINT SUPERVISION WITH

ÉCOLE NATIONALE DES TRAVAUX PUBLICS DE L'ÉTAT
Département Génie Civil et Bâtiment
École doctorale: MEGA (Mécanique, Énergétique, Génie civil, Acoustique
Spécialité: Mécanique des solides, des matériaux des structures et des surfaces

PH.D. THESIS OF
SALVATORE GAZZO

CHARACTERISATION OF THE MECHANICAL BEHAVIOUR OF NETWORKS AND WOVEN FABRICS WITH A DISCRETE HOMOGENIZATION MODEL

Supervisors:	Prof. Massimo Cuomo
	Prof. Claude Boutin
Advisors:	Prof.ssa Loredana Contrafatto
	Prof. Leopoldo Greco

2015/2018

To my wife
and my family

Contents

Abstract

In the past decades there has been an impressive progress in the development of new materials for mechanical related applications. New generations of composites have been developed, that can offer advantages over the unidirectional fibre-reinforced mats commonly used then materials take the name of woven fabrics. The behaviour of this material is strongly influenced by the micro-structure of the material.

In the thesis mechanical models and a numerical scheme able to model the mechanical behaviour of woven fabrics and general network materials have been developed. The model takes in to account the micro-structure by means of a homogenization technique. The fibres in the network have been treated like microbeams, having both extensional and bending stiffness, with different types of connection, according to the pattern and detail of the network.

The developed procedure was applied for obtaining the homogenized mechanical models for some types of biaxial and quadriaxial networks of fibres, simulating either fibre nets (in this case rigid connection were assumed among the fibres) or tissues with negligible interaction between the fibre bundles, and with relative sliding prevented (in this case the connections were simulated by means of pivots). Different geometries were analysed, including the cases in which the fibres are not orthogonal.

A first gradient medium is usually obtained but, in some cases, the homogenization procedure itself indicates that a higher order continuum is better fit to represent the deformation of the micro-structure. Special results were obtained for the case of fibres connected by pivots. In this cases an orthotropic material with zero shear modulus was obtained. Such a material has a not elliptic constitutive tensor, thus it can lead to strain concentrations. However, it was shown that some considerations about the physical behaviour of such networks indicated that higher order terms had to be included in the expansion of the internal forces and deformations, so that a strain gradient material was obtained.

The results obtained can be used for the design of specific materials requiring ad-hoc properties. Although the reference model is a network material, the results obtained can be applied to other similar kinds of microstructures, like pantographic materials, micro devices composed by microbeams etc. They have been limited at the range of linear elasticity, that is small deformation and linear elastic behaviour.

Then, numerical simulations were focused on extension tests and bias tests. The obtained deformed configurations are consistent with the literature experimental tests, both for balanced and unbalanced tissues. Moreover, a comparison between first and second gradient numerical predictions was performed. It was observed that second gradient predictions better simulate the experimental evidences.

Chapter 1

Introduction

In the past decades there has been an impressive progress in the development of new materials for mechanical related applications. The design and modelling of new materials has become one of the leading challenges for the research in engineering, together with the need of improving existing structural analysis methods in order to take advantage of all the innovations introduced. Fibres composite materials have traditionally introduced strong innovation in the manufacturing industries, ranging from transportation to construction industries. Long fibre composites are constituted by unidirectional fibres, and their major effect is to improve the mechanical properties of the material in that direction, causing significant anisotropy. New generations of composites have been developed, that can offer advantages over the unidirectional fibre-reinforced mats commonly used then materials take the name of woven fabrics. The behaviour of this material is strongly influenced by the micro-structure of the material. The multi-scale nature and the interactions of the length scales makes the design process of textiles a challenging task.

The aim of the thesis is to develop mechanical model and a numerical scheme that able to model the mechanical behaviour of woven fabrics and network materials in general. The model takes account the micro-structure of the material by means of a homogenization technique.

In this way the constitutive equations of an homogenized medium can be estimated according the micro-structure. A first gradient medium is usually obtained but in some cases, that will be discussed in the thesis, the homogenization procedure itself indicates that a higher order continuum is better fit to represent the deformation of the micro-structure. The results obtained can easily be used in numerical simulations: in the thesis they will be applied to simulate common laboratory test, in order to show the reliability of the homogenization procedure proposed.

1.1 The woven fabrics and fibre nets

The materials studied herein are assemblages of fibres that will be generally denoted as fibre networks.

They include nets, characterised by rigid connections between the fibres (for instance, glass fibre nets used in reinforcement for masonry constructions), see figure 1.1, and tissue, constituted by two or more fibre bundles (also known as yarns), bonded together in a specific architecture.

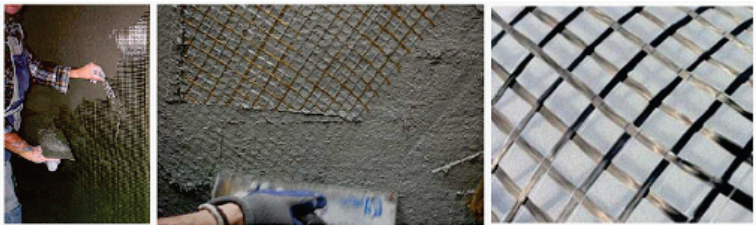

Figure 1.1: FRCM Fibre Reinforced Cementitious Matrix.

The integrity of the fabrics is maintained by the mechanical interlocking of the fibres. They provide wide range of opportunities in designing advanced structures because of their high tenacity and flexibility, high strength-to weight ratios and versatility. The yarns can be arranged in different architectures (weave patterns), that can adjust to application needs (1.2).

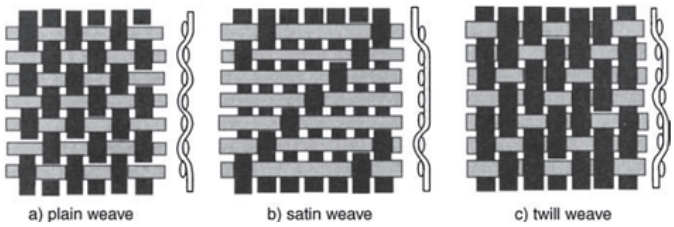

Figure 1.2: Different architecture of woven fabric.

Textiles are able to undergo large shear deformation with an highly non-linear mechanical response. In the tissues, also known as woven fabrics, yarns in different directions are free to rotate among themselves, and at last partially, to slide. For both kinds of materials, fibre nets and woven fabrics, the properties of the equivalent continuum depend from the mechanic characteristics of the fibres (glass, carbon, polymers etc. can be used), from their density, their geometry, connections etc., that is from the micro-structure of the networks.

On the other hand, the micro-structure itself can be designed in order to achieve the desired mechanical performances, choosing appropriately the fibres materials.

1.1.1 Some applications

Over the last two decades, the use of textile composites as structural parts has increased rapidly, especially in the field of aerospace, automotive and transportation [1], [2], [3], [4]. Woven fabrics composites combine a variety of desirable properties such as high stiffness, strength and low weight. Woven fabrics are commonly used in the production of composite materials due to their ease of handling, the variety of woven patterns available and the relative stability of their pattern and shape during lay up. In the manufacture of components of complex shape, the fabrics are draped onto a mould surface of varying geometric complexity resulting in changes in the fibre orientation, local fibre fraction and porosity. Woven and non-woven fabrics are now extensively used in several applications, either as reinforcement or as structural material(see, e.g. [5], [6], [7]). Finally, it should be added that this type of materials is present in nature as well, in some biological tissues [8], [9], [10], [11].

1.1.2 Mechanical behaviour

Fibre networks guarantee dimensional stability, balanced properties in the reinforcement plane, high impact resistance, good drapability, and suitability for manufacturing of doubly curved components. It is possible obtain 2D or 3D fabric. Usually high-performance materials are used for the fibres (e.g. carbon, glass, and high polymers), so that the resulting network can be considered almost inextensible in the fibre directions and mainly deform for bending or shear presenting a strong geometric hardening. More complex is the behaviour of three dimensional woven fabrics, for which the deformation in the transverse direction depends not only on the geometry of the fabric, but also on friction and interlocking among them. Friction and slippage of fibres is also a major issue in plane fabrics, when the deformation becomes large.

Given their structure, network materials are non homogeneous and highly anisotropic. Their properties manly depend of the fibres, so that even an eventual presence of plastic or resin coating has little influence a the overall properties of the composite.

For this reason, in the thesis only fibre networks will be considered, discarding further materials like polymer that can be present in the networks.

Furthermore, they present multi-scales of mechanical behaviour, as highlighted next.

Their study it can be undertaken through different dimensional scales.

- **Macro-level**

  The macro-level represents the upper level of the geometry of the final composite part. At this scale, which is usually of the order of $10^{-1} - 1m$, larger geometrical and material factors of parts such as curvature, fibre volume fraction, and global mechanical properties under different loading modes are considered. In contrast, smaller scale material characteristics, such as the yarn dimensions and architecture, are neglected.

- **Meso-level**

  The meso-level focuses on the behaviour and dimensions of the individual yarns, their interactions and weave pattern. The order of magnitude at this scale is $10^{-3} - 10^{-2}m$, depending on the size of the yarns and the fabric architecture. Previous research [12–14] has shown that this level of material hierarchy can greatly influence the macro-level mechanical behaviour of woven fabrics and, consequently, may be the most essential level to analyse. At meso-scale, each yarn is considered as a continuous domain; however, this assumption may be disputed considering micro-level behaviour where each yarn itself consists of several bundles of fibres.

- **Micro-level**

  The micro-level focuses in the arrangement of fibres in each fibrous yarn. The order of magnitude examined in this scale is close to the fibre size (typically around 5-20 μm), and is relatively small in comparison to the final part or even the yarn scale. Nonetheless, the interaction of fibers and their mechanical behavior affects the effective properties of the material at the meso-level, and eventually affects the fabric macro-level response.

The characterization of the mechanical behaviour of woven composites is a necessary condition if we want to evaluate their structural performance, analyse and design composite

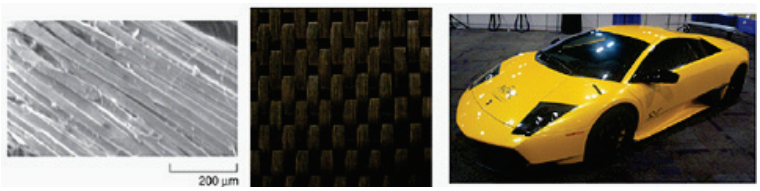

Figure 1.3: The multi-scale nature of woven fabric composites. (The figure has been reproduced from [15]).

laminates and understand their response to different loading conditions. Therefore, accurate mechanical model and efficient numerical scheme validated on the basis of laboratory tests, are needed to integrate and design structures with fibre networks.

1.2 State of the art

The characterization of the mechanical response of fibre networks and their modelling is one of the most challenging issues in material engineering. The problem is very complex since it involves many non standard tasks, considering that the material we are dealing with is not a simple material in the sense that its micro-mechanics strongly influences the observable behaviour, and this cannot be disregarded in the simulations. Some relevant aspects related to parameter identification of similar complex materials are discussed in detail in [16], [17]. Other significant issues as contact impact problems or damage evolution and identification are studied in [13, 18–21]. In the last chapter of the thesis, the results obtained from the numerical method developed will be tested against some experimental results obtained from the literature.

Standard uniaxial tests in the fibre directors are usually employed for characterizing fibre networks. In addition, other kinds of tests are used, manly for woven fabrics, particularly the bias test.

The bias extension test is an extensional test on a strip of the woven fabric constituted by two families of fibres oriented at 45° with respect to the axis of the specimen, clamped at the ends (see figure 1.4). The load elongation curve is recorded, and in order to obtain information on the shear stiffness, or on the shear stress exerted in the specimen, it is necessary to treat the data obtained from the testing apparatus. The length/width ratio of the specimen must be larger than 2.

In [23] dell'Isola et al. show that when one of the ends of the specimen is displaced of a given amount, the formation of three types of regions (A, B and C) with almost homogeneous behaviour in their interior is observed (figure 1.5). In each of these areas, the angle between the warp and weft direction is almost constant. This is due to the quasi-inextensibilty of the yarns and the rotation without slippage occurring between warp and weft yarns at the crossover points.

The transition between two different areas at constant shear angle is not concentrated on a line. In fact, it is possible to observe the onset of transition layers, in which there is a gradual variation of the angle as shown in figure 1.6. In such transition layers, the angle variation between the two constant values of the rotation is achieved by a smooth pattern, which is directly associated to the local bending of the yarns.

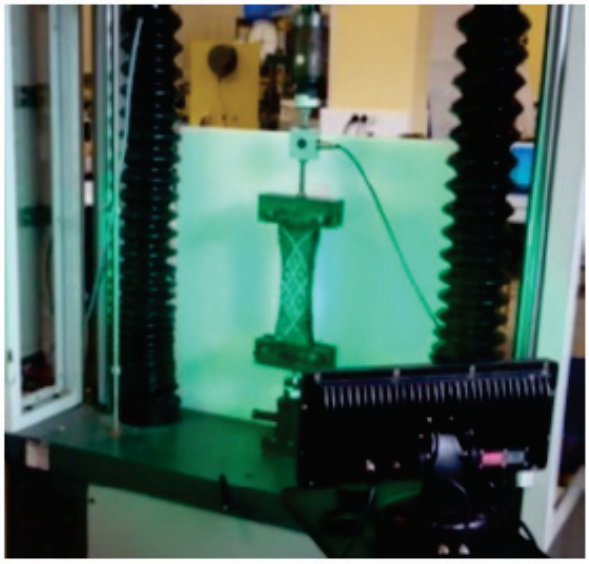

Figure 1.4: Bias test (the figure has been reproduced from [22]).

Madeo et al. [12] show how that the unbalance in the bending stiffness of the warp and weft yarns produces, macroscopic effects, such as an asymmetric S-shape, in woven fabrics subjected to Bias Extension Test, see figure 1.7.

A numerical simulation of the test is a critical task in order to develop a realistic mechanical model of the composite material, able to be employed in the analysis of more complex geometries. A numerical analysis of the extension bias test was discussed in [14], [24]. Classical continuum mechanics is an approximation based on the assumption that matter is continuously distributed throughout the body. This theory provides a reasonable basis for the analysis if the behaviour of materials at the macro-scale, where the micro-structure size-dependency can be neglected, but the strongly heterogeneity of the woven fabrics has significant effect on its macroscopic mechanical properties.

In the literature, two approaches are usually used to take into account the heterogeneity of materials with micro-structure: the generalized continuum theory and the homogenization technique.

1.2.1 Generalized continuum model

As mentioned before, fibres are may stiff in their direction. Pipkin and Rivlin developed a model of nets with inextensible cords in a seriees of pioneery papers on the kinematic of the networks [25], [26], [27]. The authors found that first gradient deformation modelling produces sharp discontinuities in the fibre rotations, that are not observed in the experiments. Therefore it was suggested, in accordance with what proposed by [28], [29], [30] to employ higher-order deformation models (see, e.g. [31], [32], [33]), able to simulate the bending energy stored in the fibres at the meso-level.

These models particularize the continuous non local theory with micro deformation introduced in the 60s by Eringen [34–37]. Differently from the classical continuum theories (local model), that assume that the stress at a material point depends on the strain at same point, the nonlocal elasticity theory establishes a relationship between macroscopic mechan-

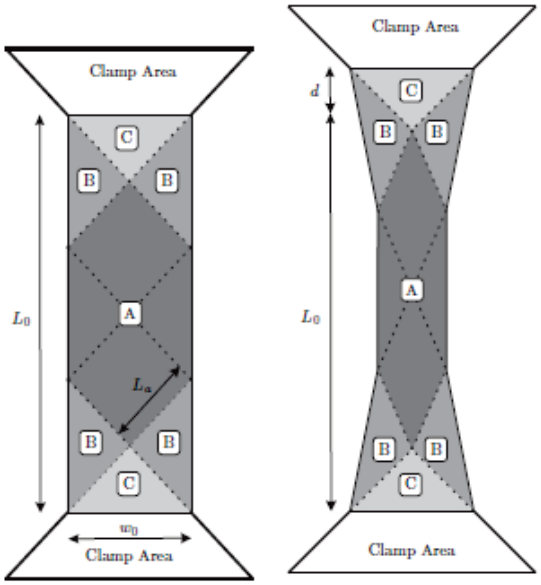

Figure 1.5: Simplified description of the shear angle pattern in the bias test extension. (The figure has been reproduced from [23]).

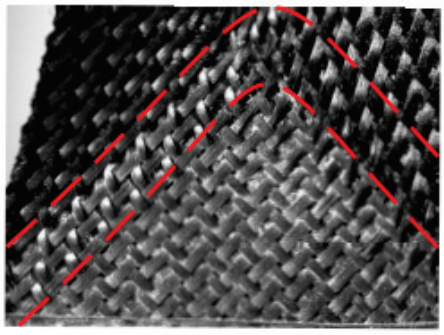

Figure 1.6: Boundary layers between two regions at constant shear. (The figure has been reproduced from [23]).

ical quantities and microscopic quantities of materials with micro-structures. The nonlocal stress at a material point is expressed as a function of the weighted values of the entire strain field, consequently including information on the size scale of the microstructure. In [38] Mindlin introduces the theory of continuum with micro-deformation; this is a continuum that in addition to the classical macro strain experiences micro-strain represented by a second order tensor, representing a gap at the micro-scale with the micro deformation. The theory extends previous theories of generalised media, like Cosserat's [39]. The latter only considers deformation of an internal triad related their to the relative rotation of the local axes. Mindlin's hypothesis also introduces deformation of the directors.

In [40] Mindlin and Eschel proposed an approximation of this theory, valid for small dimensions of the inner cell, leading to the theory of strain gradient elasticity.

The latter has been largely employed by several authors to describe the behaviour of fibres tissues and networks. Several energy models were analysed, aiming to reproduce the experimental observations. In the same spirit, it is possible to exploit the micro-polar sur-

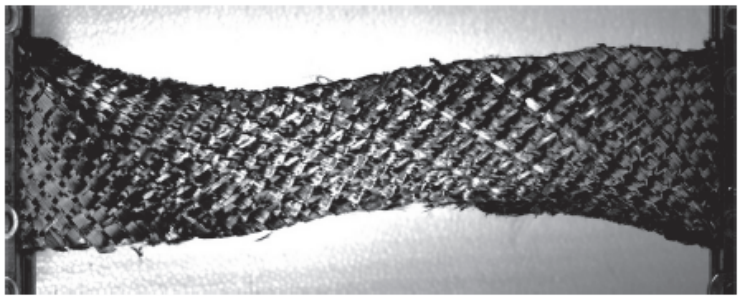

Figure 1.7: Experimental S-shape. (The figure has been reproduced from [23]).

face theory; indeed, higher-order deformation models with proper assumption [41] can be interpreted in the framework of micro-structured or micro-polar materials see [42–52] for further details. In the work of P. Boisse et al. [53] the inability of the model of Cauchy to describe the possibility of slippage between the fibres and the bending stiffness of the fibres is shown. The authors, in order to overcome these difficulties and model the mechanical behaviour of fibrous reinforcements taking into account the local fibre bending stiffness, propose a continuum first order model completed by a generalized second gradient continuum theory. According to the second gradient theory, the strain energy density depends both on the deformation tensor $\boldsymbol{C}$ and its gradient:

$$W(\boldsymbol{C}, \nabla \boldsymbol{C}) = W_I(\boldsymbol{C}) + W_{II}(\nabla \boldsymbol{C}) \tag{1.1}$$

W_I and W_{II} being the first gradient and the second gradient strain energy. The strain energy densities in Equation (1.1) are identified from elementary tests (tensile tests in the warp and weft directions, compaction test, bias extension test (in-plane shear), and transverse shear tests). These identification tests are described in detail in [54] and [55]. The second gradient strain energy takes into consideration the bending of the fibres regardless of the first gradient behaviour.

As a note, we remark that to perform numeric simulations involving higher gradient models, ad hoc tools have to be employed, since standard C^0 FEM analisys is not optimized for this purpose [56–60].

Some of the models examined in the thesis lead to the introduction of higher gradient strain, that is they lead to second gradient materials.

1.2.2 Homogenization model

In literature we can find many examples of homogenization procedures which have the purpose of obtaining a bulk macro model starting from a proper kinematical description at meso-scale. The homogenisation methods, which enable us to define an equivalent macro-continuous description from the knowledge of the micro-structure behaviour, have a large field of applications that concern mechanics of materials, geotechnics and structures. The description of the homogenization technique can be found in Bensoussan et al. [61], Sanchez-Palencia [62], Auriault et al. [63]. This theory has been used for fibre-reinforced composite and composite materials with inhomogeneities. In this context, various tissue models have been made using numerical FEM discretizations for the analysis of RVE self-equilibrium problems. Interesting development related to fibres network can be found in [64]. In this

paper the authors propose a method for combining 1-d and 2-d structural finite elements, see figure 1.8, that capture the fundamental mechanical properties of woven fabrics subjected to finite strains. A mutually constrained pantographic beam and membrane mesh is presented and a simple homogenisation theory that relates the macro-scale properties of the mesh to the properties of the elements within the mesh is introduced. The simulations are used to verify the accuracy of the homogenisation theory, the ability of the modelling approach in accurately predicting the shear force, shear kinematics and out-of-plane wrinkling behaviour of woven fabrics is shown.

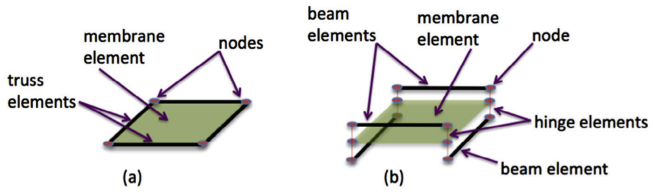

Figure 1.8: Repeat unit cells. (a) Mutually constrained truss and membrane elements, (b) mutually constrained pantographic beam and membrane mesh. (The figure has been reproduced from [64]).

Another approach is developed in [65], where the authors present finite elements for the simulation of the three-dimensional high-rate deformation of woven fabric. They employ a continuum-level modelling technique that, through the use of an appropriate unit cell, captures the evolution of the meso-structure of the fabric without explicitly modelling every yarn, see figure 1.9.

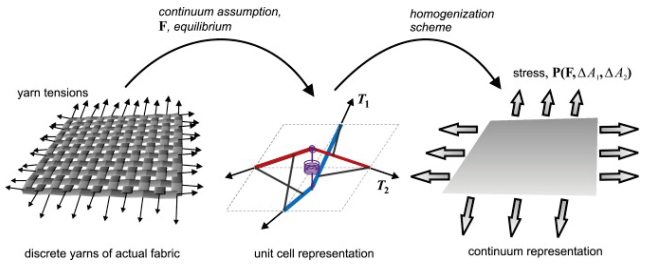

Figure 1.9: Schematic of continuum modeling technique for woven fabric: discrete yarn tensions are transformed into continuum-level stresses via the deformation of a unit cell. (The figure has been reproduced from [65]).

Similar approaches have been developed in the papers [66–70] where the authors develop different mesoscale models to derive the macroscale mechanical behaviour of woven fabrics.

The work by Durville is particularly interesting [71,72]. Durville simulates the behaviour of samples of woven fabrics, based on the individual fibres that constitute the sample modelled. Special attention is taken in identifying and modelling the the contact-friction interactions occurring within the assembly of fibres. From this model he obtains a mesoscopic model that is set within a large deformation framework.

With this approach the author models the mechanisms that govern the complex nonlinear behaviour of woven fabrics at microscopic scale.

Multilevel method has been developed by Haasemann in [73]. The fundamental principle of the multilevel method is the transition of the micro-structural response to the macroscopic structure based on the formulation of an adequate boundary value problem. The procedure of this numerical method is shown in figure 1.10.

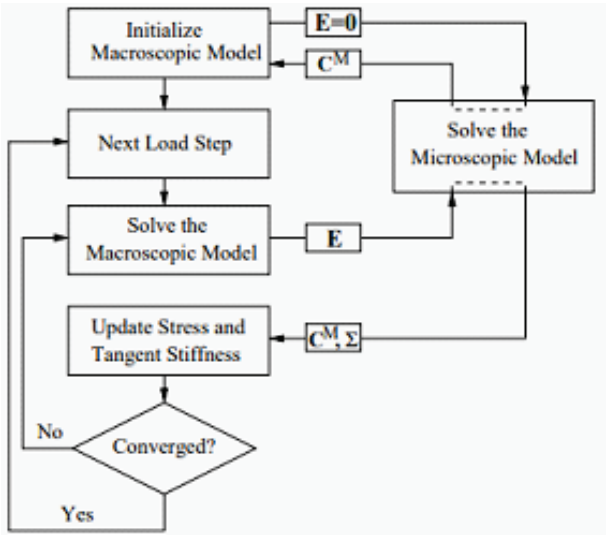

Figure 1.10: Flowchart of the multi-scale procedure. (The figure has been reproduced from [73]).

The first step of the multilevel procedure is the initialization of the macroscopic tangent stiffness with the linear elastic properties quantified by the homogenization procedure. Next, a load step is applied followed by the first solution. The strain obtained on the macroscopic FE-model is applied to the unit cell after each iteration step. The response in terms of the macro-stress Σ and the tangent stiffness CM is determined. Once the solution has converged, the macroscopic computation algorithm moves to the next step. Nevertheless, the numerical methods reviewed herein require high computational effort.

An alternative approach is represented by the homogenization method of periodic discrete medium HPDM introduced by Caillerie in [74–76].

Differently from the periodic continuous medium homogenization, the author introduced a REV (Representative Elementary Volume) composed by finite number of deformed structured elements connected by nodes. The structural elements consists in bars or bemas. In this context are the works of Boutin et al. [77] and dell'Isola et al. [78].

Boutin et al. [77] consider a linear pantographic sheet constituted by two orthogonal arrays of straight fibres interconnected by internal pivots. The authors introduce a continuous model by means of a micro-macro identification procedure, based on the asymptotic homogenization method of discrete media. Differently from Caillerie et al., that use a weak formulation for the equilibrium equation, the authors use a strong formulation and consider also the flexural deformation of the fibre. In this way the authors obtain a higher order continuum model.

In the work of dell'Isola et al. [78], the micro-structures of a pantographic lattice, see figure 1.11, is assumed to be exclusively constituted by rotational springs and rigid bars, figure 1.12. They develop an heuristic micro macro identification procedure, called Piola's heuristic homogenization method. Their method is based on the following steps:

- postulation of a micro-macro kinematical map;
- identification of micro and macro virtual work functional;
- determination of macro-constitutive equations in terms of the micro properties of considered mechanical systems by means of a suitable formal asymptotic expansion.

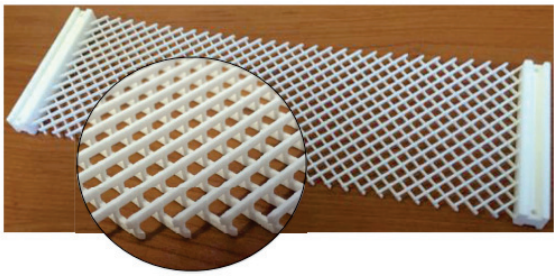

Figure 1.11: Pantographic lattice topology. (The figure has been reproduced from [78]).

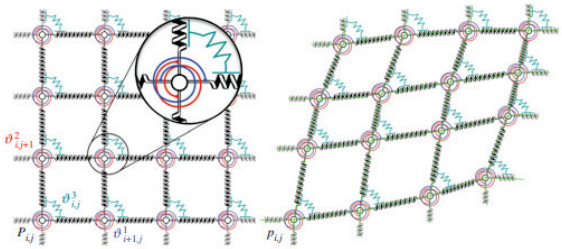

Figure 1.12: Micro-model of a pantographic sheet and Piola identification with a detail of the three rotational springs employed. (The figure has been reproduced from [78]).

In the following, a simple second gradient continuum model is deduced; this model is effective at relatively larger scales and accounts for a large class of phenomena occurring during planar extensional bias test. After presenting their theory, the authors perform numerical simulations of a pantographic structure using standard FE packages of COMSOL Multiphysics.

1.3 Outline

The aim of this thesis is the development of homogenized continuum models that have the ability to simulate the mechanical behaviour of networks and woven fabrics.

Due to the inability of the classical continuum theory to describe the mechanical behaviour of the network materials, new models will be obtained by means of the homogenization method of periodic media, originally developed in [74–76, 79] and [80–83], accounting simultaneously for both the bending deformation of the bar and the existence of internal nodes in the reference cell, that have not been treated simultaneously in the original papers.

Materials with different micro-structures will be analysed and studies on the anisotropic behaviour will be performed.

Interesting results, for future developments in the non-linear field, will be given by the model obtained considering the skew reference cell.

A second gradient homogenized material will be obtained considering a rectangular cell with pivots, based on the weak formulation. Boutin et al. [77] obtained similar solutions to the one presented herein, using however the strong formulation.

Numerical simulations of tests is a critical task in order to develop a realistic mechanical model of the composite material, that can be used in the analysis of more complex geometries. For the numerical simulations, the model was implemented in a standard FEM code.

The second gradient model was developed by means of an isogeometric analysis. A number of simulations is performed to compare the results of the developed method with experimental results available in the literature. 1.2.

Chapter 2

Homogenization model for fibres networks

Chapter 2 presents a the homogenization model for woven fabric and network materials. The model is based on the homogenization of discrete repetitive lattice, using asymptotic expansion for all field variables. The constitutive equations of the homogenized continuum are obtained from the micro-scale equilibrium equations. The latter can be derived either from strong or weak formulation.

In the calculations performed herein the inertia terms are neglected, hence all analyses are static.

2.1 Homogenization technique

Over the past decades, homogenization methodologies have been applied to several physical settings, for instance composite materials or trusses. The aim of homogenization technique is the modelling of the heterogeneous medium as a simpler, equivalent continuous medium, that can be described validly at a larger scale.

Although several homogenization methods have been developed (see [62, 63, 74–76, 79, 84, 85]) only few of them apply to strongly anisotropic multi-scale materials, (see [77], [80]).

However, a methodical homogenization technique give the possibility of identifying the micro-morphologies that lead to the macroscopic behaviour characteristics of the generalized continua. In order to apply the homogenization method to a heterogeneous material, a Representative Element of Volume (REV) must be identified. For the REV to be representative of the geometry of the heterogeneities and the properties of constituents, the element should contain a sufficiently large number of heterogeneities.

The separation of scales depends both on the geometry of the medium and the phenomenon. The REV reduces to the unit cell when the medium is periodic. Let l be the characteristic length of the REV, and L the macroscopic length. L may represent either a characteristic length of the volume of material under consideration, or a macroscopic characteristic length of the phenomenon. The separation of scales requires that:

$$\frac{l}{L} = \varepsilon << 1 \tag{2.1}$$

Using the two characteristic length scales l and L we may introduce two dimensionless

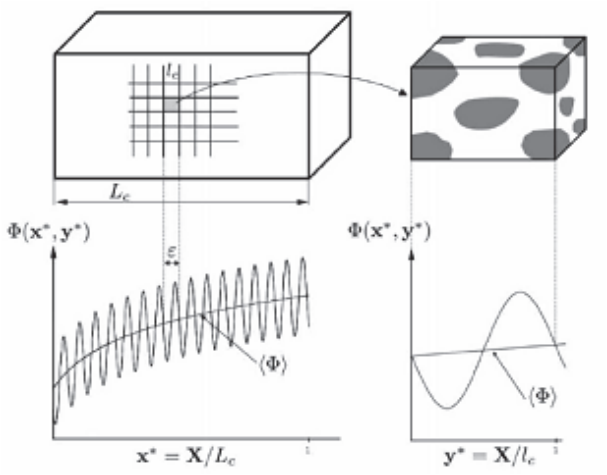

Figure 2.1: Macroscopic and microscopic variables. (The figure has been reproduced from [63]).

spatial variables $y^* = X/l$ and $x^* = X/L$, where X is the physical spatial variable. Each quantity Φ can be expressed as a function of the two dimensionless variables x^* and y^*. The variable x^* is the macroscopic (or slow) spatial variable and y^* is the microscopic (or fast) spatial variable. The fast variable y^* describes the short-range interaction, whereas the slow variable x^* describes the long-range interaction, see figure 2.1. The small parameter ε allows us to express all unknown physical quantities in the form of asymptotic expansions at multiple scales in power of ε.

The expanded form for a dimensionless quantity Φ can be written as [63]:

$$\Phi(x^*, y^*) = \Phi^0(x^*, y^*) + \varepsilon\Phi^1(x^*, y^*) + \varepsilon^2\Phi^2(x^*, y^*) + \ldots \tag{2.2}$$

The macroscopic behaviour of the equivalent continuum is described by the behaviour of the function Φ^0.

The next subsection presents the discrete homogenization method, that is developed starting from the periodic continuous medium homogenization.

2.1.1 Homogenization method of Periodic Discrete Media

In this thesis, the Homogenization method of Periodic Discrete Media (HPDM), originally developed in [74–76, 79] and [80–83] is applied to various network configurations, accounting simultaneously for both the bending deformation of the bar and for internal nodes in the cell, that have not been treated simultaneously in the original papers. The method will be presented in section 2.4.

In the papers mentioned above those arguments were treated independently; however, the study by Seppecher [86] has examined complex cells in the framework of the Γ-convergence theory. HPDM is also applicable in the case of quasi-periodic structures, see [76].

In the discrete homogenization the REV is a lattice cell composed by nodes and structural elements. We shall consider the lattice composed by beams and nodes. It is assumed that the configuration of the REV is fully described by the positions of the nodes.

Each node will be labelled by a number $n \in \mathcal{N}$ and each beam by a label $b \in \mathcal{B}$, where $\mathcal{N}$ and $\mathcal{B}$ are respectively the sets of nodes and beams of the unit cell.

The following assumptions will be made:

- linear behaviour of the element,
- small deformation,
- absence of body force.

The HPDM standard method will be presented both in strong and weak formulation in sections 2.2 and 2.3. Two cases will be considered: bar under axial deformation and bar under flexural deformation. This example is strongly inspired by the work of Caillerie [76] and aims to compare the strong and the weak homogenization formulations. In the homogenisation technique, we assume that two scale lengths coexist: the first is defined by the size l of the reference cell of the structure; the second is defined by the macro dimension L of the periodic structure. The validity condition of the homogenisation process requires that the scale ratio $\varepsilon = \dfrac{l}{L}$ is small. In such case, the cell variables vary slowly from one cell to the next one and the discrete variables represent the local values of the continuous functions to be determined. It is possible to split the homogenization technique in different steps:

- The first step of discrete homogenization consists in assuming asymptotic series expansions in powers of ε for the node displacements and the internal forces in beams. Furthermore, as the distance between nodes is very small compared to the macroscopic length L, the incremental variation of the variables between two neighbouring nodes can be expressed using truncated Taylor's series.
- The second step is the development of the balance equations of the nodes using the force-displacement relations of the beams.
- In the final step, the identification of the terms of the same power of ε allows the user to obtain the micro variables as a function of the global variables and to find the differential equations of the homogenized continuum.

The determination of the equivalent elastic property of the homogenized material requires the solution of the self-balance equations of the elementary cell. Such solution can be found analytically for simple cells and numerically for more complicated cells.

2.2 1D model - axial case

In order to highlight the procedure, in this section, the HPDM methodology will be applied for the analysis of the 1D structure shown in figure 2.2.

Let L be the length of the whole structure composed by N_c repetitive cells of length l so that $\varepsilon = \dfrac{l}{L} = \dfrac{1}{N_c}$. Each cell is identified by a natural number $\nu \in \mathcal{Z} = (1, N_c)$. It is then possible to introduce a parametric coordinate $\lambda \in (0, 1)$ defined as:

$$\lambda = \frac{\nu}{N_c} = \varepsilon\nu \tag{2.3}$$

Each cell is composed by $\mathcal{B}$ elements. The internal element of the reference cell is indicated with the notation $b \in \mathcal{B}$. O_b and E_b denote the origin and the end of the bar b, given its internal orientation.

Figure 2.2 refers to the first case studied - that of a bar characterized by length L and a cell of length l, composed by two bars of different materials joined through a rigid connection.

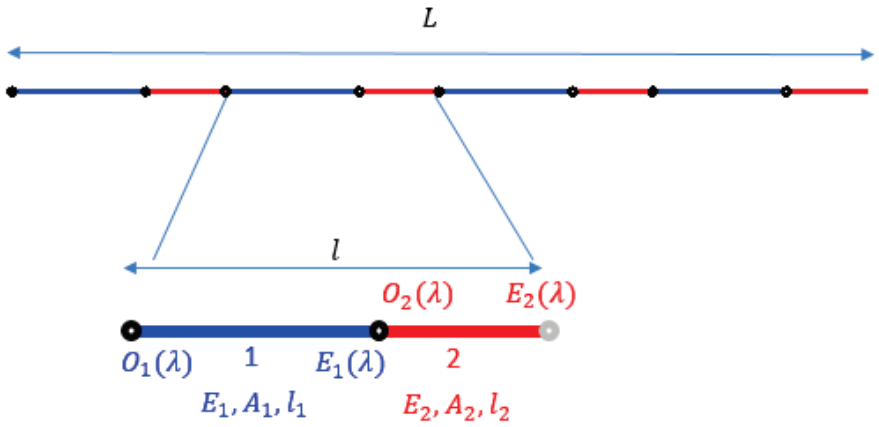

Figure 2.2: Reference cell case 1D.

In general, the (linear) relationships between the internal axial forces and the axial displacements of the bar are:

$$\begin{aligned} N_{O_b} &= \frac{EA}{L_b}\left(u_{O_b} - u_{E_b}\right) \\ N_{E_b} &= \frac{EA}{L_b}\left(u_{E_b} - u_{O_b}\right) \end{aligned} \tag{2.4}$$

It follows then that:

$$N_{O_b} = -N_{E_b} \tag{2.5}$$

To develop the method of homogenization we should perform the asymptotic expansion of the displacement function of the generic node n of the reference cell in ε. Therefore we have:

$$u_n(\lambda) = u_n^0(\lambda) + \varepsilon u_n^1(\lambda) + \varepsilon^2 u_n^2(\lambda) + \varepsilon^3 u_n^3(\lambda) + \varepsilon^4 u_n^4(\lambda) + \ldots \tag{2.6}$$

Similarly, for the external node belonging to the adjacent cell $\nu + 1$, we have:

$$u_n(\lambda+\varepsilon) = u_n^0(\lambda+\varepsilon) + \varepsilon u_n^1(\lambda+\varepsilon) + \varepsilon^2 u_n^2(\lambda+\varepsilon) + \varepsilon^3 u_n^3(\lambda+\varepsilon) + \varepsilon^4 u_n^4(\lambda+\varepsilon) + \ldots \tag{2.7}$$

Performing the Taylor expansion to the various orders we have:

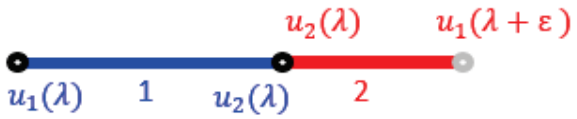

Figure 2.3: Displacement of the nodes for the reference cell.

$$\begin{aligned}
u_n^0(\lambda+\varepsilon) &= u_n^0(\lambda)+\varepsilon\frac{\partial u_n^0(\lambda)}{\partial\lambda}+\frac{\varepsilon^2}{2!}\frac{\partial^2 u_n^0(\lambda)}{\partial\lambda^2}+\dots \\
u_n^1(\lambda+\varepsilon) &= u_n^1(\lambda)+\varepsilon\frac{\partial u_n^1(\lambda)}{\partial\lambda}+\frac{\varepsilon^2}{2!}\frac{\partial^2 u_n^1(\lambda)}{\partial\lambda^2}+\dots \\
u_n^2(\lambda+\varepsilon) &= u_n^2(\lambda)+\varepsilon\frac{\partial u_n^2(\lambda)}{\partial\lambda}+\frac{\varepsilon^2}{2!}\frac{\partial^2 u_n^2(\lambda)}{\partial\lambda^2}+\dots
\end{aligned} \tag{2.8}$$

Substituting (2.8) in (2.7) we obtain:

$$u_n(\lambda+\varepsilon) = u_n^0(\lambda)+\varepsilon\left(u_n^1(\lambda)+\frac{\partial u_n^0(\lambda)}{\partial\lambda}\right)+\varepsilon^2\left(u_n^2(\lambda)+\frac{\partial u_n^1(\lambda)}{\partial\lambda}+\frac{1}{2!}\frac{\partial^2 u_n^0(\lambda)}{\partial\lambda^2}\right)+\dots \tag{2.9}$$

The nodal axial displacement of the beam can be identified in the following way (see figure 2.3):

$$\begin{aligned}
u_{O_1}(\lambda) &= u_1(\lambda) \qquad & u_{E_1}(\lambda) &= u_2(\lambda) \\
u_{O_2}(\lambda) &= u_2(\lambda) \qquad & u_{E_2}(\lambda) &= u_1(\lambda+\varepsilon)
\end{aligned} \tag{2.10}$$

Note:In the next development, for simplicity of the notation, the dependence of the displacement from the macroscopic field λ will be omitted.

Substituting the asymptotic expansions (2.6) and (2.9) in the constitutive relation of the nodal forces (2.4) and using the previous notation (2.10), we obtain the asymptotic expansion of the nodal forces in ε:
Beam 1

$$\begin{aligned}
N_{E_1}^{\varepsilon}(\lambda) &= k_{a1}\left[\left(u_2^0-u_1^0\right)+\varepsilon\left(u_2^1-u_1^1\right)+\varepsilon^2\left(u_2^2-u_1^2\right)\right] = N_{E_1}^0(\lambda)+\varepsilon N_{E_1}^1(\lambda)+\varepsilon^2 N_{E_1}^2(\lambda) \\
N_{O_1}^{\varepsilon}(\lambda) &= -N_{E_1}^{\varepsilon}(\lambda)
\end{aligned} \tag{2.11}$$

Beam 2

$$\begin{aligned}
N_{E_2}^{\varepsilon}(\lambda) &= k_{a2}\left[\left(u_1^0-u_2^0\right)+\varepsilon\left(u_1^1-u_2^1+\frac{\partial u_1^0}{\partial\lambda}\right)+\varepsilon^2\left(u_1^2-u_2^2+\frac{\partial u_1^1}{\partial\lambda}+\frac{1}{2}\frac{\partial^2 u_1^0}{\partial\lambda^2}\right)\right] = \\
&= N_{E_2}^0(\lambda)+\varepsilon N_{E_2}^1(\lambda)+\varepsilon^2 N_{E_2}^2(\lambda) \\
N_{O_2}^{\varepsilon}(\lambda) &= -N_{E_2}^{\varepsilon}(\lambda)
\end{aligned} \tag{2.12}$$

Beam 2 of the neighbouring cell $(\lambda-\varepsilon)$

$$\begin{aligned} N^{\varepsilon}_{E_2}(\lambda-\varepsilon) &= k_{a2}\left[\left(u^0_1-u^0_2\right)+\varepsilon\left(u^1_1-u^1_2+\frac{\partial u^0_2}{\partial\lambda}\right)+\varepsilon^2\left(u^2_1-u^2_2+\frac{\partial u^1_2}{\partial\lambda}-\frac{1}{2}\frac{\partial^2 u^0_1}{\partial\lambda^2}\right)\right]= \\ &= N^0_{E_2}(\lambda-\varepsilon)+\varepsilon N^1_{E_2}(\lambda-\varepsilon)+\varepsilon^2 N^2_{E_2}(\lambda-\varepsilon) \end{aligned} \tag{2.13}$$

where $k_{a1}=\dfrac{EA_1}{l_1}$ and $k_{a2}=\dfrac{EA_2}{l_2}$ are the axial stiffness of the bars 1 and 2 of the reference cell. In the following, for the sake of shortness, we will be using the following notation:

$$\begin{aligned} u^i_\Delta &= u^i_2-u^i_1 \\ u^i_m &= \frac{u^i_1+u^i_2}{2} \end{aligned} \tag{2.14}$$

2.2.1 Strong formulation

The strong formulation is based on the balance equations of the cell, see figure 2.4. The equilibrium equations in this case are:

$$\begin{array}{lll} Node & 1. & N^{\varepsilon}_{E_2}(\lambda-\varepsilon)+N^{\varepsilon}_{O_1}(\lambda)=0 \\ Node & 2. & N^{\varepsilon}_{E_1}(\lambda)+N^{\varepsilon}_{O_2}(\lambda)=0 \end{array} \tag{2.15}$$

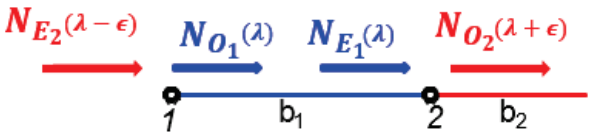

Figure 2.4: Axial nodal forces.

Equations (2.15) are expanded in powers of ε using equations (2.11) to (2.23).

Equations (2.16) to (2.23) show the development in detail. Let's start by collecting the equilibrium equation at the various order of any cell referred by λ:

Order 0 in ε:

$$\begin{array}{lll} 1. & N^0_{E_2}(\lambda-\varepsilon)+N^0_{O_1}(\lambda)=0 & \Rightarrow \quad k_{a2}(u^0_1-u^0_2)-k_{a1}(u^0_2-u^0_1)=0 \\ & & \Rightarrow \quad (k_{a1}+k_{a2})(u^0_1-u^0_2)=0 \\ & & \Rightarrow \quad u^0_1=u^0_2 \\ 2. & N^0_{E_1}(\lambda)+N^0_{O_2}(\lambda)=0 & \Rightarrow \quad k_{a1}(u^0_2-u^0_1)-k_{a2}(u^0_1-u^0_2)=0 \\ & & \Rightarrow \quad (k_{a1}+k_{a2})(u^0_1-u^0_2)=0 \\ & & \Rightarrow \quad u^0_2=u^0_1 \end{array} \tag{2.16}$$

The equilibrium equations of any cell at order 0 lead to the conclusion that $u_1^0(\lambda) = u_2^0(\lambda) = U^0(\lambda)$ and $N^0 = 0$, so that the leading order displacement is only function of the macroscopic variable. This is a typical result in homogenization, consistent with the scale separation assumption. It will be confirmed in all the subsequent applications.

Order 1 in ε:

$$\begin{aligned}
&1.\quad N^1_{E_2}(\lambda-\varepsilon)+N^1_{O_1}(\lambda)=0 \quad\Rightarrow\quad k_{a2}\left(u_1^1-u_2^1+\frac{\partial U^0}{\partial\lambda}\right)-k_{a1}(u_2^1-u_1^1)=0\\
&\qquad\qquad\qquad\qquad\Rightarrow\quad u^1_\Delta=(u_2^1-u_1^1)=\frac{k_{a2}}{k_{a1}+k_2}\frac{\partial U^0}{\partial\lambda}\\
&2.\quad N^1_{E_1}(\lambda)+N^1_{O_2}(\lambda)=0 \quad\Rightarrow\quad k_{a1}(u_2^1-u_1^1)-k_{a2}\left(u_1^1-u_2^1+\frac{\partial U^0}{\partial\lambda}\right)=0\\
&\qquad\qquad\qquad\qquad\Rightarrow\quad u^1_\Delta=(u_2^1-u_1^1)=\frac{k_{a2}}{k_{a1}+k_{a2}}\frac{\partial U^0}{\partial\lambda}
\end{aligned} \tag{2.17}$$

The equations (2.17) in the 1st-order of ε are identical. Any of the two equation (2.17) provides the micro-displacement of order 1 as function of the displacement at the macro-scale.

From the resulting equation (2.17), it follows that the leading order estimate of the axial force is:

$$N^1_{E_1}=N^1_{E_2}=N^1=K_1\frac{\partial U^0}{\partial\lambda} \tag{2.18}$$

where $K_1=\dfrac{k_{a1}k_{a2}}{k_{a1}+k_2}$ is the homogenized axial rigidity of the bar.

Order 2 in ε:

$$\begin{aligned}
&1.\quad N^2_{E_2}(\lambda-\varepsilon)+N^2_{O_1}(\lambda)=0 \quad\Rightarrow\quad k_{a2}\left(-u^2_\Delta+\frac{\partial u_2^1}{\partial\lambda}-\frac{1}{2}\frac{\partial^2U^0}{\partial\lambda^2}\right)-k_{a1}u^2_\Delta=0\\
&2.\quad N^2_{E_1}(\lambda)+N^2_{O_2}(\lambda)=0 \quad\Rightarrow\quad k_{a1}u^2_\Delta-k_{a2}\left(-u^2_\Delta+\frac{\partial u_1^1}{\partial\lambda}+\frac{1}{2}\frac{\partial^2U^0}{\partial\lambda^2}\right)=0
\end{aligned} \tag{2.19}$$

The equations (2.19) can be rearranged as follows:

$$-(k_{a1}+k_{a2})u^2_\Delta+k_{a2}\frac{\partial u_2^1}{\partial\lambda}-\frac{1}{2}k_{a2}\frac{\partial^2U^0}{\partial\lambda^2}=\ 0 \tag{2.20a}$$

$$(k_{a1}+k_{a2})u^2_\Delta-k_{a2}\frac{\partial u_1^1}{\partial\lambda}-\frac{1}{2}k_{a2}\frac{\partial^2U^0}{\partial\lambda^2}=\ 0 \tag{2.20b}$$

By adding and subtracting equations (2.20a) and (2.20b) we have:

$$k_{a2}\frac{\partial u^1_\Delta}{\partial \lambda} - k_{a2}\frac{\partial^2 U^0}{\partial \lambda^2} = 0 \tag{2.21a}$$

$$2(k_{a1}+k_{a2})u^2_\Delta - 2k_{a2}\frac{\partial u^1_m}{\partial \lambda} = 0 \;\Rightarrow u^2_\Delta = \frac{k_{a2}}{k_{a1}+k_{a2}}\frac{\partial u^1_m}{\partial \lambda} \tag{2.21b}$$

Substituting u^1_Δ given by equations (2.17) in (2.21a) we obtain the balance equations (and the homogenized stiffness K_1):

$$-K_1\frac{\partial^2 U^0}{\partial \lambda^2} = 0 \tag{2.22}$$

or

$$-\frac{\partial N^1}{\partial \lambda} = 0 \tag{2.23}$$

Equation 2.22 represents the balance equation of the heterogeneous bar. Generally, the external forces f^e_n appears at this order, but for this case it has been neglected.

Equation (2.21b) allows us to express the second order displacement contribution in terms of the first-order corrector. In order to provide an equation for u^2_Δ, higher order equations need to be considered.

Below, we summarize the results presented in equations (2.16) to (2.23).

Order 0 in ε:

$$\begin{aligned} u^0_1(\lambda) = u^0_2(\lambda) &= U^0(\lambda) \\ N^0 &= 0 \end{aligned} \tag{2.24}$$

Order 1 in ε

$$u^1_\Delta = \frac{k_{a2}}{k_{a1}+k_{a2}}\frac{\partial U^0}{\partial \lambda} \tag{2.25}$$

Order 2 in ε

$$u^2_\Delta = \frac{k_{a2}}{k_{a1}+k_{a2}}\frac{\partial u^1_m}{\partial \lambda} \tag{2.26}$$

$$-K_1\frac{\partial^2 U^0}{\partial \lambda^2} = 0 \tag{2.27}$$

2.2.2 Weak formulation

The procedure outlined in section 2.2.1 is a straightforward application of the equilibrium equations, however, its development for complex geometries may be cumbersome. In such cases, the weak formulation of the equations, obtained via the Principle Virtual Work (P.V.W.) is preferable. The weak formulation of discrete homogenization is described in [76], [75], [79] and [74], where the authors studied periodic lattices composed by bars.

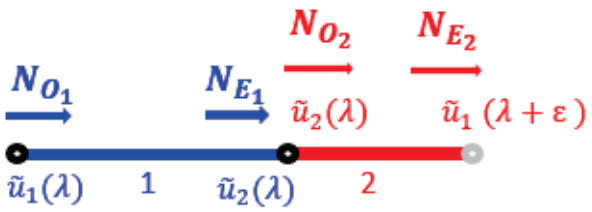

Figure 2.5: Reference cell for P.V.W with force and displacement in the cell.

In this section the homogenization of the cell represented in figure 2.5 is performed using the weak approach. This will allow us to identify the differences between the strong and weak procedure.

The P.V.W. for the discrete model is:

$$\sum_{\nu\in\mathcal{Z}}\sum_{b\in\mathcal{B}}\left(N^{\varepsilon}_{O_b}\tilde{u}^{\varepsilon}_{O_b}+N^{\varepsilon}_{E_b}\tilde{u}^{\varepsilon}_{E_b}\right)-\sum_{\nu\in\mathcal{Z}}\sum_{n\in\mathcal{N}}f^{e}_{n}\tilde{u}^{\varepsilon}_{n}=0\qquad\forall\tilde{u}^{\varepsilon}_{n}\tag{2.28}$$

where ν indicate the cell, b indicate the generic beam in the cell, $\tilde{u}^{\varepsilon}_{n}$ is the virtual displacement and f^{e}_{n} the external force in the node n. Note that in the following development f^{e}_{n} will be considered null.

In the case of the cell with one internal node, figure 2.5, the P.V.W. becomes:

$$\sum_{\nu\in\mathcal{Z}}\left(N^{\varepsilon}_{O_1}\tilde{u}^{\varepsilon}_{O_1}+N^{\varepsilon}_{E_1}\tilde{u}^{\varepsilon}_{E_1}+N^{\varepsilon}_{O_2}\tilde{u}^{\varepsilon}_{O_2}+N^{\varepsilon}_{E_2}\tilde{u}^{\varepsilon}_{E_2}-\sum_{n\in\mathcal{N}}f^{e}_{n}\tilde{u}^{\varepsilon}_{n}\right)=0\quad\forall\tilde{u}^{\varepsilon}_{n}\tag{2.29}$$

The end displacements u_{O_b} and u_{E_b} are related to the nodal degrees of freedom as follows:

$$\begin{aligned}u_{O_1}&=u_1(\lambda)\qquad u_{E_1}=u_2(\lambda)\\u_{O_2}&=u_2(\lambda)\qquad u_{E_2}=u_1(\lambda+\varepsilon)\end{aligned}\tag{2.30}$$

The nodal displacements are expanded as shown in equations (2.6), (2.9). The virtual displacements should be expanded in a similar way.

Notice that, essentially, there are only two independent sets of virtual displacements: those associated with the variation of the leading order displacement u^{0}_{n} and equipped with periodic boundary conditions at the extreme of whole body, and those associated with the variation of the higher order corrector, that own the periodicity condition and satisfy periodic boundary conditions at the end point of the cell. The expanded form of the virtual displacement of the nodes are then:

$$\begin{aligned}&\tilde{u}^{\varepsilon}_{n}(\lambda)=\tilde{u}^{0}_{n}(\lambda)+\varepsilon\tilde{u}^{1}_{n}(\lambda)\qquad n=1,2.\\&\tilde{u}^{\varepsilon}_{1}(\lambda+\varepsilon)=\tilde{u}^{0}_{1}(\lambda)+\varepsilon\left(\tilde{u}^{1}_{1}(\lambda)+\frac{\partial\tilde{u}^{0}_{1}(\lambda)}{\partial\lambda}\right)+\varepsilon^{2}\left(\frac{\partial\tilde{u}^{1}_{1}(\lambda)}{\partial\lambda}+\frac{1}{2}\frac{\partial^{2}\tilde{u}^{2}_{1}(\lambda)}{\partial\lambda^{2}}\right)+\ldots.\end{aligned}\tag{2.31}$$

The dual equilibrium equation to $\tilde{u}^{0}_{n}$ represents the generic macroscopic equilibrium, while the dual equation to $\tilde{u}^{1}_{n}$ gives the self-equilibrium equation of the cell.

Expanding equation (2.29) for the forces and for the virtual displacements we obtain (using the notation $N_b^\varepsilon = N_{E_b}^\varepsilon$ and $N_{O_b}^\varepsilon = -N_b^\varepsilon$):

$$\begin{aligned}
&\sum_{\nu\in\mathcal{Z}}\Big[-\left(N_1^0+\varepsilon N_1^1+\varepsilon^2N_1^2+\ldots\right)\left(\tilde{u}_1^0+\varepsilon\tilde{u}_1^1\right)+\\
&+\left(\left(N_1^0-N_2^0\right)+\varepsilon\left(N_1^1-N_2^1\right)+\varepsilon^2\left(N_1^2-N_2^2\right)\right)\left(\tilde{u}_2^0+\varepsilon\tilde{u}_2^1\right)+\\
&+\left(N_2^0+\varepsilon N_2^1+\varepsilon^2N_2^2+\ldots\right)\left(\tilde{u}_1^0+\varepsilon\left(\tilde{u}_1^1+\frac{\partial\tilde{u}_1^0}{\partial\lambda}\right)+\varepsilon^2\left(\frac{\partial\tilde{u}_1^1}{\partial\lambda}+\frac{1}{2}\frac{\partial^2\tilde{u}_1^2}{\partial\lambda^2}\right)+\ldots\right)-\sum_{n\in\mathcal{N}}f_n^e\tilde{u}_n\Big]=0\\
&\forall\tilde{u}_n
\end{aligned}\tag{2.32}$$

Since the virtual micro-displacement has to comply with periodicity of the boundary conditions, an arbitrary value of $\tilde{u}_1^1$ can be defined. Therefore in the case under examination, it is more convenient to refer for the virtual displacement to the difference:

$$\tilde{u}_\Delta^1=\tilde{u}_2^1-\tilde{u}_1^1\tag{2.33}$$

We will adopt a the decomposition for the nodal displacements:

$$\begin{aligned}
u_m^i&=\frac{1}{2}\left(u_1^i+u_2^i\right)\\
&\qquad\qquad i=1,\ldots\\
u_\Delta^i&=\left(u_2^i-u_1^i\right)
\end{aligned}\tag{2.34}$$

so that

$$\begin{aligned}
u_1^i&=u_m^i-\frac{1}{2}u_\Delta^i\\
&\qquad\qquad i=1,\ldots\\
u_2^i&=u_m^i+\frac{1}{2}u_\Delta^i
\end{aligned}\tag{2.35}$$

The virtual work (2.32) can be expressed consistently to (2.34) and (2.35); however, it is not shown herein for brevity.

At each order, two equilibrium equations are obtained: the micro-equilibrium equation of the cell, dual of the virtual micro-displacement $\tilde{u}_\Delta^1$, and the macro-equilibrium equation, dual of the virtual macro-displacement $\tilde{U}^0$.

Collecting the terms in power of ε, we obtain the equilibrium equations in weak form.

Order 0 in ε

The zero-order equation is:

$$\sum_{\nu\in\mathcal{Z}}\left[\left(-N_1^0+N_2^0\right)\tilde{u}_1^0+\left(N_1^0-N_2^0\right)\tilde{u}_2^0\right]=0\quad\forall\tilde{u}_n^0\quad n=1,2.\tag{2.36}$$

Given the arbitrary nature of the virtual displacements the above expression implies that:

$$N_1^0=N_2^0\tag{2.37}$$

Substituting the constitutive relations (2.11) and (2.12) into (2.37) leads to the same result found for the strong formulation:

$$k_{a1}\left(u_2^0 - u_1^0\right) = k_{a2}\left(u_1^0 - u_2^0\right) \Rightarrow u_1^0 = u_2^0 = U^0 \tag{2.38}$$

and therefore:

$$N_1^0 = N_2^0 = 0 \tag{2.39}$$

By virtue of the previous result, for the virtual macro-displacement we will accordingly assume:

$$\tilde{u}_1^0 = \tilde{u}_2^0 = \tilde{U}^0 \tag{2.40}$$

Order 1 in ε

All equation at this order, accounting the result (2.40), vanish.

Order 2 in ε

Micro-equilibrium equation

Considering the equations (2.32), (2.34) and (2.35), the virtual work dual to $\tilde{u}_\Delta^1$ at order 2 in ε becomes:

$$\varepsilon^2 \sum_{\nu \in \mathcal{Z}} \left[2\left(N_1^1 - N_2^1\right)\right] \tilde{u}_\Delta^1 = 0 \quad \forall \tilde{u}_\Delta^1 \tag{2.41}$$

that means:

$$N_1^1 - N_2^1 = 0 \tag{2.42}$$

Substituting the constitutive laws (2.11) and (2.12) into equation (2.42), we obtain equation (2.43):

$$k_{a1}\left(u_\Delta^1\right) = k_{a2}\left(-u_\Delta^1 + \frac{\partial U^0}{\partial \lambda}\right) \tag{2.43}$$

which provides the micro-displacements as function of the macro-displacements:

$$u_\Delta^1 = \frac{k_{a2}}{k_{a1} + k_{a2}} \frac{\partial U^0}{\partial \lambda} \tag{2.44}$$

substituting the equation (2.44) in the constitutive relation of the axial nodal force at order 1 in ε, we obtain:

$$N_1^1 = N_2^1 = K_1 \frac{\partial U^0}{\partial \lambda} \tag{2.45}$$

where $K_1 = \dfrac{k_{a1} k_{a2}}{k_{a1} + k_{a2}}$ is the homogenized axial rigidity, identical to the one defined in the strong formulation.

Macro-equilibrium

Considering in the P.V.W. equation (2.32), the dual to $\tilde{U}^0$ at order 2 is:

$$\varepsilon^2 \sum_{\nu \in \mathcal{Z}} \left(-N_1^2 + \left(N_1^2 - N_2^2\right) + N_2^2\right) \tilde{U}^0 + N_2^1 \frac{\partial \tilde{U}^0}{\partial \lambda} = 0 \quad \forall \tilde{U}^0 \tag{2.46}$$

The expression (2.32) holds for the whole structure, since $\tilde{U}^0$ is defined on the domain Λ.

Recalling that for the uniaxial case $\varepsilon = \dfrac{1}{N_c}$ and $\lambda = \varepsilon\nu$, we get that:

$$\lim_{\varepsilon \to 0} \varepsilon \sum_{\nu \in \mathcal{Z}} (\Delta\nu) = \int_\Lambda d\lambda \tag{2.47}$$

Taking the limit of the equation (2.46) in ε, the sum in the left hand side can be substituted by the following integral:

$$\varepsilon \int_\Lambda N_2^1 \frac{\partial \tilde{U}^0}{\partial \lambda} d\lambda = 0 \quad \forall \tilde{U}^0 \tag{2.48}$$

Integration by parts provides equation (2.49), which is the balance equation of the bar.

$$-\frac{\partial N_2^1}{\partial \lambda} = 0 \quad \Rightarrow \quad -K_1 \frac{\partial^2 U^0}{\partial \lambda^2} = 0 \tag{2.49}$$

The findings of the weak formulation presented in this subsection are summarized below:

Order 0 in ε

$$u_1^0 = u_2^0 = U^0 \quad \Rightarrow \quad N_1^0 = N_2^0 \tag{2.50}$$

Order 1 in ε

$$- \tag{2.51}$$

Order 2 in ε

$$\begin{aligned} u_\Delta^1 &= \frac{k_{a2}}{k_{a1} + k_{a2}} \frac{\partial \tilde{U}^0}{\partial \lambda} \quad (micro) \\ -K_1 \frac{\partial^2 \tilde{U}^0}{\partial \lambda^2} &= f^e \qquad (macro) \end{aligned} \tag{2.52}$$

Comparing the findings of the strong and weak formulations, we see how both formulations lead to the same expression for u_Δ^i, but shifted by one order in ε. This is due to the presence of the integral in the weak equilibrium expression.

2.3 1D model - flexural case

The second case refers to the model illustrated in figure 2.2, however, this time the element is composed by beams with only flexural deformation (see figure 2.6(b)). The main difference with the axial case is that the equilibrium equations of the elements constituting the cells are of order 4. So we expect that we will have to expand up to the fourth order in ε for obtaining the hypotheses of the homogenized material. The relationships between the end forces and the end displacements are:

$$\begin{aligned}
T^{\varepsilon}_{O_b} &= \frac{12EI}{L_b^3}\left[(v_{O_b}-v_{E_b})+\frac{L_b}{2}(\phi_{O_b}+\phi_{E_b})\right]\\
T^{\varepsilon}_{E_b} &= \frac{12EI}{L_b^3}\left[(v_{E_b}-v_{O_b})-\frac{L_b}{2}(\phi_{O_b}+\phi_{E_b})\right] = -T^{\varepsilon}_{O_b}\\
M^{\varepsilon}_{O_b} &= \frac{6EI}{L_b^2}\left[(v_{O_b}-v_{E_b})+\frac{L_b}{2}(\phi_{O_b}+\phi_{E_b})-\frac{L_b}{6}(\phi_{E_b}-\phi_{O_b})\right]\\
M^{\varepsilon}_{E_b} &= \frac{6EI}{L_b^2}\left[(v_{O_b}-v_{E_b})+\frac{L_b}{2}(\phi_{O_b}+\phi_{E_b})+\frac{L_b}{6}(\phi_{E_b}-\phi_{O_b})\right]
\end{aligned} \tag{2.53}$$

The asymptotic expansions in ε of the displacement functions $v_n(\lambda)$ and $\phi_n(\lambda)$ are:

$$\begin{aligned}
v_n(\lambda) &= v_n^0(\lambda)+\varepsilon v_n^1(\lambda)+\varepsilon^2 v_n^2(\lambda)+\varepsilon^3 v_n^3(\lambda)+\varepsilon^3 v_n^4(\lambda)+\dots\\
\phi_n(\lambda) &= \phi_n^0(\lambda)+\varepsilon\phi_n^1(\lambda)+\varepsilon^2\phi_n^2(\lambda)+\varepsilon^3\phi_n^3(\lambda)+\varepsilon^3\phi_n^4(\lambda)+\dots
\end{aligned} \tag{2.54}$$

If the considered node belongs to the neighbouring cell, we have:

$$\begin{aligned}
v_n(\lambda+\varepsilon) &= v_n^0(\lambda+\varepsilon)+\varepsilon v_n^1(\lambda+\varepsilon)+\varepsilon^2 v_n^2(\lambda+\varepsilon)+\varepsilon^3 v_n^3(\lambda+\varepsilon)+\varepsilon^3 v_n^4(\lambda+\varepsilon)+\dots\\
\phi_n(\lambda+\varepsilon) &= \phi_n^0(\lambda+\varepsilon)+\varepsilon\phi_n^1(\lambda+\varepsilon)+\varepsilon^2\phi_n^2(\lambda+\varepsilon)+\varepsilon^3\phi_n^3(\lambda+\varepsilon)+\varepsilon^3\phi_n^4(\lambda+\varepsilon)+\dots
\end{aligned} \tag{2.55}$$

Applying the Taylor expansion to the various orders, we have:

$$\begin{aligned}
v_n^0(\lambda+\varepsilon) &= v_n^0(\lambda)+\varepsilon\frac{\partial v_n^0(\lambda)}{\partial\lambda}+\frac{\varepsilon^2}{2!}\frac{\partial^2 v_n^0(\lambda)}{\partial\lambda^2}+\dots\\
v_n^1(\lambda+\varepsilon) &= v_n^1(\lambda)+\varepsilon\frac{\partial v_n^1(\lambda)}{\partial\lambda}+\frac{\varepsilon^2}{2!}\frac{\partial^2 v_n^1(\lambda)}{\partial\lambda^2}+\dots\\
v_n^2(\lambda+\varepsilon) &= v_n^2(\lambda)+\varepsilon\frac{\partial v_n^2(\lambda)}{\partial\lambda}+\frac{\varepsilon^2}{2!}\frac{\partial^2 v_n^2(\lambda)}{\partial\lambda^2}+\dots
\end{aligned} \tag{2.56}$$

$$\begin{aligned}
\phi_n^0(\lambda+\varepsilon) &= \phi_n^0(\lambda) + \varepsilon\frac{\partial\phi_n^0(\lambda)}{\partial\lambda} + \frac{\varepsilon^2}{2!}\frac{\partial^2\phi_n^0(\lambda)}{\partial\lambda^2} + \dots \\
\phi_n^1(\lambda+\varepsilon) &= \phi_n^1(\lambda) + \varepsilon\frac{\partial\phi_n^1(\lambda)}{\partial\lambda} + \frac{\varepsilon^2}{2!}\frac{\partial^2\phi_n^1(\lambda)}{\partial\lambda^2} + \dots \\
\phi_n^2(\lambda+\varepsilon) &= \phi_n^2(\lambda) + \varepsilon\frac{\partial\phi_n^2(\lambda)}{\partial\lambda} + \frac{\varepsilon^2}{2!}\frac{\partial^2\phi_n^2(\lambda)}{\partial\lambda^2} + \dots
\end{aligned} \tag{2.57}$$

Collecting the terms in equations (2.55), (2.56), (2.57), we obtain:

$$\begin{aligned}
v_n(\lambda+\varepsilon) &= v_n^0(\lambda) + \varepsilon\left(v_n^1(\lambda) + \frac{\partial v_n^0(\lambda)}{\partial\lambda}\right) + \varepsilon^2\left(v_n^2(\lambda) + \frac{\partial v_n^1(\lambda)}{\partial\lambda} + \frac{1}{2!}\frac{\partial^2 v_n^0(\lambda)}{\partial\lambda^2}\right) + \dots \\
\phi_n(\lambda+\varepsilon) &= \phi_n^0(\lambda) + \varepsilon\left(\phi_n^1(\lambda) + \frac{\partial\phi_n^0(\lambda)}{\partial\lambda}\right) + \varepsilon^2\left(\phi_n^2(\lambda) + \frac{\partial\phi_n^1(\lambda)}{\partial\lambda} + \frac{1}{2!}\frac{\partial^2\phi_n^0(\lambda)}{\partial\lambda^2}\right) + \dots
\end{aligned} \tag{2.58}$$

It can be easily shown that the leading term v_n^0 of the asymptotic expansion (2.58) is the same for all the nodes, $v_1^0 = v_2^0 = V^0$. As in the case of uniaxial deformation, discussed in subsection 2.2.1, this result is due to the zero-order translational equilibrium equations. Substituting the equations (2.54) and (2.58) in the relation (2.53), we obtain the expansion of the shear forces and bending moments up to the first order in ε:

$$\begin{aligned}
T_{O_1}^1(\lambda) &= 2k_{f1}\left[-v_\Delta^1 + \frac{l_1}{2}\varphi^0\right] \\
T_{E_1}^1(\lambda) &= 2k_{f1}\left[v_\Delta^1 - \frac{l_1}{2}\varphi^0\right] \\
T_{O_2}^1(\lambda) &= 2k_{f2}\left[\left(v_\Delta^1 - \frac{\partial V^0}{\partial\lambda}\right) + \frac{l_2}{2}\varphi^0\right] \\
T_{E_2}^1(\lambda-\varepsilon) &= 2k_{f2}\left[\left(-v_\Delta^1 + \frac{\partial V^0}{\partial\lambda}\right) - \frac{l_2}{2}\varphi^0\right]
\end{aligned} \tag{2.59}$$

$$\begin{aligned}
M_{O_1}^2(\lambda) &= k_{f1}l_1\left[-v_\Delta^1 + \frac{l_1}{2}\varphi^0 - \frac{l_1}{6}\delta\varphi^0\right] \\
M_{E_1}^2(\lambda) &= k_{f1}l_1\left[-v_\Delta^1 + \frac{l_1}{2}\varphi^0 + \frac{l_1}{6}\delta\varphi^0\right] \\
M_{O_2}^2(\lambda) &= k_{f2}l_2\left[\left(v_\Delta^1 - \frac{\partial V^0}{\partial\lambda}\right) + \frac{l_2}{2}\varphi^0 + \frac{l_2}{6}\varphi_\Delta^0\right] \\
M_{E_2}^2(\lambda-\varepsilon) &= k_{f2}l_2\left[\left(v_\Delta^1 - \frac{\partial V^0}{\partial\lambda}\right) + \frac{l_2}{2}\varphi^0 - \frac{l_2}{6}\varphi_\Delta^0\right]
\end{aligned} \tag{2.60}$$

The notations

$$v^i_\Delta = v^i_2 - v^i_1 \qquad V^i = \frac{v^i_1 + v^i_2}{2} \qquad \varphi^i = \phi^i_1 + \phi^i_2 \qquad \varphi^i_\Delta = \phi^i_2 - \phi^i_1 \qquad k_{fb} = \frac{6E_bI_b}{l_b^3}$$

will be used throughout the subsequent developments made herein.

2.3.1 Strong formulation

Similarly to the uniaxial case, we start by writing the balance equations at the nodes of the beam, as shown in Figure 2.6(b):

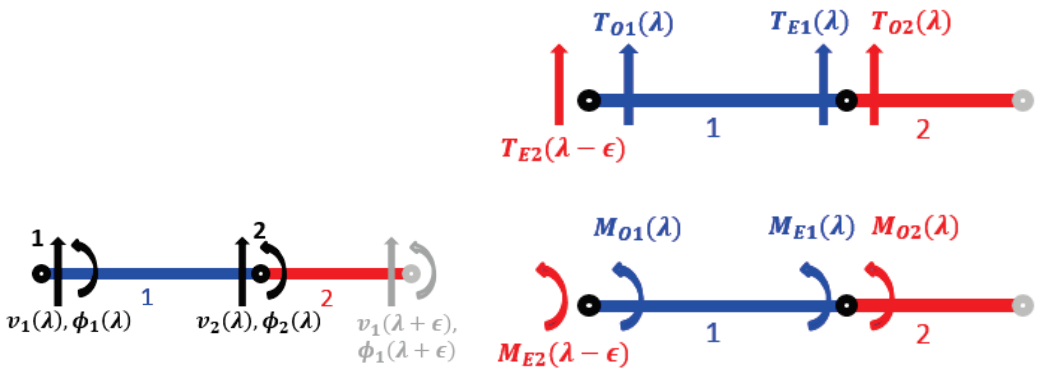

(a) Nodal vertical displacements and rotations.

(b) Nodal shear forces and bending moments.

Figure 2.6: Reference cell for Strong Formulation with forces and displacements in the cell.

The balance equations at node 1 are:

$$\begin{aligned} E_{T_1} &\Rightarrow T_{E_2}(\lambda-\varepsilon) + T_{O_1}(\lambda) = 0 \\ E_{M_1} &\Rightarrow M_{E_2}(\lambda-\varepsilon) + M_{O_1}(\lambda) = 0 \end{aligned} \tag{2.61}$$

while for node 2 the balance equations are:

$$\begin{aligned} E_{T_2} &\Rightarrow T_{E_1}(\lambda) + T_{O_2}(\lambda) = 0 \\ E_{M_2} &\Rightarrow M_{E_1}(\lambda) + M_{O_2}(\lambda) = 0 \end{aligned} \tag{2.62}$$

where $E_{T^i_n}$ and $E_{M^i_n}$ indicate respectively the force and the bending moment balance equations for the node n on the order i. Given that the unknown displacements v^1_n and ϕ^0_n appear in the shear and bending moment equilibrium equations both in the first- and second-order respectively, we should use together the translational equilibrium at order 1 and the rotational equilibrium at order 2. Substitution of the expressions (2.59) and (2.60) into the equilibrium equations (2.61) and (2.62) in matrix form gives:

$$
\begin{array}{l}
E_{T_2^1} \Rightarrow \\
E_{T_1^1} \Rightarrow \\
E_{M_2^2} \Rightarrow \\
E_{M_1^2} \Rightarrow
\end{array}
\begin{bmatrix}
k_{f1}+k_{f2} & \dfrac{-k_{f1}l_1+k_{f2}l_2}{2} & 0 \\
k_{f1}+k_{f2} & \dfrac{-k_{f1}l_1+k_{f2}l_2}{2} & 0 \\
-k_{f1}l_1+k_{f2}l_2 & \dfrac{k_{f1}l_1^2+k_{f2}l_2^2}{2} & \dfrac{k_{f1}l_1^2+k_{f2}l_2^2}{6} \\
k_{f1}l_1-k_{f2}l_2 & \dfrac{-k_{f1}l_1^2-k_{f2}l_2^2}{2} & \dfrac{k_{f1}l_1^2+k_{f2}l_2^2}{6}
\end{bmatrix}
\begin{bmatrix} v_\Delta^1 \\ \varphi^0 \\ \varphi_\Delta^0 \end{bmatrix}
= k_{f2}
\begin{bmatrix} \dfrac{\partial V^0}{\partial \lambda} \\ \dfrac{\partial V^0}{\partial \lambda} \\ l_2\dfrac{\partial V^0}{\partial \lambda} \\ -l_2\dfrac{\partial V^0}{\partial \lambda} \end{bmatrix}
\tag{2.63}
$$

To simplify the system we perform the following operations:

$$
\begin{array}{l}
(E_{T_2^1}+E_{T_1^1})/2 \quad \Rightarrow \\
(E_{T_2^1}-E_{T_1^1})/2 \quad \Rightarrow \\
(E_{M_2^2}+E_{M_1^1})/2 \quad \Rightarrow \\
(E_{M_2^2}-E_{M_1^1})/2 \quad \Rightarrow
\end{array}
\begin{bmatrix}
k_{f1}+k_{f2} & \dfrac{-k_{f1}l_1+k_{f2}l_2}{2} & 0 \\
0 & 0 & 0 \\
0 & 0 & \dfrac{k_{f1}l_1^2+k_{f2}l_2^2}{6} \\
-k_{f1}l_1+k_{f2}l_2 & \dfrac{k_{f1}l_1^2+k_{f2}l_2^2}{2} & 0
\end{bmatrix}
\begin{bmatrix} v_\Delta^1 \\ \varphi^0 \\ \varphi_\Delta^0 \end{bmatrix}
= k_{f2}\dfrac{\partial V^0}{\partial \lambda}
\begin{bmatrix} 1 \\ 0 \\ 0 \\ l_2 \end{bmatrix}
\tag{2.64}
$$

From the solution of the system (2.64), we obtain, at the first order:

$$
\begin{aligned}
v_\Delta^1 &= \frac{l_1}{l_1+l_2}\frac{\partial V^0}{\partial \lambda} \\
\varphi^0 &= \frac{2}{l_1+l_2}\frac{\partial V^0}{\partial \lambda} \\
\varphi_\Delta^0 &= 0 \\
0 &= 0
\end{aligned}
\tag{2.65}
$$

The second and the third equation of (2.65) show that the leading nodal rotations are both equal to the physical derivative of the displacement. In this way the Euler-Bernoulli beam model is obtained. Substituting the solution of the system (2.65) in (2.59) and (2.60), we obtain the shear forces and bending moments at the first order:

$$
\begin{array}{llll}
T_{O_1}^1(\lambda)=0 & T_{E_1}^1(\lambda)=0 & M_{O_1}^2(\lambda)=0 & M_{E_1}^2(\lambda)=0 \\
T_{O_2}^1(\lambda)=0 & T_{E_2}^1(\lambda-\varepsilon)=0 & M_{O_2}^2(\lambda)=0 & M_{E_2}^2(\lambda-\varepsilon)=0
\end{array}
\tag{2.66}
$$

Order 2 in ε

The asymptotic expansion of the shear forces at second order in ε is:

$$\begin{aligned}
T^2_{O_1}(\lambda) &= 2k_{f1}\left[-v^2_\Delta + \frac{l_1}{2}\varphi^1\right] \\
T^2_{E_1}(\lambda) &= -T^2_{O_1}(\lambda) \\
T^2_{O_2}(\lambda) &= 2k_{f2}\left[\left(v^2_\Delta - \frac{\partial v^1_1}{\partial\lambda} - \frac{1}{2}\frac{\partial^2 V^0}{\partial\lambda^2}\right) + \frac{l_2}{2}\left(\varphi^1 + \frac{\partial\phi^0_1}{\partial\lambda}\right)\right] \\
T^2_{E_2}(\lambda-\varepsilon) &= 2k_{f2}\left[\left(-v^2_\Delta + \frac{\partial v^1_2}{\partial\lambda} - \frac{1}{2}\frac{\partial^2 V^0}{\partial\lambda^2}\right) - \frac{l_2}{2}\left(\varphi^1 - \frac{\partial\phi^0_2}{\partial\lambda}\right)\right]
\end{aligned} \tag{2.67}$$

The corresponding bending moments are:

$$\begin{aligned}
M^3_{O_1}(\lambda) &= k_{f1}l_1\left[-v^2_\Delta + \frac{l_1}{2}\varphi^1 - \frac{l_1}{6}\delta\varphi^1\right] \\
M^3_{E_1}(\lambda) &= k_{f1}l_1\left[-v^2_\Delta + \frac{l_1}{2}\varphi^1 + \frac{l_1}{6}\delta\varphi^1\right] \\
M^3_{O_2}(\lambda) &= k_{f2}l_2\left[\left(v^2_\Delta - \frac{\partial v^1_1}{\partial\lambda} - \frac{1}{2}\frac{\partial^2 V^0}{\partial\lambda^2}\right) + \frac{l_2}{2}\varphi^1 + \frac{l_2}{6}\varphi^1_\Delta + \frac{l_2}{3}\frac{\partial\phi^0_1}{\partial\lambda}\right] \\
M^3_{E_2}(\lambda-\varepsilon) &= k_{f2}l_2\left[\left(v^2_\Delta - \frac{\partial v^1_2}{\partial\lambda} + \frac{1}{2}\frac{\partial^2 V^0}{\partial\lambda^2}\right) + \frac{l_2}{2}\varphi^1 - \frac{l_2}{6}\varphi^1_\Delta - \frac{l_2}{3}\frac{\partial\phi^0_2}{\partial\lambda}\right]
\end{aligned} \tag{2.68}$$

Substituting the expressions (2.67),(2.68) in equations (2.61),(2.62), we obtain the equilibrium equation at the order 2 in ε in matrix form:

$$\begin{aligned}
E_{T^2_2} \Rightarrow \\
E_{T^2_1} \Rightarrow \\
E_{M^3_2} \Rightarrow \\
E_{M^3_1} \Rightarrow
\end{aligned}
\begin{bmatrix}
k_{f1}+k_{f2} & \frac{-k_{f1}l_1+k_{f2}l_2}{2} & 0 \\
k_{f1}+k_{f2} & \frac{-k_{f1}l_1+k_{f2}l_2}{2} & 0 \\
-k_{f1}l_1+k_{f2}l_2 & \frac{k_{f1}l_1^2+k_{f2}l_2^2}{2} & \frac{k_{f1}l_1^2+k_{f2}l_2^2}{6} \\
k_{f1}l_1-k_{f2}l_2 & \frac{-k_{f1}l_1^2-k_{f2}l_2^2}{2} & \frac{k_{f1}l_1^2+k_{f2}l_2^2}{6}
\end{bmatrix}
\begin{bmatrix} \delta v^2 \\ \varphi^1 \\ \delta\varphi^1 \end{bmatrix}
= k_{f2}
\begin{bmatrix} \frac{\partial v^1_1}{\partial\lambda} \\ \frac{\partial v^1_2}{\partial\lambda} \\ l_2\frac{\partial v^1_1}{\partial\lambda} \\ -l_2\frac{\partial v^1_2}{\partial\lambda} \end{bmatrix}
+ \frac{k_{f2}}{2}
\begin{bmatrix} \frac{\partial^2 V^0}{\partial\lambda^2} \\ -\frac{\partial^2 V^0}{\partial\lambda^2} \\ l_2\frac{\partial^2 V^0}{\partial\lambda^2} \\ l_2\frac{\partial^2 V^0}{\partial\lambda^2} \end{bmatrix}
+ k_{f2}l_2
\begin{bmatrix} -\frac{1}{2}\frac{\partial\phi^0_1}{\partial\lambda} \\ \frac{1}{2}\frac{\partial\phi^0_2}{\partial\lambda} \\ -\frac{l_2}{3}\frac{\partial\phi^0_1}{\partial\lambda} \\ -\frac{l_2}{3}\frac{\partial\phi^0_2}{\partial\lambda} \end{bmatrix}$$

After performing row transformations we obtain the following set of equations:

$$
\begin{aligned}
(E_{T_2^2}+E_{T_1^2})/2 \quad &\Rightarrow \\
(E_{T_2^2}-E_{T_1^2})/2 \quad &\Rightarrow \\
(E_{M_2^3}+E_{M_1^3})/2 \quad &\Rightarrow \\
(E_{M_2^3}-E_{M_1^3})/2 \quad &\Rightarrow
\end{aligned}
\begin{bmatrix}
k_{f1}+k_{f2} & \dfrac{-k_{f1}l_1+k_{f2}l_2}{2} & 0 \\
0 & 0 & 0 \\
0 & 0 & \dfrac{k_{f1}l_1^2+k_{f2}l_2^2}{6} \\
-k_{f1}l_1+k_{f2}l_2 & \dfrac{k_{f1}l_1^2+k_{f2}l_2^2}{2} & 0
\end{bmatrix}
\begin{bmatrix} v_\Delta^2 \\ \varphi^1 \\ \varphi_\Delta^1 \end{bmatrix}
= \frac{k_{f2}}{2}
\begin{bmatrix}
\dfrac{\partial(v_1^1+v_2^1)}{\partial\lambda} \\
\dfrac{\partial(v_1^1-v_2^1)}{\partial\lambda} \\
l_2\dfrac{\partial(v_1^1-v_2^1)}{\partial\lambda} \\
l_2\dfrac{\partial(v_1^1+v_2^1)}{\partial\lambda}
\end{bmatrix}
+
$$

$$
+\frac{k_{f2}}{2}
\begin{bmatrix}
0 \\
\dfrac{\partial^2 V^0}{\partial\lambda^2} \\
l_2\dfrac{\partial^2 V^0}{\partial\lambda^2} \\
0
\end{bmatrix}
+\frac{k_{f2}l_2}{2}
\begin{bmatrix}
\dfrac{1}{2}\dfrac{\partial(\phi_2^0-\phi_1^0)}{\partial\lambda} \\
-\dfrac{1}{2}\dfrac{\partial(\phi_1^0+\phi_2^0)}{\partial\lambda} \\
-\dfrac{l_2}{3}\dfrac{\partial(\phi_1^0+\phi_2^0)}{\partial\lambda} \\
\dfrac{l_2}{3}\dfrac{\partial(\phi_2^0-\phi_1^0)}{\partial\lambda}
\end{bmatrix}
\tag{2.69}
$$

Combining the solution of the system (2.69) with equation (2.65) we obtain:

$$
\begin{aligned}
v_\Delta^2 &= \frac{1}{2}\frac{l_1}{l_1+l_2}\frac{\partial(v_1^1+v_2^1)}{\partial\lambda} = \frac{l_1}{l_1+l_2}\frac{\partial V^1}{\partial\lambda} \\
\varphi^1 &= \frac{1}{l_1+l_2}\frac{\partial(v_1^1+v_2^1)}{\partial\lambda} = \frac{2}{l_1+l_2}\frac{\partial V^1}{\partial\lambda} \\
\varphi_\Delta^1 &= \frac{3k_{f2}l_2}{k_{f1}l_1^2+k_{f2}l_2^2}\left(\frac{\partial^2 V^0}{\partial\lambda^2}-\frac{\partial v_\Delta^1}{\partial\lambda}-\frac{l_2}{3}\frac{\partial\varphi^0}{\partial\lambda}\right) = \frac{K_{F1}}{k_{f1}l_1^2}\frac{\partial^2 V^0}{\partial\lambda^2} \\
0 &= 0
\end{aligned}
\tag{2.70}
$$

From the second and third equations of (2.70) we can see how that also for the first order correction the average rotation is equal to the derivative of the displacement, while the rotations ϕ_n^1 of the two nodes are different. Substituting the solution (2.70) in expressions (2.67) and (2.68), we obtain the shear forces and bending moments at this order:

$$
\begin{aligned}
&T^2_{O_1}(\lambda) = 0\\
&T^2_{E_1}(\lambda) = 0\\
&T^2_{O_2}(\lambda) = 0\\
&T^2_{E_2}(\lambda - \varepsilon) = 0\\
&M^3_{O_1}(\lambda) = -K_{F1}\frac{\partial^2 V^0}{\partial \lambda^2}\\
&M^3_{E_1}(\lambda) = K_{F1}\frac{\partial^2 V^0}{\partial \lambda^2}\\
&M^3_{O_2}(\lambda) = -K_{F1}\frac{\partial^2 V^0}{\partial \lambda^2}\\
&M^3_{E_2}(\lambda - \varepsilon) = K_{F1}\frac{\partial^2 V^0}{\partial \lambda^2}
\end{aligned}
\tag{2.71}
$$

where

$$
K_{F1} = \frac{k_{f1}l_1^2 k_{f2}l_2^2}{6\left(k_{f1}l_1^2 + k_{f2}l_2^2\right)(l_1 + l_2)} = \frac{1}{L}\frac{1}{\dfrac{l_2}{E_2 I_2} + \dfrac{l_1}{E_1 I_1}} \tag{2.72}
$$

If $E_1 = E_2$, $I_1 = I_2$, then $k_f = E_1 I_1 = E_2 I_2 = EI$ and the homogeneous beam is recovered. The equation (2.72) provides the definition for the flexural stiffness of two beams in series. Notice that, differently than the axial case, no equilibrium equation for the beam is obtained at order ε^2, i.e. the last of the equations (2.70) is identically satisfied. Thus we need to proceed with the expansion at higher order of ε.

Order 3 in ε

The expansions of the shear forces at the third order in ε are :

$$
\begin{aligned}
T^3_{O_1}(\lambda) &= 2k_{f1}\left[-v^3_\Delta + \frac{l_1}{2}\varphi^2\right]\\
T^3_{E_1}(\lambda) &= -T^3_{O_1}(\lambda)\\
T^3_{O_2}(\lambda) &= 2k_{f2}\left[\left(v^3_\Delta - \frac{\partial v^2_1}{\partial \lambda} - \frac{1}{2}\frac{\partial^2 v^1_1}{\partial \lambda^2} - \frac{1}{6}\frac{\partial^3 V^0}{\partial \lambda^3}\right) + \frac{l_2}{2}\left(\varphi^2 + \frac{\partial \phi^1_1}{\partial \lambda} + \frac{1}{2}\frac{\partial^2 \phi^0_1}{\partial \lambda^2}\right)\right]\\
T^3_{E_2}(\lambda - \varepsilon) &= 2k_{f2}\left[\left(-v^3_\Delta + \frac{\partial v^2_1}{\partial \lambda} - \frac{1}{2}\frac{\partial^2 v^1_1}{\partial \lambda^2} + \frac{1}{6}\frac{\partial^3 V^0}{\partial \lambda^3}\right) - \frac{l_2}{2}\left(\varphi^2 - \frac{\partial \phi^1_2}{\partial \lambda} + \frac{1}{2}\frac{\partial^2 \phi^0}{\partial \lambda^2}\right)\right]
\end{aligned}
\tag{2.73}
$$

The bending moments equal:

$$
\begin{aligned}
M^4_{O_1}(\lambda) &= k_{f1} l_1 \left[-v^3_\Delta + \frac{l_1}{2}\varphi^2 - \frac{l_1}{6}\delta\varphi^2 \right] \\
M^4_{E_1}(\lambda) &= k_{f1} l_1 \left[-v^3_\Delta + \frac{l_1}{2}\varphi^2 + \frac{l_1}{6}\delta\varphi^2 \right] \\
M^4_{O_2}(\lambda) &= k_{f2} l_2 \left[\left(v^3_\Delta - \frac{\partial v^2_1}{\partial\lambda} - \frac{1}{2}\frac{\partial^2 v^2_1}{\partial\lambda^2} - \frac{1}{6}\frac{\partial^3 V^0}{\partial\lambda^3} \right) + \frac{l_2}{2}\varphi^2 + \frac{l_1}{6}\varphi^2_\Delta + \frac{l_2}{3}\frac{\partial\phi^1_1}{\partial\lambda} + \frac{l_2}{6}\frac{\partial^2\phi^1_1}{\partial\lambda^2} \right] \\
M^4_{E_2}(\lambda-\varepsilon) &= k_{f2} l_2 \left[\left(v^3_\Delta - \frac{\partial v^2_2}{\partial\lambda} + \frac{1}{2}\frac{\partial^2 v^1_2}{\partial\lambda^2} - \frac{1}{6}\frac{\partial^3 V^0}{\partial\lambda^3} \right) + \frac{l_2}{2}\varphi^2 - \frac{l_2}{6}\varphi^2_\Delta - \frac{l_2}{3}\frac{\partial\phi^1_2}{\partial\lambda} + \frac{l_2}{6}\frac{\partial^2\phi^0_2}{\partial\lambda^2} \right]
\end{aligned}
\tag{2.74}
$$

Substituting the expressions (2.73),(2.74) in equations (2.61),(2.62) the system to solve, in matrix form, is:

$$
\begin{aligned}
&(E_{T^3_2} + E_{T^3_1})/2 \quad \Rightarrow \\
&(E_{T^3_2} - E_{T^3_1})/2 \quad \Rightarrow \\
&(E_{M^4_2} + E_{M^4_1})/2 \quad \Rightarrow \\
&(E_{M^4_2} - E_{M^4_1})/2 \quad \Rightarrow
\end{aligned}
\begin{bmatrix}
k_{f1} + k_{f2} & \dfrac{-k_{f1}l_1 + k_{f2}l_2}{2} & 0 \\
0 & 0 & 0 \\
0 & 0 & \dfrac{k_{f1}l_1^2 + k_{f2}l_2^2}{6} \\
-k_{f1}l_1 + k_{f2}l_2 & \dfrac{k_{f1}l_1^2 + k_{f2}l_2^2}{2} & 0
\end{bmatrix}
\begin{bmatrix} v^3_\Delta \\ \varphi^2 \\ \varphi^2_\Delta \end{bmatrix}
= \frac{k_{f2}}{2}
\begin{bmatrix}
\dfrac{\partial(v^2_1 + v^2_2)}{\partial\lambda} \\
\dfrac{\partial(v^2_1 - v^2_2)}{\partial\lambda} \\
l_2\dfrac{\partial(v^2_1 - v^2_2)}{\partial\lambda} \\
l_2\dfrac{\partial(v^2_1 + v^2_2)}{\partial\lambda}
\end{bmatrix} +
$$

$$
+ \frac{1}{2}\frac{k_{f2}}{2}
\begin{bmatrix}
\dfrac{\partial^2(v^1_1 - v^1_2)}{\partial\lambda^2} \\
\dfrac{\partial^2(v^1_1 + v^1_2)}{\partial\lambda^2} \\
l_2\dfrac{\partial^2(v^1_1 + v^1_2)}{\partial\lambda^2} \\
l_2\dfrac{\partial^2(v^1_1 - v^1_2)}{\partial\lambda^2}
\end{bmatrix}
+ \frac{1}{2}\frac{k_{f2}}{3!}
\begin{bmatrix}
\dfrac{\partial^3 V^0}{\partial\lambda^3} \\ 0 \\ 0 \\ l_2\dfrac{\partial^3 V^0}{\partial\lambda^3}
\end{bmatrix}
+ \frac{k_{f2}l_2}{2}
\begin{bmatrix}
\dfrac{1}{2}\dfrac{\partial(\phi^1_2 - \phi^1_1)}{\partial\lambda} \\
-\dfrac{1}{2}\dfrac{\partial(\phi^1_1 + \phi^1_2)}{\partial\lambda} \\
-\dfrac{l_2}{3}\dfrac{\partial(\phi^1_1 + \phi^1_2)}{\partial\lambda} \\
\dfrac{l_2}{3}\dfrac{\partial(\phi^1_2 - \phi^1_1)}{\partial\lambda}
\end{bmatrix}
+ \frac{1}{2}\frac{k_{f2}l_2}{2}
\begin{bmatrix}
-\dfrac{1}{2}\dfrac{\partial^2(\phi^0_1 + \phi^0_2)}{\partial\lambda^2} \\
\dfrac{1}{2}\dfrac{\partial^2(\phi^0_2 - \phi^0_1)}{\partial\lambda^2} \\
\dfrac{l_2}{3}\dfrac{\partial^2(\phi^0_2 - \phi^0_1)}{\partial\lambda^2} \\
-\dfrac{l_2}{3}\dfrac{\partial^2(\phi^0_1 + \phi^0_2)}{\partial\lambda^2}
\end{bmatrix}
\tag{2.75}
$$

The solution of system (2.75) is:

$$
\begin{aligned}
\delta v^3 &= \frac{1}{2}\frac{l_1}{l_1 + l_2}\left(2\frac{\partial V^2}{\partial\lambda} - \frac{1}{2}\frac{\partial^2\delta v^1}{\partial\lambda^2} + \frac{2}{3!}\frac{\partial^3 V^0}{\partial\lambda^3} \right) + a\left(\frac{\partial\delta\varphi^1}{\partial\lambda} - \frac{1}{2}\frac{\partial^2\varphi^0}{\partial\lambda^2} \right) \\
\varphi^2 &= \frac{1}{l_1 + l_2}\left(2\frac{\partial V^2}{\partial\lambda} - \frac{1}{2}\frac{\partial^2\delta v^1}{\partial\lambda^2} + \frac{2}{3!}\frac{\partial^3 V^0}{\partial\lambda^3} \right) + b\left(\frac{\partial\delta\varphi^1}{\partial\lambda} - \frac{1}{2}\frac{\partial^2\varphi^0}{\partial\lambda^2} \right) \\
\delta\varphi^2 &= \frac{3k_{f2}l_2}{k_{f1}l_1^2 + k_{f2}l_2^2}\left(\frac{\partial^2 V^1}{\partial\lambda^2} - \frac{\partial\delta v^2}{\partial\lambda} - \frac{l_2}{3}\frac{\partial\varphi^1}{\partial\lambda} \right) = \frac{K_{F1}}{k_{f1}l_1^2}\frac{\partial^2 V^1}{\partial\lambda^2} \\
0 &= 0
\end{aligned}
\tag{2.76}
$$

where a and b equal:

$$
\begin{aligned}
a &= \frac{\frac{k_{f1}l_1^2l_2}{4} + \frac{k_{f2}l_2^3}{12} + \frac{k_{f1}l_1l_2^2}{6}}{k_{f1}(l_1+l_2)^2} \\
b &= \frac{\frac{k_{f1}l_2^2}{3} - \frac{k_{f2}l_2^2}{6} + \frac{k_{f1}l_1l_2}{2}}{k_{f1}(l_1+l_2)^2}
\end{aligned}
\tag{2.77}
$$

Substituting the solution (2.76) in equations (2.73) and (2.74), we obtain the shear forces and bending moments at this order:

$$
\begin{aligned}
T^3_{O_1}(\lambda) &= -\frac{K_{F1}}{(l_1+l_2)}\frac{\partial^3 V^0}{\partial\lambda^3} \\
T^3_{E_1}(\lambda) &= \frac{K_{F1}}{(l_1+l_2)}\frac{\partial^3 V^0}{\partial\lambda^3} \\
T^3_{O_2}(\lambda) &= \frac{K_{F1}}{(l_1+l_2)}\frac{\partial^3 V^0}{\partial\lambda^3} - \frac{k_{f2}l_2}{l_1+l_2}\frac{\partial^2 v_2^1}{\partial\lambda^2} \\
T^3_{E_2}(\lambda-\varepsilon) &= -\frac{K_{F1}}{(l_1+l_2)}\frac{\partial^3 V^0}{\partial\lambda^3} - \frac{k_{f2}l_2}{l_1+l_2}\frac{\partial^2 v_2^1}{\partial\lambda^2}
\end{aligned}
\tag{2.78}
$$

$$
\begin{aligned}
M^4_{O_1}(\lambda) &= -K_{F1}\frac{\partial^2 v_2^1}{\partial\lambda^2} - K_{F1}\frac{-3k_{f1}l_1^2 + k_{f2}l_2^2}{4(l_1+l_2)k_{f1}l_1}\frac{\partial^3 V^0}{\partial\lambda^3} \\
M^4_{E_1}(\lambda) &= -K_{F1}\frac{\partial^2 v_2^1}{\partial\lambda^2} - K_{F1}\frac{-3k_{f1}l_1^2 + k_{f2}l_2^2}{4(l_1+l_2)k_{f1}l_1}\frac{\partial^3 V^0}{\partial\lambda^3} \\
M^4_{O_2}(\lambda) &= -K_{F1}\frac{-3k_{f1}l_1^2 + k_{f2}l_2^2}{4(l_1+l_2)k_{f1}l_1^2k_{f2}l_2^2}\frac{\partial^3 V^0}{\partial\lambda^3} - K_{F1}\frac{\partial^2 v_2^1}{\partial\lambda^2} \\
M^4_{E_2}(\lambda-\varepsilon) &= K_{F1}\frac{\partial^2 v_2^1}{\partial\lambda^2} + K_{F1}\frac{-k_{f1}l_1^2(l_1-2l_2) + k_{f2}l_2^2(3l_1+2l_2)}{4(l_1+l_2)k_{f1}l_1^2}\frac{\partial^3 V^0}{\partial\lambda^3}
\end{aligned}
\tag{2.79}
$$

Order 4 in ε

The equilibrium equations are:

$$
\begin{aligned}
(E_{T_2^4}+E_{T_1^4})/2 \quad &\Rightarrow \\
(E_{T_2^4}-E_{T_1^4})/2 \quad &\Rightarrow \\
(E_{M_2^5}+E_{M_1^5})/2 \quad &\Rightarrow \\
(E_{M_2^5}-E_{M_1^5})/2 \quad &\Rightarrow
\end{aligned}
\begin{bmatrix}
k_{f1}+k_{f2} & \dfrac{-k_{f1}l_1+k_{f2}l_2}{2} & 0 \\
0 & 0 & 0 \\
0 & 0 & \dfrac{k_{f1}l_1^2+k_{f2}l_2^2}{6} \\
-k_{f1}l_1+k_{f2}l_2 & \dfrac{k_{f1}l_1^2+k_{f2}l_2^2}{2} & 0
\end{bmatrix}
\begin{bmatrix} v_\Delta^4 \\ \varphi^3 \\ \varphi_\Delta^3 \end{bmatrix}
= \frac{k_{f2}}{2}
\begin{bmatrix}
2\dfrac{\partial V^3}{\partial\lambda} \\
-\dfrac{\partial v_\Delta^3}{\partial\lambda} \\
-l_2\dfrac{\partial v_\Delta^3}{\partial\lambda} \\
2l_2\dfrac{\partial V^3}{\partial\lambda}
\end{bmatrix}+
$$

$$
+\frac{1}{2}\frac{k_{f2}}{2}
\begin{bmatrix}
-\dfrac{\partial^2 v_\Delta^2}{\partial\lambda^2} \\
2\dfrac{\partial^2 V^2}{\partial\lambda^2} \\
2l_2\dfrac{\partial^2 V^2}{\partial\lambda^2} \\
-l_2\dfrac{\partial^2 v_\Delta^2}{\partial\lambda^2}
\end{bmatrix}+\frac{1}{2}\frac{k_{f2}}{3!}
\begin{bmatrix}
2\dfrac{\partial^3 V^1}{\partial\lambda^3} \\
-\dfrac{\partial^3 v_\Delta^1}{\partial\lambda^3} \\
-l_2\dfrac{\partial^3 v_\Delta^1}{\partial\lambda^3} \\
2l_2\dfrac{\partial^3 V_\Delta^1}{\partial\lambda^3}
\end{bmatrix}+\frac{1}{2}\frac{k_{f2}}{4!}
\begin{bmatrix}
0 \\
\dfrac{\partial^4 V^0}{\partial\lambda^4} \\
l_2\dfrac{\partial^4 V^0}{\partial\lambda^4} \\
0
\end{bmatrix}+
\tag{2.80}
$$

$$
+\frac{k_{f2}l_2}{2}
\begin{bmatrix}
\dfrac{1}{2}\dfrac{\partial\varphi_\Delta^2}{\partial\lambda} \\
-\dfrac{1}{2}\dfrac{\partial\varphi^2}{\partial\lambda} \\
-\dfrac{l_2}{3}\dfrac{\partial\varphi^2}{\partial\lambda} \\
\dfrac{l_2}{3}\dfrac{\partial\varphi_\Delta^2}{\partial\lambda}
\end{bmatrix}+\frac{1}{2}\frac{k_{f2}l_2}{2}
\begin{bmatrix}
-\dfrac{1}{2}\dfrac{\partial^2\varphi^1}{\partial\lambda^2} \\
\dfrac{1}{2}\dfrac{\partial^2\varphi_\Delta^1}{\partial\lambda^2} \\
\dfrac{l_2}{3}\dfrac{\partial^2\varphi_\Delta^1}{\partial\lambda^2} \\
-\dfrac{l_2}{3}\dfrac{\partial^2\varphi^1}{\partial\lambda^2}
\end{bmatrix}+\frac{1}{2}\frac{k_{f2}l_2}{3!}
\begin{bmatrix}
\dfrac{1}{2}\dfrac{\partial^3\varphi_\Delta^0}{\partial\lambda^3} \\
-\dfrac{1}{2}\dfrac{\partial^3\varphi^0}{\partial\lambda^3} \\
-\dfrac{l_2}{3}\dfrac{\partial^3\varphi^0}{\partial\lambda^3} \\
\dfrac{l_2}{3}\dfrac{\partial^3\varphi_\Delta^0}{\partial\lambda^3}
\end{bmatrix}
$$

The solution of the system (2.80) is:

$$
\begin{aligned}
v_\Delta^4 &= \frac{1}{2}\frac{l_1}{l_1+l_2}\left(2\frac{\partial V^3}{\partial\lambda}-\frac{1}{2}\frac{\partial^2 v_\Delta^2}{\partial\lambda^2}+\frac{2}{5!}\frac{\partial^3 V^1}{\partial\lambda^3}-\frac{1}{4!}\frac{\partial^4\delta V^0}{\partial\lambda^4}\right)+a\left(\frac{\partial\delta\varphi^2}{\partial\lambda}-\frac{1}{2}\frac{\partial^2\varphi^1}{\partial\lambda^2}+\frac{1}{3!}\frac{\partial^3\delta\varphi^0}{\partial\lambda^3}\right) \\
\varphi^3 &= \frac{1}{l_1+l_2}\left(2\frac{\partial V^3}{\partial\lambda}-\frac{1}{2}\frac{\partial^2 v_\Delta^2}{\partial\lambda^2}+\frac{2}{5!}\frac{\partial^3 V^1}{\partial\lambda^3}-\frac{1}{4!}\frac{\partial^4 V^0}{\partial\lambda^4}\right)+b\left(\frac{\partial\varphi_\Delta^2}{\partial\lambda}-\frac{1}{2}\frac{\partial^2\varphi^1}{\partial\lambda^2}+\frac{1}{3!}\frac{\partial^3\varphi_\Delta^0}{\partial\lambda^3}\right) \\
\varphi_\Delta^3 &= \frac{3k_{f2}l_2^2}{\left(k_{f1}l_1^2+k_{f2}l_2^2\right)(l_1+l_2)}\left(-\frac{\partial v_\Delta^3}{\partial\lambda}+\frac{\partial^2 V^2}{\partial\lambda^2}+\frac{1}{3!}\frac{\partial^3 v_\Delta^1}{\partial\lambda^3}+\frac{2}{4!}\frac{\partial^4 V^0}{\partial\lambda^4}+\frac{l_2}{6}\frac{\partial^2\varphi_\Delta^1}{\partial\lambda^2}-\frac{l_2}{3}\frac{\partial\varphi^2}{\partial\lambda}-\frac{l_2}{3!3}\frac{\partial^3\varphi^0}{\partial\lambda^3}\right) \\
0 &= \frac{k_{f2}}{2}\left[-\frac{\partial v_\Delta^3}{\partial\lambda}+\frac{\partial^2 V^2}{\partial\lambda^2}-\frac{1}{2}l_2\frac{\partial\varphi^2}{\partial\lambda}-\frac{1}{3!}\frac{\partial^3 v_\Delta^1}{\partial\lambda^3}+\frac{2}{4!}\frac{\partial^4 V^0}{\partial\lambda^4}+\frac{l_2}{2}\left(\frac{1}{2}\frac{\partial^2\varphi_\Delta^1}{\partial\lambda^2}-\frac{1}{3!}\frac{\partial^3\varphi^0}{\partial\lambda^3}\right)\right]
\end{aligned}
\tag{2.81}
$$

Substituting the previous results in the last of the equations (2.81) we obtain the equilibrium equation of the beam:

$$\frac{K_{F1}}{l_1+l_2}\frac{\partial^4 V^0}{\partial\lambda^4}=0 \tag{2.82}$$

2.3.2 Weak formulation

The procedure of the method is identical to the one used in section 2.2.2 for the axial case. The P.V.W., in the general case, is:

$$\sum_{\nu\in\mathcal{Z}}\sum_{b\in\mathcal{B}}\left(T^{\varepsilon}_{O_b}\tilde{v}_{O_b}+T^{\varepsilon}_{E_b}\tilde{v}_{E_b}+M^{\varepsilon}_{O_b}\tilde{\phi}_{O_b}+M^{\varepsilon}_{E_b}\tilde{\phi}_{E_b}\right)-\sum_{\nu\in\mathcal{Z}}\sum_{n\in\mathcal{N}}f^{e,n}\tilde{v}_n=0\quad\forall\tilde{v}_n,\tilde{\phi}_n \tag{2.83}$$

Applying the following compatibility conditions to the system of figure 2.6(b),

$$\begin{array}{llll}\tilde{v}_{O_1} & =\tilde{v}_1(\lambda) & \tilde{v}_{E_1} & =\tilde{v}_2(\lambda)\\ \tilde{v}_{O_2} & =\tilde{v}_2(\lambda) & \tilde{v}_{E_2} & =\tilde{v}_1(\lambda+\varepsilon)\\ \tilde{\phi}_{O_1} & =\tilde{\phi}_1(\lambda) & \tilde{\phi}_{E_1} & =\tilde{\phi}_2(\lambda)\\ \tilde{\phi}_{O_2} & =\tilde{\phi}_2(\lambda) & \tilde{\phi}_{E_2} & =\tilde{\phi}_1(\lambda+\varepsilon)\end{array} \tag{2.84}$$

and the equilibrium operator (2.53) ($T_{E_b}=-T_{O_b}$), the P.V.W., equations (2.83), for the case considered becomes:

$$\begin{aligned}&\sum_{\nu\in\mathcal{Z}}\Big[T^{\varepsilon}_{E_1}\left(\tilde{v}_2(\lambda)-\tilde{v}_1(\lambda)\right)+T^{\varepsilon}_{E_2}\left(\tilde{v}_1(\lambda+1)-\tilde{v}_2(\lambda)\right)+M^{\varepsilon}_{O_1}\tilde{\phi}_1(\lambda)+\\&+\left(M^{\varepsilon}_{E_1}+M^{\varepsilon}_{O_2}\right)\tilde{\phi}_2(\lambda)+M^{\varepsilon}_{E_2}\tilde{\phi}_1(\lambda+1)-\sum_{n\in\mathcal{N}}f^{e}_{n}\tilde{v}_n(\lambda)\Big]=0\quad\forall\tilde{v}_n,\tilde{\phi}_n\end{aligned} \tag{2.85}$$

For the reader's convenience, we rewrite the constitutive equations for the end forces of the two beams, given in section 2.3. The following notations shall be used from now on:

$$v^i_\Delta=v^i_2-v^i_1\qquad\varphi^i_\Delta=\phi^i_2-\phi^i_1\qquad k_{fb}=\frac{6E_bI_b}{l_b^3}$$

The internal forces are expanded as series of ε up to order 1:
Beam 1

$$\begin{array}{ll}T^{\varepsilon}_{O_1}(\lambda) & =2k_{f1}\left[-v^0_\Delta-\varepsilon v^1_\Delta+\varepsilon\frac{l_1}{2}\left(\phi^0_1+\phi^0_2\right)\right]=T^0_{O_1}+\varepsilon T^1_{O_1}+\ldots\\ T^{\varepsilon}_{E_1}(\lambda) & =-T^{\varepsilon}_{O_1}(\lambda)\\ M^{\varepsilon}_{O_1}(\lambda) & =k_{f1}l_1\left[-\varepsilon v^0_\Delta-\varepsilon^2 v^1_\Delta+\varepsilon^2\frac{l_1}{3}\left(2\phi^0_1+\phi^0_2\right)\right]=\varepsilon M^1_{O_1}+\varepsilon^2 M^2_{O_1}+\ldots\\ M^{\varepsilon}_{E_1}(\lambda) & =k_{f1}l_1\left[-\varepsilon v^0_\Delta-\varepsilon^2 v^1_\Delta+\varepsilon^2\frac{l_1}{3}\left(\phi^0_1+2\phi^0_2\right)\right]=\varepsilon M^1_{E_1}+\varepsilon^2 M^2_{E_1}+\ldots\end{array} \tag{2.86}$$

Beam 2:

$$\begin{aligned}
T^{\varepsilon}_{O_2}(\lambda) &= 2k_{f2}\left[v^0_\Delta + \varepsilon\left(v^1_\Delta + \frac{\partial v^0_1}{\partial\lambda}\right) + \varepsilon\frac{l_2}{2}\left(\phi^0_2+\phi^0_1\right)\right] = T^0_{O_2} + \varepsilon T^1_{O_2} + ..\\
T^{\varepsilon}_{E_2}(\lambda) &= -T^{\varepsilon}_{O_2}(\lambda)\\
M^{\varepsilon}_{O_2}(\lambda) &= k_{f2}l_2\left[\varepsilon v^0_\Delta + \varepsilon^2\left(v^1_\Delta - \frac{\partial v^0_1}{\partial\lambda}\right) + \varepsilon^2\frac{l_2}{3}\left(2\phi^0_2+\phi^0_1\right)\right] = \varepsilon M^1_{O_2} + \varepsilon^2 M^2_{O_2} + \ldots\\
M^{\varepsilon}_{E_2}(\lambda) &= k_{f2}l_2\left[\varepsilon v^0_\Delta + \varepsilon^2\left(v^1_\Delta - \frac{\partial v^0_1}{\partial\lambda}\right) + \varepsilon^2\frac{l_2}{3}\left(\phi^0_2+2\phi^0_1\right)\right] = \varepsilon M^1_{E_2} + \varepsilon^2 M^2_{E_2} + ..
\end{aligned} \tag{2.87}$$

The virtual displacements are expanded as shown below:

$$\begin{aligned}
&\tilde{v}_1(\lambda) = \tilde{v}^0_1(\lambda) + \varepsilon\tilde{v}^1_1(\lambda)\\
&\tilde{v}_2(\lambda) = \tilde{v}^0_2(\lambda) + \varepsilon\tilde{v}^1_2(\lambda)\\
&\tilde{\phi}_1(\lambda) = \tilde{\phi}^0_1(\lambda) + \varepsilon\tilde{\phi}^1_1(\lambda)\\
&\tilde{\phi}_2(\lambda) = \tilde{\phi}^0_2(\lambda) + \varepsilon\tilde{\phi}^1_2(\lambda)\\
&\tilde{v}_1(\lambda+\varepsilon) = \tilde{v}^0_1(\lambda) + \varepsilon\left(\tilde{v}^1_1(\lambda) + \frac{\partial\tilde{v}^0_1(\lambda)}{\partial\lambda}\right) + \varepsilon^2\left(\frac{\partial\tilde{v}^1_1(\lambda)}{\partial\lambda} + \frac{1}{2}\frac{\partial^2\tilde{v}^0_1(\lambda)}{\partial\lambda^2}\right) + \ldots.\\
&\tilde{\phi}_1(\lambda+\varepsilon) = \tilde{\phi}^0_1(\lambda) + \varepsilon\left(\tilde{\phi}^1_1(\lambda) + \frac{\partial\tilde{\phi}^0_1(\lambda)}{\partial\lambda}\right) + \varepsilon^2\left(\frac{\partial\tilde{\phi}^1_1(\lambda)}{\partial\lambda} + \frac{1}{2}\frac{\partial^2\tilde{\phi}^1_1(\lambda)}{\partial\lambda^2}\right) + \ldots
\end{aligned} \tag{2.88}$$

For the micro virtual displacements v^1_n, ϕ^1_n we adopt the decomposition introduced by Caillerie et al. in [74], [76], [75]. This assumption is a reformulation of the one used in the axial case (equation (2.31)).

It is assumed that:

$$\tilde{v}^1_n(\lambda) = \tilde{v}^1_n\theta(\lambda) \qquad \tilde{\phi}^1_n(\lambda) = \tilde{\phi}^1_n\eta(\lambda)$$

where $\tilde{v}^1_n$ and $\tilde{\phi}^1_n$ are periodic functions and $\theta(\lambda), \eta(\lambda)$ depend on the macro-scale.

Under this assumption, the asymptotic expansions for the micro virtual displacements become:

$$\begin{aligned}
&\tilde{v}_{O_1} = \vartheta(\lambda)\varepsilon\tilde{v}^1_1 \qquad \tilde{v}_{E_1} = \vartheta(\lambda)\varepsilon\tilde{v}^1_2\\
&\tilde{v}_{O_2} = \vartheta(\lambda)\varepsilon\tilde{v}^1_2 \qquad \tilde{v}_{E_2} = \varepsilon\tilde{v}^1_1\left(\vartheta(\lambda) + \varepsilon\frac{\partial\vartheta(\lambda)}{\partial\lambda} + \frac{\varepsilon^2}{2!}\frac{\partial^2\vartheta(\lambda)}{\partial\lambda^2} + \frac{\varepsilon^3}{3!}\frac{\partial^3\vartheta(\lambda)}{\partial\lambda^3} + \frac{\varepsilon^4}{4!}\frac{\partial^4\vartheta(\lambda)}{\partial\lambda^4}\right)\\
&\tilde{\phi}_{O_1} = \eta(\lambda)\varepsilon\tilde{\phi}^1_1 \qquad \tilde{\phi}_{E_1} = \eta(\lambda)\varepsilon\tilde{\phi}^1_2\\
&\tilde{\phi}_{O_2} = \eta(\lambda)\varepsilon\tilde{\phi}^1_2 \qquad \tilde{\phi}_{E_2} = \varepsilon\tilde{\phi}^1_1\left(\eta(\lambda) + \varepsilon\frac{\partial\eta(\lambda)}{\partial\lambda} + \frac{\varepsilon^2}{2!}\frac{\partial^2\eta(\lambda)}{\partial\lambda^2} + \frac{\varepsilon^3}{3!}\frac{\partial^3\eta(\lambda)}{\partial\lambda^3} + \frac{\varepsilon^4}{4!}\frac{\partial^4\eta(\lambda)}{\partial\lambda^4}\right)
\end{aligned}$$

The equilibrium equations dual to the virtual displacements $\tilde{v}^0_n, \tilde{\phi}^0_n$ are the equations defining the macro-field, while the equilibrium equations dual to the virtual displacements $\tilde{v}^1_n, \tilde{\phi}^1_n$ define the self-equilibrium of the cell.

Order 0 in ε

The macro equilibrium equation for the P.V.W., equation (2.85), using the virtual displacement $\tilde{v}_n^0$ yields:

$$\sum_{\nu\in\mathcal{Z}}\left[T_{E_1}^0\left(\tilde{v}_2^0-\tilde{v}_1^0\right)+T_{E_2}^0\left(\tilde{v}_1^0-\tilde{v}_2^0\right)\right]=\sum_{\nu\in\mathcal{Z}}\left[\left(T_{E_1}^0-T_{E_2}^0\right)\tilde{v}_\Delta^0\right]=0\quad\forall\tilde{v}_\Delta^0 \tag{2.89}$$

Notice that the bending moment equations at this order vanish.
From equation (2.89) we obtain:

$$T_{E_1}^0=T_{E_2}^0 \tag{2.90}$$

Substituting the constitutive equations (2.86) and (2.87) in the equilibrium equation (2.90), we obtain:

$$2k_{f1}\left(v_2^0-v_1^0\right)=2k_{f2}\left(v_1^0-v_2^0\right)\quad\Rightarrow\quad 2\left(k_{f1}+k_{f2}\right)\left(v_2^0-v_1^0\right)=0\quad\Rightarrow\quad v_2^0=v_1^0 \tag{2.91}$$

Therefore, from the last equation in (2.91) we have a restriction on the displacement field:

$$v_2^0=v_1^0=V^0 \tag{2.92}$$

Substituting the equation 2.92 in equations 2.86 and 2.86, we get that:

$$\begin{aligned}&T_{E_1}^0=T_{E_2}^0=0\\&M_{O_1}^0=M_{E_1}^1=M_{O_2}^1=M_{E_2}^1=0\end{aligned} \tag{2.93}$$

Hence, alike for the strong formulation, the forces and the bending moment at leading order are equal to zero.

Order 1 in ε

Accounting for the results (2.92) and (2.93) the virtual work of equation (2.85) at order 1 vanishes identically. So at this order we find no macro or micro-equilibrium conditions.

Order 2 in ε

Micro equilibrium

At order 2 the bending moment equations vanish. In order to obtain a complete system for calculating the micro displacements, it is then necessary to make use of the bending moment equations of the micro-scale at the next order. This will be true for all the higher orders. The micro-equilibrium equations so obtained are:

$$\varepsilon^2\textstyle\sum_{\nu\in\mathcal{Z}}\vartheta(\lambda)\left[T_{E_1}^1\left(\tilde{v}_2^1-\tilde{v}_1^1\right)+T_{E_2}^1\left(\tilde{v}_1^1-\tilde{v}_2^1\right)\right]=0\quad\forall\tilde{v}_n^1,\vartheta(\lambda) \tag{2.94a}$$

$$\varepsilon^3\textstyle\sum_{\nu\in\mathcal{Z}}\eta(\lambda)\left[\left(M_{O_1}^2+M_{E_2}^2\right)\tilde{\phi}_1^1+\left(M_{E_1}^2+M_{O_2}^2\right)\tilde{\phi}_2^1\right]=0\quad\forall\tilde{\phi}_n^1,\eta(\lambda) \tag{2.94b}$$

From equations (2.94a) and (2.94b) we obtain the following system:

$$\begin{cases} T^1_{E_1} - T^1_{E_2} = 0 \\ M^2_{O_1} + M^2_{E_2} = 0 \\ M^2_{E_1} + M^2_{O_2} = 0 \end{cases} \tag{2.95}$$

$$\begin{cases} 2k_{f1}\left(v^1_\Delta - \dfrac{l_1}{2}\left(\phi^0_1 + \phi^0_2\right)\right) - 2k_{f2}\left(\left(-v^1_\Delta + \dfrac{\partial V^0}{\partial \lambda}\right) - \dfrac{l_2}{2}\left(\phi^0_2 + \phi^0_1\right)\right) = 0 \\ k_{f1}l_1\left(-v^1_\Delta + \dfrac{l_1}{3}\left(2\phi^0_1 + \phi^0_2\right)\right) + k_{f2}l_2\left(\left(v^1_\Delta - \dfrac{\partial V^0}{\partial \lambda}\right) + \dfrac{l_2}{3}\left(\phi^0_2 + 2\phi^0_1\right)\right) = 0 \\ k_{f1}l_1\left(-v^1_\Delta + \dfrac{l_1}{3}\left(\phi^0_1 + 2\phi^0_2\right)\right) + k_{f2}l_2\left(\left(v^1_\Delta - \dfrac{\partial V^0}{\partial \lambda}\right) + \dfrac{l_{b2}}{3}\left(2\phi^0_2 + \phi^0_1\right)\right) = 0 \end{cases} \tag{2.96}$$

The solution of the system gives the micro-variables v^1_Δ and ϕ^0_1, ϕ^0_2 as a function of the macroscopic displacement:

$$v^1_\Delta = \frac{l_1}{l_1 + l_2}\frac{\partial V^0}{\partial \lambda}, \quad \phi^0_1 = \phi^0_2 = \frac{1}{l_1 + l_2}\frac{\partial V^0}{\partial \lambda} \tag{2.97}$$

The second of equations (2.97) confirms the result found with the strong formulation, i.e. the rotations ϕ^0_1 and ϕ^0_2 are equal and given by the derivative of the displacements.

Macro equilibrium

At order 2 in ε, accounting for the virtual fields $\tilde{v}^0$ and the second result of (2.97) for the virtual rotation, the P.V.W. becomes:

$$\varepsilon^2 \sum_{v \in \mathcal{Z}} \left[T^1_{E_2}\frac{\partial \tilde{V}^0}{\partial \lambda} + \left(M^2_{O_1} + M^2_{E_2} + M^2_{E_1} + M^2_{O_2}\right)\frac{1}{l_1 + l_2}\frac{\partial \tilde{V}^0}{\partial \lambda} - \sum_{n \in \mathcal{N}} f^{e,n}\tilde{V}^0 \right] = 0 \quad \forall \tilde{V}^0 \tag{2.98}$$

Substituting equation (2.97) in the shear forces and bending moment in formulas (2.86) and (2.87) we get:

$$\begin{array}{lll} T^1_{E_1} = 0 & M^2_{O_1} = 0 & M^2_{E_1} = 0 \\ T^1_{E_2} = 0 & M^2_{O_2} = 0 & M^2_{E_2} = 0 \end{array} \tag{2.99}$$

Since the equation at the macro-scale (2.98) vanishes, we should move on to the next order.

Order 3 in ε

Micro-equilibrium

The expansion of the internal forces at this order is:

Beam 1

$$\begin{aligned} T^2_{O_1} &= 2k_{f1}\left[-v^2_\Delta + \frac{l_1}{2}\varphi^1\right] \\ T^2_{E_1} &= -T^2_{O_1} \\ M^3_{O_1} &= k_{f1}l_1\left[-v^2_\Delta + \frac{l_1}{2}\varphi^1 - \frac{l_1}{6}\delta\varphi^1\right] \\ M^3_{E_1} &= k_{f1}l_1\left[-v^2_\Delta + \frac{l_1}{2}\varphi^1 + \frac{l_1}{6}\delta\varphi^1\right] \end{aligned} \tag{2.100}$$

Beam 2

$$\begin{aligned} T^2_{O_2} &= 2k_{f2}\left[\left(v^2_\Delta - \frac{\partial v^1_1}{\partial\lambda} - \frac{1}{2}\frac{\partial^2 V^0}{\partial\lambda^2}\right) + \frac{l_2}{2}\left(\varphi^1 + \frac{\partial\phi^0_1}{\partial\lambda}\right)\right] \\ T^2_{E_2} &= -T^2_{O_2} \\ M^3_{O_2} &= k_{f2}l_2\left[\left(v^2_\Delta - \frac{\partial v^1_1}{\partial\lambda} - \frac{1}{2}\frac{\partial^2 V^0}{\partial\lambda^2}\right) + \frac{l_2}{2}\varphi^1 + \frac{l_2}{6}\delta\varphi^1 + \frac{l_2}{3}\frac{\partial\phi^0_1}{\partial\lambda}\right] \\ M^3_{E_2} &= k_{f2}l_2\left[\left(v^2_\Delta - \frac{\partial v^1_1}{\partial\lambda} - \frac{1}{2}\frac{\partial^2 V^0}{\partial\lambda^2}\right) + \frac{l_2}{2}\varphi^1 - \frac{l_2}{6}\delta\varphi^1 + \frac{2l_2}{3}\frac{\partial\phi^0_1}{\partial\lambda}\right] \end{aligned} \tag{2.101}$$

As in the previous order, the force equilibrium at order ε^3 and the bending moment equilibrium at the subsequent order are examined together:

$$\varepsilon^3 \textstyle\sum_{\nu\in\mathcal{Z}} \vartheta(\lambda)\left[T^2_{E_1}\left(\tilde{v}^1_2 - \tilde{v}^1_1\right) + T^2_{E_2}\left(\tilde{v}^1_1 - \tilde{v}^1_2\right)\right] = 0 \quad \forall\tilde{v}^1_n, \vartheta(\lambda) \tag{2.102a}$$

$$\varepsilon^4 \textstyle\sum_{\nu\in\mathcal{Z}} \eta(\lambda)\left[\left(M^3_{O_1} + M^3_{E_2}\right)\tilde{\phi}^1_1 + \left(M^3_{E_1} + M^3_{O_2}\right)\tilde{\phi}^1_2\right] = 0 \quad \forall\tilde{\phi}^1_n, \eta(\lambda) \tag{2.102b}$$

From equations (2.102a) and (2.102b) we obtain the following system:

$$\begin{cases} T^2_{E_1} - T^2_{E_2} = 0 \\ M^3_{O_1} + M^3_{E_2} = 0 \\ M^3_{E_1} + M^3_{O_2} = 0 \end{cases} \tag{2.103}$$

From the solution of the system (2.103) we obtain:

$$\begin{aligned} v^2_1 - v^2_2 &= -\frac{l_1^2}{2(l_1+l_2)^2}\frac{\partial^2 V^0}{\partial\lambda^2} - \frac{l_1}{l_1+l_2}\frac{\partial v^1_1}{\partial\lambda} \\ \phi^1_1 &= \frac{k_{f1}l_1^3 - k_{f2}l_2^3}{2(l_1+l_2)^2(k_{f1}l_1^2 + k_{f2}l_2^2)}\frac{\partial^2 V^0}{\partial\lambda^2} + \frac{1}{l_1+l_2}\frac{\partial v^1_1}{\partial\lambda} \\ \phi^1_2 &= \frac{k_{f1}l_1^3 + k_{f2}l_2^2(2l_1+l_2)}{2(l_1+l_2)^2(k_{f1}l_1^2 + k_{f2}l_2^2)}\frac{\partial^2 V^0}{\partial\lambda^2} + \frac{1}{l_1+l_2}\frac{\partial v^1_1}{\partial\lambda} \end{aligned} \tag{2.104}$$

Substituting equations (2.104) in equations (2.100) and (2.101), we obtain the forces on the macroscopic field:

$$\begin{aligned} T^2_{E_1} &= 0 \quad M^3_{O_1} = -K_{F1}\frac{\partial^2 V^0}{\partial \lambda^2} \quad M^3_{O_2} = -K_{F1}\frac{\partial^2 V^0}{\partial \lambda^2} \\ T^2_{E_2} &= 0 \quad M^3_{E_1} = K_{F1}\frac{\partial^2 V^0}{\partial \lambda^2} \quad M^3_{E_2} = K_{F1}\frac{\partial^2 V^0}{\partial \lambda^2} \\ K_{F1} &= \frac{k_{f1}l_1^2 k_{f2}l_2^2}{6\left(k_{f1}l_1^2 + k_{f2}l_2^2\right)(l_1+l_2)} \end{aligned} \tag{2.105}$$

where K_{F1} is the homogenized flexural modulus , that is identical to the one obtained using the strong formulation.

Macro-equilibrium

The P.V.W. is

$$\varepsilon^3 \sum_{\nu \in \mathcal{Z}} \left[T^2_{E_2}\frac{\partial \tilde{V}^0}{\partial \lambda} + \left(M^3_{O_1} + M^3_{E_2} + M^3_{E_1} + M^3_{O_2}\right)\frac{1}{l_1+l_2}\frac{\partial \tilde{V}^0}{\partial \lambda}\right] = 0 \quad \forall \tilde{V}^0 \tag{2.106}$$

Using equations (2.105) we obtain the identity equation, so we need to go to the next order.

Order 4 in ε

The expansion of the internal forces at this order is:
Beam 1:

$$\begin{aligned} T^3_{O_1} &= 2k_{f1}\left[-v^3_\Delta + \frac{l_1}{2}\varphi^2\right] \\ T^3_{E_1} &= -T^3_{O_1} \\ M^4_{O_1} &= k_{f1}l_1\left[-v^3_\Delta + \frac{l_1}{2}\varphi^2 - \frac{l_1}{6}\delta\varphi^2\right] \\ M^4_{E_1} &= k_{f1}l_1\left[-v^3_\Delta + \frac{l_1}{2}\varphi^2 + \frac{l_1}{6}\delta\varphi^2\right] \end{aligned} \tag{2.107}$$

Beam 2:

$$\begin{aligned}
T^3_{O_2} &= 2k_{f2}\left[\left(v^3_\Delta - \frac{\partial v^2_1}{\partial\lambda} + \frac{1}{2}\frac{\partial^2 v^1_1}{\partial\lambda^2} - \frac{1}{6}\frac{\partial^3 V^0}{\partial\lambda^3}\right) + \frac{l_2}{2}\left(\varphi^2 - \frac{\partial\phi^1_2}{\partial\lambda} + \frac{1}{2}\frac{\partial^2\phi^0}{\partial\lambda^2}\right)\right] \\
T^3_{E_2} &= -T^3_{O_2} \\
M^4_{O_2} &= k_{f2}l_2\left[\left(v^3_\Delta - \frac{\partial v^2_1}{\partial\lambda} - \frac{1}{2}\frac{\partial^2 v^2_1}{\partial\lambda^2} - \frac{1}{6}\frac{\partial^3 V^0}{\partial\lambda^3}\right) + \frac{l_2}{2}\varphi^2 + \frac{l_1}{6}\delta\varphi^2 + \frac{l_2}{3}\frac{\partial\phi^1_1}{\partial\lambda} + \frac{l_2}{6}\frac{\partial^2\phi^1_1}{\partial\lambda^2}\right] \\
M^4_{E_2} &= k_{f2}l_2\left[\left(v^3_\Delta - \frac{\partial v^2_2}{\partial\lambda} + \frac{1}{2}\frac{\partial^2 v^1_2}{\partial\lambda^2} - \frac{1}{6}\frac{\partial^3 V^0}{\partial\lambda^3}\right) + \frac{l_2}{2}\varphi^2 - \frac{l_2}{6}\delta\varphi^2 - \frac{l_2}{3}\frac{\partial\phi^1_2}{\partial\lambda} + \frac{l_2}{6}\frac{\partial^2\phi^0_2}{\partial\lambda^2}\right]
\end{aligned} \tag{2.108}$$

Micro-equilibrium

Proceeding as before, the P.V.W. at the microscopic scale is:

$$\varepsilon^4 \sum_{v\in\mathcal{Z}} \vartheta(\lambda)\left[T^3_{E_1}\left(\tilde{v}^1_2 - \tilde{v}^1_1\right) + T^3_{E_2}\left(\tilde{v}^1_1 - \tilde{v}^1_2\right)\right] = 0 \quad \forall \tilde{v}^1_n, \vartheta(\lambda) \tag{2.109a}$$

$$\varepsilon^5 \sum_{v\in\mathcal{Z}} \eta(\lambda)\left[\left(M^4_{O_1} + M^4_{E_2}\right)\tilde{\phi}^1_1 + \left(M^4_{E_1} + M^4_{O_2}\right)\tilde{\phi}^1_2\right] + M^3_{E_2}\tilde{\phi}^1_1\frac{\partial\eta(\lambda)}{\partial\lambda} = 0 \quad \forall \tilde{\phi}^1_n, \eta(\lambda) \tag{2.109b}$$

Taking the limit of equations (2.109a) and (2.109b) as ε approaches 0, we obtain the self-balance equation of the cell:

$$\begin{cases} T^3_{E_1} - T^3_{E_2} = 0 \\ M^4_{O_1} + M^4_{E_2} + \dfrac{\partial M^3_{E_2}}{\partial\lambda} = 0 \\ M^4_{E_1} + M^4_{O_2} = 0 \end{cases} \tag{2.110}$$

From the solution of the system (2.110) we obtain the micro-variable as a function its macroscopic variables:

$$\begin{aligned}
v^3_1 - v^3_2 &= -\frac{l_1}{l_1+l_2}\frac{\partial v^2_1}{\partial\lambda} - \frac{l_1^2}{2(l_1+l_2)^2}\frac{\partial^2 v^1_1}{\partial\lambda^2} - \frac{k_{f1}l_1^4(l_1-l_2) + k_{f2}l_1l_2^2(l_1^2+l_2^2)}{6(l_1+l_2)^3(k_{f1}l_1^2+k_{f2}l_2^2)}\frac{\partial^3 V^0}{\partial\lambda^3} \\
\phi^2_1 &= \frac{1}{l_1+l_2}\frac{\partial v^2_1}{\partial\lambda} + \frac{k_{f1}l_1^3 - k_{f2}l_2^3}{2(l_1+l_2)^2(k_{f1}l_1^2+k_{f2}l_2^2)}\frac{\partial^2 v^1_1}{\partial\lambda^2} + \frac{(k_{f1}l_1^3 - k_{f2}l_2^3)(l_1-l_2)}{6(l_1+l_2)^3(k_{f1}l_1^2+k_{f2}l_2^2)}\frac{\partial^3 V^0}{\partial\lambda^3} \\
\phi^2_2 &= \frac{1}{l_1+l_2}\frac{\partial v^2_1}{\partial\lambda} + \frac{k_{f1}l_1^3 + k_{f2}l_2^2(2l_1+l_2)}{2(l_1+l_2)^2(k_{f1}l_1^2+k_{f2}l_2^2)}\frac{\partial^2 v^1_1}{\partial\lambda^2} + \frac{(k_{f1}l_1^3(l_1-l_2) + k_{f2}l_2^2(3l_1^2+2l_1l_2+l_2^2))}{6(l_1+l_2)^3(k_{f1}l_1^2+k_{f2}l_2^2)}\frac{\partial^3 V^0}{\partial\lambda^3}
\end{aligned} \tag{2.111}$$

Substituting equation (2.111) in equations (2.107) and (2.108), we obtain the internal forces

on the macroscopic field:

$$\begin{aligned}
T^3_{O_1} &= \frac{K_{F1}}{l_1+l_2}\frac{\partial^3 V^0}{\partial\lambda^3} & T^3_{E_1} &= -T^3_{O_1}\\
M^4_{O_1} &= -K_{F1}\frac{\partial^2 v^1_1}{\partial\lambda^2} & M^4_{E_1} &= \frac{l_1}{l_1+l_2}K_{F1}\left(\frac{\partial^3 V^0}{\partial\lambda^3}+\frac{\partial^2 v^1_1}{\partial\lambda^2}\right)\\
T^3_{O_2} &= K_{F1}\frac{\partial^3 V^0}{\partial\lambda^3} & T^3_{E_2} &= -T^3_{O_2}\\
M^4_{O_2} &= -K_{F1}\left(\frac{l_1}{l_1+l_2}\frac{\partial^3 V^0}{\partial\lambda^3}-\frac{\partial^2 v^1_1}{\partial\lambda^2}\right) & M^4_{E_2} &= K_{F1}\left(\frac{\partial^3 V^0}{\partial\lambda^3}+\frac{\partial^2 v^1_1}{\partial\lambda^2}\right)
\end{aligned} \tag{2.112}$$

$$K_{F1} = \frac{k_{f1}l_1^2 k_{f2}l_2^2}{6\left(k_{f1}l_1^2+k_{f2}l_2^2\right)(l_1+l_2)}$$

Macro-equilibrium
The P.V.W. at the order ε^4 is:

$$\varepsilon^4\sum_{\nu\in\mathcal{Z}}\left[T^3_{E_2}\frac{\partial\tilde{V}^0}{\partial\lambda}+\left(M^4_{O_1}+M^4_{E_2}+M^4_{E_1}+M^4_{O_2}\right)\frac{1}{l_1+l_2}\frac{\partial\tilde{V}^0}{\partial\lambda}+\frac{1}{l_1+l_2}M^3_{E_2}\frac{\partial^2\tilde{V}^0}{\partial\lambda^2}\right]=0 \quad \forall\tilde{V}^0 \tag{2.113}$$

Replacing equation (2.112) in equation (2.113), and taking the limit as ε approaches zero, and introducing the Jacobian $J=(l_1+l_2)$, that allows us to express the weak formulation in physical coordinates, we obtain:

$$\varepsilon^3\int_\Lambda \frac{1}{(l_1+l_2)^2}M^3_{E_2}\frac{\partial^2\tilde{V}^0}{\partial\lambda^2}(l_1+l_2)\,d\lambda=0 \quad \forall\tilde{V}^0 \tag{2.114}$$

Substituting the forces calculated in (2.105) in equation (2.114), we obtain:

$$\int_\Lambda K_{F1}\frac{\partial^2 V^0}{\partial\lambda^2}\frac{1}{(l_1+l_2)^2}\frac{\partial^2\tilde{V}^0}{\partial\lambda^2}(l_1+l_2)\,d\lambda=0 \quad \forall\tilde{V}^0 \tag{2.115}$$

After integrating by parts the left hand side of equation (2.115), we obtain the homogenized balance equation:

$$\frac{K_{F1}}{l_1+l_2}\frac{\partial^4 V^0}{\partial\lambda^4}=0 \tag{2.116}$$

It can be easily shown that the results obtained at the various order using the weak formulation coincide with the ones obtained using the strong procedure.

The equilibrium equation of the continuum is obtained expanding up to the order 4 in ε, when the elements deform for bending. In the case that the elements experience only axial deformation it was different to expand the displacement up to the second order in ε.

In a general case it is then expect that a combination of the two cases be encountered.

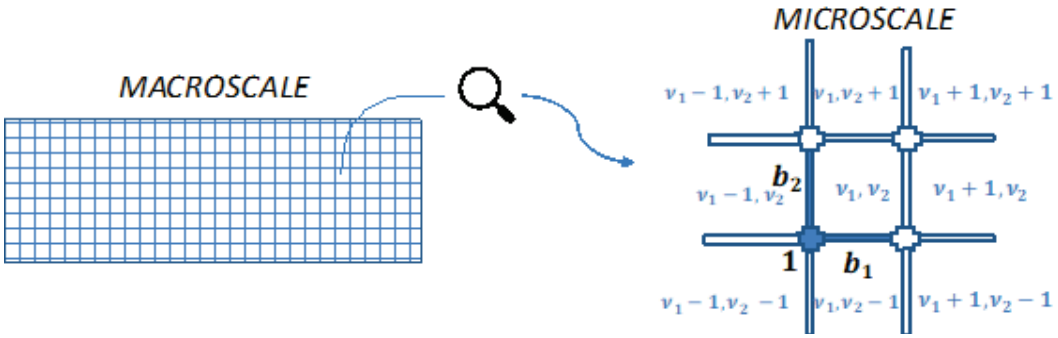

Figure 2.7: Homogenization 2D case

2.4 Discrete homogenization for 2D networks

In this section the HPDM is applied to 2D networks characterized by periodic cell with internal node and described by beams.

This approach is different from that one proposed in [76] because the axial and bending deformation of the bars are simultaneously accounted, Boutin and Hans in [81] introduce similar case with the strong formulation and without internal nodes. In this study only the plane case is examined. The present formulation can be extended to two-dimensional lattices constrained to lie on a curved surfaces. However, the details of such implementation are not straightforward, hence this case will be treated in future studies. The homogenization will be carried out under the follow hypotheses:

- the lattice is periodic.
- The elements are linearly elastic.
- The deformations are assumed to be small, so that the equilibrium refers to the referent configuration of the cell.

The discrete homogenization procedure will be carried out by means of the weak formulation, following the steps developed in sections 2.2.2 and 2.3.2.

2.4.1 Geometry Description

In the following procedure, we shall refer to $\boldsymbol{t}_b$ as the vector joining the end point of the beam b in the current configuration. Only straight plane elements are considered in the work, therefore each beam is defined by a normal vector $\boldsymbol{n}_b = z \times \boldsymbol{t}_b$ where z is the vector normal to the surface of the lattice. We now present a method of the numbering, introduced for the first time by Caillerie et al. in [76], of nodes, bars and pairs of interacting bars that will be convenient in the use of the discrete homogenization method. We consider lattices structure obtained by repetition of a given elementary cell. We define $\hat{\mathcal{N}}$, the set of nodes in a unit cell, $\hat{\mathcal{B}}$ the set of beams in a unit cell, and $\mathcal{Z}$, the set of cells of the macroscopic structure. The cells are numbered by a system of two integers $(\nu_1, \nu_2) \in \mathcal{Z}$, the nodes are then numbered by a triplet $\hat{n} = (n, \nu_1, \nu_2) \in \tilde{\mathcal{N}}$ and in the same way the numbering of the bars

are $\hat{b} = (b, \nu_1, \nu_2) \in \hat{\mathcal{B}}$. The beam links two nodes and is oriented in the direction of the vector $\boldsymbol{t}_b$, where $O_{\hat{b}}$ is the origin of the beam and $E_{\hat{b}}$ the end of the bar:

$$\boldsymbol{t}_b = \boldsymbol{P}_{E_b} - \boldsymbol{P}_{O_b} \tag{2.117}$$

Figure 2.8 shows a typical case study, where the numbering of nodes and bars is indicated. The position of a point in the continuum will be referred to a pair of parametric coordinates

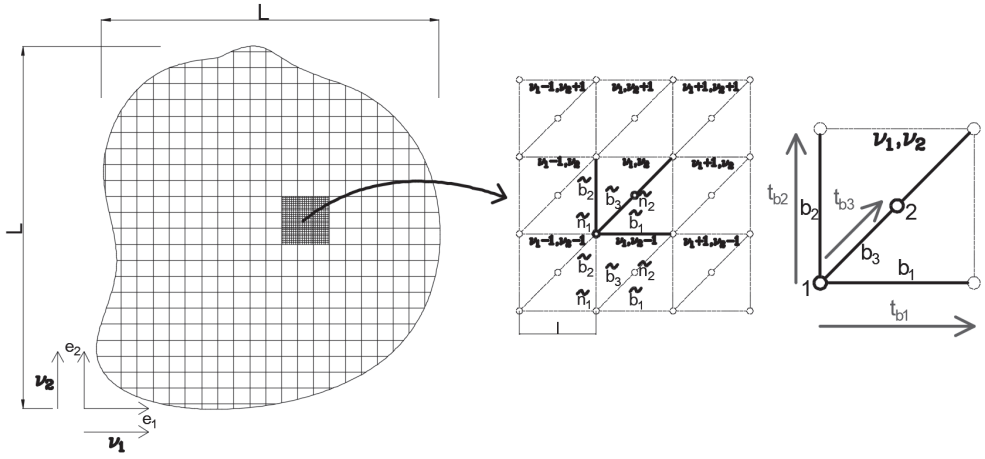

Figure 2.8: Numbering of the bars and nodes

λ_i (generally they are covariant coordinates), defined as:

$$\lambda_i = \varepsilon \nu_i \in (0, 1) \tag{2.118}$$

$\varepsilon = \dfrac{1}{\sqrt{N_c}}$ is a small parameter where N_c is the number of cells in the structure. In fact, we see that $N_c = N_x \times N_y \cong \dfrac{L}{l} \times \dfrac{L}{l} = \dfrac{1}{\varepsilon^2}$.
The mapping for the parametric domain $\Gamma = (0, 1) \times (0, 1)$ to the physical continuum is shown in figure 2.9. The basis vectors of the continuum are defined as:

$$\boldsymbol{g}_\alpha = \frac{\partial \boldsymbol{P}}{\partial \lambda^\alpha} \tag{2.119}$$

The length of the bar is then given by the following equation:

$$l_b^\varepsilon = \|P_{E_b} - P_{O_b}\| = \varepsilon \|\boldsymbol{t}_b\| = \varepsilon l_b \tag{2.120}$$

Therefore the length of the bar depends on the scale parameter ε at the first power. In the application that follows we shall assume that the height of the beam in the plain scales with ε^1, while the width orthogonal to the plane remains constant.

2.4.2 Expansion of the degrees of freedom for the beam elements

For a plane beam lattice each node has three degrees of freedom. Let us call $\boldsymbol{u}_{\hat{n}}(\lambda_1, \lambda_2)$, $\varphi_{\hat{n}}(\lambda_1, \lambda_2)$ the displacement and the rotation of a node with respect to a reference configura-

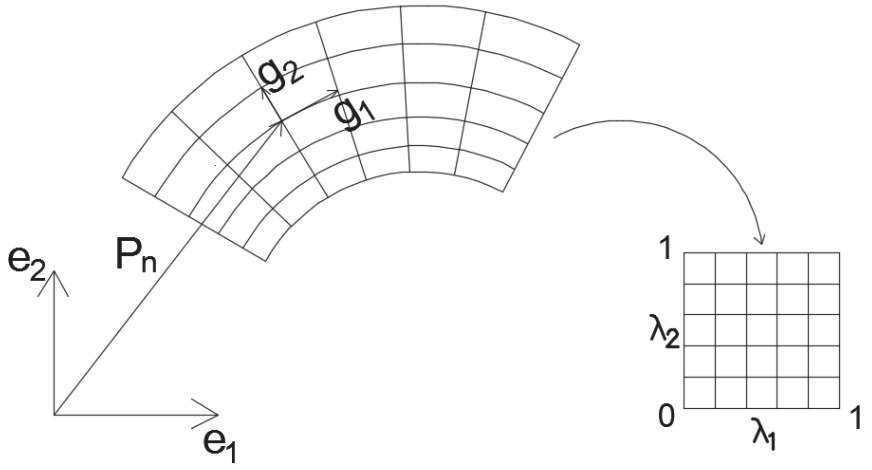

Figure 2.9: Mapping for the parametric space

tion. The deformation is given by an asymptotic expansion of the form:

$$\boldsymbol{u}^{\varepsilon}_{\hat{n}}(\lambda_1,\lambda_2) \cong \boldsymbol{u}^{0}(\lambda_1,\lambda_2) + \varepsilon \boldsymbol{u}^{1}_{n}(\lambda_1,\lambda_2) + \varepsilon^2 \boldsymbol{u}^{2}_{n}(\lambda_1,\lambda_2) + \ldots \tag{2.121a}$$

$$\varphi^{\varepsilon}_{\hat{n}}(\lambda_1,\lambda_2) \cong \varphi^{0}_{n}(\lambda_1,\lambda_2) + \varepsilon \varphi^{1}_{n}(\lambda_1,\lambda_2) + \varepsilon^2 \varphi^{2}_{n}(\lambda_1,\lambda_2) + \ldots \tag{2.121b}$$

We have made the assumption that $\boldsymbol{u}^0$ does not depend on n, as shown in the paragraph 2.2.1. This means that this leading term is the same for all nodes in the reference cell. Therefore, it locates the actual position of this cell, and consequently will be interpreted as the displacement function of the equivalent continuous medium. For this reason in the following developments we shall set $\boldsymbol{u}^0(\lambda_1,\lambda_2) = \boldsymbol{U}^0(\lambda_1,\lambda_2)$. The following terms $\boldsymbol{u}^1_n, \boldsymbol{u}^2_n, \ldots$ of the expansions depend on n and (λ_1,λ_2), and provide at different orders the position of node n in the reference cell relatively to $\boldsymbol{U}^0$.

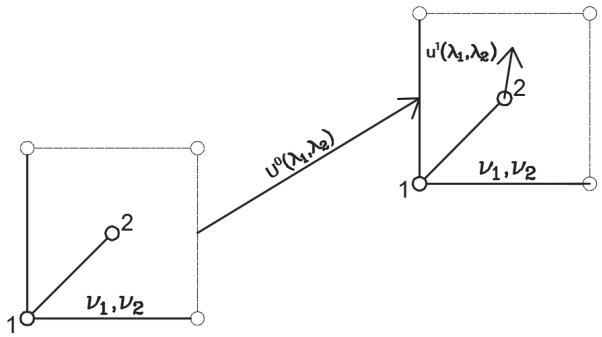

Figure 2.10: The figure show the displacement of the reference cell $\boldsymbol{U}^0(\lambda_1,\lambda_2)$, and the displacement of the internal node $\boldsymbol{u}^1_n(\lambda_1,\lambda_2)$ at the first order.

We assume that for each beam element b of the cell, the origin is a node belonging to the cell, while the end node can be a node of the cell or a node of a neighbouring cell. Using the previous notation the expansion for the degrees of freedom (DOFs) of the node O_b becomes:

$$\boldsymbol{u}^{\varepsilon}_{O_b} \cong \boldsymbol{U}^0(\lambda_1,\lambda_2) + \varepsilon \boldsymbol{u}^1_{O_b}(\lambda_1,\lambda_2) + \varepsilon^2 \boldsymbol{u}^2_{O_b}(\lambda_1,\lambda_2) + \ldots \tag{2.122}$$

for the end node E_b different cases may apply:

- if E_b belongs to a cell forward in the 1-direction to the reference cell, then:

$$\boldsymbol{u}^{\varepsilon}_{E_b} \cong \boldsymbol{U}^0(\lambda_1+\varepsilon,\lambda_2) + \varepsilon \boldsymbol{u}^1_{E_b}(\lambda_1+\varepsilon,\lambda_2) + \varepsilon^2 \boldsymbol{u}^2_{E_b}(\lambda_1+\varepsilon,\lambda_2) + \ldots \tag{2.123}$$

where the Taylor's expansion of each term of equation (2.123) is given by:

$$\begin{aligned}
\boldsymbol{U}^0(\lambda_1+\varepsilon,\lambda_2) &\cong \boldsymbol{U}^0(\lambda_1,\lambda_2) + \varepsilon \frac{\partial \boldsymbol{U}^0(\lambda_1,\lambda_2)}{\partial \lambda_1} + \frac{\varepsilon^2}{2}\frac{\partial^2 \boldsymbol{U}^0(\lambda_1,\lambda_2)}{\partial \lambda_1^2} + \ldots \\
\boldsymbol{u}^1_{E_b}(\lambda_1+\varepsilon,\lambda_2) &\cong \boldsymbol{u}^1_{E_b}(\lambda_1,\lambda_2) + \varepsilon \frac{\partial \boldsymbol{u}^1_{E_b}(\lambda_1,\lambda_2)}{\partial \lambda_1} + \ldots \\
&\ldots. \\
\boldsymbol{u}^i_{E_b}(\lambda_1+\varepsilon,\lambda_2) &\cong \ldots
\end{aligned} \tag{2.124}$$

Substituting equation (2.124) in (2.123) we obtain:

$$\begin{aligned}
\boldsymbol{u}^{\varepsilon}_{E_b} \cong \boldsymbol{U}^0(\lambda_1,\lambda_2) &+ \varepsilon \left(\frac{\partial \boldsymbol{U}^0(\lambda_1,\lambda_2)}{\partial \lambda_1} + \boldsymbol{u}^1_{E_b}(\lambda_1,\lambda_2) \right) + \\
&+ \varepsilon^2 \left(\frac{1}{2}\frac{\partial^2 \boldsymbol{U}^0(\lambda_1,\lambda_2)}{\partial \lambda_1^2} + \frac{\partial \boldsymbol{u}^1_{E_b}(\lambda_1,\lambda_2)}{\partial \lambda_1} + \boldsymbol{u}^2_{E_b}(\lambda_1,\lambda_2) \right) + \ldots
\end{aligned} \tag{2.125}$$

- if E_b belongs to the reference cell then

$$\boldsymbol{u}^{\varepsilon}_{E_b} \cong \boldsymbol{U}^0(\lambda_1,\lambda_2) + \varepsilon \boldsymbol{u}^1_{E_b}(\lambda_1,\lambda_2) + \varepsilon^2 \boldsymbol{u}^2_{E_b}(\lambda_1,\lambda_2) + \ldots \tag{2.126}$$

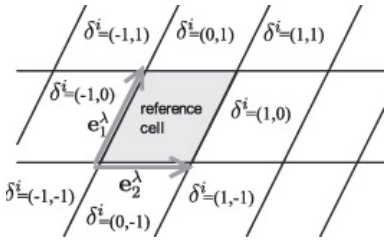

Figure 2.11: Significance of the shift parameters δ_{ib} (the figure has been reproduced from [87])

Similar expressions are obtained for nodes belonging to neighbouring cells in the 2-direction. The expansions (2.122),(2.125) can be generalized introducing for each beam a vector $\boldsymbol{\delta^b}$, as done in [76], whose component δ^{ib} is -1,0,1 according to [87], [88], [89], [90].

The range of value that this vector may take assume in neighbouring cells is given in figure 2.11. The displacement of the end node, under this notation, becomes:

$$\boldsymbol{u}^{\varepsilon}_{E_b} \cong \boldsymbol{U}^0\left(\lambda_1+\varepsilon\delta^{ib},\lambda_2+\varepsilon\delta^{ib}\right)+\varepsilon\boldsymbol{u}^1_{E_b}\left(\lambda_1+\varepsilon\delta^{ib},\lambda_2+\varepsilon\delta^{ib}\right)+\varepsilon^2\boldsymbol{u}^2_{E_b}\left(\lambda_1+\varepsilon\delta^{ib},\lambda_2+\varepsilon\delta^{ib}\right)+\ldots \tag{2.127}$$

After expanding in Taylor series the terms $\boldsymbol{U}^0\left(\lambda_1+\varepsilon\delta^{ib},\lambda_2+\varepsilon\delta^{ib}\right)$, $\boldsymbol{u}^1_{E_b}\left(\lambda_1+\varepsilon\delta^{ib},\lambda_2+\varepsilon\delta^{ib}\right)$, $\boldsymbol{u}^2_{E_b}\left(\lambda_1+\varepsilon\delta^{ib},\lambda_2+\varepsilon\delta^{ib}\right)$ equation (2.127) takes the form:

$$\begin{aligned}\boldsymbol{u}^{\varepsilon}_{E_b} \cong \boldsymbol{U}^0(\lambda_1,\lambda_2)+\varepsilon\left(\frac{\partial\boldsymbol{U}^0(\lambda_1,\lambda_2)}{\partial\lambda_i}\delta^{ib}+\boldsymbol{u}^1_{E_b}(\lambda_1,\lambda_2)\right)+\\ +\varepsilon^2\left(\frac{\left(\delta^{ib}\right)^2}{2}\frac{\partial^2\boldsymbol{U}^0(\lambda_1,\lambda_2)}{\partial^2\lambda_i}+\frac{\partial\boldsymbol{u}^1_{E_b}(\lambda_1,\lambda_2)}{\partial\lambda_i}\delta^{ib}+\boldsymbol{u}^2_{E_b}(\lambda_1,\lambda_2)\right)+\ldots\end{aligned} \tag{2.128}$$

Analogous expansion can be performed for the rotation of the origin of the beam:

$$\phi^{\varepsilon}_{O_b}(\lambda_1,\lambda_2)=\phi^0_{O_b}(\lambda_1,\lambda_2)+\varepsilon\phi^1_{O_b}(\lambda_1,\lambda_2)+\varepsilon^2\phi^1_{O_b}(\lambda_1,\lambda_2)+\ldots \tag{2.129}$$

and for the rotation of the end node:

$$\begin{aligned}\phi^{\varepsilon}_{E_b}\left(\lambda_1+\varepsilon\delta^{ib},\lambda_2+\varepsilon\delta^{ib}\right)=&\phi^0_{E_b}\left(\lambda_1+\varepsilon\delta^{ib},\lambda_2+\varepsilon\delta^{ib}\right)+\varepsilon\phi^1_{E_b}\left(\lambda_1+\varepsilon\delta^{ib},\lambda_2+\varepsilon\delta^{ib}\right)+\\ &+\varepsilon^2\phi^2_{E_b}\left(\lambda_1+\varepsilon\delta^{ib},\lambda_2+\varepsilon\delta^{ib}\right)\end{aligned} \tag{2.130}$$

The previous expression, after expansion in Taylor's series, yields:

$$\begin{aligned}&\phi^0_{E_b}\left(\lambda_1+\varepsilon\delta^{ib},\lambda_2+\varepsilon\delta^{ib}\right)=\phi^0_{E_b}(\lambda_1,\lambda_2)+\varepsilon\frac{\partial\phi^0_{E_b}(\lambda_1,\lambda_2)}{\partial\lambda_i}\delta^{ib}+\frac{\left(\varepsilon\delta^{ib}\right)^2}{2}\frac{\partial^2\phi^0_{E_b}(\lambda_1,\lambda_2)}{\partial\lambda_i^2}+\ldots\\ &\phi^1_{E_b}\left(\lambda_1+\varepsilon\delta^{ib},\lambda_2+\varepsilon\delta^{ib}\right)=\phi^1_{E_b}(\lambda_1,\lambda_2)+\varepsilon\frac{\partial\phi^1_{E_b}(\lambda_1,\lambda_2)}{\partial\lambda_i}\delta^{ib}+\ldots\\ &\phi^2_{E_b}\left(\lambda_1+\varepsilon\delta^{ib},\lambda_2+\varepsilon\delta^{ib}\right)=\phi^2_{E_b}(\lambda_1,\lambda_2)+\ldots\\ &\ldots.\end{aligned} \tag{2.131}$$

Substituting equation (2.131) in equation (2.130) we obtain:

$$\phi^{\varepsilon}_{E_b}\left(\lambda_1+\varepsilon\delta^{ib},\lambda_2+\varepsilon\delta^{ib}\right)=\phi^{0}_{E_b}\left(\lambda_1,\lambda_2\right)+\varepsilon\left(\frac{\partial\phi^{0}_{E_b}\left(\lambda_1,\lambda_2\right)}{\partial\lambda_i}\delta^{ib}+\phi^{1}_{E_b}\left(\lambda_1,\lambda_2\right)\right)+ \\ +\varepsilon^2\left(\frac{\left(\delta^{ib}\right)^2}{2}\frac{\partial^2\phi^{0}_{E_b}\left(\lambda_1,\lambda_2\right)}{\partial\lambda_i^2}+\frac{\partial\phi^{1}_{E_b}\left(\lambda_1,\lambda_2\right)}{\partial\lambda_i}\delta^{ib}+\phi^{2}_{E_b}\left(\lambda_1,\lambda_2\right)\right)+\ldots \tag{2.132}$$

2.4.3 Beam element of the lattice

The lattice is composed by slender beams, rigidly connected at the nodes. Eventually, internal pins can also be considered. It is assumed that each element behaves as an Euler-Bernoulli beam. Consequently, the (linear) relationships between the end forces and the end displacements of a beam are:

$$\begin{aligned}
N^{\varepsilon}_{O_b}\hat{\boldsymbol{t}}_b&=\left[\frac{EA^{\varepsilon}}{l^{\varepsilon}_b}\left(\boldsymbol{u}^{\varepsilon}_{O_b}-\boldsymbol{u}^{\varepsilon}_{E_b}\right)\cdot\hat{\boldsymbol{t}}_b\right]\hat{\boldsymbol{t}}_b\\
N^{\varepsilon}_{E_b}\hat{\boldsymbol{t}}_b&=-N^{\varepsilon}_{O_b}\hat{\boldsymbol{t}}_b\\
T^{\varepsilon}_{O_b}\hat{\boldsymbol{n}}_b&=\left[\frac{12EI^{\varepsilon}}{(l^{\varepsilon}_b)^3}\left(\boldsymbol{u}^{\varepsilon}_{O_b}-\boldsymbol{u}^{\varepsilon}_{E_b}\right)\cdot\hat{\boldsymbol{n}}_b+\frac{6EI^{\varepsilon}}{(l^{\varepsilon}_b)^2}\left(\phi^{\varepsilon}_{O_b}+\phi^{\varepsilon}_{E_b}\right)\right]\hat{\boldsymbol{n}}_b\\
T^{\varepsilon}_{E_b}\hat{\boldsymbol{n}}_b&=-T^{\varepsilon}_{O_b}\hat{\boldsymbol{n}}_b\\
M^{\varepsilon}_{O_b}&=\frac{6EI^{\varepsilon}}{(l^{\varepsilon}_b)^2}\left(\boldsymbol{u}^{\varepsilon}_{O_b}-\boldsymbol{u}^{\varepsilon}_{E_b}\right)\cdot\hat{\boldsymbol{n}}_b+\frac{2EI^{\varepsilon}}{l^{\varepsilon}_b}\left(2\phi^{\varepsilon}_{O_b}+\phi^{\varepsilon}_{E_b}\right)\\
M^{\varepsilon}_{E_b}&=\frac{6EI^{\varepsilon}}{(l^{\varepsilon}_b)^2}\left(\boldsymbol{u}^{\varepsilon}_{O_b}-\boldsymbol{u}^{\varepsilon}_{E_b}\right)\cdot\hat{\boldsymbol{n}}_b+\frac{2EI^{\varepsilon}}{l^{\varepsilon}_b}\left(\phi^{\varepsilon}_{O_b}+2\phi^{\varepsilon}_{E_b}\right)
\end{aligned} \tag{2.133}$$

where $I^{\varepsilon}=\dfrac{\varepsilon^3h^3\times s}{12}$, h is the height of the beam, s is its width of the beam (which doesn't scale with ε since only plane periodicity is considered) , $A^{\varepsilon}=\varepsilon h\times s$, and $l^{\varepsilon}_b=\varepsilon l_b$, and l^{ε}_b is the length of the generic bar that composes the reference cell. Using the asymptotic expansion obtained in section 2.4.2 we get the following expressions for the quantities appearing in equations (2.133):

$$\begin{aligned}\boldsymbol{u}^{\varepsilon}_{O_b}-\boldsymbol{u}^{\varepsilon}_{E_b}\cong{}&\boldsymbol{U}^0(\lambda_1,\lambda_2)+\varepsilon\boldsymbol{u}^1_{O_b}(\lambda_1,\lambda_2)+\varepsilon^2\boldsymbol{u}^2_{O_b}(\lambda_1,\lambda_2)-\boldsymbol{U}^0(\lambda_1,\lambda_2)+\\&-\varepsilon\frac{\partial\boldsymbol{U}^0(\lambda_1,\lambda_2)}{\partial\lambda_i}\delta^{ib}-\frac{\left(\varepsilon\delta^{ib}\right)^2}{2}\frac{\partial^2\boldsymbol{U}^0(\lambda_1,\lambda_2)}{\partial\lambda_i^2}-\varepsilon\boldsymbol{u}^1_{E_b}(\lambda_1,\lambda_2)+\\&-\varepsilon\frac{\partial\boldsymbol{u}^1(\lambda_1,\lambda_2)}{\partial\lambda_i}\delta^{ib}-\varepsilon^2\boldsymbol{u}^2_{E_b}(\lambda_1,\lambda_2)=\\&=\varepsilon\left(\boldsymbol{u}^1_{O_b}-\boldsymbol{u}^1_{E_b}-\frac{\partial\boldsymbol{U}^0}{\partial\lambda_i}\delta^{ib}\right)+\varepsilon^2\left(\boldsymbol{u}^2_{O_b}-\boldsymbol{u}^2_{E_b}-\frac{\partial\boldsymbol{u}^1_{E_b}}{\partial\lambda_i}\delta^{ib}-\frac{\left(\delta^{ib}\right)^2}{2}\frac{\partial^2\boldsymbol{U}^0}{\partial\lambda_i^2}\right)\end{aligned}\tag{2.134}$$

$$\begin{aligned}\phi^{\varepsilon}_{O_b}+\phi^{\varepsilon}_{E_b}={}&\phi^0_{O_b}(\lambda_1,\lambda_2)+\varepsilon\phi^1_{O_b}(\lambda_1,\lambda_2)+\varepsilon^2\phi^1_{O_b}(\lambda_1,\lambda_2)+\\&+\phi^0_{E_b}(\lambda_1,\lambda_2)+\varepsilon\left(\frac{\partial\phi^0_{E_b}(\lambda_1,\lambda_2)}{\partial\lambda_i}\delta^{ib}+\phi^1_{E_b}(\lambda_1,\lambda_2)\right)+\\&+\varepsilon^2\left(\frac{\left(\delta^{ib}\right)^2}{2}\frac{\partial^2\phi^0_{E_b}(\lambda_1,\lambda_2)}{\partial\lambda_i^2}+\frac{\partial\phi^1_{E_b}(\lambda_1,\lambda_2)}{\partial\lambda_i}\delta^{ib}+\phi^2_{E_b}(\lambda_1,\lambda_2)\right)=\\&=\phi^0_{O_b}+\phi^0_{E_b}+\varepsilon\left(\frac{\partial\phi^0_{E_b}}{\partial\lambda_i}\delta^{ib}+\phi^1_{O_b}+\phi^1_{E_b}\right)+\\&+\varepsilon^2\left(\frac{\left(\delta^{ib}\right)^2}{2}\frac{\partial^2\phi^0_{E_b}}{\partial\lambda_i^2}+\frac{\partial\phi^1_{E_b}}{\partial\lambda_i}\delta^{ib}+\phi^2_{O_b}+\phi^2_{E_b}\right)\end{aligned}\tag{2.135}$$

$$\begin{aligned}2\phi^{\varepsilon}_{O_b}+\phi^{\varepsilon}_{E_b}={}&2\left(\phi^0_{O_b}(\lambda_1,\lambda_2)+\varepsilon\phi^1_{O_b}(\lambda_1,\lambda_2)+\varepsilon^2\phi^1_{O_b}(\lambda_1,\lambda_2)\right)+\\&+\phi^0_{E_b}(\lambda_1,\lambda_2)+\varepsilon\left(\frac{\partial\phi^0_{E_b}(\lambda_1,\lambda_2)}{\partial\lambda_i}\delta^{ib}+\phi^1_{E_b}(\lambda_1,\lambda_2)\right)+\\&+\varepsilon^2\left(\frac{\left(\delta^{ib}\right)^2}{2}\frac{\partial^2\phi^0_{E_b}(\lambda_1,\lambda_2)}{\partial\lambda_i^2}+\frac{\partial\phi^1_{E_b}(\lambda_1,\lambda_2)}{\partial\lambda_i}\delta^{ib}+\phi^2_{E_b}(\lambda_1,\lambda_2)\right)=\\&=2\phi^0_{O_b}+\phi^0_{E_b}+\varepsilon\left(\frac{\partial\phi^0_{E_b}}{\partial\lambda_i}\delta^{ib}+2\phi^1_{O_b}+\phi^1_{E_b}\right)+\\&+\varepsilon^2\left(\frac{\left(\delta^{ib}\right)^2}{2}\frac{\partial^2\phi^0_{E_b}}{\partial\lambda_i^2}+\frac{\partial\phi^1_{E_b}}{\partial\lambda_i}\delta^{ib}+2\phi^2_{O_b}+\phi^2_{E_b}\right)\end{aligned}\tag{2.136}$$

$$\begin{aligned}
\phi^{\varepsilon}_{O_b} + 2\phi^{\varepsilon}_{E_b} =& \phi^0_{O_b}(\lambda_1,\lambda_2) + \varepsilon\phi^1_{O_b}(\lambda_1,\lambda_2) + \varepsilon^2\phi^1_{O_b}(\lambda_1,\lambda_2) + \\
&+ 2\left(\phi^0_{E_b}(\lambda_1,\lambda_2) + \varepsilon\left(\frac{\partial\phi^0_{E_b}(\lambda_1,\lambda_2)}{\partial\lambda_i}\delta^{ib} + \phi^1_{E_b}(\lambda_1,\lambda_2)\right)\right) + \\
&+ 2\left(\varepsilon^2\left(\frac{\left(\delta^{ib}\right)^2}{2}\frac{\partial^2\phi^0_{E_b}(\lambda_1,\lambda_2)}{\partial\lambda_i^2} + \frac{\partial\phi^1_{E_b}(\lambda_1,\lambda_2)}{\partial\lambda_i}\delta^{ib} + \phi^2_{E_b}(\lambda_1,\lambda_2)\right)\right) = \\
&= \phi^0_{O_b} + 2\phi^0_{E_b} + \varepsilon\left(2\frac{\partial\phi^0_{E_b}}{\partial\lambda_i}\delta^{ib} + \phi^1_{O_b} + 2\phi^1_{E_b}\right) + \\
&+ \varepsilon^2\left(\left(\delta^{ib}\right)^2\frac{\partial^2\phi^0_{E_b}}{\partial\lambda_i^2} + 2\frac{\partial\phi^1_{E_b}}{\partial\lambda_i}\delta^{ib} + \phi^2_{O_b} + 2\phi^2_{E_b}\right)
\end{aligned} \tag{2.137}$$

Substituting the equations (2.134), (2.135), (2.136) and (2.137) into equation (2.133) we can write the end forces of each beam.

Axial forces:

$$\begin{aligned}
N^{\varepsilon}_{O_b} = -N^{\varepsilon}_{E_b} &= \frac{\varepsilon EA}{\varepsilon l_b}\left(\boldsymbol{u}^{\varepsilon}_{O_b}(\lambda_1,\lambda_2) - \boldsymbol{u}^{\varepsilon}_{E_b}\left(\lambda_1+\varepsilon\delta^{1b},\lambda_2+\varepsilon\delta^{2b}\right)\right)\hat{\boldsymbol{t}}_b = \\
&= \frac{EA}{l_b}\varepsilon\left(\boldsymbol{u}^1_{O_b} - \boldsymbol{u}^1_{E_b} - \frac{\partial\boldsymbol{U}^0}{\partial\lambda_i}\delta^{ib}\right)\hat{\boldsymbol{t}}_b + \\
&+ \frac{EA}{l_b}\varepsilon^2\left(\boldsymbol{u}^2_{O_b} - \boldsymbol{u}^2_{E_b} - \frac{\partial\boldsymbol{u}^1_{E_b}}{\partial\lambda_i}\delta^{ib} - \frac{\left(\delta^{ib}\right)^2}{2}\frac{\partial^2\boldsymbol{U}^0}{\partial\lambda_i^2}\right)\hat{\boldsymbol{t}}_b
\end{aligned} \tag{2.138}$$

Shear forces:

$$\begin{aligned}
T^{\varepsilon}_{O_b} = -T^{\varepsilon}_{E_b} &= \frac{\varepsilon^3 12EI}{\varepsilon^3 l_b^3}\left(\boldsymbol{u}^{\varepsilon}_{O_b} - \boldsymbol{u}^{\varepsilon}_{E_b}\right)\hat{\boldsymbol{n}}_b + \frac{\varepsilon^3 6EI}{\varepsilon^2 2_b}\left(\phi^{\varepsilon}_{O_b} + \phi^{\varepsilon}_{E_b}\right) = \\
&= \frac{12EI}{l_b^3}\varepsilon\left(\boldsymbol{u}^1_{O_b} - \boldsymbol{u}^1_{E_b} - \frac{\partial\boldsymbol{U}^0}{\partial\lambda_i}\delta^{ib}\right)\hat{\boldsymbol{n}}_b + \\
&+ \frac{12EI}{l_b^3}\varepsilon^2\left(\boldsymbol{u}^2_{O_b} - \boldsymbol{u}^2_{E_b} - \frac{\partial\boldsymbol{u}^1_{E_b}}{\partial\lambda_i}\delta^{ib} - \frac{\left(\delta^{ib}\right)^2}{2}\frac{\partial^2\boldsymbol{U}^0}{\partial\lambda_i^2}\right)\hat{\boldsymbol{n}}_b + \\
&+ \frac{6EI}{l_b^2}\left(\varepsilon\left(\phi^0_{O_b} + \phi^0_{E_b}\right) + \varepsilon^2\left(\frac{\partial\phi^0_{E_b}}{\partial\lambda_i}\delta^{ib} + \phi^1_{O_b} + \phi^1_{E_b}\right)\right) \\
&+ \frac{6EI}{l_b^2}\varepsilon^3\left(\frac{\left(\delta^{ib}\right)^2}{2}\frac{\partial^2\phi^0_{E_b}}{\partial\lambda_i^2} + \frac{\partial\phi^1_{E_b}}{\partial\lambda_i}\delta^{ib} + \phi^2_{O_b} + \phi^2_{E_b}\right)
\end{aligned} \tag{2.139}$$

Bending moment at the origin of the beam:

$$
\begin{aligned}
M^{\varepsilon}_{O_b} &= \frac{\varepsilon^3 6EI}{\varepsilon^2 l_b^2}\left(\boldsymbol{u}^{\varepsilon}_{O_b}-\boldsymbol{u}^{\varepsilon}_{E_b}\right)\hat{\boldsymbol{n}}_b+\frac{\varepsilon^3 2EI}{\varepsilon l_b}\left(2\phi^{\varepsilon}_{O_b}+\phi^{\varepsilon}_{E_b}\right)= \\
&= \frac{6EI}{l_b^2}\left(\varepsilon^2\left(\boldsymbol{u}^1_{O_b}-\boldsymbol{u}^1_{E_b}-\frac{\partial \boldsymbol{U}^0}{\partial\lambda_i}\delta^{ib}\right)+\varepsilon^3\left(\boldsymbol{u}^2_{O_b}-\boldsymbol{u}^2_{E_b}-\frac{\partial \boldsymbol{u}^1_{E_b}}{\partial\lambda_i}\delta^{ib}-\frac{\left(\delta^{ib}\right)^2}{2}\frac{\partial^2\boldsymbol{U}^0}{\partial\lambda_i^2}\right)\right)\hat{\boldsymbol{n}}_b+ \\
&+\frac{2EI}{l_b}\left(\varepsilon^2\left(2\phi^0_{O_b}+\phi^0_{E_b}\right)+\varepsilon^3\left(\frac{\partial\phi^0_{E_b}}{\partial\lambda_i}\delta^{ib}+2\phi^1_{O_b}+\phi^1_{E_b}\right)\right)+ \\
&+\frac{2EI}{l_b}\varepsilon^4\left(\frac{\left(\delta^{ib}\right)^2}{2}\frac{\partial^2\phi^0_{E_b}}{\partial\lambda_i^2}+\frac{\partial\phi^1_{E_b}}{\partial\lambda_i}\delta^{ib}+2\phi^2_{O_b}+\phi^2_{E_b}\right)
\end{aligned}
\tag{2.140}
$$

Bending moment at the end of the beam:

$$
\begin{aligned}
M^{\varepsilon}_{E_b} &= \frac{\varepsilon^3 6EI}{\varepsilon^2 l_b^2}\left(\boldsymbol{u}^{\varepsilon}_{O_b}-\boldsymbol{u}^{\varepsilon}_{E_b}\right)\hat{\boldsymbol{n}}_b+\frac{\varepsilon^3 2EI}{\varepsilon l_b}\left(\phi^{\varepsilon}_{O_b}+2\phi^{\varepsilon}_{E_b}\right)= \\
&= \frac{6EI}{l_b^2}\left(\varepsilon^2\left(\boldsymbol{u}^1_{O_b}-\boldsymbol{u}^1_{E_b}-\frac{\partial \boldsymbol{U}^0}{\partial\lambda_i}\delta^{ib}\right)+\varepsilon^3\left(\boldsymbol{u}^2_{O_b}-\boldsymbol{u}^2_{E_b}-\frac{\partial \boldsymbol{u}^1_{E_b}}{\partial\lambda_i}\delta^{ib}-\frac{\left(\delta^{ib}\right)^2}{2}\frac{\partial^2\boldsymbol{U}^0}{\partial\lambda_i^2}\right)\right)\hat{\boldsymbol{n}}_b+ \\
&+\frac{2EI}{l_b}\left(\varepsilon^2\left(\phi^0_{O_b}+2\phi^0_{E_b}\right)+\varepsilon^3\left(2\frac{\partial\phi^0_{E_b}}{\partial\lambda_i}\delta^{ib}+\phi^1_{O_b}+2\phi^1_{E_b}\right)\right)+ \\
&+\frac{2EI}{l_b}\varepsilon^4\left(\frac{\partial^2\phi^0_{E_b}}{\partial\lambda_i^2}\left(\delta^{ib}\right)^2+2\frac{\partial\phi^1_{E_b}}{\partial\lambda_i}\delta^{ib}+\phi^2_{O_b}+2\phi^2_{E_b}\right)
\end{aligned}
\tag{2.141}
$$

Note that in the previous relations we have omitted the dependence of the deformation and rotation on (λ_1,λ_2). The constitutive equations (2.138), (2.139), (2.140) and (2.141) can be eventually modified to account for shear deformation, using the Timoshenko beam model.

2.4.4 The virtual work formulation

The equilibrium equations of the periodic lattice structure are obtained via the P.V.W. that can be written as:

$$
\begin{aligned}
&\sum_{\nu_1,\nu_2\in\mathcal{Z}}\sum_{b\in\mathcal{B}}\left[N^{\varepsilon}_{O_b}\tilde{\boldsymbol{u}}^{\varepsilon}_{O_b}\cdot\hat{\boldsymbol{t}}_b+N^{\varepsilon}_{E_b}\tilde{\boldsymbol{u}}^{\varepsilon}_{E_b}\cdot\hat{\boldsymbol{t}}_b+T^{\varepsilon}_{O_b}\tilde{\boldsymbol{u}}^{\varepsilon}_{O_b}\cdot\hat{\boldsymbol{n}}_b+T^{\varepsilon}_{E_b}\tilde{\boldsymbol{u}}^{\varepsilon}_{E_b}\cdot\hat{\boldsymbol{n}}_b+M^{\varepsilon}_{O_b}\tilde{\phi}^{\varepsilon}_{O_b}+M^{\varepsilon}_{E_b}\tilde{\phi}^{\varepsilon}_{E_b}\right]+ \\
&-\sum_{\nu_1,\nu_2\in\mathcal{Z}}\sum_{n\in\mathcal{N}}\boldsymbol{f}^{\varepsilon}_n\tilde{\boldsymbol{u}}^{\varepsilon}_{\hat{n}}=0\quad\forall\tilde{\boldsymbol{u}}_n,\tilde{\phi}_n
\end{aligned}
\tag{2.142}
$$

Depending on the definition of the virtual displacement, different equilibrium conditions may be obtained. If in the virtual deformation only the macroscopic terms are included, the equilibrium equations of the equivalent continuum are obtained. On other hand, if only the higher terms are considered in the virtual deformations, equation (2.142) yields the micro-equilibrium equation for the cell. This observations lead to the following two steps:

1. First we choose $\underline{\tilde{\boldsymbol{u}}^{\varepsilon}_{\hat{n}}(\lambda_1,\lambda_2) = \tilde{\boldsymbol{U}}^0(\lambda_1,\lambda_2)}$ and $\underline{\tilde{\phi}^{\varepsilon}_{\hat{n}}(\lambda_1,\lambda_2) = \tilde{\phi}^0_n(\lambda_1,\lambda_2)}$, where $\tilde{\boldsymbol{U}}^0(\lambda_1,\lambda_2)$ and $\tilde{\phi}^0_n(\lambda_1,\lambda_2)$ are respectively the macroscopic virtual displacement and the virtual rotation null on the constrained boundary. The Taylor expansion of the macroscopic virtual deformations can be written as:

$$\begin{aligned}
\tilde{\boldsymbol{u}}^{\varepsilon}_{O_b} &\cong \tilde{\boldsymbol{U}}^0(\lambda_1,\lambda_2)\\
\tilde{\boldsymbol{u}}^{\varepsilon}_{E_b} &\cong \tilde{\boldsymbol{U}}^0(\lambda_1,\lambda_2) + \varepsilon\frac{\partial\tilde{\boldsymbol{U}}^0(\lambda_1,\lambda_2)}{\partial\lambda_i}\delta^{ib} + \frac{\left(\varepsilon\delta^{ib}\right)^2}{2}\frac{\partial^2\tilde{\boldsymbol{U}}^0(\lambda_1,\lambda_2)}{\partial^2\lambda_i} + \dots\\
\tilde{\phi}^{\varepsilon}_{O_b} &\cong \tilde{\phi}^0_{O_b}(\lambda_1,\lambda_2)\\
\tilde{\phi}^{\varepsilon}_{E_b} &\cong \tilde{\phi}^0_{E_b}(\lambda_1,\lambda_2) + \varepsilon\frac{\partial\tilde{\phi}^0_{E_b}(\lambda_1,\lambda_2)}{\partial\lambda_i}\delta^{ib} + \frac{\left(\varepsilon\delta^{ib}\right)^2}{2}\frac{\partial^2\tilde{\phi}^0_{E_b}(\lambda_1,\lambda_2)}{\partial\lambda_i^2} + \dots
\end{aligned} \tag{2.143}$$

From the constitutive equations (2.138), (2.139), (2.140) and (2.141) at the lower order in ε we have:

$$\begin{aligned}
N^{\varepsilon}_{E_b} &\sim \varepsilon\\
T^{\varepsilon}_{E_b} &\sim \varepsilon\\
M^{\varepsilon}_{O_b} &\sim \varepsilon^2\\
M^{\varepsilon}_{E_b} &\sim \varepsilon^2
\end{aligned}$$

Substituting the equation (2.143), up to the order 1 in ε and the expansion of constitutive equation (from (2.138) to (2.141)), in equation (2.142) we have the following expression for the P.V.W.:

$$\begin{aligned}
&\sum_{\nu_1,\nu_2\in\mathcal{Z}}\sum_{b\in\mathcal{B}}\Big[\varepsilon\left(N^1_{O_b}+N^1_{E_b}\right)\tilde{\boldsymbol{U}}^0\cdot\hat{\boldsymbol{t}}_b + \varepsilon\left(T^1_{O_b}+T^1_{E_b}\right)\tilde{\boldsymbol{U}}^0\cdot\hat{\boldsymbol{n}}_b +\\
&+\varepsilon^2 N^1_{E_b}\frac{\partial\tilde{\boldsymbol{U}}^0}{\partial\lambda_i}\delta^{ib}\cdot\hat{\boldsymbol{t}}_b + \varepsilon^2 T^1_{E_b}\frac{\partial\tilde{\boldsymbol{U}}^0}{\partial\lambda_i}\delta^{ib}\cdot\hat{\boldsymbol{n}}_b + \varepsilon^2\left(M^2_{O_b}\tilde{\phi}^0_{O_b} + M^2_{E_b}\tilde{\phi}^0_{E_b}\right)\Big] +\\
&-\sum_{\nu_1,\nu_2\in\mathcal{Z}}\sum_{n\in\mathcal{N}}\varepsilon^2\boldsymbol{f}^2_n\tilde{\boldsymbol{U}}^0 = 0 \quad \forall\tilde{\boldsymbol{U}}^0,\tilde{\phi}^0_n
\end{aligned} \tag{2.144}$$

The leading term yields the elementary equilibrium condition:

$$\begin{aligned} N^{\varepsilon}_{O_b} &= -N^{\varepsilon}_{E_b} \\ T^{\varepsilon}_{O_b} &= -T^{\varepsilon}_{E_b} \end{aligned} \tag{2.145}$$

so that the P.V.W. (2.142) can also be written as:

$$\begin{aligned} &\sum_{\nu_1,\nu_2\in\mathcal{Z}}\sum_{b\in\mathcal{B}}\left[N^{\varepsilon}_{E_b}\left(\tilde{\boldsymbol{u}}^{\varepsilon}_{E_b}-\tilde{\boldsymbol{u}}^{\varepsilon}_{O_b}\right)\cdot\hat{\boldsymbol{t}}_b+T^{\varepsilon}_{E_b}\left(\tilde{\boldsymbol{u}}^{\varepsilon}_{E_b}-\tilde{\boldsymbol{u}}^{\varepsilon}_{O_b}\right)\cdot\hat{\boldsymbol{n}}_b+M^{\varepsilon}_{O_b}\tilde{\phi}^{\varepsilon}_{O_b}+M^{\varepsilon}_{E_b}\tilde{\phi}^{\varepsilon}_{E_b}\right]+ \\ &-\sum_{\nu_1,\nu_2\in\mathcal{Z}}\sum_{n\in\mathcal{N}}\boldsymbol{f}^{\varepsilon}_n\tilde{\boldsymbol{u}}^{\varepsilon}_n=0\quad\forall\tilde{\boldsymbol{u}}_n,\tilde{\phi}_n \end{aligned} \tag{2.146}$$

From (2.146) we obtain:

$$\begin{aligned} &\sum_{\nu_1,\nu_2\in\mathcal{Z}}\sum_{b\in\mathcal{B}}\left[\varepsilon^2N^1_{E_b}\frac{\partial\tilde{\boldsymbol{U}}^0}{\partial\lambda_i}\delta^{ib}\cdot\hat{\boldsymbol{t}}_b+\varepsilon^2T^1_{E_b}\frac{\partial\tilde{\boldsymbol{U}}^0}{\partial\lambda_i}\delta^{ib}\cdot\hat{\boldsymbol{n}}_b+\varepsilon^2\left(M^2_{O_b}\tilde{\phi}^0_{O_b}+M^2_{E_b}\tilde{\phi}^0_{E_b}\right)\right]+ \\ &-\sum_{\nu_1,\nu_2\in\mathcal{Z}}\sum_{n\in\mathcal{N}}\varepsilon^2\boldsymbol{f}^2\tilde{\boldsymbol{U}}^0=0\quad\forall\tilde{\boldsymbol{U}}^0,\tilde{\phi}^0_n \end{aligned} \tag{2.147}$$

Notice that this equation includes the forces at order 1 coupled with the bending moment at order 2 as it happened with the straight beam.
Since ε is very small, the sums $\varepsilon^2\sum_{\nu_1,\nu_2\in\mathcal{Z}}$ can be approximated by the integrals $\int_\Lambda d\lambda_1 d\lambda_2$ and hence the equation (2.147) becomes:

$$\int_\Lambda\Big[\sum_{b\in\mathcal{B}}\left(N^1_{E_b}\frac{\partial\tilde{\boldsymbol{U}}^0}{\partial\lambda_i}\delta^{ib}\cdot\hat{\boldsymbol{t}}_b+T^1_{E_b}\frac{\partial\tilde{\boldsymbol{U}}^0}{\partial\lambda_i}\delta^{ib}\cdot\hat{\boldsymbol{n}}_b+M^2_{O_b}\tilde{\phi}^0_{O_b}+M^2_{E_b}\tilde{\phi}^0_{E_b}\right)-\boldsymbol{f}^2\tilde{\boldsymbol{U}}^0\Big]d\lambda_1d\lambda_2=0 \tag{2.148}$$

In order to express the equations in the physical domain, we introduce the Jacobian $J_0=\|\boldsymbol{g}_1\times\boldsymbol{g}_2\cdot\hat{\boldsymbol{z}}\|$ in equation (2.148):

$$\int_\Lambda\Big[\sum_{b\in\mathcal{B}}\frac{1}{J_0}\left(N^1_{E_b}\frac{\partial\tilde{\boldsymbol{U}}^0}{\partial\lambda_i}\delta^{ib}\cdot\hat{\boldsymbol{t}}_b+T^1_{E_b}\frac{\partial\tilde{\boldsymbol{U}}^0}{\partial\lambda_i}\delta^{ib}\cdot\hat{\boldsymbol{n}}_b+M^2_{O_b}\tilde{\phi}^0_{O_b}+M^2_{E_b}\tilde{\phi}^0_{E_b}\right)-\boldsymbol{f}^2\tilde{\boldsymbol{U}}^0\Big]J_0d\lambda_1d\lambda_2=0 \tag{2.149}$$

In the next subsection we shall see how the comparison of the P.V.W. (2.149) and the weak formulation of the classic continuous medium provides the equilibrium equations of the equivalent continuous medium.

2. Introducing in (2.146) a virtual displacement in the form $\underline{\tilde{\boldsymbol{u}}^{\varepsilon}_n(\lambda_1,\lambda_2)=\varepsilon\boldsymbol{\theta}(\lambda_1,\lambda_2)\tilde{\boldsymbol{u}}^1_n}$ and a virtual rotation in the form $\underline{\tilde{\phi}^{\varepsilon}_n(\lambda_1,\lambda_2)=\varepsilon\eta(\lambda_1,\lambda_2)\tilde{\phi}^n}$, where $\boldsymbol{\theta}(\lambda_1,\lambda_2)$ and

$\eta(\lambda_1, \lambda_2)$ are a vector function and a function defined on the macroscopic field and $\tilde{\boldsymbol{u}}^1_n, \tilde{\phi}^1_n$ are defined in the microscopic field. Considering these terms in the P.V.W. equation (2.146) we obtain the self-balance equations of the cell:

$$\begin{aligned}&\int_\Lambda \sum_{b\in\mathcal{B}} \left[N^1_{E_b}\left(\tilde{\boldsymbol{u}}^1_{E_b} - \tilde{\boldsymbol{u}}^1_{O_b}\right)\cdot\hat{\boldsymbol{t}}_b + T^1_{E_b}\left(\tilde{\boldsymbol{u}}^1_{E_b} - \tilde{\boldsymbol{u}}^1_{O_b}\right)\cdot\hat{\boldsymbol{n}}_b\right]\boldsymbol{\theta}\, d\lambda_1 d\lambda_2 + \\ &+\varepsilon\int_\Lambda \sum_{b\in\mathcal{B}} \left[M^2_{O_b}\tilde{\phi}^1_{O_b} + M^2_{E_b}\tilde{\phi}^1_{E_b}\right]\eta\, d\lambda_1 d\lambda_2 = 0 \qquad \forall\boldsymbol{\theta}, \tilde{\boldsymbol{u}}^1_n, \tilde{\phi}^1_n\end{aligned} \tag{2.150}$$

From equation (2.150) follow the equilibrium equations:

$$\sum_{b\in\mathcal{B}}\left[N^1_{E_b}\left(\tilde{\boldsymbol{u}}^1_{E_b} - \tilde{\boldsymbol{u}}^1_{O_b}\right)\cdot\hat{\boldsymbol{t}}_b + T^1_{E_b}\left(\tilde{\boldsymbol{u}}^1_{E_b} - \tilde{\boldsymbol{u}}^1_{O_b}\right)\cdot\hat{\boldsymbol{n}}_b\right] = 0 \quad \forall \quad \tilde{\boldsymbol{u}}^n \tag{2.151a}$$

$$\varepsilon\sum_{b\in\mathcal{B}}\left[M^2_{O_b}\tilde{\phi}^1_{O_b} + M^2_{E_b}\tilde{\phi}^1_{E_b}\right] = 0 \quad \forall\tilde{\phi}^n \tag{2.151b}$$

for each cell. The equation (2.151a) describes the self-balance of the cell, expressed as equilibrium of the nodes from which we will obtain the micro-deformation as function of macro-deformation. The equation (2.151b) describes the bending equilibrium of the node that is similar to the angular momentum balance in the Cauchy continuum.

$$M_i = 0$$

The above equation provides the symmetry condition, necessary for the Cauchy continuum. We now examine the balance of the bending moments; substitution of the constitutive relationships (2.140) and (2.141) in equation (2.151b) we obtain an equation that relates the rotation to the gradient of the displacement. This expression depends of the geometry of the unit cell, and will be presented in the following section for some cases.

Chapter 3

Application to 2D networks

The method developed in chapter 2 has been applied to some networks and fabrics, characterised by the unit cells illustrated in figures 3.1.

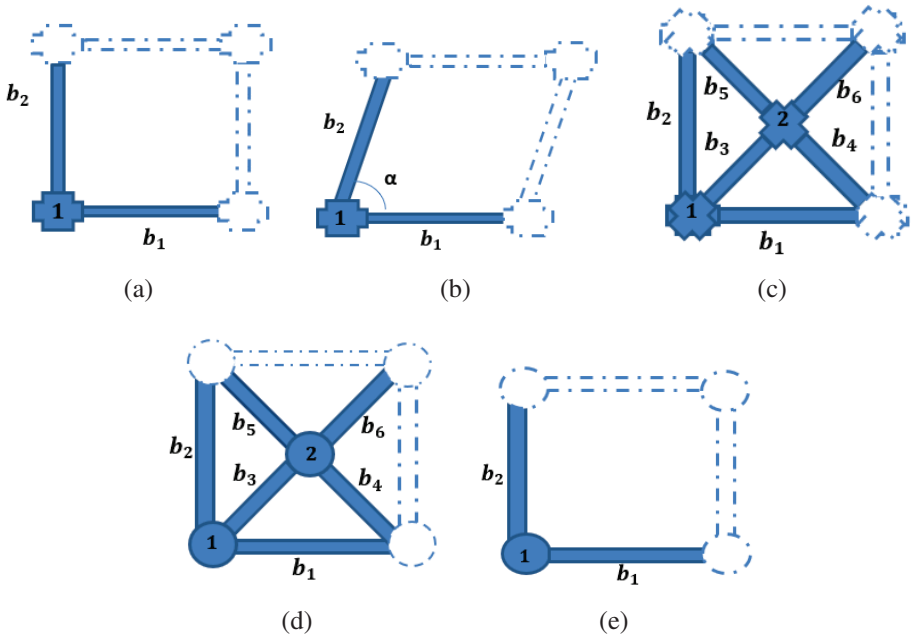

Figure 3.1: (a) Rectangular cell with rigid connection, (b) Skew cell with rigid connection, (c) Rectangular cell braced with rigid connection, (d) Rectangular cell braced with pivots, (e) Rectangular cell with pivot

3.1 Rectangular cell with rigid connection

We consider a lattice that in the natural configuration is constituted by two orthogonal arrays of straight fibres interconnected by internal joints as described in figure 3.2. A similar case was treated by Boutin and Hans in [81].

Using the constitutive equation, calculated in section 2.4.3, we have in this case at the leading order:

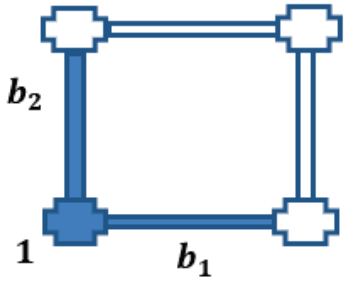

Figure 3.2: Unit cell of quadrilateral plane lattice with joint

axial forces

$$\begin{aligned} N^{\varepsilon}_{E_1} &= \varepsilon \frac{(EA)_1}{l_1} \frac{\partial \boldsymbol{U}^0}{\partial \lambda_1} \cdot \hat{\boldsymbol{t}}_1 = \varepsilon \frac{(EA)_1}{l_1} \frac{\partial U^0_1}{\partial \lambda_1} \\ N^{\varepsilon}_{E_2} &= \varepsilon \frac{(EA)_2}{l_2} \frac{\partial \boldsymbol{U}^0}{\partial \lambda_2} \cdot \hat{\boldsymbol{t}}_2 = \varepsilon \frac{(EA)_2}{l_2} \frac{\partial U^0_2}{\partial \lambda_2} \end{aligned} \tag{3.1}$$

shear forces

$$\begin{aligned} T^{\varepsilon}_{E_1} &= \varepsilon \frac{12\,(EI)_1}{l_1^3} \frac{\partial \boldsymbol{U}^0}{\partial \lambda_1} \cdot \hat{\boldsymbol{n}}_1 - \varepsilon \frac{12\,(EI)_1}{l_1^2} \phi^0 = \varepsilon \frac{12\,(EI)_{b1}}{l_1^3} \frac{\partial U^0_2}{\partial \lambda_1} - \varepsilon \frac{12\,(EI)_1}{l_1^2} \phi^0 \\ T^{\varepsilon}_{E_2} &= \varepsilon \frac{12\,(EI)_2}{l_2^3} \frac{\partial \boldsymbol{U}^0}{\partial \lambda_2} \cdot \hat{\boldsymbol{n}}_2 - \varepsilon \frac{12\,(EI)_2}{l_2^2} \phi^0 = -\varepsilon \frac{12\,(EI)_2}{l_2^3} \frac{\partial U^0_1}{\partial \lambda_2} - \varepsilon \frac{12\,(EI)_2}{l_2^2} \phi^0 \end{aligned} \tag{3.2}$$

bending moment at the origin of the beam

$$\begin{aligned} M^{\varepsilon}_{O_1} &= -\varepsilon^2 \frac{6\,(EI)_1}{l_1^2} \frac{\partial \boldsymbol{U}^0}{\partial \lambda_1} \cdot \hat{\boldsymbol{n}}_1 + \varepsilon^2 \frac{6\,(EI)_1}{l_1} \phi^0 = -\varepsilon^2 \frac{6\,(EI)_1}{l_1^2} \frac{\partial U^0_2}{\partial \lambda_1} + \varepsilon^2 \frac{6\,(EI)_1}{l_1} \phi^0 \\ M^{\varepsilon}_{O_2} &= -\varepsilon^2 \frac{6\,(EI)_2}{l_2^2} \frac{\partial \boldsymbol{U}^0}{\partial \lambda_2} \cdot \hat{\boldsymbol{n}}_2 + \varepsilon^2 \frac{6\,(EI)_2}{l_2} \phi^0 = \varepsilon^2 \frac{6\,(EI)_2}{l_2^2} \frac{\partial U^0_1}{\partial \lambda_2} + \varepsilon^2 \frac{6\,(EI)_2}{l_2} \phi^0 \end{aligned} \tag{3.3}$$

bending moment at the end of the beams

$$\begin{aligned} M^{\varepsilon}_{E_1} &= -\varepsilon^2 \frac{6\,(EI)_1}{l_1^2} \frac{\partial U^0_2}{\partial \lambda_1} + \varepsilon^2 \frac{6\,(EI)_1}{l_1} \phi^0 \\ M^{\varepsilon}_{E_2} &= \varepsilon^2 \frac{6\,(EI)_2}{l_2^2} \frac{\partial U^0_1}{\partial \lambda_2} + \varepsilon^2 \frac{6\,(EI)_2}{l_2} \phi^0 \end{aligned} \tag{3.4}$$

Following the procedure presented in subsection 2.4.4, we start by taking a macroscopic virtual displacement in the P.V.W. The first significant equation is obtained at order ε^2 (that

is then included in the integral):

$$\begin{aligned}&\int_\Lambda \sum_{b\in\mathcal{B}} \frac{1}{J_0}\left[N^1_{E_b}\frac{\partial\tilde{\boldsymbol{U}}^0}{\partial\lambda_i}\cdot\hat{\boldsymbol{t}}_b\delta^{ib}+T^1_{E_b}\frac{\partial\tilde{\boldsymbol{U}}^0}{\partial\lambda_i}\cdot\hat{\boldsymbol{n}}_b\delta^{ib}+M^2_{O_b}\tilde{\phi}^0_{O_b}+M^2_{E_b}\tilde{\phi}^0_{E_b}\right]J_0 d\lambda_1 d\lambda_2+\\ &-\int_\Lambda \boldsymbol{f}^\varepsilon_n\tilde{\boldsymbol{U}}^0 J_0 d\lambda_1 d\lambda_2=0\end{aligned} \tag{3.5}$$

At this step the shear forces and the bending moment depend on the rotation ϕ^0_n. In order to determine the rotation as function of the macroscopic deformation we need to write the P.V.W. at the microscopic scale, equation (2.150), that yields:

$$\begin{aligned}&\int_\Lambda \sum_{b\in\mathcal{B}}\left(N_{E_b}\left(\tilde{\boldsymbol{u}}^1_1-\tilde{\boldsymbol{u}}^1_1\right)\cdot\hat{\boldsymbol{t}}_b+T_{E_b}\left(\tilde{\boldsymbol{u}}^1_1-\tilde{\boldsymbol{u}}^1_1\right)\cdot\hat{\boldsymbol{n}}_b\right)\boldsymbol{\theta}\,d\lambda_1 d\lambda_2+\\ &+\varepsilon\int_\Lambda\sum_{b\in\mathcal{B}}\left(M_{O_b}+M_{E_b}\right)\tilde{\phi}^1_n\eta\,d\lambda_1 d\lambda_2=0\qquad\forall\boldsymbol{\theta},\tilde{\boldsymbol{u}}^1_n,\eta,\tilde{\phi}^1_n\end{aligned} \tag{3.6}$$

The first integral vanishes (this is typical for cell without internal nodes), while for the second integral appearing in equation (3.6) we obtain the following condition:

$$\sum_{b\in\mathcal{B}}\left(M_{O_b}+M_{E_b}\right)\tilde{\phi}^1=0\qquad\forall\tilde{\phi}^1$$

The latter equation provides the moment balance at the node:

$$M_{O_1}+M_{O_2}+M_{E_1}+M_{E_2}=0 \tag{3.7}$$

Introducing equations (3.3) and (3.4) into equation (3.7) we obtain the rotation at the leading order:

$$\phi^0=\frac{\dfrac{(EI)_1}{l_1^2}\dfrac{\partial U^0_2}{\partial\lambda_1}-\dfrac{(EI)_2}{l_2^2}\dfrac{\partial U^0_1}{\partial\lambda_2}}{\left(\dfrac{(EI)_1}{l_1}+\dfrac{(EI)_2}{l_2}\right)} \tag{3.8}$$

Defining the dimensionless parameter

$$\alpha=\frac{(EI)_1}{(EI)_2}\frac{l_2}{l_1} \tag{3.9}$$

equation (3.8) becomes:

$$\phi^0=\frac{\alpha\dfrac{\partial U^0_2}{\partial\lambda_1}\dfrac{1}{l_1}-\dfrac{\partial U^0_1}{\partial\lambda_2}\dfrac{1}{l_2}}{1+\alpha} \tag{3.10}$$

If $(EI)_1=(EI)_1=EI$ and $l_1=l_2=l_b$, then $\alpha=1$ and we find that the macroscopic rotation is equal to the skew part of the gradient of displacement:

$$\phi^0 = \frac{1}{2l_b}\left(\frac{\partial U_2^0}{\partial \lambda_1} - \frac{\partial U_1^0}{\partial \lambda_2}\right) \tag{3.11}$$

This result was assumed *a priori* by Ganghoffer in his works [91], [92]. Here, we have shown that this assumption is consistent only for anisotropic lattices where the length of the beams are the same. For the general isotropic case, we introduce the following two parametric coordinates:

$$\xi^1 = \frac{1+\alpha}{2}\frac{l_1}{\alpha l}\lambda_1 \qquad \xi^2 = \frac{1+\alpha}{2}\frac{l_2}{\alpha l}\lambda_2 \tag{3.12}$$

$$\xi^1 = \frac{1+\alpha}{2}\frac{l_1}{\alpha l}\lambda_1 \qquad \xi^2 = \frac{1+\alpha}{2}\frac{l_2}{\alpha l}\lambda_2 \tag{3.13}$$

with $l = \sqrt{l_1 l_2}$. The rotation ϕ^0 is now equal to:

$$\phi^0 = \frac{1}{2}\left(\frac{\partial U_2^0}{\partial \xi_1} - \frac{\partial U_1^0}{\partial \xi_2}\right) \tag{3.14}$$

that is the skew part of the gradient of the displacement with respect to the transformed parametric coordinates.
Let the case of a square isotropic cell be considered, so that $\alpha = 1$.

Substituting equation (3.11) in the equations (3.2), (3.3) and (3.4) we have the following expression for the internal forces:

$$\begin{aligned} N_{E_1} &= \frac{EA}{l_b}\frac{\partial U_1^0}{\partial \lambda_1} \\ N_{E_2} &= \frac{EA}{l_b}\frac{\partial U_2^0}{\partial \lambda_2} \end{aligned} \tag{3.15a}$$

$$\begin{aligned} T_{E_1} &= \frac{12EI}{l_b^3}\frac{\partial U_2^0}{\partial \lambda_1} - \frac{12EI}{l_b^2}\frac{1}{2l_b}\left(\frac{\partial U_2^0}{\partial \lambda_1} - \frac{\partial U_1^0}{\partial \lambda_2}\right) = \frac{6EI}{l_b^3}\left(\frac{\partial U_2^0}{\partial \lambda_1} + \frac{\partial U_1^0}{\partial \lambda_2}\right) \\ T_{E_2} &= -\frac{12EI}{l_b^3}\frac{\partial U_1^0}{\partial \lambda_2} - \varepsilon\frac{12EI}{l_b^2}\frac{1}{2l_b}\left(\frac{\partial U_2^0}{\partial \lambda_1} - \frac{\partial U_1^0}{\partial \lambda_2}\right) = -\frac{6EI}{l_b^3}\left(\frac{\partial U_2^0}{\partial \lambda_1} + \frac{\partial U_1^0}{\partial \lambda_2}\right) \end{aligned} \tag{3.15b}$$

$$\begin{aligned} M_{O_1} &= -\frac{6EI}{l_b^2}\frac{\partial U_2^0}{\partial \lambda_1} + \frac{3EI}{l_b^2}\frac{\partial U_2^0}{\partial \lambda_1} - \frac{3EI}{l_b^2}\frac{\partial U_1^0}{\partial \lambda_2} = -\frac{3EI}{l_b^2}\left(\frac{\partial U_2^0}{\partial \lambda_1} + \frac{\partial U_1^0}{\partial \lambda_2}\right) \\ M_{O_2} &= \frac{6EI}{l_b^2}\frac{\partial U_1^0}{\partial \lambda_2} + \frac{3EI}{l_b^2}\frac{\partial U_2^0}{\partial \lambda_1} - \frac{3EI}{l_b^2}\frac{\partial U_1^0}{\partial \lambda_2} = \frac{3EI}{l_b^2}\left(\frac{\partial U_2^0}{\partial \lambda_1} + \frac{\partial U_1^0}{\partial \lambda_2}\right) \end{aligned} \tag{3.15c}$$

$$\begin{aligned} M_{E_1} &= -\frac{3EI}{l_b^2}\left(\frac{\partial U_2^0}{\partial \lambda_1} + \frac{\partial U_1^0}{\partial \lambda_2}\right) \\ M_{E_2} &= \frac{3EI}{l_b^2}\left(\frac{\partial U_2^0}{\partial \lambda_1} + \frac{\partial U_1^0}{\partial \lambda_2}\right) \end{aligned} \tag{3.15d}$$

The continuum balance equation is obtained from equation (3.17) using as virtual rotation:

$$\tilde{\phi}^0 = \frac{1}{2l_b}\left(\frac{\partial \tilde{U}_2^0}{\partial \lambda_1} - \frac{\partial \tilde{U}_1^0}{\partial \lambda_2}\right) \tag{3.16}$$

The P.V.W than can be written as:

$$\begin{aligned}&\int_\Lambda \sum_{b\in\mathcal{B}} \frac{1}{J_0}\left[N_{E_b}\frac{\partial \tilde{\boldsymbol{U}}^0}{\partial \lambda_i}\delta^{ib}\cdot\hat{\boldsymbol{t}}_b + T_{E_b}\frac{\partial \tilde{\boldsymbol{U}}^0}{\partial \lambda_i}\delta^{ib}\cdot\hat{\boldsymbol{n}}_b\right] J_0 d\lambda_1 d\lambda_2 + \\ &-\int_\Lambda \boldsymbol{f}^e \tilde{\boldsymbol{U}}^0 J_0 d\lambda_1 d\lambda_2 = 0\end{aligned} \tag{3.17}$$

In order to identify the components of the stress tensor, we write the P.V.W. of the continuum in the form:

$$\int_\Lambda S^{\alpha,\beta}\frac{1}{\|t_\beta\|}\frac{\partial \tilde{\boldsymbol{u}}}{\partial \lambda^\beta}\cdot\hat{\boldsymbol{t}}_\alpha J_0 d\lambda_1 d\lambda_2 - \int_\Lambda \boldsymbol{f}^e \tilde{\boldsymbol{u}} J_0 d\lambda_1 d\lambda_2 = 0 \tag{3.18}$$

The stress components $\boldsymbol{S}$ are components of the Cauchy stress. However, the procedure can be extended to the case of large displacements and small deformations; in this case the components of the second Piola tensor would have been obtained. This motivates the symbol used in the formula.

Notice that the integration, in the balance equation (3.17), is performed in the physical space OXY; for this reason we introduce the Jacobian $J_0 = sl_1l_2$, where s is the thickness of the bars. Equating the expressions (3.17) and (3.18) provides the components of the second Piola-Kirchhoff stress tensor as:

$$\begin{aligned}S^{XX} &= \frac{N_{E_1}}{sl_b} = \frac{EA}{sl_b^2}\frac{\partial U_1^0}{\partial \lambda_1} = \frac{EA}{sl_b}\frac{\partial U_1^0}{\partial X} \\ S^{YY} &= \frac{N_{E_2}}{sl_b} = \frac{EA}{sl_b^2}\frac{\partial U_2^0}{\partial \lambda_2} = \frac{EA}{sl_b}\frac{\partial U_2^0}{\partial Y} \\ S^{XY} &= -\frac{T_{E_2}}{sl_b} = \frac{6EI}{sl_b^4}\left(\frac{\partial U_2^0}{\partial \lambda_1} + \frac{\partial U_1^0}{\partial \lambda_2}\right) = \frac{6EI}{sl_b^3}\left(\frac{\partial U_2^0}{\partial X} + \frac{\partial U_1^0}{\partial Y}\right) \\ S^{YX} &= \frac{T_{E_1}}{sl_b} = \frac{6EI}{sl_b^4}\left(\frac{\partial U_2^0}{\partial \lambda_1} + \frac{\partial U_1^0}{\partial \lambda_2}\right) = \frac{6EI}{sl_b^3}\left(\frac{\partial U_2^0}{\partial X} + \frac{\partial U_1^0}{\partial Y}\right)\end{aligned} \tag{3.19}$$

that in matrix form can be written as:

$$\begin{bmatrix} S^{XX} \\ S^{YY} \\ S^{XY} \\ S^{YX} \end{bmatrix} = \begin{bmatrix} \frac{EA}{sl_b} & 0 & 0 & 0 \\ 0 & \frac{EA}{sl_b} & 0 & 0 \\ 0 & 0 & \frac{6EI}{sl_b^3} & \frac{6EI}{sl_b^3} \\ 0 & 0 & \frac{6EI}{sl_b^3} & \frac{6EI}{sl_b^3} \end{bmatrix} \begin{bmatrix} \frac{\partial U_1}{\partial X} \\ \frac{\partial U_2}{\partial Y} \\ \frac{\partial U_2}{\partial X} \\ \frac{\partial U_1}{\partial Y} \end{bmatrix} \tag{3.20}$$

Remarks 1. The result obtained for the components of the stress tensor can be easily interpreted observing figure 3.3.

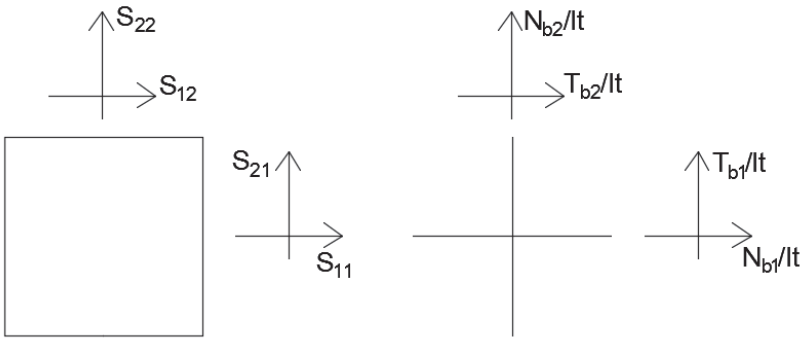

Figure 3.3: Components of the stress tensor

Remarks 2. The obtained stress components are physical components, indeed they are functions of the physical gradient of $\boldsymbol{u}$ with respect to the Lagrangian coordinators X_1, X_2, that has been obtained multiplying the parametric abscissa by l_{b1} or l_{b2}. It is important to understand the meaning and the limits of the constitutive equation (3.19). The procedure implemented is based on the assumption of small deformations, so that the beam constitutive equations (2.133) are valid only in incremental form. Therefore, the equation (3.19) relates increments of the stress tensor to increments of the strain.
Remarks 3. From the constitutive conditions (3.19) we obtain a Cauchy continuum where Poisson's ratio ν equals 0. The last two rows of (3.20) provide the shear modulus, i.e.:

$$S^{XY} = S^{YX} = \frac{6EI}{sl_b^3}\left(\frac{\partial U_1}{\partial Y} + \frac{\partial U_2}{\partial X}\right) \tag{3.21}$$

The material is orthotropic, with $E_1 = E_2$. Remarks 4. The gradient of displacement has been expressed through its covariant components. In the case of small deformations, equation (3.20) can be used to obtain the components of Cauchy stress.
Consider now a rectangular cell with $\alpha \neq 1$.
The internal forces can be obtained from the constitutive equations after substituting the value found for ϕ^0 (3.10):

$$T_{E_1} = \frac{12\,(EI)_{b1}}{l_{b1}^3}\frac{\partial U_2^0}{\partial \lambda_1} - \frac{12\,(EI)_{b1}}{l_{b1}^2}\left(\frac{\alpha}{1+\alpha}\frac{\partial U_2^0}{\partial \lambda_1}\frac{1}{l_{b1}} - \frac{1}{1+\alpha}\frac{\partial U_1^0}{\partial \lambda_2}\frac{1}{l_{b2}}\right) =$$
$$= \frac{1}{1+\alpha}\left(\frac{12\,(EI)_{b1}}{l_{b1}^3}\frac{\partial U_2^0}{\partial \lambda_1} + \frac{12\,(EI)_{b1}}{l_{b1}^2 l_{b2}}\frac{\partial U_1^0}{\partial \lambda_2}\right)$$

$$T_{E_2} = -\frac{12\,(EI)_{b2}}{l_{b2}^3}\frac{\partial U_1^0}{\partial \lambda_2} - \frac{12\,(EI)_{b2}}{l_{b2}^2}\left(\frac{\alpha}{1+\alpha}\frac{\partial U_2^0}{\partial \lambda_1}\frac{1}{l_{b1}} - \frac{1}{1+\alpha}\frac{\partial U_1^0}{\partial \lambda_2}\frac{1}{l_{b2}}\right) =$$
$$= -\frac{\alpha}{1+\alpha}\left(\frac{12\,(EI)_{b2}}{l_{b2}^2 l_{b1}}\frac{\partial U_2^0}{\partial \lambda_1} + \frac{12\,(EI)_{b2}}{l_{b2}^3}\frac{\partial U_1^0}{\partial \lambda_2}\right) =$$
$$= -\frac{1}{1+\alpha}\left(\frac{12\,(EI)_{b1}}{l_{b1}^2 l_{b2}}\frac{\partial U_2^0}{\partial \lambda_1} + \frac{12\,(EI)_{b1}}{l_{b1} l_{b2}^2}\frac{\partial U_1^0}{\partial \lambda_2}\right)$$

Substituting the above expressions in the P.V.W. we obtain the internal stresses, referring to the parametric coordinates:

$$\begin{aligned}
S^{11}\frac{1}{\|t_{b1}\|}\frac{\partial \tilde{\boldsymbol{U}}^0}{\partial \lambda^1}\cdot\hat{\boldsymbol{t}}_{b1} &= \frac{N_{E_{b1}}}{s l_{b1} l_{b2}}\frac{\partial \tilde{\boldsymbol{U}}^0}{\partial \lambda^1}\cdot\hat{\boldsymbol{t}}_{b1} = \frac{(EA)_1}{s l_{b1}^2 l_{b2}}\frac{\partial U_1^0}{\partial \lambda_1}\frac{\partial \tilde{u}^0}{\partial \lambda^1}\hat{\boldsymbol{t}}_{b1} \\
S^{22}\frac{1}{\|t_{b2}\|}\frac{\partial \tilde{\boldsymbol{U}}^0}{\partial \lambda^2}\cdot\hat{\boldsymbol{t}}_{b2} &= \frac{N_{E_{b2}}}{s l_{b1} l_{b2}}\frac{\partial \tilde{\boldsymbol{U}}^0}{\partial \lambda^2}\cdot\hat{\boldsymbol{t}}_{b2} = \frac{(EA)_2}{s l_{b1} l_{b2}^2}\frac{\partial U_2^0}{\partial \lambda_2}\frac{\partial \tilde{u}_2^0}{\partial \lambda^2} \\
S^{12}\frac{1}{\|t_{b2}\|}\frac{\partial \tilde{\boldsymbol{U}}^0}{\partial \lambda^2}\cdot\hat{\boldsymbol{t}}_{b1} &= -\frac{T_{E_{b2}}}{s l_{b1} l_{b2}}\frac{\partial \tilde{\boldsymbol{U}}^0}{\partial \lambda^2}\cdot\hat{\boldsymbol{t}}_{b1} = \\
&= \frac{1}{(1+\alpha)\,(s l_{b1} l_{b2})}\left(\frac{12\,(EI)_{b1}}{l_{b1}^2 l_{b2}}\frac{\partial U_2^0}{\partial \lambda_1} + \frac{12\,(EI)_{b1}}{l_{b1} l_{b2}^2}\frac{\partial U_1^0}{\partial \lambda_2}\right)\frac{\partial \tilde{u}_1^0}{\partial \lambda^2} \\
S^{21}\frac{1}{\|t_{b1}\|}\frac{\partial \tilde{\boldsymbol{U}}^0}{\partial \lambda^1}\cdot\hat{\boldsymbol{t}}_{b2} &= \frac{T_{E_{b1}}}{s l_{b1} l_{b2}}\frac{\partial \tilde{\boldsymbol{u}}^0}{\partial \lambda^1}\cdot\hat{\boldsymbol{t}}_{b2} = \\
&= \frac{1}{(1+\alpha)\,(s l_{b1} l_{b2})}\left(\frac{12\,(EI)_{b1}}{l_{b1}^3}\frac{\partial U_2^0}{\partial \lambda_1} + \frac{12\,(EI)_{b1}}{l_{b1}^2 l_{b2}}\frac{\partial U_1^0}{\partial \lambda_2}\right)\frac{\partial \tilde{U}_2^0}{\partial \lambda^1}
\end{aligned} \tag{3.22}$$

Therefore, in physical coordinates, we have that:

$$S^{XX} = \frac{N_{E_1}}{s l_{b2}} = \frac{(EA)_1}{s l_{b1} l_{b2}}\frac{\partial U_1^0}{\partial \lambda_1} = \frac{(EA)_1}{s l_{b2}}\frac{\partial U_1^0}{\partial X}$$
$$S^{YY} = \frac{N_{E_2}}{s l_{b1}} = \frac{(EA)_2}{s l_{b1} l_{b2}}\frac{\partial U_2^0}{\partial \lambda_2} = \frac{(EA)_2}{s l_{b1}}\frac{\partial U_2^0}{\partial Y}$$

$$S^{XY} = -\frac{T_{E_2}}{sl_{b1}} = \frac{1}{1+\alpha}\left(\frac{12\,(EI)_{b1}}{sl_{b1}^3 l_{b2}}\frac{\partial U_2^0}{\partial \lambda_1} + \frac{12\,(EI)_{b1}}{sl_{b1}^2 l_{b2}^2}\frac{\partial U_1^0}{\partial \lambda_2}\right) =$$
$$= \frac{1}{1+\alpha}\frac{12\,(EI)_{b1}}{sl_{b1}^2 l_{b2}}\left(\frac{\partial U_2^0}{\partial X} + \frac{\partial U_1^0}{\partial Y}\right)$$
$$S^{YX} = \frac{T_{E_1}}{sl_{b2}} = \frac{1}{1+\alpha}\left(\frac{12\,(EI)_{b1}}{sl_{b1}^3 l_{b2}}\frac{\partial U_2^0}{\partial \lambda_1} + \frac{12\,(EI)_{b1}}{sl_{b1}^2 l_{b2}^2}\frac{\partial U_1^0}{\partial \lambda_2}\right) =$$
$$= \frac{1}{1+\alpha}\frac{12\,(EI)_{b1}}{sl_{b1}^2 l_{b2}}\left(\frac{\partial U_2^0}{\partial X} + \frac{\partial U_1^0}{\partial Y}\right)$$

The stress components in matrix form become:

$$\begin{bmatrix} S^{XX} \\ S^{YY} \\ S^{XY} \\ S^{YX} \end{bmatrix} = \begin{bmatrix} \frac{(EA)_1}{sl_{b2}} & 0 & 0 & 0 \\ 0 & \frac{(EA)_2}{sl_{b1}} & 0 & 0 \\ 0 & 0 & \frac{1}{1+\alpha}\frac{12\,(EI)_{b1}}{sl_{b1}^2 l_{b2}} & \frac{1}{1+\alpha}\frac{12\,(EI)_{b1}}{sl_{b1}^2 l_{b2}} \\ 0 & 0 & \frac{1}{1+\alpha}\frac{12\,(EI)_{b1}}{sl_{b1}^2 l_{b2}} & \frac{1}{1+\alpha}\frac{12\,(EI)_{b1}}{sl_{b1}^2 l_{b2}} \end{bmatrix} \begin{bmatrix} \frac{\partial U_1}{\partial X} \\ \frac{\partial U_2}{\partial Y} \\ \frac{\partial U_2}{\partial X} \\ \frac{\partial U_1}{\partial Y} \end{bmatrix} \tag{3.23}$$

Note that in this case we also find $\nu = 0$.

Remarks 5. From the stress components (3.23) results the symmetry of the tangential stress $S^{12} = S^{21}$. The matrix (3.23) has, obviously, rank 3, and at the zero eigenvalue is associated to the eigenvector $\frac{\partial U_2}{\partial X_1} = -\frac{\partial U_1}{\partial X_2}$, that is the rigid rotation is given by the skew part of the gradient of displacement, as should be expected since we have found a Cauchy continuum.

3.2 Skew cell with rigid connection

In this section we will analyze the case where the fibres of the tissue are not orthogonal, see figure 3.4, and therefore the material coordinate system is not orthogonal either.

Indicating by $\boldsymbol{t}_i$ the covariant basis of the cell, the controvariant basis is given by:

$$\boldsymbol{t}^\alpha = G^{\alpha\beta}\boldsymbol{t}_\beta \tag{3.24}$$

where $G^{\alpha\beta}$ is the inverse of the covariant metric $G^{\alpha\beta} = \boldsymbol{t}_\alpha \cdot \boldsymbol{t}_\beta$.

For the case of the skew cell with straight beams shown in figure 3.4, we have:

$$\begin{aligned} \boldsymbol{t_1} &= l_1(1,0) & \boldsymbol{t^1} &= (\frac{1}{l_1}, -\frac{\cos\alpha}{l_1 \sin\alpha}) \\ \boldsymbol{t_2} &= l_2(\cos\alpha, \sin\alpha) & \boldsymbol{t^2} &= \left(0, \frac{1}{l_2 \sin\alpha}\right) \end{aligned} \tag{3.25}$$

The displacement can be expressed in the covariant system as follows:

$$\boldsymbol{u} = (u_1 \boldsymbol{t^1} + u_2 \boldsymbol{t^2}) \tag{3.26}$$

where $u_i = \boldsymbol{u} \cdot \boldsymbol{t}_i$.

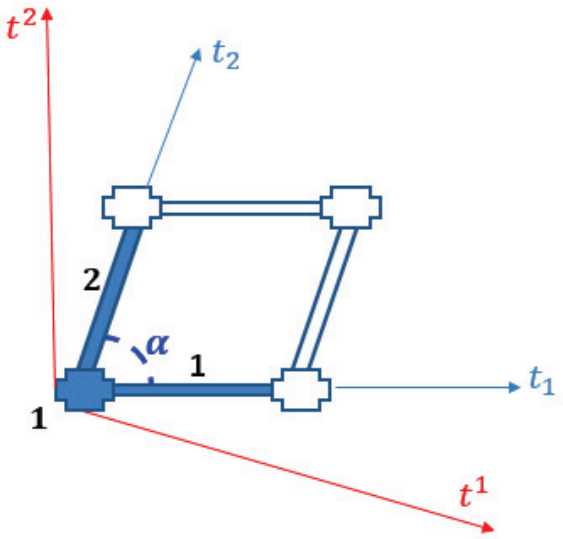

Figure 3.4: Reference cell rhomboedral case with rigid connection

In the expression of the internal forces reported in section (2.4.3) appear the components of the displacement on the unit tangent and the normal to the beams, $\hat{\boldsymbol{t}}_i = \dfrac{\boldsymbol{t}_i}{\|\boldsymbol{t}_i\|}$, $\hat{\boldsymbol{n}}_i = \boldsymbol{e}_z \cdot \boldsymbol{t}_i$. In the case under examination it is:

$$\begin{aligned} \hat{\boldsymbol{t}}_{\boldsymbol{1}} &= (1,0) & \hat{\boldsymbol{n}}_{\boldsymbol{1}} &= (0,1) \\ \hat{\boldsymbol{t}}_{\boldsymbol{2}} &= (\cos\alpha, \sin\alpha) & \hat{\boldsymbol{n}}_{\boldsymbol{2}} &= (-\sin\alpha, \cos\alpha) \end{aligned} \tag{3.27}$$

The physical components of the displacement on the local orthonormal system of the beams are therefore equal to:

$$\begin{aligned} u_{\hat{t}_i} &= \boldsymbol{u} \cdot \hat{\boldsymbol{t}}_i = u_\alpha \boldsymbol{t}^\alpha \cdot \hat{\boldsymbol{t}}_i \\ u_{\hat{\boldsymbol{n}}_i} &= \boldsymbol{u} \cdot \hat{\boldsymbol{n}}_i = u_\alpha \boldsymbol{t}^\alpha \cdot \hat{\boldsymbol{n}}_i \end{aligned} \tag{3.28}$$

Combining the components (3.28) with the definitions (3.2) for the local axes, the internal forces-displacement relations becomes:

$$
\begin{aligned}
N^1_{E1} &= k_{a1}\frac{\partial U^0_1}{\partial \lambda_1}\\
N^1_{E2} &= k_{a2}\frac{\partial U^0_2}{\partial \lambda_2}\\
T^1_{E1} &= 2k_{f1}\left(\frac{1}{l_2\sin\alpha}\frac{\partial U^0_2}{\partial \lambda_1}-\frac{\partial U^0_1}{\partial \lambda_1}\frac{\cos\alpha}{l_1\sin\alpha}-l_1\phi^0\right)\\
T^1_{E2} &= 2k_{f2}\left(-\frac{1}{l_1\sin\alpha}\frac{\partial U^0_1}{\partial \lambda_2}+\frac{\partial U^0_2}{\partial \lambda_2}\frac{\cos\alpha}{l_2\sin\alpha}-l_2\phi^0\right)\\
M^2_{O1} &= k_{f1}l_1\left(-\frac{1}{l_2\sin\alpha}\frac{\partial U^0_2}{\partial \lambda_1}+\frac{\cos\alpha}{l_1\sin\alpha}\frac{\partial U^0_1}{\partial \lambda_1}+l_1\phi^0\right)\\
M^2_{E1} &= k_{f1}l_1\left(-\frac{1}{l_2\sin\alpha}\frac{\partial U^0_2}{\partial \lambda_1}+\frac{\cos\alpha}{l_1\cos\alpha}\frac{\partial U^0_1}{\partial \lambda_1}+l_1\phi^0\right)\\
M^2_{O2} &= k_{f2}l_2\left(\frac{1}{l_1\sin\alpha}\frac{\partial U^0_1}{\partial \lambda_2}-\frac{\cos\alpha}{l_2\sin\alpha}\frac{\partial U^0_2}{\partial \lambda_2}+l_2\phi^0\right)\\
M^2_{E2} &= k_{f2}l_2\left(\frac{1}{l_1\sin\alpha}\frac{\partial U^0_1}{\partial \lambda_2}-\frac{\cos\alpha}{l_2\sin\alpha}\frac{\partial U^0_2}{\partial \lambda_2}+l_2\phi^0\right)
\end{aligned}
\tag{3.29}
$$

The P.V.W obtained using the virtual displacement and the virtual rotation at order 1 gives the self-balance equation of the cell that allow to express the rotation as a function of the displacements, exactly as in the previously considered case.

$$
\phi^0=\frac{1}{\left(k_{f1}l_1^3l_2+k_{f2}l_1l_2^3\right)\sin\alpha}\left(k_{f1}l_1^2\frac{\partial U^0_2}{\partial \lambda_1}-k_{f2}l_2^2\frac{\partial U^0_1}{\partial \lambda_2}-k_{f1}l_1l_2\cos\alpha\frac{\partial U^0_1}{\partial \lambda_1}+k_{f2}l_1l_2\cos\alpha\frac{\partial U^0_2}{\partial \lambda_2}\right)
\tag{3.30}
$$

The equilibrium equation (3.18) can be once more used to identify the components of the stress tensor as a function of the displacement gradient on the covariant basis:

$$
\begin{bmatrix}S^{11}\\S^{22}\\S^{12}\\S^{21}\end{bmatrix}=\begin{bmatrix}K_1 & K_{F1}\cos^2\alpha & -K_{F1}\frac{l_2}{l_1}\cos\alpha & -K_{F1}\frac{l_2}{l_1}\cos\alpha\\ K_{F1}\cos^2\alpha & K_2 & -K_{F1}\frac{l_1}{l_2}\cos\alpha & -K_{F1}\frac{l_1}{l_2}\cos\alpha\\ -K_{F1}\frac{l_2}{l_1}\cos\alpha & -K_{F1}\frac{l_1}{l_2}\cos\alpha & K_{F1} & K_{F1}\\ -K_{F1}\frac{l_2}{l_1}\cos\alpha & -K_{F1}\frac{l_1}{l_2}\cos\alpha & K_{F1} & K_{F1}\end{bmatrix}\begin{bmatrix}\frac{\partial U_1}{\partial \lambda_1}\\ \frac{\partial U_2}{\partial \lambda_2}\\ \frac{\partial U_2}{\partial \lambda_1}\\ \frac{\partial U_1}{\partial \lambda_2}\end{bmatrix}
\tag{3.31}
$$

where

$$\begin{aligned} K_{F1} &= \frac{2k_{f1}k_{f2}}{\left(k_{f1}l_1^3 l_2 + k_{f2}l_1 l_2^3\right)\sin^3\alpha} \quad K_{F2} = \frac{k_{f1}l_1^2 + k_{f2}l_2^2}{\left(k_{f1}l_1^5 l_2 + k_{f2}l_1^3 l_2^3\right)\sin\alpha} \\ K_1 &= k_{a1}K_{F2} + K_{F1}\left(\frac{l_1}{l_2}\right)^2\cos^2\alpha \quad K_2 = k_{a2}\frac{K_{F2}}{(l_1 l_2)^2} + K_{F1}\left(\frac{l_2}{l_1}\right)^2\cos^2\alpha \end{aligned} \tag{3.32}$$

The matrix formulation (3.31) makes reference to the material axes of the cell. In order to express the constitutive law in the external reference Cartesian frame of unit vector $\boldsymbol{e}_i \quad i = 1,2$ it is necessary to perform the rotation of the fourth order tensor of the elastic constant as follows:

$$S^{ij} = E^{\alpha\beta\gamma\delta}(\boldsymbol{t}_\alpha \cdot \boldsymbol{e}_i)(\boldsymbol{t}_\beta \cdot \boldsymbol{e}_j)(\boldsymbol{t}_\gamma \cdot \boldsymbol{e}_k)(\boldsymbol{t}_\delta \cdot \boldsymbol{e}_l)\frac{\partial u_k}{\partial X_l} \tag{3.33}$$

Therefore, the rotation of the elastic constant tensor is:

$$E^{ijkl} = E^{\alpha\beta\gamma\delta}(\boldsymbol{t}_\alpha \cdot \boldsymbol{e}_i)(\boldsymbol{t}_\beta \cdot \boldsymbol{e}_j)(\boldsymbol{t}_\gamma \cdot \boldsymbol{e}_k)(\boldsymbol{t}_\delta \cdot \boldsymbol{e}_l) \tag{3.34}$$

where $\alpha, \beta, \gamma, \delta = 1,2$ and $i, j, k, l = 1,2$.

Applying the relation (3.34) in the expression (3.31) we find the stress components, in the cartesian frame OXY:

$$\begin{bmatrix} S^{XX} \\ S^{YY} \\ S^{XY} \\ S^{YX} \end{bmatrix} = \begin{bmatrix} a_{11} & a_{12} & a_{13} & a_{14} \\ a_{21} & a_{22} & a_{23} & a_{24} \\ a_{31} & a_{32} & a_{33} & a_{34} \\ a_{41} & a_{42} & a_{43} & a_{44} \end{bmatrix} \begin{bmatrix} \dfrac{\partial U_1}{\partial X} \\ \dfrac{\partial U_2}{\partial Y} \\ \dfrac{\partial U_2}{\partial X} \\ \dfrac{\partial U_1}{\partial Y} \end{bmatrix} \tag{3.35}$$

where

$$
\begin{aligned}
a_{11} &= K_1 l_1^4 + \left(K_2 l_2^4 - 2K_{F1} l_1^2 l_2^2\right)\cos^4\alpha \\
a_{12} &= l_2^2\left(K_2 l_2^2 - K_{F1} l_1^2\right)\cos^2\alpha \sin^2\alpha \\
a_{13} &= l_2^2 \cos\alpha \left[K_{F1} l_1^2 + \left(K_2 l_2^2 - 2K_{F1} l_1^2\right)\cos^2\alpha\right]\sin\alpha \\
a_{14} &= l_2^2 \cos\alpha \left[K_{F1} l_1^2 + \left(K_2 l_2^2 - 2K_{F1} l_1^2\right)\cos^2\alpha\right]\sin\alpha
\end{aligned}
$$

$$
\begin{aligned}
a_{21} &= l_2^2\left(K_2 l_2^2 - K_{F1} l_1^2\right)\cos^2\alpha \sin^2\alpha \\
a_{22} &= K_2 l_2^4 \sin^4\alpha \\
a_{23} &= l_2^2\left(K_2 l_2^2 - K_{F1} l_1^2\right)\cos\alpha \sin^3\alpha \\
a_{24} &= l_2^2\left(K_2 l_2^2 - K_{F1} l_1^2\right)\cos\alpha \sin^3\alpha
\end{aligned}
$$

$$
\begin{aligned}
a_{31} &= l_2^2 \cos\alpha \left[K_{F1} l_1^2 + \left(K_2 l_2^2 - 2K_{F1} l_1^2\right)\cos^2\alpha\right]\sin\alpha \\
a_{32} &= l_2^2\left(K_2 l_2^2 - K_{F1} l_1^2\right)\cos\alpha \sin^3\alpha \\
a_{33} &= l_2^2\left[K_{F1} l_1^2 + \left(K_2 l_2^2 - 2K_{F1} l_1^2\right)\cos^2\alpha\right]\sin^2\alpha \\
a_{34} &= l_2^2\left[K_{F1} l_1^2 + \left(K_2 l_2^2 - 2K_{F1} l_1^2\right)\cos^2\alpha\right]\sin^2\alpha
\end{aligned}
$$

$$
\begin{aligned}
a_{41} &= l_2^2 \cos\alpha \left[K_{F1} l_1^2 + \left(K_2 l_2^2 - 2K_{F1} l_1^2\right)\cos^2\alpha\right]\sin\alpha \\
a_{42} &= l_2^2\left(K_2 l_2^2 - K_{F1} l_1^2\right)\cos\alpha \sin^3\alpha \\
a_{43} &= l_2^2\left[K_{F1} l_1^2 + \left(K_2 l_2^2 - 2K_{F1} l_1^2\right)\cos^2\alpha\right]\sin^2\alpha \\
a_{44} &= l_2^2\left[K_{F1} l_1^2 + \left(K_2 l_2^2 - 2K_{F1} l_1^2\right)\cos^2\alpha\right]\sin^2\alpha
\end{aligned}
$$

The constitutive tensor obtained is anisotropic.
For $\alpha = \dfrac{\pi}{2}$ the rectangular cell case equation (3.23) is recovered.
It is interesting to examine the case when two beams are equal, that is when the cell becomes rhombohedral, figure 3.5.

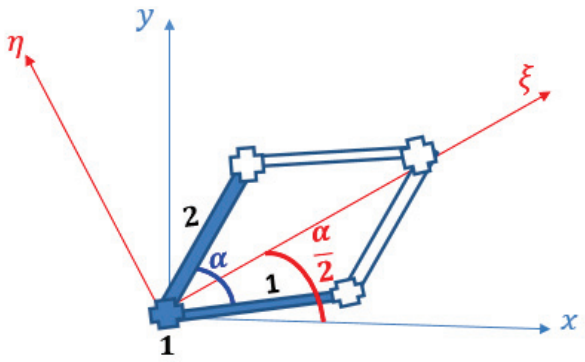

Figure 3.5: Reference cell rhomboedral case with rigid connection

In this case the cell is symmetric about the axis ξ, rotated by an angle of $\dfrac{\alpha}{2}$ with respect to the Cartesian axis X. Rotating the constitutive tensor to the new couple of axis (ξ,η) [1],

[1]The rotation is performed in a manner analogue to the equation (3.34) substituting $\boldsymbol{t}_\alpha$ with $\boldsymbol{e}_i$ and $\boldsymbol{e}_i$ with $\boldsymbol{g}_i$. $(\boldsymbol{g}_1, \boldsymbol{g}_2)$ denote the unit vectors of the axes (ξ,η)

the constitutive matrix, for $\alpha = \frac{\pi}{3}$,takes the form:

$$\begin{bmatrix} \frac{\sqrt{3}}{4}\left(3k_a+2k_f\right) & \frac{\sqrt{3}}{4}\left(k_a-2k_f\right) & 0 & 0 \\ \frac{\sqrt{3}}{4}\left(k_a-2k_f\right) & \frac{\sqrt{3}}{12}\left(k_a+6k_f\right) & 0 & 0 \\ 0 & 0 & \frac{\sqrt{3}}{4}k_a & \frac{\sqrt{3}}{4}k_a \\ 0 & 0 & \frac{\sqrt{3}}{4}k_a & \frac{\sqrt{3}}{4}k_a \end{bmatrix} \tag{3.36}$$

The expression (3.36) shows that, in the case of a romboedral cell, the material becomes orthotropic, as it is expected.

3.3 Rectangular cell braced with rigid connection

This cell and the developed one in the next subsection, can be representative of a quadrilateral tissue shown in figure 3.6. We consider a periodic structure composed by a rectangular reference cell braced with rigid connection. In general, the P.V.W. is given by equations (2.146).

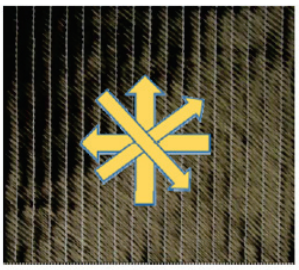

Figure 3.6: Quadrilateral tissue

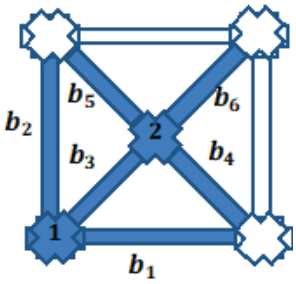

Figure 3.7: Reference cell rectangular braced with rigid connection

In the case shown in figure 3.7 we have:

$$\sum_{\nu\in\mathcal{Z}}\left[N^{\varepsilon}_{E_b}\left(\tilde{\boldsymbol{u}}^{\varepsilon}_{E_b}-\tilde{\boldsymbol{u}}^{\varepsilon}_{O_b}\right)\cdot\hat{\boldsymbol{t}}_b+T^{\varepsilon}_{E_b}\left(\tilde{\boldsymbol{u}}^{\varepsilon}_{E_b}-\tilde{\boldsymbol{u}}^{\varepsilon}_{O_b}\right)\cdot\hat{\boldsymbol{n}}_b+M^{\varepsilon}_{O_b}\tilde{\phi}_{O_b}+M^{\varepsilon}_{E_b}\tilde{\phi}_{E_b}-\sum_{n\in\mathcal{N}}\mathbf{f}^{e}_{n}\cdot\tilde{\boldsymbol{u}}^{\varepsilon}_{n}\right]=0$$

$$b=1,..,6\qquad\forall\tilde{\boldsymbol{u}}^{\varepsilon}_{n},\tilde{\phi}^{\varepsilon}_{n}\tag{3.37}$$

It is possible to identify the nodal displacement in the following way:

$$\begin{array}{lll}
\tilde{\boldsymbol{u}}^{\varepsilon}_{O_1}(\lambda)=\tilde{\boldsymbol{u}}^{\varepsilon}_{1}(\lambda) & \tilde{\boldsymbol{u}}^{\varepsilon}_{O_2}(\lambda)=\tilde{\boldsymbol{u}}^{\varepsilon}_{1}(\lambda) & \tilde{\boldsymbol{u}}^{\varepsilon}_{O_3}(\lambda)=\tilde{\boldsymbol{u}}^{\varepsilon}_{1}(\lambda)\\
\tilde{\boldsymbol{u}}^{\varepsilon}_{O_4}(\lambda)=\tilde{\boldsymbol{u}}^{\varepsilon}_{2}(\lambda) & \tilde{\boldsymbol{u}}^{\varepsilon}_{O_5}(\lambda)=\tilde{\boldsymbol{u}}^{\varepsilon}_{2}(\lambda) & \tilde{\boldsymbol{u}}^{\varepsilon}_{O_6}(\lambda)=\tilde{\boldsymbol{u}}^{\varepsilon}_{2}(\lambda)\\
\\
\tilde{\boldsymbol{u}}^{\varepsilon}_{E_1}(\lambda)=\tilde{\boldsymbol{u}}^{\varepsilon}_{2}(\lambda_1+\varepsilon,\lambda_2) & \tilde{\boldsymbol{u}}^{\varepsilon}_{E_2}(\lambda)=\tilde{\boldsymbol{u}}^{\varepsilon}_{1}(\lambda_1,\lambda_2+\varepsilon) & \tilde{\boldsymbol{u}}^{\varepsilon}_{E_3}(\lambda)=\tilde{\boldsymbol{u}}^{\varepsilon}_{2}(\lambda)\\
\tilde{\boldsymbol{u}}^{\varepsilon}_{E_4}(\lambda)=\tilde{\boldsymbol{u}}^{\varepsilon}_{2}(\lambda_1+\varepsilon,\lambda_2) & \tilde{\boldsymbol{u}}^{\varepsilon}_{E_5}(\lambda)=\tilde{\boldsymbol{u}}^{\varepsilon}_{1}(\lambda_1,\lambda_2+\varepsilon) & \tilde{\boldsymbol{u}}^{\varepsilon}_{E_6}(\lambda)=\tilde{\boldsymbol{u}}^{\varepsilon}_{2}(\lambda_1+\varepsilon,\lambda_2+\varepsilon)\\
\\
\tilde{\phi}^{\varepsilon}_{O_1}(\lambda)=\tilde{\phi}^{\varepsilon}_{1}(\lambda) & \tilde{\phi}^{\varepsilon}_{O_2}(\lambda)=\tilde{\phi}^{\varepsilon}_{1}(\lambda) & \tilde{\phi}^{\varepsilon}_{O_3}(\lambda)=\tilde{\phi}^{\varepsilon}_{1}(\lambda)\\
\tilde{\phi}^{\varepsilon}_{O_4}(\lambda)=\tilde{\phi}^{\varepsilon}_{2}(\lambda) & \tilde{\phi}^{\varepsilon}_{O_5}(\lambda)=\tilde{\phi}^{\varepsilon}_{2}(\lambda) & \tilde{\phi}^{\varepsilon}_{O_6}(\lambda)=\tilde{\phi}^{\varepsilon}_{2}(\lambda)\\
\\
\tilde{\phi}^{\varepsilon}_{E_1}(\lambda)=\tilde{\phi}^{\varepsilon}_{1}(\lambda_1+\varepsilon,\lambda_2) & \tilde{\phi}^{\varepsilon}_{E_2}(\lambda)=\tilde{\phi}^{\varepsilon}_{1}(\lambda_1,\lambda_2+\varepsilon) & \tilde{\phi}^{\varepsilon}_{E_3}(\lambda)=\tilde{\phi}^{\varepsilon}_{2}(\lambda)\\
\tilde{\phi}^{\varepsilon}_{E_4}(\lambda)=\tilde{\phi}^{\varepsilon}_{1}(\lambda_1+\varepsilon,\lambda_2) & \tilde{\phi}^{\varepsilon}_{E_5}(\lambda)=\tilde{\phi}^{\varepsilon}_{1}(\lambda_1,\lambda_2+\varepsilon) & \tilde{\phi}^{\varepsilon}_{E_6}(\lambda)=\tilde{\phi}^{\varepsilon}_{1}(\lambda_1+\varepsilon,\lambda_2+\varepsilon)
\end{array}\tag{3.38}$$

where λ indicates the couple of variables λ_1,λ_2.

Micro-equilibrium

Substitution of the asymptotic expansion for the forces (2.138), (2.139), (2.140), (2.141) and for the displacements (2.128), (2.132) in equation (3.37), yields:

$$\begin{aligned}
&\varepsilon^2\sum_{\nu\in\mathcal{Z}}\left[N^{1}_{E_3}\left(\tilde{\boldsymbol{u}}^{1}_{2}-\tilde{\boldsymbol{u}}^{1}_{1}\right)\cdot\hat{\boldsymbol{t}}_3+N^{1}_{E_4}\left(\tilde{\boldsymbol{u}}^{1}_{1}-\tilde{\boldsymbol{u}}^{1}_{2}\right)\cdot\hat{\boldsymbol{t}}_4+N^{1}_{E_5}\left(\tilde{\boldsymbol{u}}^{1}_{1}-\tilde{\boldsymbol{u}}^{1}_{2}\right)\cdot\hat{\boldsymbol{t}}_5+N^{1}_{E_6}\left(\tilde{\boldsymbol{u}}^{1}_{1}-\tilde{\boldsymbol{u}}^{1}_{2}\right)\cdot\hat{\boldsymbol{t}}_6\right]\theta_x+\\
&+\varepsilon^2\sum_{\nu\in\mathcal{Z}}\left[T^{1}_{E_3}\left(\tilde{\boldsymbol{u}}^{1}_{2}-\tilde{\boldsymbol{u}}^{1}_{1}\right)\cdot\hat{\boldsymbol{n}}_3+T^{1}_{E_4}\left(\tilde{\boldsymbol{u}}^{1}_{1}-\tilde{\boldsymbol{u}}^{1}_{2}\right)\cdot\hat{\boldsymbol{n}}_4+T^{1}_{E_5}\left(\tilde{\boldsymbol{u}}^{1}_{1}-\tilde{\boldsymbol{u}}^{1}_{2}\right)\cdot\hat{\boldsymbol{n}}_5+T^{1}_{E_6}\left(\tilde{\boldsymbol{u}}^{1}_{1}-\tilde{\boldsymbol{u}}^{1}_{2}\right)\cdot\hat{\boldsymbol{n}}_6\right]\theta_y+\\
&+\varepsilon^3\sum_{\nu\in\mathcal{Z}}\Big[\left(M^{2}_{O_1}+M^{2}_{O_2}+M^{2}_{O_3}+M^{2}_{E_1}+M^{2}_{E_2}+M^{2}_{E_4}+M^{2}_{E_5}+M^{2}_{E_6}\right)\eta_1\tilde{\phi}^{1}_{1}+\\
&\quad+\left(M^{2}_{E_3}+M_{O_4}+M_{O_5}+M_{O_6}\right)\eta_2\tilde{\phi}^{1}_{2}\Big]=0\qquad\forall\boldsymbol{\theta},\tilde{\boldsymbol{u}}^{1}_{n},\eta_n,\tilde{\phi}^{1}_{n}
\end{aligned}\tag{3.39}$$

The self-equilibrium equations are given bellow:

$$\begin{cases}
-N^{1}_{3}c(\alpha_3)+N^{1}_{4}c(\alpha_4)+N^{1}_{5}c(\alpha_5)+N^{1}_{6}s(\alpha_6)+T^{1}_{3}s(\alpha_3)-T^{1}_{4}s(\alpha_4)-T^{1}_{5}s(\alpha_5)-T^{1}_{6}s(\alpha_6)=0\\
-T^{1}_{3}c(\alpha_3)+T^{1}_{4}c(\alpha_4)+T^{1}_{5}c(\alpha_5)+T^{1}_{6}c(\alpha_6)-N^{1}_{3}s(\alpha_3)+N^{1}_{4}s(\alpha_4)+N^{1}_{5}s(\alpha_5)+N^{1}_{6}s(\alpha_6)=0\\
M^{2}_{E_1}+M^{2}_{E_2}+M^{2}_{E_4}+M^{2}_{E_5}+M^{2}_{E_6}+M^{2}_{O_1}+M^{2}_{O_2}+M^{2}_{O_3}=0\\
M^{2}_{E_3}+M^{2}_{O4}+M^{2}_{O_5}+M^{2}_{O_6}=0
\end{cases}\tag{3.40}$$

The solution of the system given in Equation (3.41) refers to the particular case where $E_1I_1 = E_2I_2 = E_eI_e$, $E_3I_3 = E_4I_4 = E_5I_5 = E_6I_6 = E_iI_i$, $l_1 = l_2 = l$ and the internal node is in the center of the cell:

$$\begin{aligned} u^1_\Delta &= \frac{1}{2}\frac{\partial U^0}{\partial \lambda_1} + \frac{\partial U^0}{\partial \lambda_2} \\ v^1_\Delta &= \frac{1}{2}\frac{\partial V^0}{\partial \lambda_1} + \frac{\partial V^0}{\partial \lambda_2} \\ \phi^0_1 &= \frac{1}{2l}\frac{\partial V^0}{\partial \lambda_1} - \frac{\partial U^0}{\partial \lambda_2} \\ \phi^0_2 &= \frac{1}{2l}\frac{\partial V^0}{\partial \lambda_1} - \frac{\partial U^0}{\partial \lambda_2} \end{aligned} \tag{3.41}$$

The relations (3.41) give the micro-variable as function of the macro-variables.

Macro-equilibrium

Considering the equilibrium equation in weak form dual of the macroscopic displacement U^0, provides the following macro-equilibrium equation:

$$\begin{aligned} &\int_\Lambda \Big[N^1_{E_1}\frac{\partial \tilde{\boldsymbol{U}}^0}{\partial \lambda_1}\cdot\hat{\boldsymbol{t}}_3 + N^1_{E_2}\frac{\partial \tilde{\boldsymbol{U}}^0}{\partial \lambda_2}\cdot\hat{\boldsymbol{t}}_2 + N^1_{E_4}\frac{\partial \tilde{\boldsymbol{U}}^0}{\partial \lambda_1}\cdot\hat{\boldsymbol{t}}_4 + N^1_{E_5}\frac{\partial \tilde{\boldsymbol{U}}^0}{\partial \lambda_2}\cdot\hat{\boldsymbol{t}}_5 + N^1_{E_6}\left(\frac{\partial \tilde{\boldsymbol{U}}^0}{\partial \lambda_1}+\frac{\partial \tilde{\boldsymbol{U}}^0}{\partial \lambda_2}\right)\cdot\hat{\boldsymbol{t}}_6 + \\ &+T^1_{E_1}\frac{\partial \tilde{\boldsymbol{U}}^0}{\partial \lambda_1}\cdot\hat{\boldsymbol{n}}_1 + T^1_{E_2}\frac{\partial \tilde{\boldsymbol{U}}^0}{\partial \lambda_2}\cdot\hat{\boldsymbol{n}}_2 + T^1_{E_4}\frac{\partial \tilde{\boldsymbol{U}}^0}{\partial \lambda_1}\cdot\hat{\boldsymbol{n}}_4 + T^1_{E_5}\frac{\partial \tilde{\boldsymbol{U}}^0}{\partial \lambda_2}\cdot\hat{\boldsymbol{n}}_5 + T^1_{E_6}\left(\frac{\partial \tilde{\boldsymbol{U}}^0}{\partial \lambda_1}+\frac{\partial \tilde{\boldsymbol{U}}^0}{\partial \lambda_2}\right)\cdot\hat{\boldsymbol{n}}_6 + \\ &+\left(M^2_{O_1}+M^2_{O_2}+M^2_{O_3}++M^2_{E_1}+M^2_{E_2}+M^2_{E_4}+M^2_{E_5}+M^2_{E_6}\right)\tilde{\phi}^0_1 + \\ &+\left(M^2_{O_4}+M^2_{O_5}+M^2_{O_6}+M^2_{E_3}\right)\tilde{\phi}^0_2\Big] d\lambda_1 d\lambda_2 = 0 \qquad \forall \tilde{\boldsymbol{U}}^0, \tilde{\phi}^0 \end{aligned} \tag{3.42}$$

Substitution of equations (3.41), the constitutive relation (2.4.3) in expression (3.42) and use of the Jacobian of the transormation, provides the component of the stress tensor in physical coordinates.
In matrix form the stress components are:

$$\begin{bmatrix} S^{XX} \\ S^{YY} \\ S^{XY} \\ S^{YX} \end{bmatrix} = \begin{bmatrix} k_{fi}+k_{ae}+\frac{k_{ai}}{2} & \frac{1}{2}\left(k_{ai}-2k_{fi}\right) & 0 & 0 \\ \frac{1}{2}\left(k_{ai}-2k_{fi}\right) & k_{fi}+k_{ae}+\frac{k_{ai}}{2} & 0 & 0 \\ 0 & 0 & \frac{k_{ai}}{2}+k_{fe} & \frac{k_{ai}}{2}+k_{fe} \\ 0 & 0 & \frac{k_{ai}}{2}+k_{fe} & \frac{k_{ai}}{2}+k_{fe} \end{bmatrix} \begin{bmatrix} \frac{\partial U}{\partial X} \\ \frac{\partial V}{\partial Y} \\ \frac{\partial V}{\partial X} \\ \frac{\partial U}{\partial Y} \end{bmatrix} \tag{3.43}$$

where:

$k_{fi} = (6E_iI_i)/(l\sqrt{2}/2)^3$ is the flexural rigidity of the internal bar

$k_{fe} = (6E_eI_e)/l^3$ is the flexural rigidity of the external bar

$k_{ai} = (E_iA_i)/(l\sqrt{2}/2)$ is the axial rigidity of the internal bar

$k_{ae} = (E_eA_e)/l$ is the axial rigidity of the external bar

Remarks 6

The constitutive matrix (3.43) has rank 3. As in the case of the cell without braces, the eigenvector related to the zero eigenvalue that represents the rigid macro-rotation is $\frac{\partial U}{\partial Y} - \frac{\partial V}{\partial X}$. Therefore a Cauchy continuum is found.

Remarks 7

The material obtained is orthotropic with $\nu_{12} \neq 0$

3.4 Rectangular cell braced with pivots

In this section we consider a braced rectangular lattice. The beams are connected by pivots, so in this case we will consider different rotations for each node. The DOFs of cell are:

- node 1: $u_1, v_1, \phi_{1,1}, \phi_{1,2}, \phi_{1,3}, \phi_{1,4}$
- node 2: $u_2, v_2, \phi_{2,1}, \phi_{2,2}$

Figure 3.9 shows the rotational degree of freedom given by the pivots.

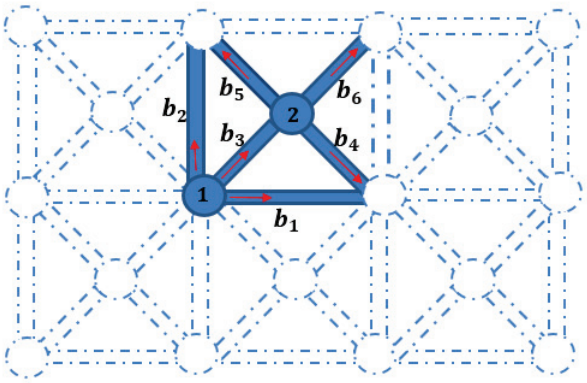

Figure 3.8: Reference cell rectangular braced with pivot

The P.V.W. takes the same form of equation (3.37). It is possible to identify the nodal displacement in the following way:

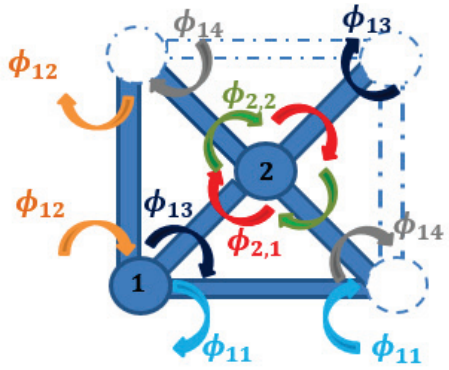

Figure 3.9: Reference cell rectangular braced with pivots and rotational degrees of freedom

$$
\begin{array}{lll}
\tilde{\boldsymbol{u}}^{\varepsilon}_{O_1}(\lambda) = \tilde{\boldsymbol{u}}^{\varepsilon}_{1}(\lambda) & \tilde{\boldsymbol{u}}^{\varepsilon}_{O_2}(\lambda) = \tilde{\boldsymbol{u}}^{\varepsilon}_{1}(\lambda) & \tilde{\boldsymbol{u}}^{\varepsilon}_{O_3}(\lambda) = \tilde{\boldsymbol{u}}^{\varepsilon}_{1}(\lambda) \\
\tilde{\boldsymbol{u}}^{\varepsilon}_{O_4}(\lambda) = \tilde{\boldsymbol{u}}^{\varepsilon}_{2}(\lambda) & \tilde{\boldsymbol{u}}^{\varepsilon}_{O_5}(\lambda) = \tilde{\boldsymbol{u}}^{\varepsilon}_{2}(\lambda) & \tilde{\boldsymbol{u}}^{\varepsilon}_{O_6}(\lambda) = \tilde{\boldsymbol{u}}^{\varepsilon}_{2}(\lambda) \\
\\
\tilde{\boldsymbol{u}}^{\varepsilon}_{E_1}(\lambda) = \tilde{\boldsymbol{u}}^{\varepsilon}_{2}(\lambda_1+\varepsilon,\lambda_2) & \tilde{\boldsymbol{u}}^{\varepsilon}_{E_2}(\lambda) = \tilde{\boldsymbol{u}}^{\varepsilon}_{1}(\lambda_1,\lambda_2+\varepsilon) & \tilde{\boldsymbol{u}}^{\varepsilon}_{E_3}(\lambda) = \tilde{\boldsymbol{u}}^{\varepsilon}_{2}(\lambda) \\
\tilde{\boldsymbol{u}}^{\varepsilon}_{E_4}(\lambda) = \tilde{\boldsymbol{u}}^{\varepsilon}_{2}(\lambda_1+\varepsilon,\lambda_2) & \tilde{\boldsymbol{u}}^{\varepsilon}_{E_5}(\lambda) = \tilde{\boldsymbol{u}}^{\varepsilon}_{1}(\lambda_1,\lambda_2+\varepsilon) & \tilde{\boldsymbol{u}}^{\varepsilon}_{E_6}(\lambda) = \tilde{\boldsymbol{u}}^{\varepsilon}_{2}(\lambda_1+\varepsilon,\lambda_2+\varepsilon) \\
\\
\tilde{\phi}^{\varepsilon}_{O_1}(\lambda) = \tilde{\phi}^{\varepsilon}_{1,1}(\lambda) & \tilde{\phi}^{\varepsilon}_{O_2}(\lambda) = \tilde{\phi}^{\varepsilon}_{1,2}(\lambda) & \tilde{\phi}^{\varepsilon}_{O_3}(\lambda) = \tilde{\phi}^{\varepsilon}_{1,3}(\lambda) \\
\tilde{\phi}^{\varepsilon}_{O_4}(\lambda) = \tilde{\phi}^{\varepsilon}_{2,2}(\lambda) & \tilde{\phi}^{\varepsilon}_{O_5}(\lambda) = \tilde{\phi}^{\varepsilon}_{2,2}(\lambda) & \tilde{\phi}^{\varepsilon}_{O_6}(\lambda) = \tilde{\phi}^{\varepsilon}_{2,1}(\lambda) \\
\\
\tilde{\phi}^{\varepsilon}_{E_1}(\lambda) = \tilde{\phi}^{\varepsilon}_{1,1}(\lambda_1+\varepsilon,\lambda_2) & \tilde{\phi}^{\varepsilon}_{E_2}(\lambda) = \tilde{\phi}^{\varepsilon}_{2,2}(\lambda_1,\lambda_2+\varepsilon) & \tilde{\phi}^{\varepsilon}_{E_3}(\lambda) = \tilde{\phi}^{\varepsilon}_{2,1}(\lambda) \\
\tilde{\phi}^{\varepsilon}_{E_4}(\lambda) = \tilde{\phi}^{\varepsilon}_{1,4}(\lambda_1+\varepsilon,\lambda_2) & \tilde{\phi}^{\varepsilon}_{E_5}(\lambda) = \tilde{\phi}^{\varepsilon}_{1,4}(\lambda_1,\lambda_2+\varepsilon) & \tilde{\phi}^{\varepsilon}_{E_6}(\lambda) = \tilde{\phi}^{\varepsilon}_{1,3}(\lambda_1+\varepsilon,\lambda_2+\varepsilon)
\end{array}
\tag{3.44}
$$

where λ indicates the couple of variables λ_1, λ_2

Micro-equilibrium

Substitution of the asymptotic expansion of the force (2.138), (2.139), (2.140), (2.141) and displacements (2.128), (2.132) in the P.V.W. equation provides:

$$
\begin{aligned}
&\varepsilon^2 \sum_{\nu\in\mathcal{Z}} \left[N^1_{E_3} \left(\tilde{\boldsymbol{u}}^1_2 - \tilde{\boldsymbol{u}}^1_1\right)\cdot\hat{\boldsymbol{t}}_3 + N^1_{E_4} \left(\tilde{\boldsymbol{u}}^1_1 - \tilde{\boldsymbol{u}}^1_2\right)\cdot\hat{\boldsymbol{t}}_4 + N^1_{E_5} \left(\tilde{\boldsymbol{u}}^1_1 - \tilde{\boldsymbol{u}}^1_2\right)\cdot\hat{\boldsymbol{t}}_5 + N^1_{E_6} \left(\tilde{\boldsymbol{u}}^1_1 - \tilde{\boldsymbol{u}}^1_2\right)\cdot\hat{\boldsymbol{t}}_6 \right]\theta_x + \\
&+\varepsilon^2 \sum_{\nu\in\mathcal{Z}} \left[T^1_{E_3} \left(\tilde{\boldsymbol{u}}^1_2 - \tilde{\boldsymbol{u}}^1_1\right)\cdot\hat{\boldsymbol{n}}_3 + T^1_{E_4} \left(\tilde{\boldsymbol{u}}^1_1 - \tilde{\boldsymbol{u}}^1_2\right)\cdot\hat{\boldsymbol{n}}_4 + T^1_{E_5} \left(\tilde{\boldsymbol{u}}^1_1 - \tilde{\boldsymbol{u}}^1_2\right)\cdot\hat{\boldsymbol{n}}_5 + T^1_{E_6} \left(\tilde{\boldsymbol{u}}^1_1 - \tilde{\boldsymbol{u}}^1_2\right)\cdot\hat{\boldsymbol{n}}_6 \right]\theta_y + \\
&+\varepsilon^3 \sum_{\nu\in\mathcal{Z}} \left[\left(M^2_{O_1} + M^2_{E_1}\right)\eta_{1,1}\tilde{\phi}^1_{1,1} + \left(M^2_{O_2} + M^2_{E_2}\right)\eta_{2,2}\tilde{\phi}^1_{1,2} + \left(M^2_{O_3} + M^2_{E_6}\right)\eta_{1,3}\tilde{\phi}^1_{1,3} + \right. \\
&\left. + \left(M^2_{O_4} + M^2_{O_5}\right)\eta_{2,2}\tilde{\phi}^1_{2,2} + \left(M^2_{E_3} + M^2_{O_6}\right)\eta_{2,1}\tilde{\phi}^1_{2,1} + \left(M^2_{E_4} + M^2_{E_5}\right)\eta_{1,4}\tilde{\phi}^1_{1,4} \right] = 0 \quad \forall \boldsymbol{\theta}, \tilde{\boldsymbol{u}}^1_n, \eta_n, \tilde{\phi}^1_n
\end{aligned}
\tag{3.45}
$$

The self-equilibrium equations are:

$$\begin{cases} -N_3^1 c(\alpha_3) + N_4^1 c(\alpha_4) + N_5^1 c(\alpha_5) + N_6^1 s(\alpha_6) + T_3^1 s(\alpha_3) - T_4^1 s(\alpha_4) - T_5^1 s(\alpha_5) - T_6^1 s(\alpha_6) = 0 \\ -T_3^1 c(\alpha_3) + T_4^1 c(\alpha_4) + T_5^1 c(\alpha_5) + T_6^1 c(\alpha_6) - N_3^1 s(\alpha_3) + N_4^1 s(\alpha_4) + N_5^1 s(\alpha_5) + N_6^1 s(\alpha_6) = 0 \\ M_{O_1}^2 + M_{E_1}^2 = 0 \\ M_{O_2}^2 + M_{E_2}^2 = 0 \\ M_{O_3}^2 + M_{E_6}^2 = 0 \\ M_{O_4}^2 + M_{O_5}^2 = 0 \\ M_{E_3}^2 + M_{O_6}^2 = 0 \\ M_{E_4}^2 + M_{E_5}^2 = 0 \end{cases} \tag{3.46}$$

where $c(\alpha_b) = \cos(\alpha_b)$, $s(\alpha_b) = \sin(\alpha_b)$ and α_b is the angle formed by the beam b and the abscissa axis x.

The solution of the system can be found for the particular case where $E_1 I_1 = E_2 I_2 = E_e I_e$, $E_3 I_3 = E_4 I_4 = E_5 I_5 = E_6 I_6 = E_i I_i$, $l_1 = l_2 = l$ and the internal node is in the center of the cell:

$$\begin{array}{ll} u_\Delta^1 = \dfrac{1}{2}\left(\dfrac{\partial U^0}{\partial \lambda_1} + \dfrac{\partial U^0}{\partial \lambda_2}\right) & \phi_{1,3}^0 = -\dfrac{1}{2l}\left(\dfrac{\partial U^0}{\partial \lambda_1} + \dfrac{\partial U^0}{\partial \lambda_2} - \dfrac{\partial V^0}{\partial \lambda_1} - \dfrac{\partial V^0}{\partial \lambda_2}\right) \\ v_\Delta^1 = \dfrac{1}{2}\left(\dfrac{\partial V^0}{\partial \lambda_1} + \dfrac{\partial V^0}{\partial \lambda_2}\right) & \phi_{1,4}^0 = -\dfrac{1}{2l}\left(-\dfrac{\partial U^0}{\partial \lambda_1} + \dfrac{\partial U^0}{\partial \lambda_2} - \dfrac{\partial V^0}{\partial \lambda_1} + \dfrac{\partial V^0}{\partial \lambda_2}\right) \\ \phi_{1,1}^0 = \dfrac{1}{l}\dfrac{\partial V^0}{\partial \lambda_1} & \phi_{2,1}^0 = -\dfrac{1}{2l}\left(\dfrac{\partial U^0}{\partial \lambda_1} + \dfrac{\partial U^0}{\partial \lambda_2} - \dfrac{\partial V^0}{\partial \lambda_1} - \dfrac{\partial V^0}{\partial \lambda_2}\right) \\ \phi_{1,2}^0 = -\dfrac{1}{l}\dfrac{\partial U^0}{\partial \lambda_2} & \phi_{2,2}^0 = -\dfrac{1}{2l}\left(-\dfrac{\partial U^0}{\partial \lambda_1} + \dfrac{\partial U^0}{\partial \lambda_2} - \dfrac{\partial V^0}{\partial \lambda_1} + \dfrac{\partial V^0}{\partial \lambda_2}\right) \end{array} \tag{3.47}$$

The relations (3.47) give the micro-variable as a function of the macro-variables.

Macro-equilibrium

Considering the equilibrium equation in weak form, dual of the macroscopic displacement U^0, yields the macro-equilibrium equation:

$$\begin{aligned} \int_\Lambda \Big[& N_{E_1}^1 \frac{\partial \tilde{\boldsymbol{U}}^0}{\partial \lambda_1} \hat{\boldsymbol{t}}_3 + N_{E_2}^1 \frac{\partial \tilde{\boldsymbol{U}}^0}{\partial \lambda_2} \hat{\boldsymbol{t}}_2 + N_{E_4}^1 \frac{\partial \tilde{\boldsymbol{U}}^0}{\partial \lambda_1} \hat{\boldsymbol{t}}_4 + N_{E_5}^1 \frac{\partial \tilde{\boldsymbol{U}}^0}{\partial \lambda_2} \hat{\boldsymbol{t}}_5 + N_{E_6}^1 \left(\frac{\partial \tilde{\boldsymbol{U}}^0}{\partial \lambda_1} + \frac{\partial \tilde{\boldsymbol{U}}^0}{\partial \lambda_2} \right) \hat{\boldsymbol{t}}_6 + \\ & + T_{E_1}^1 \frac{\partial \tilde{\boldsymbol{U}}^0}{\partial \lambda_1} \hat{\boldsymbol{n}}_1 + T_{E_2}^1 \frac{\partial \tilde{\boldsymbol{U}}^0}{\partial \lambda_2} \hat{\boldsymbol{n}}_2 + T_{E_4}^1 \frac{\partial \tilde{\boldsymbol{U}}^0}{\partial \lambda_1} \hat{\boldsymbol{n}}_4 + T_{E_5}^1 \frac{\partial \tilde{\boldsymbol{U}}^0}{\partial \lambda_2} \hat{\boldsymbol{n}}_5 + T_{E_6}^1 \left(\frac{\partial \tilde{\boldsymbol{U}}^0}{\partial \lambda_1} + \frac{\partial \tilde{\boldsymbol{U}}^0}{\partial \lambda_2} \right) \hat{\boldsymbol{n}}_6 + \\ & + \left(M_{O_1}^2 + M_{E_1}^2 \right) \tilde{\phi}_{1,1}^0 + \left(M_{O_2}^2 + M_{E_2}^2 \right) \tilde{\phi}_{1,2}^0 + \left(M_{O_3}^2 + M_{E_6}^2 \right) \tilde{\phi}_{1,3}^0 + \left(M_{O_4}^2 + M_{O_5}^2 \right) \tilde{\phi}_{2,2}^0 + \\ & + \left(M_{E_3}^2 + M_{O_6}^2 \right) \tilde{\phi}_{2,1}^0 + \left(M_{E_4}^2 + M_{E_5}^2 \right) \tilde{\phi}_{1,4}^0 \Big] d\lambda_1 d\lambda_2 = 0 \qquad \forall \tilde{\boldsymbol{U}}^0, \tilde{\phi}_n^0 \end{aligned} \tag{3.48}$$

Substituting the result (3.47) and the constitutive relation (see subsection 2.4.3) in (3.48) and using the Jacobian of the transformation, as made in equation 3.19, we obtain the component of the stress tensor in physical coordinates.

The stress components in matrix notation are:

$$\begin{bmatrix} S^{XX} \\ S^{YY} \\ S^{XY} \\ S^{YX} \end{bmatrix} = \begin{bmatrix} k_{ae} + \frac{k_{ai}}{2} & \frac{k_{ai}}{2} & 0 & 0 \\ \frac{k_{ai}}{2} & k_{ae} + \frac{k_{ai}}{2} & 0 & 0 \\ 0 & 0 & \frac{k_{ai}}{2} & \frac{k_{ai}}{2} \\ 0 & 0 & \frac{k_{ai}}{2} & \frac{k_{ai}}{2} \end{bmatrix} \begin{bmatrix} \frac{\partial U_1}{\partial X} \\ \frac{\partial U_2}{\partial Y} \\ \frac{\partial U_2}{\partial X} \\ \frac{\partial U_1}{\partial Y} \end{bmatrix} \tag{3.49}$$

where:

$k_{ai} = E_i A_i/(l\sqrt{2}/2)$ is the axial rigidity of the internal bar

$k_{ae} = E_e A_e/l$ is the axial rigidity of the external bar

Remarks 8

The elastic stiffness parameters at the leading order (3.49) depend on the axial rigidity of the beams. Only considering higher order terms would account also of the flexural rigidity of the elements, as will be found in the next application.

3.5 Discrete homogenization method weak formulation with higher order terms

3.5.1 Rectangular case with pivot

In this section we will consider a periodic pantograph network of fibres formed by two sets of continuous fibres arranged perpendicularly along the axes X and Y. The two sets may differ from one another. The fibres are connected by perfect pivots, where the axis Z is perpendicular to the $\{X,Y\}$ plane, see figure 3.10.

The equilibrium weak formulation for the reference cell is:

$$\begin{aligned} &\sum_{\nu\in\mathcal{Z}} \Big[N^{\varepsilon}_{E_1}\left(\tilde{u}^{\varepsilon}_{E_1} - \tilde{u}^{\varepsilon}_{O_1}\right) + N^{\varepsilon}_{E_2}\left(\tilde{v}^{\varepsilon}_{E_2} - \tilde{v}^{\varepsilon}_{O_2}\right) + T^{\varepsilon}_{E_1}\left(\tilde{v}^{\varepsilon}_{E_1} - \tilde{v}^{\varepsilon}_{O_1}\right) + T^{\varepsilon}_{E_2}\left(\tilde{u}^{\varepsilon}_{E_2} - \tilde{u}^{\varepsilon}_{O_2}\right) + \\ &\quad + M^{\varepsilon}_{O_1}\tilde{\phi}^{\varepsilon}_{O_1} + M^{\varepsilon}_{E_1}\tilde{\phi}^{\varepsilon}_{E_1} + M^{\varepsilon}_{O_2}\tilde{\phi}^{\varepsilon}_{O_2} + M^{\varepsilon}_{E_2}\tilde{\phi}^{\varepsilon}_{E_2} - \sum_{n\in\mathcal{N}} f^{e}_{n}\tilde{u}_n \Big] = 0 \qquad \forall \tilde{u}_n \tilde{v}_n, \tilde{\phi}_n \end{aligned} \tag{3.50}$$

Due to the periodicity of the micro-structure of the pantographic sheet, we may identify the nodal displacement in the following way:

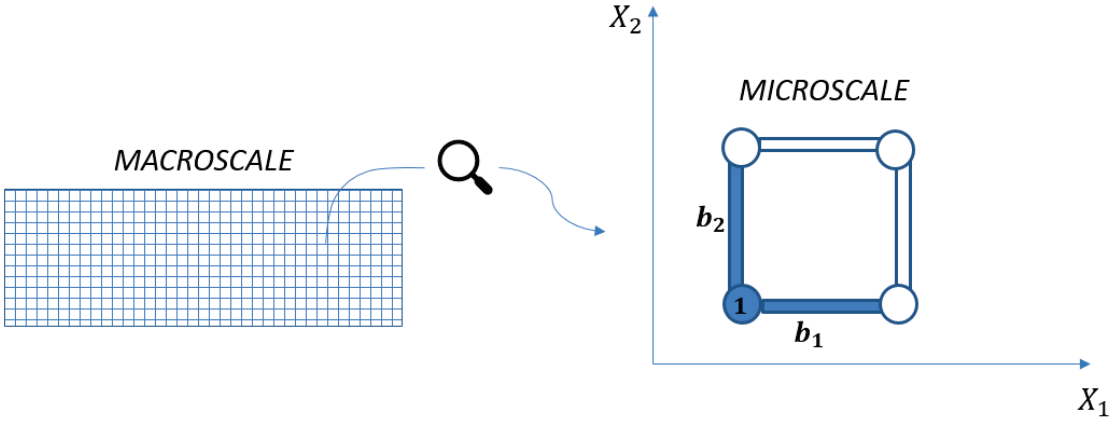

Figure 3.10: Rectangular case with pivot

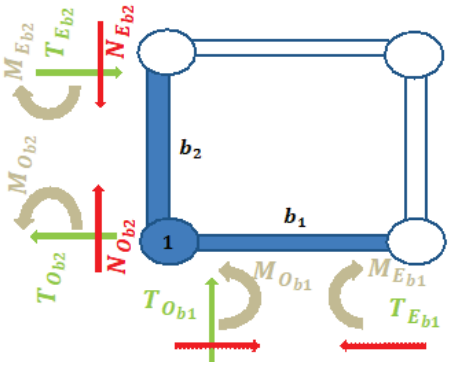

Figure 3.11: Force in the reference cell

$$\begin{array}{ll} u^{\varepsilon}_{O_1} = u^{\varepsilon}_1(\lambda_1,\lambda_2) & u^{\varepsilon}_{E_1} = u^{\varepsilon}_1(\lambda_1+\varepsilon,\lambda_2) \\ u^{\varepsilon}_{O_2} = u^{\varepsilon}_1(\lambda_1,\lambda_2) & u^{\varepsilon}_{E_2} = u^{\varepsilon}_1(\lambda_1,\lambda_2+\varepsilon) \\ v^{\varepsilon}_{O_1} = v^{\varepsilon}_1(\lambda_1,\lambda_2) & v^{\varepsilon}_{E_1} = v^{\varepsilon}_1(\lambda_1+\varepsilon,\lambda_2) \\ v^{\varepsilon}_{O_2} = v^{\varepsilon}_1(\lambda_1,\lambda_2) & v^{\varepsilon}_{E_2} = v^{\varepsilon}_1(\lambda_1,\lambda_2+\varepsilon) \end{array} \tag{3.51}$$

The rotation of the two fibres linked by the pivot are different to each other and given by:

$$\begin{array}{ll} \phi^{\varepsilon}_{O_1} = \phi^{\varepsilon}_1(\lambda_1,\lambda_2) & \phi^{\varepsilon}_{E_1} = \phi^{\varepsilon}_1(\lambda_1+\varepsilon,\lambda_2) \\ \phi^{\varepsilon}_{O_2} = \phi^{\varepsilon}_2(\lambda_1,\lambda_2) & \phi^{\varepsilon}_{E_2} = \phi^{\varepsilon}_2(\lambda_1,\lambda_2+\varepsilon) \end{array} \tag{3.52}$$

The asymptotic expansion of the nodal forces, shown in figure (3.11), is given in equations (3.53), (3.54) for the beam 1 and (3.55), (3.56) for the beam 2. While many of the expressions shown below have been already developed in lower orders of ε, herein they are developed up to order 4 (forces) and 5 (moments).

$$
\begin{aligned}
N^{\varepsilon}_{E_1} =& \varepsilon k_{a1}\frac{\partial U^0}{\partial \lambda_1}+\varepsilon^2 k_{a1}\left(\frac{1}{2}\frac{\partial^2 U^0}{\partial \lambda_1^2}+\frac{\partial u_1^1}{\partial \lambda_1}\right)+\varepsilon^3 k_{a1}\left(\frac{1}{6}\frac{\partial^3 U^0}{\partial \lambda_1^3}+\frac{1}{2}\frac{\partial^2 u_1^1}{\partial \lambda_1^2}+\frac{\partial u_1^2}{\partial \lambda_1}\right)+\\
&+\varepsilon^4 k_{a1}\left(\frac{1}{24}\frac{\partial^4 U^0}{\partial \lambda_1^4}+\frac{1}{6}\frac{\partial^3 u_1^1}{\partial \lambda_1^3}+\frac{1}{2}\frac{\partial^2 u_1^2}{\partial \lambda_1^2}+\frac{\partial u_1^3}{\partial \lambda_1}\right)=\\
&=\varepsilon N^1_{E_1}+\varepsilon^2 N^2_{E_1}+\varepsilon^3 N^3_{E_1}+\varepsilon^4 N^4_{E_1}
\end{aligned}
$$

$$
\begin{aligned}
T^{\varepsilon}_{E_1} =& \varepsilon 2k_{f1}\left(\frac{\partial V^0}{\partial \lambda_1}-l_1\phi_1^0\right)+\varepsilon^2 2k_{f1}\left[\frac{1}{2}\frac{\partial^2 V^0}{\partial \lambda_1^2}+\frac{\partial v_1^1}{\partial \lambda_1}-\frac{l_1}{2}\left(\frac{\partial \phi_1^0}{\partial \lambda_1}+2\phi_1^1\right)\right]+\\
&+\varepsilon^3 2k_{f1}\left[\frac{1}{6}\frac{\partial^3 V^0}{\partial \lambda_1^3}+\frac{1}{2}\frac{\partial^2 v_1^1}{\partial \lambda_1^2}+\frac{\partial v_1^2}{\partial \lambda_1}-\frac{l_1}{2}\left(\frac{1}{2}\frac{\partial^2 \phi_1^0}{\partial \lambda_1^2}+\frac{\partial \phi_1^1}{\partial \lambda_1}+2\phi_1^2\right)\right]+\\
&+\varepsilon^4 2k_{f1}\left[\frac{1}{24}\frac{\partial^4 V^0}{\partial \lambda_1^4}+\frac{1}{6}\frac{\partial^3 v_1^1}{\partial \lambda_1^3}+\frac{1}{2}\frac{\partial^2 v_1^2}{\partial \lambda_1^2}+\frac{\partial v_1^3}{\partial \lambda_1}-\frac{l_1}{2}\left(\frac{1}{6}\frac{\partial^3 \phi_1^0}{\partial \lambda_1^3}+\frac{1}{2}\frac{\partial^2 \phi_1^1}{\partial^2 \lambda_1}+\frac{\partial \phi_1^2}{\partial \lambda_1}+2\phi_1^3\right)\right]=\\
&=\varepsilon T^1_{E_1}+\varepsilon^2 T^2_{E_1}+\varepsilon^3 T^3_{E_1}+\varepsilon^4 T^4_{E_1}
\end{aligned}
\tag{3.53}
$$

$$
\begin{aligned}
M^{\varepsilon}_{O_1} =& \varepsilon^2 k_{f1} l_1\left(-\frac{\partial V^0}{\partial \lambda_1}+l_1\phi_1^0\right)+\varepsilon^3 k_{f1} l_1\left[-\frac{1}{2}\frac{\partial^2 V^0}{\partial \lambda_1^2}-\frac{\partial v_1^1}{\partial \lambda_1}+\frac{l_1}{3}\left(\frac{\partial \phi_1^0}{\partial \lambda_1}+3\phi_1^1\right)\right]+\\
&+\varepsilon^4 k_{f1} l_1\left[-\frac{1}{6}\frac{\partial^3 V^0}{\partial \lambda_1^3}-\frac{1}{2}\frac{\partial^2 v_1^1}{\partial \lambda_1^2}-\frac{\partial v_1^2}{\partial \lambda_1}+\frac{l_1}{3}\left(\frac{1}{2}\frac{\partial^2 \phi_1^0}{\partial \lambda_1^2}+\frac{\partial \phi_1^1}{\partial \lambda_1}+3\phi_1^2\right)\right]+\\
&+\varepsilon^5 k_{f1} l_1\left[-\frac{1}{24}\frac{\partial^4 V^0}{\partial \lambda_1^4}-\frac{1}{6}\frac{\partial^3 v_1^1}{\partial \lambda_1^3}-\frac{1}{2}\frac{\partial^2 v_1^2}{\partial \lambda_1^2}-\frac{\partial v_1^3}{\partial \lambda_1}+\frac{l_1}{3}\left(\frac{1}{6}\frac{\partial^3 \phi_1^0}{\partial \lambda_1^3}+\frac{1}{2}\frac{\partial^2 \phi_1^1}{\partial^2 \lambda_1}+\frac{\partial \phi_1^2}{\partial \lambda_1}+3\phi_1^3\right)\right]=\\
&=\varepsilon^2 M^2_{O_1}+\varepsilon^3 M^3_{O_1}+\varepsilon^4 M^4_{O_1}+\varepsilon^5 M^5_{O_1}
\end{aligned}
$$

$$
\begin{aligned}
M^{\varepsilon}_{E_1} =& \varepsilon^2 k_{f1} l_1\left(-\frac{\partial V^0}{\partial \lambda_1}+l_1\phi_1^0\right)+\varepsilon^3 k_{f1} l_1\left[-\frac{1}{2}\frac{\partial^2 V^0}{\partial \lambda_1^2}-\frac{\partial v_1^1}{\partial \lambda_1}+\frac{l_1}{3}\left(2\frac{\partial \phi_1^0}{\partial \lambda_1}+3\phi_1^1\right)\right]+\\
&+\varepsilon^4 k_{f1} l_1\left[-\frac{1}{6}\frac{\partial^3 V^0}{\partial \lambda_1^3}-\frac{1}{2}\frac{\partial^2 v_1^1}{\partial \lambda_1^2}-\frac{\partial v_1^2}{\partial \lambda_1}+\frac{l_1}{3}\left(\frac{\partial^2 \phi_1^0}{\partial \lambda_1^2}+2\frac{\partial \phi_1^1}{\partial \lambda_1}+3\phi_1^2\right)\right]+\\
&+\varepsilon^5 k_{f1} l_1\left[-\frac{1}{24}\frac{\partial^4 V^0}{\partial \lambda_1^4}-\frac{1}{6}\frac{\partial^3 v_1^1}{\partial \lambda_1^3}-\frac{1}{2}\frac{\partial^2 v_1^2}{\partial \lambda_1^2}-\frac{\partial v_1^3}{\partial \lambda_1}+\frac{l_1}{3}\left(\frac{1}{3}\frac{\partial^3 \phi_1^0}{\partial \lambda_1^3}+\frac{\partial^2 \phi_1^1}{\partial^2 \lambda_1}+2\frac{\partial \phi_1^2}{\partial \lambda_1}+3\phi_1^3\right)\right]=\\
&=\varepsilon^2 M^2_{E_1}+\varepsilon^3 M^3_{E_1}+\varepsilon^4 M^4_{E_1}+\varepsilon^5 M^5_{E_1}
\end{aligned}
\tag{3.54}
$$

$$
\begin{aligned}
N^{\varepsilon}_{E_2} =& \varepsilon k_{a2}\frac{\partial V^0}{\partial \lambda_2} + \varepsilon^2 k_{a2}\left(\frac{1}{2}\frac{\partial^2 V^0}{\partial \lambda_2^2} + \frac{\partial v_1^1}{\partial \lambda_2}\right) + \varepsilon^3 k_{a2}\left(\frac{1}{6}\frac{\partial^3 V^0}{\partial \lambda_2^3} + \frac{1}{2}\frac{\partial^2 v_1^1}{\partial \lambda_2^2} + \frac{\partial v_1^2}{\partial \lambda_2}\right) + \\
&+ \varepsilon^4 k_{a2}\left(\frac{1}{24}\frac{\partial^4 V^0}{\partial \lambda_2^4} + \frac{1}{6}\frac{\partial^3 v_1^1}{\partial \lambda_2^3} + \frac{1}{2}\frac{\partial^2 v_1^2}{\partial \lambda_2^2} + \frac{\partial v_1^3}{\partial \lambda_2}\right) = \\
&= \varepsilon N^1_{E_2} + \varepsilon^2 N^2_{E_2} + \varepsilon^3 N^3_{E_2} + \varepsilon^4 N^4_{E_2}
\end{aligned}
$$

$$
\begin{aligned}
T^{\varepsilon}_{E_2} =& \varepsilon 2k_{f2}\left(-\frac{\partial U^0}{\partial \lambda_2} - l_2\phi_2^0\right) + \varepsilon^2 2k_{f2}\left[-\frac{1}{2}\frac{\partial^2 U^0}{\partial \lambda_2^2} - \frac{\partial u_1^1}{\partial \lambda_2} - \frac{l_2}{2}\left(\frac{\partial \phi_2^0}{\partial \lambda_2} + 2\phi_2^1\right)\right] \\
&+ \varepsilon^3 2k_{f2}\left[-\frac{1}{6}\frac{\partial^3 U^0}{\partial \lambda_2^3} - \frac{1}{2}\frac{\partial^2 u_1^1}{\partial \lambda_2^2} - \frac{\partial u_1^2}{\partial \lambda_2} - \frac{l_2}{2}\left(\frac{1}{2}\frac{\partial^2 \phi_2^0}{\partial \lambda_2^2} + \frac{\partial \phi_2^1}{\partial \lambda_2} + 2\phi_2^2\right)\right] + \\
&+ \varepsilon^4 2k_{f2}\left[-\frac{1}{24}\frac{\partial^4 U^0}{\partial \lambda_2^4} - \frac{1}{6}\frac{\partial^3 u_1^1}{\partial \lambda_2^3} - \frac{1}{2}\frac{\partial^2 u_1^2}{\partial \lambda_2^2} - \frac{\partial u_1^3}{\partial \lambda_2} - \frac{l_2}{2}\left(\frac{1}{6}\frac{\partial^3 \phi_2^0}{\partial \lambda_2^3} + \frac{1}{2}\frac{\partial^2 \phi_2^1}{\partial^2 \lambda_2} + \frac{\partial \phi_2^2}{\partial \lambda_2} + 2\phi_2^3\right)\right] = \\
&= \varepsilon T^1_{E_2} + \varepsilon^2 T^2_{E_2} + \varepsilon^3 T^3_{E_2} + \varepsilon^4 T^4_{E_2}
\end{aligned}
\tag{3.55}
$$

$$
\begin{aligned}
M^{\varepsilon}_{O_2} =& \varepsilon^2 k_{f2} l_2\left(\frac{\partial U^0}{\partial \lambda_2} + l_2\phi_2^0\right) + \varepsilon^3 k_{f2} l_2\left[\frac{1}{2}\frac{\partial^2 U^0}{\partial \lambda_2^2} + \frac{\partial u_1^1}{\partial \lambda_2} + \frac{l_2}{3}\left(\frac{\partial \phi_2^0}{\partial \lambda_2} + 3\phi_2^1\right)\right] + \\
&+ \varepsilon^4 k_{f2} l_2\left[\frac{1}{6}\frac{\partial^3 U^0}{\partial \lambda_2^3} + \frac{1}{2}\frac{\partial^2 u_1^1}{\partial \lambda_2^2} + \frac{\partial u_1^2}{\partial \lambda_2} + \frac{l_2}{3}\left(\frac{1}{2}\frac{\partial^2 \phi_2^0}{\partial \lambda_2^2} + \frac{\partial \phi_2^1}{\partial \lambda_2} + 3\phi_2^2\right)\right] + \\
&+ \varepsilon^5 k_{f2} l_2\left[\frac{1}{24}\frac{\partial^4 U^0}{\partial \lambda_2^4} + \frac{1}{6}\frac{\partial^3 u_1^1}{\partial \lambda_2^3} + \frac{1}{2}\frac{\partial^2 u_1^2}{\partial \lambda_2^2} + \frac{\partial u_1^3}{\partial \lambda_2} + \frac{l_2}{3}\left(\frac{1}{6}\frac{\partial^3 \phi_2^0}{\partial \lambda_2^3} + \frac{1}{2}\frac{\partial^2 \phi_2^1}{\partial^2 \lambda_2} + \frac{\partial \phi_2^2}{\partial \lambda_2} + 3\phi_2^3\right)\right] = \\
&= \varepsilon^2 M^2_{O_2} + \varepsilon^3 M^3_{O_2} + \varepsilon^4 M^4_{O_2} + \varepsilon^5 M^5_{O_2}
\end{aligned}
$$

$$
\begin{aligned}
M^{\varepsilon}_{E_2} =& \varepsilon^2 k_{f2} l_2\left(\frac{\partial U^0}{\partial \lambda_2} + l_2\phi_2^0\right) + \varepsilon^3 k_{f2} l_2\left[\frac{1}{2}\frac{\partial^2 U^0}{\partial \lambda_2^2} + \frac{\partial u_1^1}{\partial \lambda_2} + \frac{l_2}{3}\left(2\frac{\partial \phi_2^0}{\partial \lambda_2} + 3\phi_2^1\right)\right] + \\
&+ \varepsilon^4 k_{f2} l_2\left[\frac{1}{6}\frac{\partial^3 U^0}{\partial \lambda_2^3} + \frac{1}{2}\frac{\partial^2 u_1^1}{\partial \lambda_2^2} + \frac{\partial u_1^2}{\partial \lambda_2} + \frac{l_2}{3}\left(\frac{\partial^2 \phi_2^0}{\partial \lambda_2^2} + 2\frac{\partial \phi_2^1}{\partial \lambda_2} + 3\phi_2^2\right)\right] + \\
&+ \varepsilon^5 k_{f2} l_2\left[\frac{1}{24}\frac{\partial^4 U^0}{\partial \lambda_2^4} + \frac{1}{6}\frac{\partial^3 u_1^1}{\partial \lambda_2^3} + \frac{1}{2}\frac{\partial^2 u_1^2}{\partial \lambda_2^2} + \frac{\partial u_1^3}{\partial \lambda_2} + \frac{l_2}{3}\left(\frac{1}{3}\frac{\partial^3 \phi_2^0}{\partial \lambda_2^3} + \frac{\partial^2 \phi_2^1}{\partial^2 \lambda_2} + 2\frac{\partial \phi_2^2}{\partial \lambda_2} + 3\phi_2^3\right)\right] = \\
&= \varepsilon^2 M^2_{E_2} + \varepsilon^3 M^3_{E_2} + \varepsilon^4 M^4_{E_2} + \varepsilon^5 M^5_{E_2}
\end{aligned}
\tag{3.56}
$$

where $k_{fi} = \dfrac{6E_iI_i}{l_i^3}$ and $k_{ai} = \dfrac{E_iA_i}{l_i}$.

Note: We have already demonstrated in section (2.2.2) that the leading terms of the

displacement are independent of the node; this shows that the displacement depends only on the macroscopic field: $U_1^0(\lambda_1,\lambda_2) = U^0(\lambda_1,\lambda_2)$ and $V_1^0(\lambda_1,\lambda_2) = V^0(\lambda_1,\lambda_2)$.
The proposed procedure of homogenization in weak formulation gives raise to two groups of equilibrium equations:
1. Taking a virtual displacement in the macro-displacement field and performing the Taylor expansions of the macroscopic field, we have:

$$\begin{aligned}
\tilde{u}^{\varepsilon}_{O_1} &= \tilde{u}^{\varepsilon}_{O_2} = \tilde{U}^0(\lambda_1,\lambda_2)\\
\tilde{u}^{\varepsilon}_{E_1} &= \tilde{U}^0(\lambda_1+\varepsilon,\lambda_2) = \tilde{U}^0 + \varepsilon\frac{\partial\tilde{U}^0}{\partial\lambda_1} + \varepsilon^2\frac{1}{2}\frac{\partial^2\tilde{U}^0}{\partial\lambda_1^2} + \varepsilon^3\frac{1}{6}\frac{\partial^3\tilde{U}^0}{\partial\lambda_1^3} + \varepsilon^4\frac{1}{24}\frac{\partial^4\tilde{U}^0}{\partial\lambda_1^4}\\
\tilde{u}^{\varepsilon}_{E_2} &= \tilde{U}^0(\lambda_1,\lambda_2+\varepsilon) = \tilde{U}^0 + \varepsilon\frac{\partial\tilde{U}^0}{\partial\lambda_2} + \varepsilon^2\frac{1}{2}\frac{\partial^2\tilde{U}^0}{\partial\lambda_2^2} + \varepsilon^3\frac{1}{6}\frac{\partial^3\tilde{U}^0}{\partial\lambda_2^3} + \varepsilon^4\frac{1}{24}\frac{\partial^4\tilde{U}^0}{\partial\lambda_2^4}\\
\tilde{v}^{\varepsilon}_{O_1} &= \tilde{v}_{O_2} = \tilde{V}^0(\lambda_1,\lambda_2)\\
\tilde{v}^{\varepsilon}_{E_1} &= \tilde{V}^0(\lambda_1+\varepsilon,\lambda_2) = \tilde{V}^0 + \varepsilon\frac{\partial\tilde{V}^0}{\partial\lambda_1} + \varepsilon^2\frac{1}{2}\frac{\partial^2\tilde{V}^0}{\partial\lambda_1^2} + \varepsilon^3\frac{1}{6}\frac{\partial^3\tilde{V}^0}{\partial\lambda_1^3} + \varepsilon^4\frac{1}{24}\frac{\partial^4\tilde{V}^0}{\partial\lambda_1^4}\\
\tilde{v}^{\varepsilon}_{E_2} &= \tilde{V}^0(\lambda_1,\lambda_2+\varepsilon) = \tilde{V}^0 + \varepsilon\frac{\partial\tilde{V}^0}{\partial\lambda_2} + \varepsilon^2\frac{1}{2}\frac{\partial^2\tilde{V}^0}{\partial\lambda_2^2} + \varepsilon^3\frac{1}{6}\frac{\partial^3\tilde{V}^0}{\partial\lambda_2^3} + \varepsilon^4\frac{1}{24}\frac{\partial^4\tilde{V}^0}{\partial\lambda_2^4}
\end{aligned} \tag{3.57}$$

for the rotation we have:

$$\begin{aligned}
\tilde{\phi}^{\varepsilon}_{O_1} &= \tilde{\phi}^0_1(\lambda_1,\lambda_2)\\
\tilde{\phi}^{\varepsilon}_{E_1} &= \tilde{\phi}^0_1(\lambda_1+\varepsilon,\lambda_2) = \tilde{\phi}^0_1 + \varepsilon\frac{\partial\tilde{\phi}^0_1}{\partial\lambda_1} + \varepsilon^2\frac{1}{2}\frac{\partial^2\tilde{\phi}^0_1}{\partial\lambda_1^2} + \varepsilon^3\frac{1}{6}\frac{\partial^3\tilde{\phi}^0_1}{\partial\lambda_1^3} + \varepsilon^4\frac{1}{24}\frac{\partial^4\tilde{\phi}^0_1}{\partial\lambda_1^4}\\
\tilde{\phi}^{\varepsilon}_{O_2} &= \tilde{\phi}^0_2(\lambda_1,\lambda_2)\\
\tilde{\phi}^{\varepsilon}_{E_2} &= \tilde{\phi}^0_2(\lambda_1+\varepsilon,\lambda_2) = \tilde{\phi}^0_2 + \varepsilon\frac{\partial\tilde{\phi}^0_2}{\partial\lambda_1} + \varepsilon^2\frac{1}{2}\frac{\partial^2\tilde{\phi}^0_2}{\partial\lambda_1^2} + \varepsilon^3\frac{1}{6}\frac{\partial^3\tilde{\phi}^0_2}{\partial\lambda_1^3} + \varepsilon^4\frac{1}{24}\frac{\partial^4\tilde{\phi}^0_2}{\partial\lambda_1^4}
\end{aligned} \tag{3.58}$$

Note that in order to simplify writing, symbols $\tilde{U}^0$, $\tilde{V}^0$ and $\tilde{\phi}^0_1$, $\tilde{\phi}^0_2$, were used instead of $\tilde{U}^0(\lambda_1,\lambda_2)$, $\tilde{V}^0(\lambda_1,\lambda_2)$ and $\tilde{\phi}^0_1(\lambda_1,\lambda_2)$, $\tilde{\phi}^0_2(\lambda_1,\lambda_2)$.
Similar formulation are used by Rahali et al. in [92], from which higher properties of a pantographic lattice are obtained. They only develop the rotation at the first order, maintaining the subsequent terms are inessential; also the displacement are developed up to the second order. In the developments present here, displacement and rotation are fully expended and all terms in the asymptotic expansion are taken in account, leading to somewhat difference result, instead similar to the obtained by Boutin et al. in [77].
Substituting the expressions for the forces (3.53), (3.55) and (3.57) in equation (3.50), we obtain the P.V.W. in the macroscopic field:

$$
\begin{aligned}
&\varepsilon^2 \sum_{\nu\in\mathcal{Z}} \Big[N^1_{E_1} \frac{\partial \tilde{U}^0}{\partial \lambda_1} + T^1_{E_1} \frac{\partial \tilde{V}^0}{\partial \lambda_1} + N^1_{E_2} \frac{\partial \tilde{V}^0}{\partial \lambda_2} - T^1_{E_2} \frac{\partial \tilde{U}^0}{\partial \lambda_2} + \left(M^2_{E_1} + M^2_{O_1} \right) \tilde{\phi}^0_1 + \left(M^2_{E_2} + M^2_{O_2} \right) \tilde{\phi}^0_2 \Big] + \\
&+\varepsilon^3 \sum_{\nu\in\mathcal{Z}} \Big[\frac{1}{2} N^1_{E_1} \frac{\partial^2 \tilde{U}^0}{\partial \lambda_1^2} + N^2_{E_1} \frac{\partial \tilde{U}^0}{\partial \lambda_1} + \frac{1}{2} T^1_{E_1} \frac{\partial^2 \tilde{V}^0}{\partial \lambda_1^2} + T^2_{E_1} \frac{\partial \tilde{V}^0}{\partial \lambda_1} + \frac{1}{2} N^1_{E_2} \frac{\partial^2 \tilde{V}^0}{\partial \lambda_2^2} + N^2_{E_2} \frac{\partial \tilde{V}^0}{\partial \lambda_2} + \\
&\quad - \frac{1}{2} T^1_{E_2} \frac{\partial^2 \tilde{U}^0}{\partial \lambda_2^2} - T^2_{E_2} \frac{\partial \tilde{U}^0}{\partial \lambda_2} + M^2_{E_1} \frac{\partial \tilde{\phi}^0_1}{\partial \lambda_1} + M^2_{E_2} \frac{\partial \tilde{\phi}^0_2}{\partial \lambda_2} + \left(M^3_{E_1} + M^3_{O_1} \right) \tilde{\phi}^0_1 + \left(M^3_{E_2} + M^3_{O_2} \right) \tilde{\phi}^0_2 \Big] + \\
&+\varepsilon^4 \sum_{\nu\in\mathcal{Z}} \Big[\frac{1}{6} N^1_{E_1} \frac{\partial^3 \tilde{U}^0}{\partial \lambda_1^3} + \frac{1}{2} N^2_{E_1} \frac{\partial^2 \tilde{U}^0}{\partial \lambda_1^2} + N^3_{E_1} \frac{\partial \tilde{U}^0}{\partial \lambda_1} + \frac{1}{6} T^1_{E_1} \frac{\partial^3 \tilde{V}^0}{\partial \lambda_1^3} + \frac{1}{2} T^2_{E_1} \frac{\partial^2 \tilde{V}^0}{\partial \lambda_1^2} + T^3_{E_1} \frac{\partial \tilde{V}^0}{\partial \lambda_1} + \\
&\quad + \frac{1}{6} N^1_{E_2} \frac{\partial^3 \tilde{V}^0}{\partial \lambda_2^3} + \frac{1}{2} N^2_{E_2} \frac{\partial^2 \tilde{V}^0}{\partial \lambda_2^2} + N^3_{E_2} \frac{\partial \tilde{V}^0}{\partial \lambda_2} - \frac{1}{6} T^1_{E_2} \frac{\partial^3 \tilde{U}^0}{\partial \lambda_2^3} - \frac{1}{2} T^2_{E_2} \frac{\partial^2 \tilde{U}^0}{\partial \lambda_2^2} - T^3_{E_2} \frac{\partial \tilde{U}^0}{\partial \lambda_2} + \\
&\quad + \frac{1}{2} M^2_{E_1} \frac{\partial^2 \tilde{\phi}^0_1}{\partial \lambda_1^2} + M^3_{E_1} \frac{\partial \tilde{\phi}^0_1}{\partial \lambda_1} + \left(M^4_{E_1} + M^4_{O_1} \right) \tilde{\phi}^0_1 + \left(M^4_{E_2} + M^4_{O_2} \right) \tilde{\phi}^0_2 + \frac{1}{2} M^2_{E_2} \frac{\partial^2 \tilde{\phi}^0_2}{\partial \lambda_2^2} + M^3_{E_2} \frac{\partial \tilde{\phi}^0_2}{\partial \lambda_2} \Big] + \\
&-\varepsilon^2 \sum_{\nu\in\mathcal{Z}} \sum_{n\in\mathcal{N}} f^{e,n} \tilde{U}^0 - \sum_{\nu\in\mathcal{Z}} \sum_{n\in\mathcal{N}} f^{e,n} \tilde{V}^0 = 0 \qquad \forall \tilde{U}^0, \tilde{V}^0, \tilde{\phi}^0_1, \tilde{\phi}^0_2
\end{aligned}
\tag{3.59}
$$

In equation (3.59) the axial, the shear forces and the bending moments depends on the macroscopic variable $U^0(\lambda_1, \lambda_2)$, $V^0(\lambda_1, \lambda_2)$ and on the microscopic variable $u^i_n(\lambda_1, \lambda_2)$, $v^i_n(\lambda_1, \lambda_2)$, $\phi^i_n(\lambda_1, \lambda_2)$. Hence, if we want to find the constitutive law of the homogenized continuum we need to express the microscopic variable as a function of macroscopic variable. Or in other words, we need to find the self-equilibrium equations at the micro-scale.
2. Taking the virtual displacement and the virtual rotation in the micro field $\tilde{u}^\varepsilon_n = \varepsilon \tilde{u}^1_n \vartheta_x(\lambda_1, \lambda_2)$, $\tilde{v}^\varepsilon_n = \varepsilon \tilde{v}^1_n \vartheta_y(\lambda_1, \lambda_2)$, $\tilde{\phi}^\varepsilon_1 = \varepsilon \tilde{\phi}^1_1 \eta_x(\lambda_1, \lambda_2)$ and $\tilde{\phi}^\varepsilon_2 = \varepsilon \tilde{\phi}^1_2 \eta_y(\lambda_1, \lambda_2)$, where $\tilde{v}^1_n$, $\tilde{v}^1_n$, $\tilde{\phi}^1_1$ and $\tilde{\phi}^1_2$ are periodical, while $\vartheta_x(\lambda_1, \lambda_2)$, $\vartheta_y(\lambda_1, \lambda_2)$, $\eta_x(\lambda_1, \lambda_2)$ and $\eta_y(\lambda_1, \lambda_2)$ depend only on the macroscopic field and are zero at the boundary, we find:

$$
\begin{aligned}
&\tilde{u}^\varepsilon_{O_1} = \tilde{u}^\varepsilon_{O_2} = \varepsilon \tilde{u}^1_1 \vartheta_x(\lambda_1, \lambda_2) \\
&\tilde{u}^\varepsilon_{E_1} = \varepsilon \tilde{u}^1_1 \vartheta_x(\lambda_1 + \varepsilon, \lambda_2) = \tilde{u}^1_1 \left(\varepsilon \vartheta_x + \varepsilon^2 \frac{\partial \vartheta_x}{\partial \lambda_1} + \varepsilon^3 \frac{1}{2} \frac{\partial^2 \vartheta_x}{\partial \lambda_1^2} + \varepsilon^4 \frac{1}{6} \frac{\partial^3 \vartheta_x}{\partial \lambda_1^3} \right) \\
&\tilde{u}^\varepsilon_{E_2} = \varepsilon \tilde{u}^1_1 \vartheta_x(\lambda_1, \lambda_2 + \varepsilon) = \tilde{u}^1_1 \left(\varepsilon \vartheta_x + \varepsilon^2 \frac{\partial \vartheta_x}{\partial \lambda_2} + \varepsilon^3 \frac{1}{2} \frac{\partial^2 \vartheta_x}{\partial \lambda_2^2} + \varepsilon^4 \frac{1}{6} \frac{\partial^3 \vartheta_x}{\partial \lambda_2^3} \right) \\
&\tilde{v}^\varepsilon_{O_1} = \tilde{v}^\varepsilon_{O_{b2}} = \varepsilon \tilde{v}^1_1 \vartheta_y(\lambda_1, \lambda_2) \\
&\tilde{v}^\varepsilon_{E_1} = \varepsilon \tilde{v}^1_1 \vartheta_y(\lambda_1 + \varepsilon, \lambda_2) = \tilde{v}^1_1 \left(\varepsilon \vartheta_y + \varepsilon^2 \frac{\partial \vartheta_y}{\partial \lambda_1} + \varepsilon^3 \frac{1}{2} \frac{\partial^2 \vartheta_y}{\partial \lambda_1^2} + \varepsilon^4 \frac{1}{6} \frac{\partial^3 \vartheta_y}{\partial \lambda_1^3} \right) \\
&\tilde{v}^\varepsilon_{E_2} = \varepsilon \tilde{v}^1_1 \vartheta_y(\lambda_1, \lambda_2 + \varepsilon) = \tilde{v}^1_1 \left(\varepsilon \vartheta_y + \varepsilon^2 \frac{\partial \vartheta_y}{\partial \lambda_2} + \varepsilon^3 \frac{1}{2} \frac{\partial^2 \vartheta_y}{\partial \lambda_2^2} + \varepsilon^4 \frac{1}{6} \frac{\partial^3 \vartheta_y}{\partial \lambda_2^3} \right)
\end{aligned}
$$

$$\tilde{\phi}^{\varepsilon}_{O_1} = \varepsilon\tilde{\phi}^1_1\eta_x(\lambda_1,\lambda_2)$$
$$\tilde{\phi}^{\varepsilon}_{E_1} = \varepsilon\tilde{\phi}^1_1\eta_x(\lambda_1+\varepsilon,\lambda_2) = \tilde{\phi}^1_1\left(\varepsilon\eta_x + \varepsilon^2\frac{\partial\eta_x}{\partial\lambda_1} + \varepsilon^3\frac{1}{2}\frac{\partial^2\eta_x}{\partial\lambda_1^2} + \varepsilon^4\frac{1}{6}\frac{\partial^3\eta_x}{\partial\lambda_1^3}\right)$$
$$\tilde{\phi}^{\varepsilon}_{O_2} = \varepsilon\tilde{\phi}^1_2\eta_y(\lambda_1,\lambda_2)$$
$$\tilde{\phi}^{\varepsilon}_{E_2} = \varepsilon\tilde{\phi}^1_2\eta_y(\lambda_1+\varepsilon,\lambda_2) = \tilde{\phi}^1_2\left(\varepsilon\eta_y + \varepsilon^2\frac{\partial\eta_y}{\partial\lambda_1} + \varepsilon^3\frac{1}{2}\frac{\partial^2\eta_y}{\partial\lambda_1^2} + \varepsilon^4\frac{1}{6}\frac{\partial^3\eta_y}{\partial\lambda_1^3}\right)$$

Therefore, the P.V.W. becomes:

$$\begin{aligned}
&\varepsilon^3\sum_{\nu\in\mathcal{Z}}\Big[\left(N^1_{E_1}\frac{\partial\vartheta_x}{\partial\lambda_1} - T^1_{E_2}\frac{\partial\vartheta_x}{\partial\lambda_2}\right)\tilde{u}^1_1 + \left(T^1_{E_1}\frac{\partial\vartheta_y}{\partial\lambda_1} + N^1_{E_2}\frac{\partial\vartheta_y}{\partial\lambda_2}\right)\tilde{v}^1_1 + \\
&\quad + \left(M^2_{E_1} + M^2_{O_1}\right)\tilde{\phi}^1_1\eta_x + \left(M^2_{E_2} + M^2_{O_2}\right)\tilde{\phi}^1_2\eta_y\Big] + \\
&+\varepsilon^4\sum_{\nu\in\mathcal{Z}}\Big[\left(\frac{1}{2}N^1_{E_1}\frac{\partial^2\vartheta_x}{\partial\lambda_1^2} + N^2_{E_1}\frac{\partial\vartheta_x}{\partial\lambda_1} - \frac{1}{2}T^1_{E_2}\frac{\partial^2\vartheta_x}{\partial\lambda_2^2} - T^2_{E_2}\frac{\partial\vartheta_x}{\partial\lambda_2}\right)\tilde{u}^1_1 + \\
&\quad + \left(\frac{1}{2}T^1_{E_{b1}}\frac{\partial^2\vartheta_y}{\partial\lambda_1^2} + T^2_{E_1}\frac{\partial\vartheta_y}{\partial\vartheta_y\lambda_1} + \frac{1}{2}N^1_{E_2}\frac{\partial^2\vartheta_y}{\partial\lambda_2^2} + N^2_{E_2}\frac{\partial\vartheta_y}{\partial\lambda_2}\right)\tilde{v}^1_1 + \\
&\quad + \left(M^2_{E_1}\frac{\partial\eta_x}{\partial\lambda_1} + \left(M^3_{E_1} + M^3_{O_1}\right)\eta_x\right)\tilde{\phi}^1_1 + \left(M^2_{E_2}\frac{\partial\eta_y}{\partial\lambda_2} + \left(M^3_{E_2} + M^3_{O_2}\right)\eta_y\right)\tilde{\phi}^1_2\Big] + \\
&+\varepsilon^5\sum_{\nu\in\mathcal{Z}}\Big[\left(\frac{1}{6}N^1_{E_1}\frac{\partial^3\vartheta_x}{\partial\lambda_1^3} + \frac{1}{2}N^2_{E_1}\frac{\partial^2\vartheta_x}{\partial\lambda_1^2} + N^3_{E_1}\frac{\partial\vartheta_x}{\partial\lambda_1} - \frac{1}{6}T^1_{E_2}\frac{\partial^3\vartheta_x}{\partial\lambda_2^3} - \frac{1}{2}T^2_{E_2}\frac{\partial^2\vartheta_x}{\partial\lambda_2^2} - T^3_{E_2}\frac{\partial\vartheta_x}{\partial\lambda_2}\right)\tilde{u}^1_1 + \\
&\quad + \left(\frac{1}{6}N^1_{E_2}\frac{\partial^3\vartheta_y}{\partial\lambda_2^3} + \frac{1}{2}N^2_{E_2}\frac{\partial^2\vartheta_y}{\partial\lambda_2^2} + N^3_{E_2}\frac{\partial\vartheta_y}{\partial\lambda_2} + \frac{1}{6}T^1_{E_1}\frac{\partial^3\vartheta_y}{\partial\lambda_1^3} + \frac{1}{2}T^2_{E_1}\frac{\partial^2\vartheta_y}{\partial\lambda_1^2} + T^3_{E_1}\frac{\partial\vartheta_y}{\partial\lambda_1}\right)\tilde{v}^1_1 + \\
&\quad + \left(\frac{1}{2}M^2_{E_1}\frac{\partial^2\eta_x}{\partial\lambda_1^2} + M^3_{E_1}\frac{\partial\eta_x}{\partial\lambda_1} + \left(M^4_{E_1} + M^4_{O_1}\right)\eta_x\right)\tilde{\phi}^1_1 + \\
&\quad + \left(\frac{1}{2}M^2_{E_2}\frac{\partial^2\eta_y}{\partial\lambda_2^2} + M^3_{E_2}\frac{\partial\eta_y}{\partial\lambda_2} + \left(M^4_{E_2} + M^4_{O_2}\right)\eta_y\right)\tilde{\phi}^1_2\Big] = 0 \qquad \forall\tilde{u}^1_1\vartheta_x, \tilde{v}^1_1\vartheta_y, \tilde{\phi}^1_1\eta_x, \tilde{\phi}^1_2\eta_y
\end{aligned} \tag{3.60}$$

For $\varepsilon^2 \to 0$ the summation $\sum_{\nu\in\mathcal{Z}}$ becomes an integral, therefore at order ε we have the following expression:

$$\begin{aligned}
\varepsilon\int_\Lambda\Big[&\left(N^1_{E_1}\frac{\partial\vartheta_x}{\partial\lambda_1} - T^1_{E_2}\frac{\partial\vartheta_x}{\partial\lambda_2}\right)\tilde{u}^1_1 + \left(T^1_{E_1}\frac{\partial\vartheta_y}{\partial\lambda_1} + N^1_{E_2}\frac{\partial\vartheta_y}{\partial\lambda_2}\right)\tilde{v}^1_1 + \\
&\left(M^2_{E_1} + M^2_{O_1}\right)\tilde{\phi}^1_1\eta_x + \left(M^2_{E_2} + M^2_{O_2}\right)\tilde{\phi}^1_2\eta_y\Big]d\lambda_1 d\lambda_2 = 0 \\
&\forall\tilde{u}^1_1\vartheta_x, \tilde{v}^1_1\vartheta_y, \tilde{\phi}^1_1\eta_x, \tilde{\phi}^1_2\eta_y
\end{aligned} \tag{3.61}$$

After applying integration by parts in the left hand side of equation (3.61) we obtain the following system of equations:

$$\begin{cases} \left(\dfrac{\partial N^1_{E_1}}{\partial \lambda_1} - \dfrac{\partial T^1_{E_2}}{\partial \lambda_2}\right)\vartheta_x \tilde{u}^1_1 = 0 \\ \left(\dfrac{\partial T^1_{E_1}}{\partial \lambda_1} + \dfrac{\partial N^1_{E_2}}{\partial \lambda_2}\right)\vartheta_y \tilde{v}^1_1 = 0 \\ \left(M^2_{E_1} + M^2_{O_1}\right)\tilde{\phi}^1_1 \eta_x = 0 \\ \left(M^2_{E_2} + M^2_{O_2}\right)\tilde{\phi}^1_2 \eta_y = 0 \end{cases} \tag{3.62}$$

Substituting equations (3.53) and (3.55) in equation (3.62), we obtain

$$\begin{cases} -k_{a1}\dfrac{\partial^2 U^0}{\partial \lambda_1^2} = 0 \\ -k_{a2}\dfrac{\partial^2 V^0}{\partial \lambda_2^2} = 0 \\ \tilde{\phi}^0_1 = \dfrac{1}{l_1}\dfrac{\partial V^0}{\partial \lambda_1} \\ \tilde{\phi}^0_2 = -\dfrac{1}{l_2}\dfrac{\partial U^0}{\partial \lambda_2} \end{cases} \tag{3.63}$$

Following the same steps at order 2 in ε we obtain:

$$\begin{aligned} \varepsilon^2 \int_\Lambda \Big[& \left(\frac{1}{2}N^1_{E_1}\frac{\partial^2 \vartheta_x}{\partial \lambda_1^2} + N^2_{E_1}\frac{\partial \vartheta_x}{\partial \lambda_1} - \frac{1}{2}T^1_{E_2}\frac{\partial^2 \vartheta_x}{\partial \lambda_2^2} - T^2_{E_2}\frac{\partial \vartheta_x}{\partial \lambda_2}\right)\tilde{u}^1_1 + \\ & + \left(\frac{1}{2}T^1_{E_1}\frac{\partial^2 \vartheta_y}{\partial \lambda_1^2} + T^2_{E_1}\frac{\partial \vartheta_y}{\partial \lambda_1} + \frac{1}{2}N^1_{E_2}\frac{\partial^2 \vartheta_y}{\partial \lambda_2^2} + N^2_{E_2}\frac{\partial \vartheta_y}{\partial \lambda_2}\right)\tilde{v}^1_1 + \\ & + \left(M^2_{E_1}\frac{\partial \eta_x}{\partial \lambda_1} + \left(M^3_{E_1} + M^3_{O_1}\right)\eta_x\right)\tilde{\phi}^1_1 + \left(M^2_{E_2}\frac{\partial \eta_y}{\partial \lambda_2} + \left(M^3_{E_2} + M^3_{O_2}\right)\eta_y\right)\tilde{\phi}^1_2 \Big] d\lambda_1 d\lambda_2 = 0 \end{aligned} \tag{3.64}$$

$$\begin{cases} \left(\dfrac{1}{2}\dfrac{\partial^2 N^1_{E_1}}{\partial \lambda_1^2} - \dfrac{\partial N^2_{E_1}}{\partial \lambda_1} - \dfrac{1}{2}\dfrac{\partial^2 T^1_{E_2}}{\partial \lambda_2^2} + \dfrac{\partial T^2_{E_2}}{\partial \lambda_2}\right)\vartheta_x \tilde{u}^1_1 = 0 \\ \left(\dfrac{1}{2}\dfrac{\partial^2 T^1_{E_1}}{\partial \lambda_1^2} - \dfrac{\partial T^2_{E_1}}{\partial \lambda_1} + \dfrac{1}{2}\dfrac{\partial^2 N^1_{E_2}}{\partial \lambda_2^2} - \dfrac{\partial N^2_{E_2}}{\partial \lambda_2}\right)\vartheta_y \tilde{v}^1_1 = 0 \\ \left(M^3_{E_1} + M^3_{O_1} - \dfrac{\partial M^2_{E_1}}{\partial \lambda_1}\right)\eta_x \tilde{\phi}^1_1 = 0 \\ \left(M^3_{E_2} + M^3_{O_2} - \dfrac{\partial M^2_{E_2}}{\partial \lambda_2}\right)\eta_y \tilde{\phi}^1_2 = 0 \end{cases} \tag{3.65}$$

Substitution of equations (3.53) and (3.55) in equation (3.65), yields:

$$\begin{cases} -k_{a1}\dfrac{\partial^2 u^1}{\partial \lambda_1^2} = 0 \\ -k_{a2}\dfrac{\partial^2 v^1}{\partial \lambda_2^2} = 0 \\ \tilde{\phi}_1^1 = \dfrac{1}{l_1}\dfrac{\partial v^1}{\partial \lambda_1} \\ \tilde{\phi}_2^1 = -\dfrac{1}{l_2}\dfrac{\partial u^1}{\partial \lambda_2} \end{cases} \tag{3.66}$$

At the order 3 in ε we obtain:

$$\begin{aligned} \varepsilon^3 \int_\Lambda \Big[& \left(\frac{1}{6} N_{E_1}^1 \frac{\partial^3 \vartheta_x}{\partial \lambda_1^3} + \frac{1}{2} N_{E_1}^2 \frac{\partial^2 \vartheta_x}{\partial \lambda_1^2} + N_{E_1}^3 \frac{\partial \vartheta_x}{\partial \lambda_1} - \frac{1}{6} T_{E_2}^1 \frac{\partial^3 \vartheta_x}{\partial \lambda_2^3} - \frac{1}{2} T_{E_2}^2 \frac{\partial^2 \vartheta_x}{\partial \lambda_2^2} - T_{E_2}^3 \frac{\partial \vartheta_x}{\partial \lambda_2} \right) \tilde{u}_1^1 + \\ & + \left(\frac{1}{6} N_{E_2}^1 \frac{\partial^3 \vartheta_y}{\partial \lambda_2^3} + \frac{1}{2} N_{E_2}^2 \frac{\partial^2 \vartheta_y}{\partial \lambda_2^2} + N_{E_2}^3 \frac{\partial \vartheta_y}{\partial \lambda_2} + \frac{1}{6} T_{E_1}^1 \frac{\partial^3 \vartheta_y}{\partial \lambda_1^3} + \frac{1}{2} T_{E_1}^2 \frac{\partial^2 \vartheta_y}{\partial \lambda_1^2} + T_{E_1}^3 \frac{\partial \vartheta_y}{\partial \lambda_1} \right) \tilde{v}_1^1 + \\ & + \left(\frac{1}{2} M_{E_1}^2 \frac{\partial^2 \eta_x}{\partial \lambda_1^2} + M_{E_1}^3 \frac{\partial \eta_x}{\partial \lambda_1} + \left(M_{E_1}^4 + M_{O_1}^4 \right) \eta_x \right) \tilde{\phi}_1^1 + \\ & + \left(\frac{1}{2} M_{E_2}^2 \frac{\partial^2 \eta_y}{\partial \lambda_2^2} + M_{E_2}^3 \frac{\partial \eta_y}{\partial \lambda_2} + \left(M_{E_2}^4 + M_{O_2}^4 \right) \eta_y \right) \tilde{\phi}_2^1 \Big] d\lambda_1 d\lambda_2 = 0 \end{aligned} \tag{3.67}$$

$$\begin{cases} \left(-\dfrac{1}{6}\dfrac{\partial^3 N_{E_1}^1}{\partial \lambda_1^3} + \dfrac{1}{2}\dfrac{\partial^2 N_{E_1}^2}{\partial \lambda_1^2} - \dfrac{\partial N_{E_1}^3}{\partial \lambda_1} + \dfrac{1}{6}\dfrac{\partial^3 T_{E_2}^1}{\partial \lambda_2^3} - \dfrac{1}{2}\dfrac{\partial^2 T_{E_2}^2}{\partial \lambda_2^2} + \dfrac{\partial T_{E_2}^3}{\partial \lambda_2} \right) \vartheta_x \tilde{u}_1^1 = 0 \\ \left(-\dfrac{1}{6}\dfrac{\partial^3 N_{E_2}^1}{\partial \lambda_2^3} + \dfrac{1}{2}\dfrac{\partial^2 N_{E_2}^2}{\partial \lambda_2^2} - \dfrac{\partial N_{E_2}^3}{\partial \lambda_2} - \dfrac{1}{6}\dfrac{\partial^3 T_{E_1}^1}{\partial \lambda_1^3} + \dfrac{1}{2}\dfrac{\partial^2 T_{E_1}^2}{\partial \lambda_1^2} - \dfrac{\partial T_{E_1}^3}{\partial \lambda_1} \right) \vartheta_y \tilde{v}_1^1 = 0 \\ \left(M_{E_1}^4 + M_{O_1}^4 + \dfrac{1}{2}\dfrac{\partial^2 M_{E_1}^2}{\partial \lambda_1^2} - \dfrac{\partial M_{E_1}^3}{\partial \lambda_1} \right) \eta_x \tilde{\phi}_1^1 = 0 \\ \left(M_{E_2}^4 + M_{O_2}^4 + \dfrac{1}{2}\dfrac{\partial^2 M_{E_2}^2}{\partial \lambda_2^2} - \dfrac{\partial M_{E_2}^3}{\partial \lambda_2} \right) \eta_y \tilde{\phi}_2^1 = 0 \end{cases} \tag{3.68}$$

Substitution of equations (3.53) and (3.55) in equation (3.68), gives the balance equation and the expressions of the rotations at this order:

$$\begin{cases} -k_{a1}\left(\dfrac{1}{12}\dfrac{\partial^4 U^0}{\partial\lambda_1^4}+\dfrac{\partial^2 u^2}{\partial\lambda_1^2}\right)+\dfrac{1}{6}k_{f2}\dfrac{\partial^4 U^0}{\partial\lambda_2^4}=0 \\ -k_{a2}\left(\dfrac{1}{12}\dfrac{\partial^4 V^0}{\partial\lambda_2^4}+\dfrac{\partial^2 v^2}{\partial\lambda_2^2}\right)+\dfrac{1}{6}k_{f1}\dfrac{\partial^4 V^0}{\partial\lambda_1^4}=0 \\ \tilde{\phi}_1^2=\dfrac{1}{l_1}\dfrac{\partial v^2}{\partial\lambda_1} \\ \tilde{\phi}_2^2=-\dfrac{1}{l_2}\dfrac{\partial u^2}{\partial\lambda_2} \end{cases} \tag{3.69}$$

In this way we have obtained the variable at the micro-scale as a function of the macro-scale variable and the balance equation for the different orders. Adding the balance equations ((3.63) to (3.69)), we obtain the following balance equations at different orders:

$$\begin{aligned} &-\varepsilon k_{a1}\frac{\partial^2 U^0}{\partial\lambda_1^2}+\varepsilon^3\left[-k_{a1}\left(\frac{1}{12}\frac{\partial^4 U^0}{\partial\lambda_1^4}+\frac{\partial^2 u^2}{\partial\lambda_1^2}\right)+\frac{1}{6}k_{f2}\frac{\partial^4 U^0}{\partial\lambda_2^4}\right]=0 \\ &-\varepsilon k_{a2}\frac{\partial^2 V^0}{\partial\lambda_2^2}+\varepsilon^3\left[-k_{a2}\left(\frac{1}{12}\frac{\partial^4 V^0}{\partial\lambda_2^4}+\frac{\partial^2 v^2}{\partial\lambda_2^2}\right)+\frac{1}{6}k_{f1}\frac{\partial^4 V^0}{\partial\lambda_1^4}\right]=0 \end{aligned} \tag{3.70}$$

This result, similarly to the one found in [77], was obtained because we implicitly used the hypothesis that

$$\begin{aligned} \frac{\partial U^0}{\partial\lambda_1}&=O\left(\frac{\partial U^0}{\partial\lambda_2}\right) \\ \frac{\partial V^0}{\partial\lambda_2}&=O\left(\frac{\partial V^0}{\partial\lambda_1}\right) \end{aligned} \tag{3.71}$$

This hypothesis is natural in the continuum mechanics. However, in pantographic sheets, formed by beam like elements, the transverse gradient $\dfrac{\partial U^0}{\partial\lambda_2}$ dominates in comparison to the axial gradient $\dfrac{\partial U^0}{\partial\lambda_1}$ that is:

$$\begin{aligned} \frac{\partial U^0}{\partial\lambda_1}&\ll\frac{\partial U^0}{\partial\lambda_2} \\ \frac{\partial V^0}{\partial\lambda_2}&\ll\frac{\partial V^0}{\partial\lambda_1} \end{aligned} \tag{3.72}$$

Hence, in order to model the behaviour of this material we need to use the hypothesis that

$$\begin{aligned}\frac{\partial U^0}{\partial \lambda_1} &\sim \varepsilon(\frac{\partial U^0}{\partial \lambda_2})\\ \frac{\partial V^0}{\partial \lambda_2} &\sim \varepsilon(\frac{\partial V^0}{\partial \lambda_1})\end{aligned} \tag{3.73}$$

$$\begin{aligned}\frac{\partial^2 U^0}{\partial \lambda_1^2} &\sim \varepsilon^2(\frac{\partial^2 U^0}{\partial \lambda_2^2})\\ \frac{\partial^2 V^0}{\partial \lambda_2^2} &\sim \varepsilon^2(\frac{\partial^2 V^0}{\partial \lambda_1^2})\end{aligned} \tag{3.74}$$

The presence of a higher contrast in the components of the strain tensor, as given by expression (3.73) is unconventional in the elastic composite medium but naturally arises in the case of weakly compressible viscous fluids, where the trace of the strain rate tensor is negligible compared to its deviatoric component, and in beams and plates, where the deformation in the section of the beam in the thickness of the plates are negligible.
Replacing the estimate (3.73) in the expression (3.70) we find that at the leading order

$$\begin{aligned}\varepsilon^3\left(\frac{1}{6}k_{f2}\frac{\partial^4 U^0}{\partial \lambda_2^4} - k_{a1}\frac{\partial^2 U^0}{\partial \lambda_1^2}\right) = 0\\ \varepsilon^3\left(\frac{1}{6}k_{f1}\frac{\partial^4 V^0}{\partial \lambda_1^4} - k_{a2}\frac{\partial^2 V^0}{\partial \lambda_2^2}\right) = 0\end{aligned} \tag{3.75}$$

The expressions (3.75) are the balance equations of the second order of homogenized continuum, similar result was obtain with the strong formulation by Boutin et al [77].
In order to get the constitutive law at the macro-scale, we substitute the rotation estimated for the micro-scale, equations (3.62), (3.65) and (3.68) in equation (3.60):

$$
\begin{aligned}
&\varepsilon^2 \sum_{\nu\in\mathcal{Z}} \left[N^1_{E_1} \frac{\partial \tilde{U}^0}{\partial \lambda_1} + N^1_{E_2} \frac{\partial \tilde{V}^0}{\partial \lambda_2} \right] + \\
&+\varepsilon^3 \sum_{\nu\in\mathcal{Z}} \left[\frac{1}{2} N^1_{E_1} \frac{\partial^2 \tilde{U}^0}{\partial \lambda_1^2} + N^2_{E_1} \frac{\partial \tilde{U}^0}{\partial \lambda_1} + \frac{1}{2} N^1_{E_2} \frac{\partial^2 \tilde{V}^0}{\partial \lambda_2^2} + N^2_{E_2} \frac{\partial \tilde{V}^0}{\partial \lambda_2} \right] + \\
&+\varepsilon^4 \sum_{\nu\in\mathcal{Z}} \left[\frac{1}{6} N^1_{E_1} \frac{\partial^3 \tilde{U}^0}{\partial \lambda_1^3} + \frac{1}{2} N^2_{E_1} \frac{\partial^2 \tilde{U}^0}{\partial \lambda_1^2} + N^3_{E_1} \frac{\partial \tilde{U}^0}{\partial \lambda_1} + \right. \\
&\quad + \frac{1}{6} N^1_{E_2} \frac{\partial^3 \tilde{V}^0}{\partial \lambda_2^3} + \frac{1}{2} N^2_{E_2} \frac{\partial^2 \tilde{V}^0}{\partial \lambda_2^2} + N^3_{E_2} \frac{\partial \tilde{V}^0}{\partial \lambda_2} + \\
&\quad \left. + M^3_{E_1} \frac{\partial \tilde{\phi}^0_1}{\partial \lambda_1} + M^3_{E_2} \frac{\partial \tilde{\phi}^0_2}{\partial \lambda_2} \right] + \\
&-\varepsilon^2 \sum_{\nu\in\mathcal{Z}} \sum_{n\in\mathcal{N}} f^{e,n} \tilde{U}^0 - \sum_{\nu\in\mathcal{Z}} \sum_{n\in\mathcal{N}} f^{e,n} \tilde{V}^0 = 0 \qquad \forall \tilde{U}^0, \tilde{V}^0, \tilde{\phi}^0_1, \tilde{\phi}^0_2.
\end{aligned}
\tag{3.76}
$$

For $\varepsilon^2 \to 0$ the sum becomes an integral, therefore we have

$$
\begin{aligned}
&\int_\Lambda \left(N^1_{E_1} \frac{\partial \tilde{U}^0}{\partial \lambda_1} + N^1_{E_2} \frac{\partial \tilde{V}^0}{\partial \lambda_2} \right) d\lambda_1 d\lambda_2 + \\
&+\varepsilon \int_\Lambda \Big[\frac{1}{2} N^1_{E_1} \frac{\partial^2 \tilde{U}^0}{\partial \lambda_1^2} + N^2_{E_1} \frac{\partial \tilde{U}^0}{\partial \lambda_1} + \frac{1}{2} N^1_{E_2} \frac{\partial^2 \tilde{V}^0}{\partial \lambda_2^2} + N^2_{E_2} \frac{\partial \tilde{V}^0}{\partial \lambda_2} \Big] d\lambda_1 d\lambda_2 + \\
&+\varepsilon^2 \int_\Lambda \Big[\frac{1}{6} N^1_{E_1} \frac{\partial^3 \tilde{U}^0}{\partial \lambda_1^3} + \frac{1}{2} N^2_{E_1} \frac{\partial^2 \tilde{U}^0}{\partial \lambda_1^2} + N^3_{E_1} \frac{\partial \tilde{U}^0}{\partial \lambda_1} + \\
&\quad + \frac{1}{6} N^1_{E_2} \frac{\partial^3 \tilde{V}^0}{\partial \lambda_2^3} + \frac{1}{2} N^2_{E_2} \frac{\partial^2 \tilde{V}^0}{\partial \lambda_2^2} + N^3_{E_2} \frac{\partial \tilde{V}^0}{\partial \lambda_2} + M^3_{E_1} \frac{1}{l_1} \frac{\partial^2 \tilde{V}^0}{\partial \lambda_1^2} - M^3_{E_2} \frac{1}{l_2} \frac{\partial^2 \tilde{U}^0}{\partial \lambda_2^2} \Big] d\lambda_1 d\lambda_2 + \\
&- \int_\Lambda \Big[\sum_{n\in\mathcal{N}} f^{e,n} \tilde{U}^0 + \sum_{n\in\mathcal{N}} f^{e,n} \tilde{V}^0 \Big] d\lambda_1 d\lambda_2 = 0 \qquad \forall \tilde{U}^0, \tilde{V}^0.
\end{aligned}
\tag{3.77}
$$

Using the estimate 3.73, we obtain

$$
\begin{aligned}
&\varepsilon^2 \int_\Lambda \Big[\left(N^1_{E_1} \frac{\partial \tilde{U}^0}{\partial \lambda_1} + N^1_{E_2} \frac{\partial \tilde{V}^0}{\partial \lambda_2} \right) + M^3_{E_1} \frac{1}{l_1} \frac{\partial^2 \tilde{V}^0}{\partial \lambda_1^2} - M^3_{E_2} \frac{1}{l_2} \frac{\partial^2 \tilde{U}^0}{\partial \lambda_2^2} + \\
&\quad - \sum_{n\in\mathcal{N}} f^{e,n} \tilde{U}^0 - \sum_{n\in\mathcal{N}} f^{e,n} \tilde{V}^0 \Big] d\lambda_1 d\lambda_2 = 0 \quad \forall \tilde{U}^0, \tilde{V}^0
\end{aligned}
\tag{3.78}
$$

that, equating to the internal virtual work of the continuum and using the Jacobian of the transformation, as made in 3.19, we derive the components of the stress tensor in physical coordinates. In this case of a second gradient continuum the P.V.W., becomes:

$$\int_\Lambda S_{\alpha,\beta}\frac{\partial \tilde{\boldsymbol{u}}_\alpha}{\partial X_\beta}\cdot\hat{\boldsymbol{t}}_\alpha dX_1dX_2+\int_\Lambda S_{\alpha,\beta,\gamma}\frac{\partial^2\tilde{\boldsymbol{u}}_\alpha}{\partial X^2_{\beta,\gamma}}\cdot\hat{\boldsymbol{t}}_\alpha dX_1dX_2-\int_\Lambda \boldsymbol{f}^e\tilde{\boldsymbol{u}}dX_1dX_2=0 \tag{3.79}$$

For the first gradient, in Voight representation we have:

$$\begin{bmatrix}S_{XX}\\S_{YY}\\S_{XY}\\S_{YX}\end{bmatrix}=\begin{bmatrix}\frac{k_{a1}l_1}{l_2} & 0 & 0 & 0\\ 0 & \frac{k_{a2}l_2}{l_1} & 0 & 0\\ 0 & 0 & 0 & 0\\ 0 & 0 & 0 & 0\end{bmatrix}\begin{bmatrix}\frac{\partial U}{\partial X}\\ \frac{\partial V}{\partial Y}\\ \frac{\partial V}{\partial X}\\ \frac{\partial U}{\partial Y}\end{bmatrix} \tag{3.80}$$

For the second gradient, in Voight representation we have:

$$\begin{bmatrix}S_{XXX}\\S_{YXX}\\S_{XYX}\\S_{YYX}\\S_{XYY}\\S_{YYY}\end{bmatrix}=\begin{bmatrix}0 & 0 & 0 & 0 & 0 & 0\\ 0 & \frac{k_{f1}l_1^3}{6l_2} & 0 & 0 & 0 & 0\\ 0 & 0 & 0 & 0 & 0 & 0\\ 0 & 0 & 0 & 0 & 0 & 0\\ 0 & 0 & 0 & 0 & \frac{k_{f2}l_2^3}{6l_1} & 0\\ 0 & 0 & 0 & 0 & 0 & 0\end{bmatrix}\begin{bmatrix}\frac{\partial^2 U}{\partial X^2}\\ \frac{\partial^2 V}{\partial X^2}\\ \frac{\partial^2 U}{\partial X\partial Y}\\ \frac{\partial^2 V}{\partial X\partial Y}\\ \frac{\partial^2 U}{\partial Y^2}\\ \frac{\partial^2 V}{\partial Y^2}\end{bmatrix} \tag{3.81}$$

Note once more that $k_{fi}=\dfrac{6E_iI_i}{l_i^3}$ and $k_{ai}=\dfrac{E_iA_i}{l_i}$.

Remarks 9

The constitutive matrix (3.80) is singular, since the shear modulus is 0. This is a consequence of the presence of the pivot. Therefore, the existence of the solution depends on the boundary conditions of the problem considered.

The first gradient term, equation (3.80), would have been obtained if the hypotheses (3.73) and (3.74) would have not been made.

It is know, in fact, that the homogenization theory at the leading order procedures standard Cauchy material models. However, as was underlined in [86], different assumption on the relative magnitude of the rigidities of the elements can lead to alternative models reach like Kirchoff and Mindlin models can be obtained in shells with different hypothesis on the ratio between the shear and the bending stiffness.

In the present case, the effect of the pivots is enhance the bending deformation in the system, so that, in the limit of slender rod elements, like those didn't are considered in this section, the axial stiffness becomes dominant over the bending stiffness. This is the motivation of the hypothesis (3.73), (3.74), that lead to the second gradient model found in matrix (3.81).

Remarks 10

Experimental results from bias-test of tissues show that the bending deformation of the fibres is not negligible, see [93], [94], [31], [30], [24]. Therefore the assumption (3.74) holds true, and we need to add at the deformation also the second derivatives of displacement (3.80).
A higher gradient material is then obtained. Notice that in such case the obtained constitutive matrix is singular, and as a result the solution is strongly affected by boundary conditions, (this is typical however of micromorphic models).

3.6 Discussion on theoretical results

3.6.1 Evaluation of the contrast of anisotropy

The design of lattice structure, like woven fabrics and networks, with controlled anisotropy and mechanical properties is of critical importance for various applications. In order to evaluate the characteristic of anisotropy of networks having as elementary cell one of those examined in the previous sections, it is evaluated the constitutive response of the network to an uniaxial stress state applied along an axis ξ rotated by an angle θ respect to the axis X, always taken coincident with the direction of fibre 1, see figure 3.12.

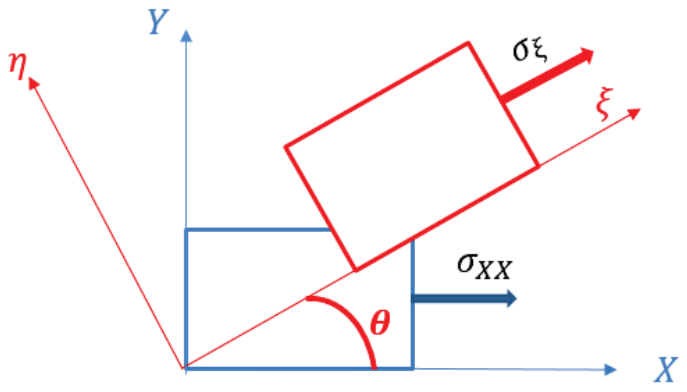

Figure 3.12: Evaluation of uniaxial stiffness as a function of rotation angle θ

The constitutive relation evaluated in the previous section are:

$$S = E\nabla \boldsymbol{U} \tag{3.82}$$

where S and $\nabla \boldsymbol{U}$ are respectively the stress tensor and the displacement gradient in the Cartesian system.

Applying at the equation (3.82) the rotation matrix (3.84) we obtain the constitutive relation in a rotated Cartesian system as follow:

$$\bar{S} = \bar{E}\bar{\nabla}\bar{\boldsymbol{U}} \tag{3.83}$$

$$\boldsymbol{R} = \begin{bmatrix} c^2 & s^2 & cs & cs \\ s^2 & c^2 & -cs & -cs \\ -cs & cs & c^2 & -s^2 \\ -cs & cs & -s^2 & c^2 \end{bmatrix} \tag{3.84}$$

where $\bar{E} = RER^{-1}$ and $c = \cos\theta$ and $s = \sin\theta$.

Applying the uniaxial stress $S_{\xi,\xi} = 1$, from equation (3.83) is obtained the strain state.

Denoting by $\epsilon_{\xi\xi} = \partial \boldsymbol{U}/\partial\xi$, the ratio $C_{\xi\xi} = \epsilon_{\xi\xi}/\sigma_{\xi\xi}$ represents the uniaxial compliance in the direction ξ, and its inverse is the uniaxial stiffness $D_{\xi\xi}$.
Their variation with the angle θ allows to evaluate the anisotropy of the network.

It will be exam the cases of:

- rectangular cell with rigid connection;
- skew cell with rigid connection;
- square and rectangular braced cell with rigid connection;
- square and rectangular braced cell with pivot.

Notation for rectangular and skew cell with rigid connection

In this section the case of the rectangular cell 3.3 and skew cell 3.2 are examined.

For both cases the following definitions are used:

$$\begin{aligned} k_{a1} &= \frac{E_1 A_1}{l_1} & k_{a2} &= \frac{E_2 A_2}{l_2} \\ k_{f1} &= \frac{6E_1 I_1}{l_1^3} & k_{f2} &= \frac{6E_2 I_2}{l_2^3} \\ A_1 &= h_1 s_1 & A_2 &= h_2 s_2 \qquad s_1 = s_2 = 1 \\ I_1 &= \frac{s_2 h_1^3}{12} & I_2 &= \frac{s_1 h_2^3}{12} \end{aligned} \tag{3.85}$$

Defining the dimensionless parameters

$$\alpha = \frac{l_2}{l_1} \quad \beta = \frac{h_2}{h_1} \quad \gamma = \frac{E_2}{E_1} \quad \lambda_1 = \frac{l_1}{h_1} \tag{3.86}$$

the expressions (3.85) become:

$$\begin{aligned} k_{a1} &= \frac{E_1}{\lambda_1} & k_{a2} &= \frac{\gamma\beta}{\alpha} k_{a1} \quad l_2 = \alpha l_1 \\ k_{f2} &= k_{f1}\gamma\left(\frac{\beta}{\alpha}\right)^3 & k_{f1} &= \frac{E_1}{2\lambda_1^3} \end{aligned} \tag{3.87}$$

Rectangular cell with rigid connection

In the case of a network with rectangular cell with rigid connection, the component $\varepsilon_{\xi\xi}$ of the deformation as a function of the angle θ is:

$$\varepsilon_{\xi\xi} = \frac{\lambda_1 \left[\cos 4\theta \left(-\alpha^2\lambda_1^2 - \alpha\beta^3\gamma\left(\lambda_1^2 - 1\right) + \beta^2\right) + \alpha\beta^3\gamma\left(\lambda_1^2 + 3\right) + 4\beta^2\cos 2\theta(\alpha\beta\gamma - 1) + 3\beta^2 + \alpha^2\lambda_1^2\right]}{8\beta^3\gamma E_1} \tag{3.88}$$

The uniaxial compliance and the uniaxial stiffness obtained from relation (3.88) are normalized with respect to the modulus E_1 and represented in polar plots in figures 3.13(a) and 3.13(b), respectively.

The different curves refer to cells having different length of the beams, equal section $\beta = 1$, equal modulus $\gamma = 1$, and slenderness $\lambda_1 = 5$.

The material examined shows an orthotropic behaviour, and the greater the ratio l_2/l_1 the larger is the contrast of anisotropy. This result derives from the fact that the rectangular cells elongated in the two-direction, the density of the fibres in that direction is greater.

From figure 3.13(a) it is seen that the direction of maximum compliance is at approximately 45° from the 1-axis. The same result are also reported in a linear plot in figures 3.13(c) and 3.13(d), when the ratio between the maximum and minimum stiffness or anisotropy is easier to calculate. The maximum stiffness at 0° is obtained for the square cell, and is equal to about $0.2D_1$

Skew cell with rigid connection

Polar plots of the dimensionless uniaxial compliance and stiffness are presented in figures 3.14 and 3.15, that examine the cases of cells with $l_2/l_1 = 1$ and $l_2/l_1 = 4$.
In each plot the results varying the angle α between the fibres in the range of $\pi/9, \pi/2$ are reported.

As a general comment, the skew cell, as expected, presents two direction of higher stiffness, coincident with the directions of the fibres.

However, when $l_2/l_1 = 1$, for small value of the angle α, the stiffness is almost uniform for all the directions $\theta \in (0, \alpha)$, while a bi-directionality of the cell is regained when α approaches $\pi/2$.

The same is yet true when $l_2/l_1 = 4$. In this case, the greatest stiffness is always reached along the direction 2, and a small peak of stiffness is detected in direction 1.

From the linear plots of figures 3.14(c) and 3.14(d) it is observed that the largest compliance occurs at an angle θ varying from $3/4\pi$ and $\pi/2$. The largest stiffness is obtained for $\alpha = \pi/9$, and reaches $0.6D_{11}$.

However, in this case the contrast of anisotropy is very large. Similar results are obtained for a skew cell with $l_2/l_1 = 4$ (figure 3.15), but in this case the contrast of anisotropies is much larger.

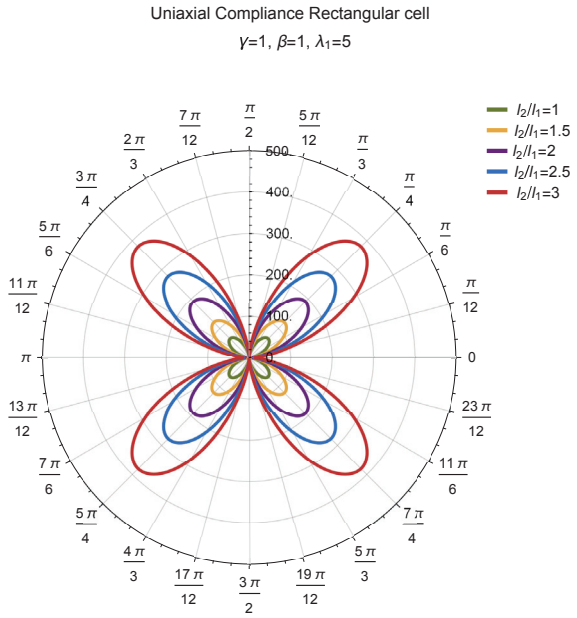

(a) Polar plot of the uniaxial compliance $\epsilon_{\xi\xi}$

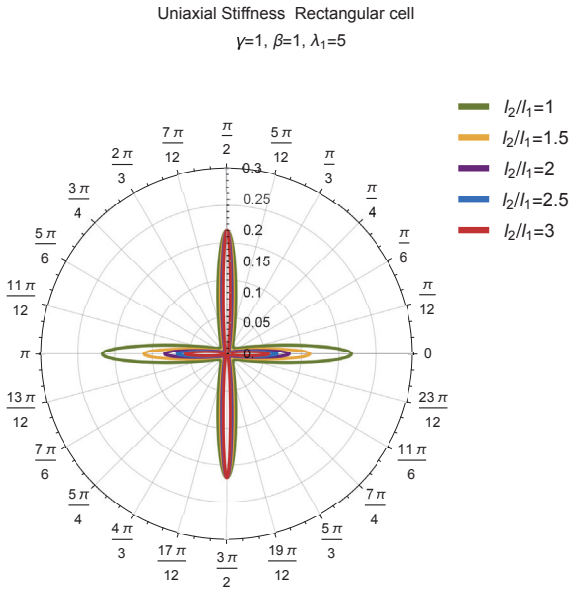

(b) Polar plot of the uniaxial stiffness D_{11}

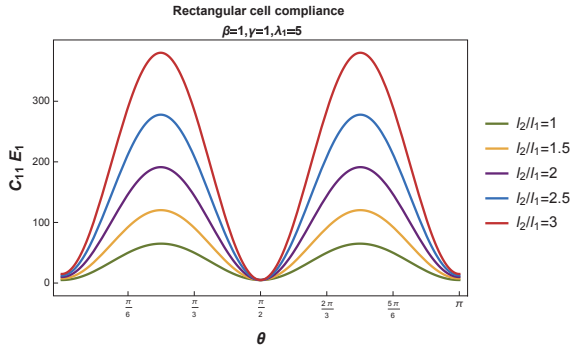

(c) Plot of the uniaxial stiffness D_{11}

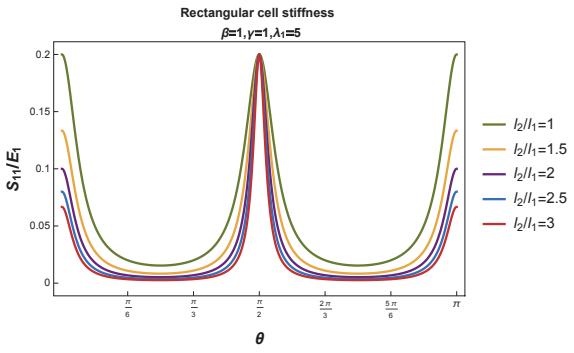

(d) Plot of the uniaxial compliance $\epsilon_{\xi\xi}$

Figure 3.13: Uniaxial compliance and stiffness of a material formed by rectangular reference cell with rigid connection as function of the load directions for differents aspect ratio of the length

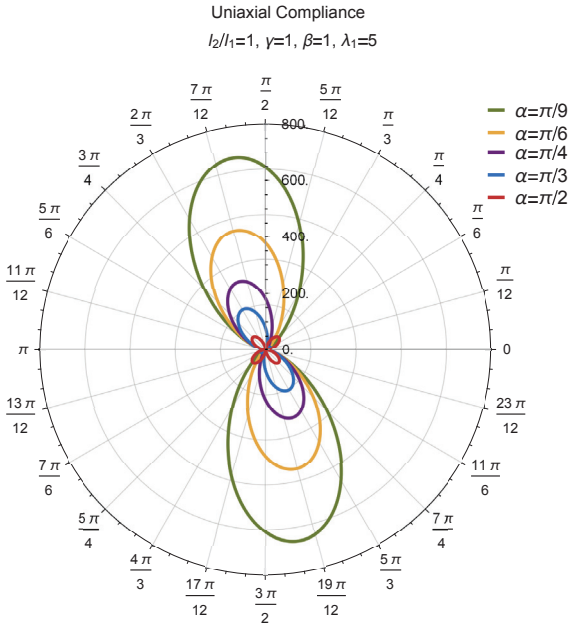

(a) Polar plot of the uniaxial compliance $\epsilon_{\xi\xi}$

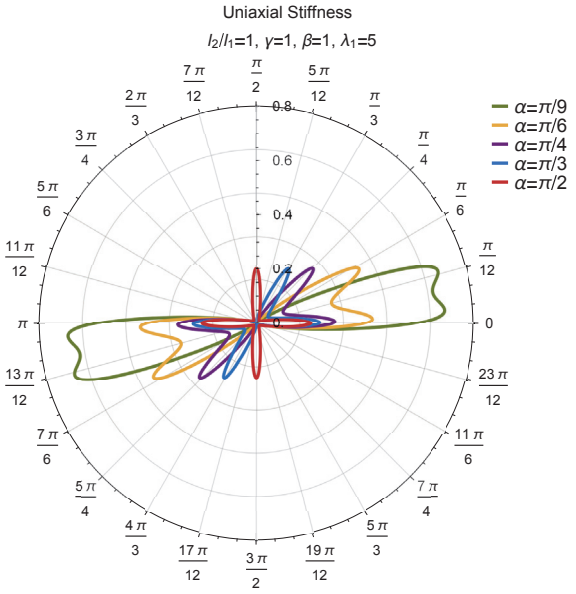

(b) Polar plot of the uniaxial stiffness D_{11}

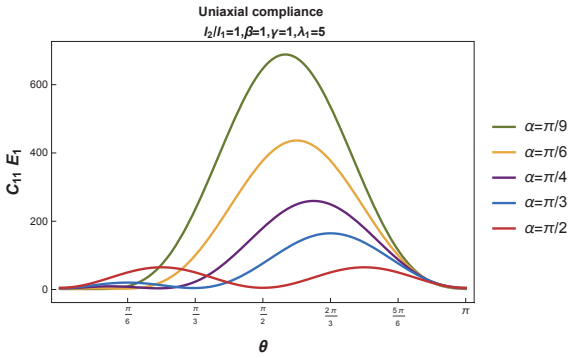

(c) Plot of the uniaxial compliance $\epsilon_{\xi\xi}$

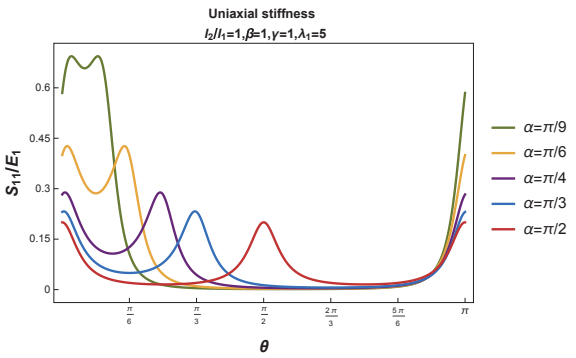

(d) Plot of the uniaxial stiffness D_{11}

Figure 3.14: Uniaxial compliance and stiffness of a material formed by skew reference cell with rigid connection as function of the load directions for differents angles between the two fibres and aspect ratio of the length 1.

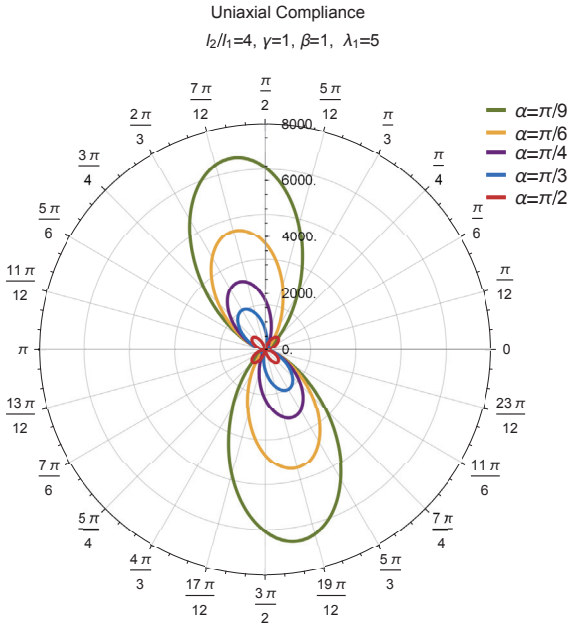

(a) Polar plot of the uniaxial compliance $\epsilon_{\xi\xi}$

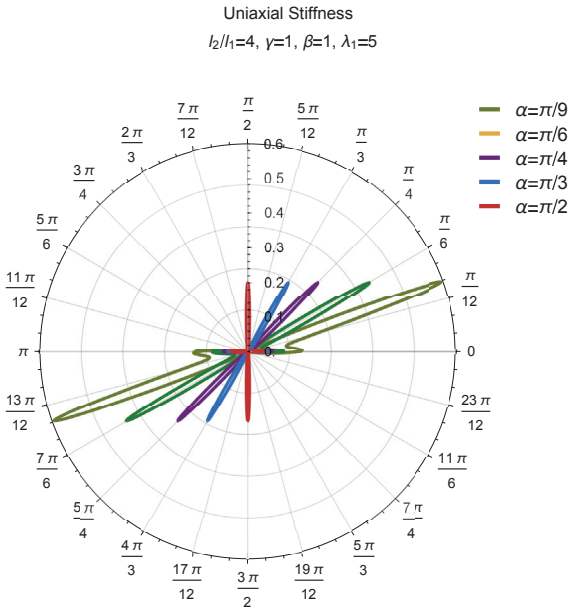

(b) Polar plot of the uniaxial stiffness D_{11}

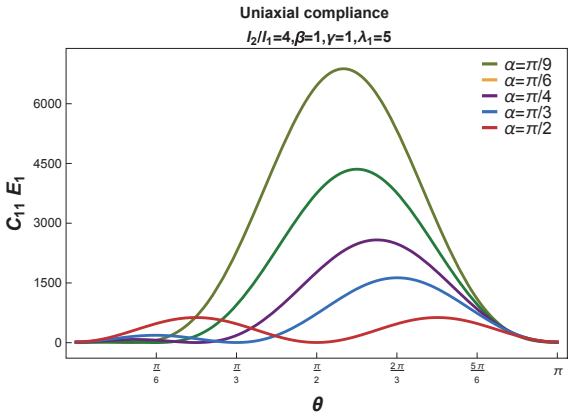

(c) Plot of the uniaxial compliance $\epsilon_{\xi\xi}$

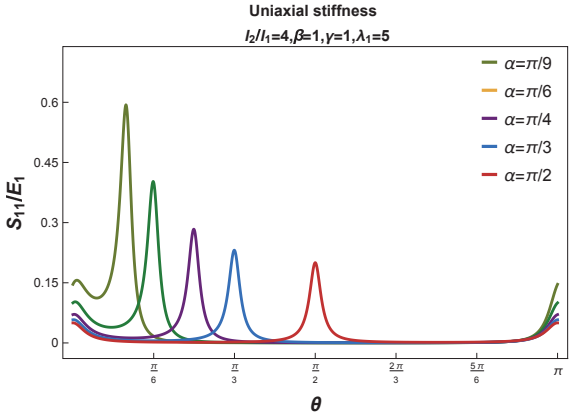

(d) Plot of the uniaxial stiffness D_{11}

Figure 3.15: Uniaxial compliance and stiffness of a material formed by skew reference cell with rigid connection as function of the load direction for differents angles between the two fibres and aspect ratio of the length 4.

Braced cell with rigid connection

The general case of a network with a rectangular braced reference cell was examined in subsection 3.3. Here we consider a configuration commonly met in a quadrilateral networks of fibres.

The two external fibres, 1 and 2, can be different among themselves, while the internal fibres along the diagonals (usually less stiff) are identical, although different from 1 and 2.

However, the internal node is located at the centre of the cell.

With reference to this case, let's introduce the following dimensionless parameters:

$$\gamma_1 = \frac{E_2}{E_1} \quad \gamma_2 = \frac{E_{in}}{E_1} \quad \beta_1 = \frac{h_2}{h_1} \quad \beta_2 = \frac{h_{in}}{h_1} \quad \rho = \frac{l_2}{l_1} \tag{3.89}$$

where E_{in}, h_{in} are the Young modulus and the thickness of internal fibres. The length of the internal fibres is $l_{in} = l_1/2\sqrt{1+\rho^2}$. The slenderness of the external fibre 1 is denoted by $\lambda_1 = l_1/h_1$.

Note that the slenderness of the second internal fibres are $\lambda_2 = \lambda_1 \frac{\rho}{\beta}$ and $\lambda_{in} = \frac{\lambda_1}{\beta_2}\sqrt{\frac{1}{4}+\frac{\rho^2}{4}}$.

First, the case of a square braced cell $\rho = 1$ with two equal external fibres $\beta_1 = 1, \gamma_1 = 1$ is examined.

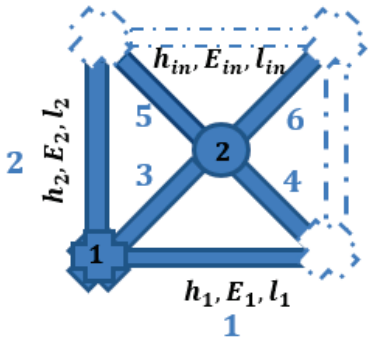

Figure 3.16: Braced cell

Plots of the uniaxial stiffness and compliance are reported in figure 3.17, for different β_2, with $\gamma_2 = 1$ and $\lambda_1 = 5$.

The ratio β_2 has been varied from 0.3 to 2. When the internal fibres have a larger thickness than the external ($\beta_2 > 1$), the uniaxial stiffness in the braces direction (45°), becomes greater than the stiffness in the direction 1 and 2, figures 3.17(b),3.17(d). The opposite condition occurs when $\beta_2 < 1$.

In the latter case, an anisotropic behaviour similar to the one found for the rectangular cell is obtained. However, the effect of the internal fibres is to reduce in any case the contrast of anisotropy.

From figure 3.17(c) it is observed that when $\beta_2 = 1$ the compliance is almost constant for all directions. Consequently, the polar plots of figures 3.17(a), 3.17(b) tend to get the form of a square.

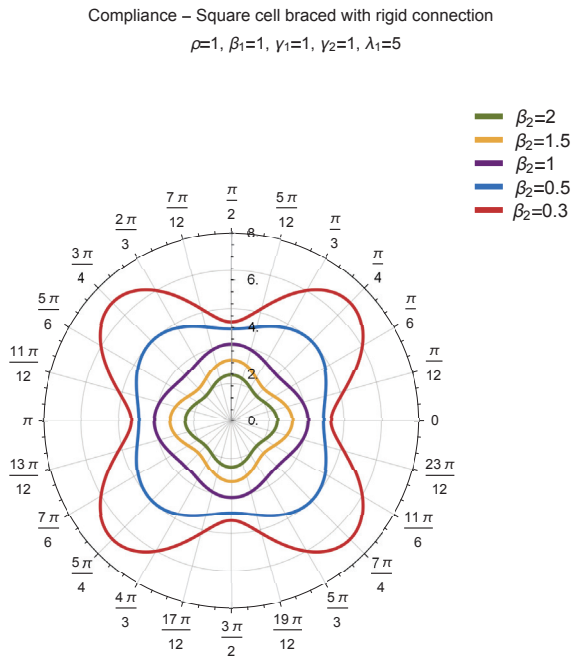

(a) Polar plot of the uniaxial compliance $\epsilon_{\xi\xi}$

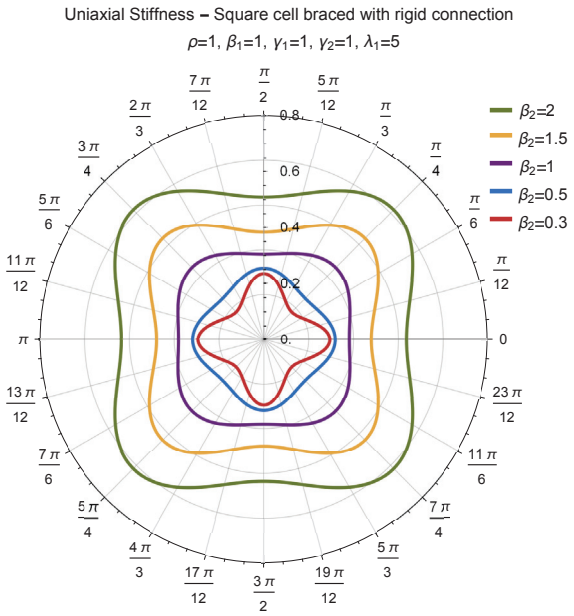

(b) Polar plot of the uniaxial stiffness D_{11}

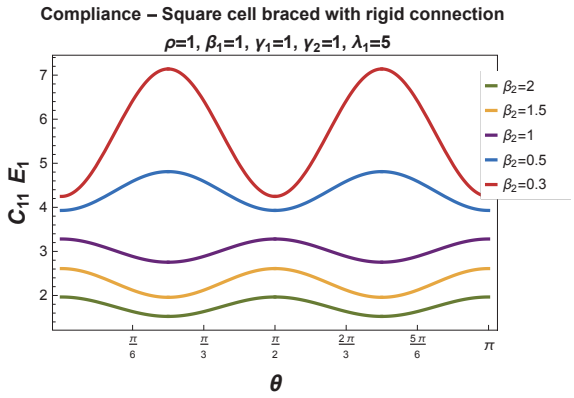

(c) Plot of the uniaxial compliance $\epsilon_{\xi\xi}$

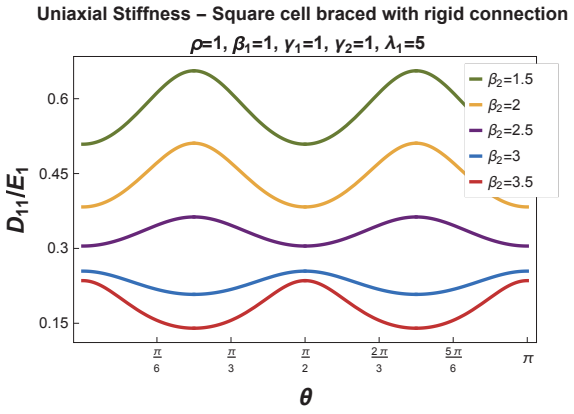

(d) Plot of the uniaxial stiffness D_{11}

Figure 3.17: Uniaxial compliance and stiffness of a material formed by square braced cell with rigid connections as function of the load directions for different thickness ratio β_2.

In the following, the case of a braced rectangular cell is examined. Figure 3.18 refers to the case where $\gamma_1 = \gamma_2 = 1$, $\beta_1 = \beta_2 = 1$, that is the fibres are all equal, but the aspect ratio of the cell, ρ, is varied in the range (1,3). For all cases the slenderness of the fibre 1 is fixed to $\lambda_1 = 5$.

Looking at figure 3.18(b), the plot of uniaxial stiffness changes from the square balanced form, already obtained for the case of a square cell ($\rho = 1$), to a strongly anisotropic shape when $\rho > 1$.

Comparing the plots of figures 3.18(a) and 3.18(b) with the figures 3.13(a) and 3.13(b) referring to a rectangular cell without internal fibres, it can be observed that the insertion of diagonal fibres makes the transition of the stiffness from direction 1 to direction 2 more smooth.

Interesting is the plot of figure 3.18(d) when $\rho = 1$ the greatest stiffness occurs along the diagonal directions. As ρ grows, the maximum stiffness is obtained in the direction 2, and reaches $0.5E_1$ for $\rho = 3$, which is greater of the maximum stiffness obtained in the rectangular cell without braces with the same aspect ratio (in this case $D_{11} = 0.2E_1$).

The diagonal fibres make, therefore, the network much stiffer.

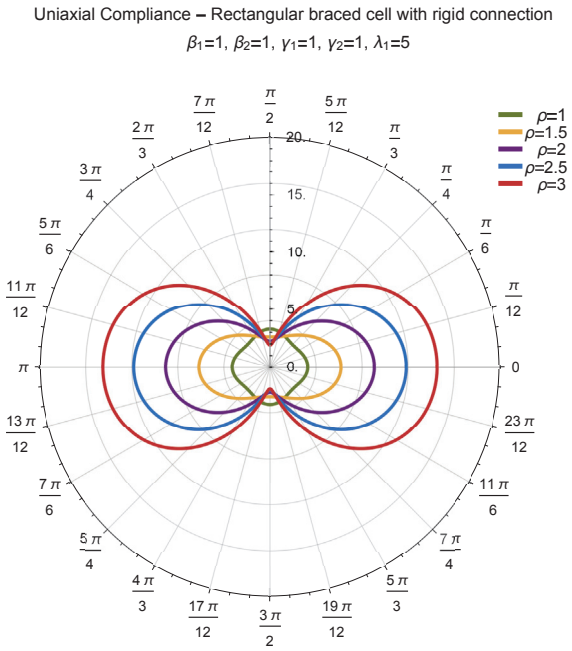

(a) Polar plot of the uniaxial compliance $\epsilon_{\xi\xi}$

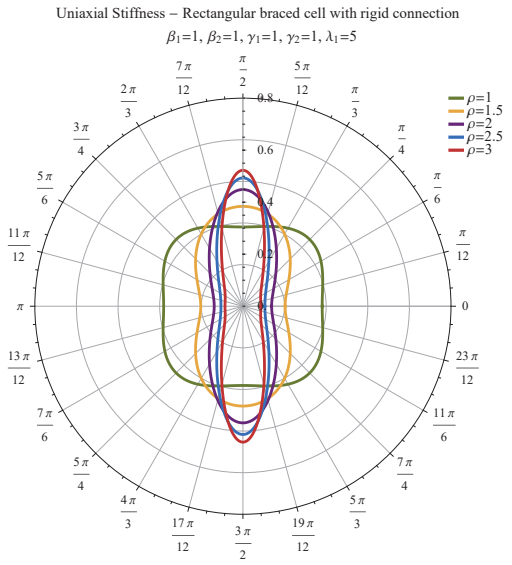

(b) Polar plot of the uniaxial stiffness D_{11}

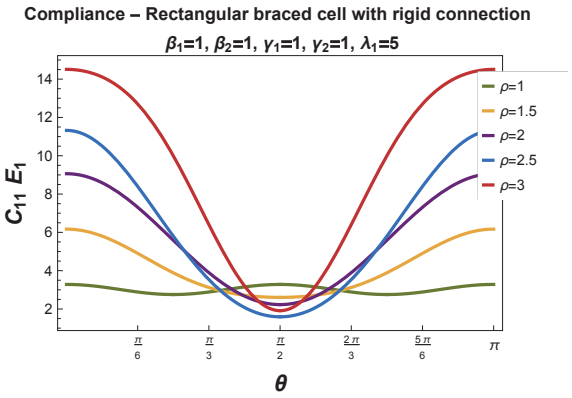

(c) Plot of the uniaxial compliance $\epsilon_{\xi\xi}$

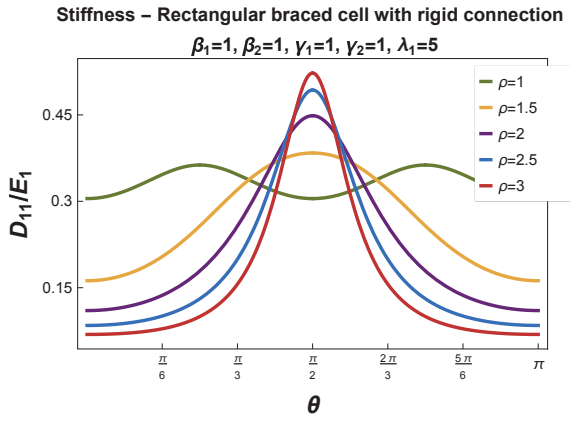

(d) Plot of the uniaxial stiffness D_{11}

Figure 3.18: Uniaxial compliance and stiffness of a material formed by rectangular braced cell with rigid connections as function of the load direction for different aspect ratio ρ.

In figure 3.19 is shown the Poisson ratio of the material resulting from a network with square braced cell with rigid connection.

Remembering the matrix of the elastic constant found in the subsection 3.3, it is possible to define an equivalent Poisson ratio as:

$$\nu_{eq} = \frac{E_{12}}{E_{11}} \tag{3.90}$$

For the case $\theta = 0$ and $\rho = 1, \beta_1 = 1$ we obtain the result:

$$\nu_{eq} = \frac{1 - 24\dfrac{1}{\lambda_{in}^2}}{24\dfrac{1}{\lambda_{in}^2} + \dfrac{\sqrt{2}}{\beta_2} + 1} \tag{3.91}$$

The figure 3.19 represents the equivalent Poisson ratio defined as a function of β_2 and of the

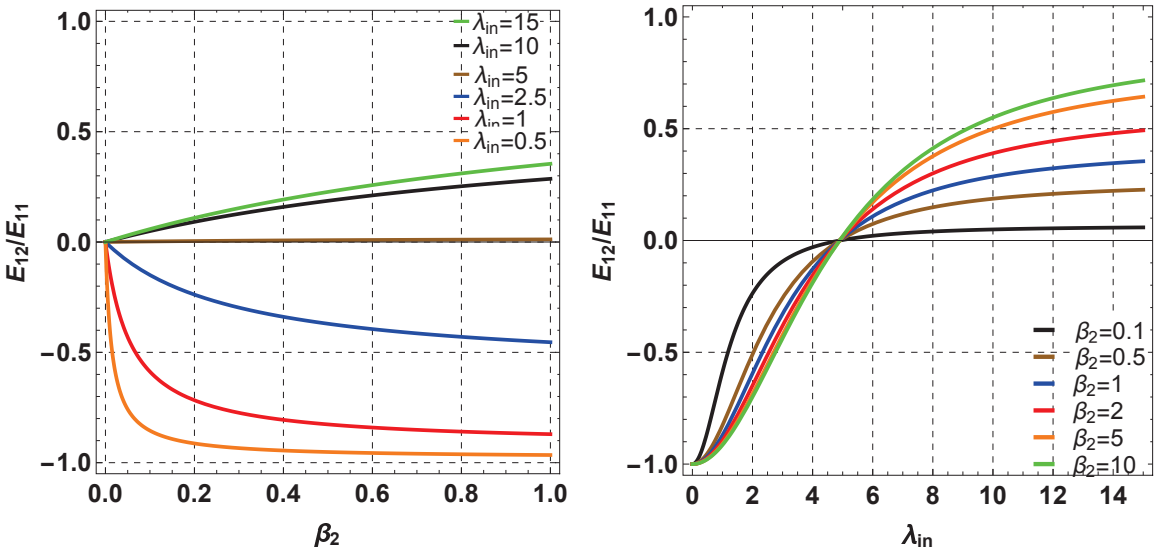

(a) Equivalent Poisson ratio in function of β_2 varying λ_{in}

(b) Equivalent Poisson ratio in function of λ_{in} varying β_2

Figure 3.19: Equivalent Poisson ratio in the case of material with reference cell square braced with rigid connections

slenderness of the internal fibres λ_{in}.

It can be observed that for $\lambda_{in} = 5$ a zero Poisson ratio is obtained. For slenderness $\lambda_{in} < 5$ a negative Poisson ratio is obtained, that means that the material has an auxetic behaviour. This result is highlighted in figure 3.19(b) where in the abscissae is reported the slenderness λ_{in}.

From equation (3.91) is evident that the auxetic behaviour is determined by the the negative flexural coefficient present in the term E_{12}, prevails when the flexural rigidity if internal beams is bigger respect the axial rigidity of the internal beams $k_{fi} \gg k_{ai}$. The result obtained is only a mathematical result, as is not easy feasible to build element with these properties.

Braced cell with pivots

The case examined in section 3.4, refers to a quadriaxial tissue, where the connections can be, in a first approximation, modelled as perfect pivots.

Figure 3.21 refers to the case of a square cell, figure 3.22 to the case of a rectangular cell.

For the square cell, figure 3.21, it has been assumed that all the fibres have the same modulus $\gamma_1 = \gamma_2 = 1$, that the external fibres are equal, $\beta_1 = 1, \rho = 1$, but the thickness of the internal fibres has been varied in the range $\beta_2 \in (0.3, 2)$ as done for the case of the square cell with rigid connection of figure 3.17.

The comparison of the two cases (cell with rigid connection, figure 3.17, and cell with pivots, figure 3.21) shows that the effects of the pivots is to increase the contrast of anisotropy for the cases in which $\beta_2 \neq 1$.

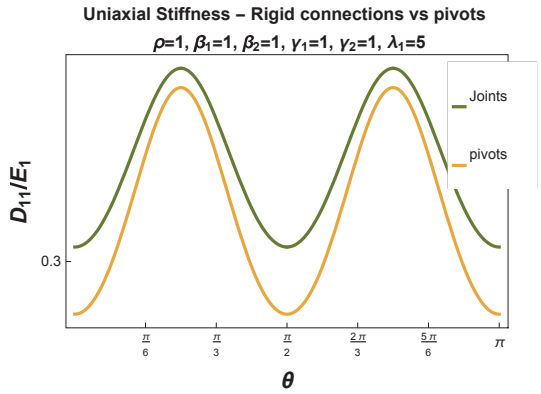

Figure 3.20: Comparison between the uniaxia stiffness in the square braced case with rigid connection and with pivots

When $\beta_2 = 1$, instead, almost identical result are found for the two cells (see figure 3.20).

For $\beta_2 < 1$ the results are similar to the two cases considered. On the contrary, when $\beta_2 > 1$, the cell with pivots has a more pronounced anisotropy behaviour than the analogous cell with rigid connection (figure 3.22(c), 3.22(b)).

The maximum stiffness for the value $\beta_2 = 3$, for this case, is larger than $0.6E_1$, similar to the maximum stiffness of the cell with rigid connections. However, the stiffness in the direction 1 and 2, for this case, is only $0.3E_1$, (it is larger in the case of square braced cell with rigid connections).

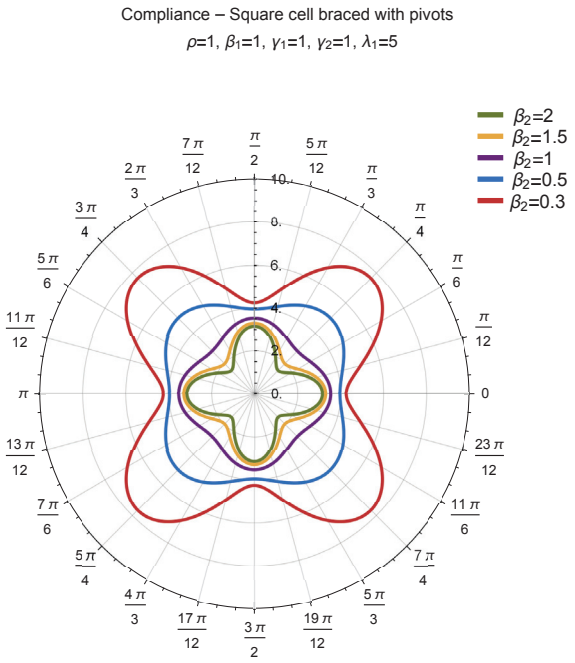

(a) Polar plot of the uniaxial compliance $\epsilon_{\xi\xi}$

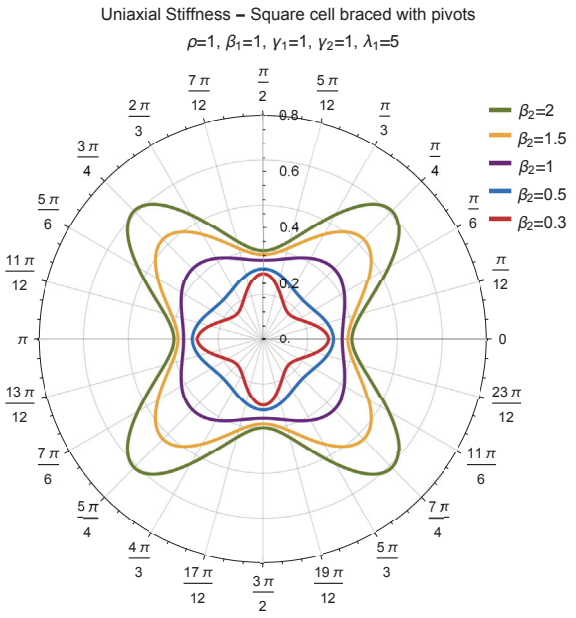

(b) Polar plot of the uniaxial stiffness D_{11}

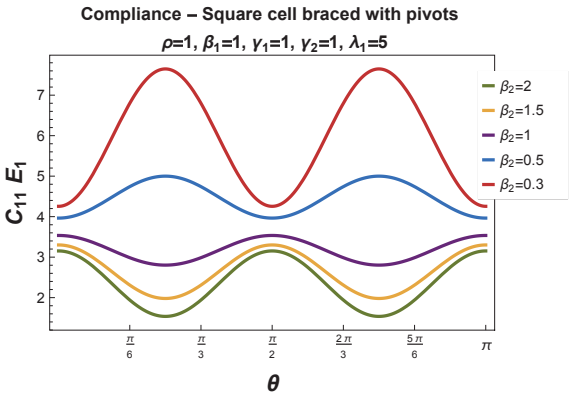

(c) Plot of the uniaxial compliance $\epsilon_{\xi\xi}$

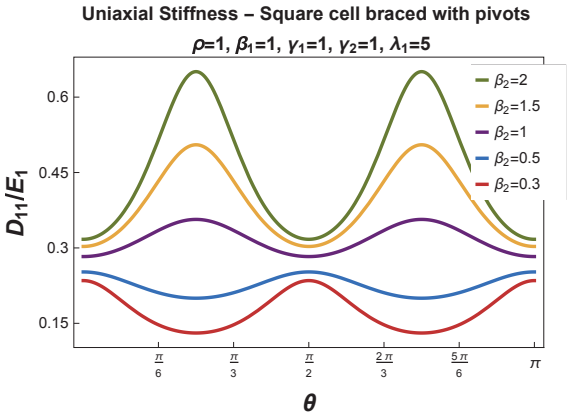

(d) Plot of the uniaxial stiffness D_{11}

Figure 3.21: Uniaxial compliance and stiffness of a material formed by square braced cell with pivots as function of the load directions for different thickness ratio β_2.

When we consider a rectangular quadriaxial cell with pivots, and set $\beta_2 = 1$, figure 3.22, we obtain for the uniaxial stiffness and compliance, almost the same results as for the rectangular cell with rigid connections.

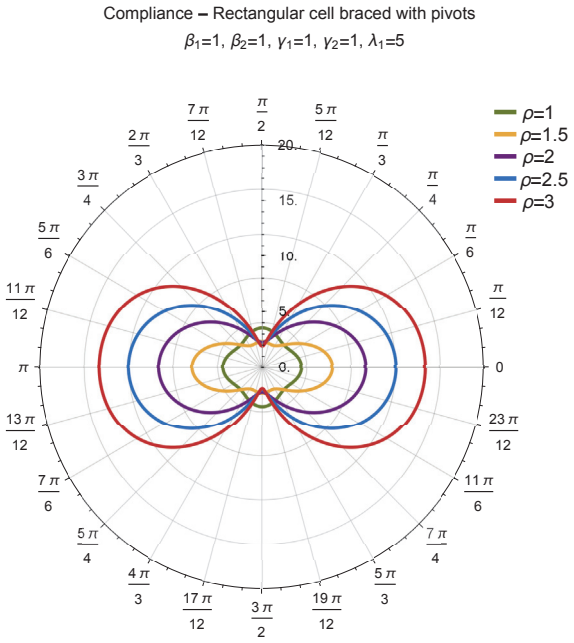

(a) Polar plot of the uniaxial compliance $\epsilon_{\xi\xi}$

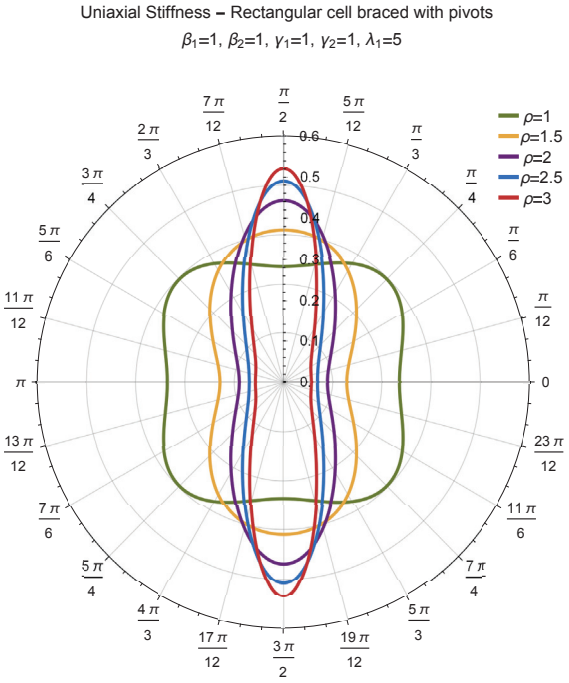

(b) Polar plot of the uniaxial stiffness D_{11}

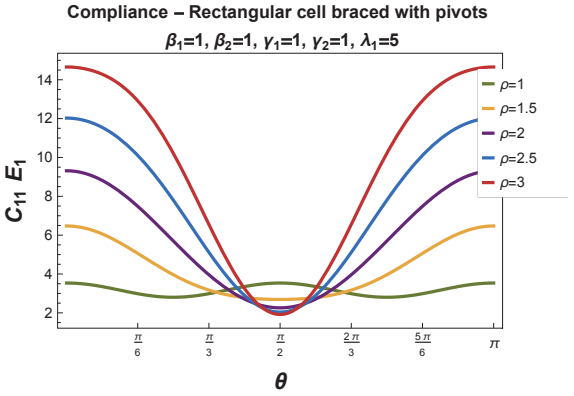

(c) Plot of the uniaxial compliance $\epsilon_{\xi\xi}$

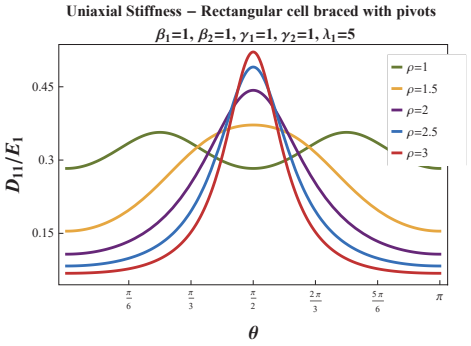

(d) Plot of the uniaxial stiffness D_{11}

Figure 3.22: Uniaxial compliance and stiffness of a material formed by rectangular braced cell with pivots as function of the load direction for different aspect ratio ρ.

This result appears to be true also for different ratio of the cross section area of internal and external fibres; for instance figure 3.23 shows the uniaxial stiffness as function of the angle θ varying the aspect ratio ρ when $\beta_2 = 0.3$ considering the material formed by rectangular cell with rigid connections and material formed by rectangular cell with pivots.

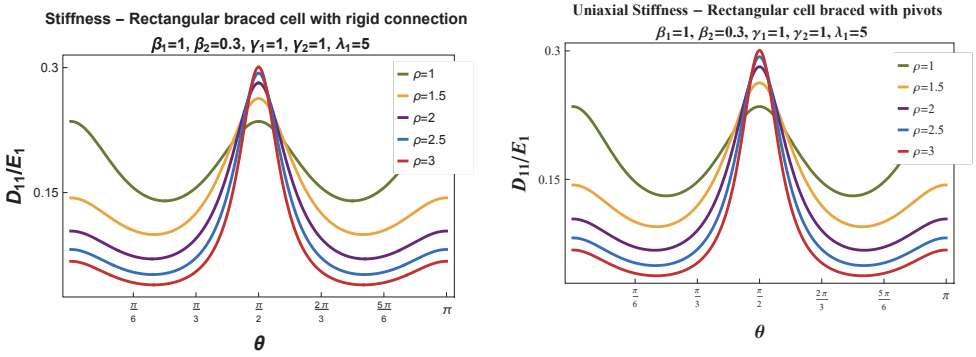

(a) Rectangular braced reference cell with rigid connections

(b) Rectangular braced reference cell with pivots

Figure 3.23: Uniaxial stiffness D_{11} as function of the angle θ with $\beta_2 = 0.3$ and varying the aspect ratio ρ.

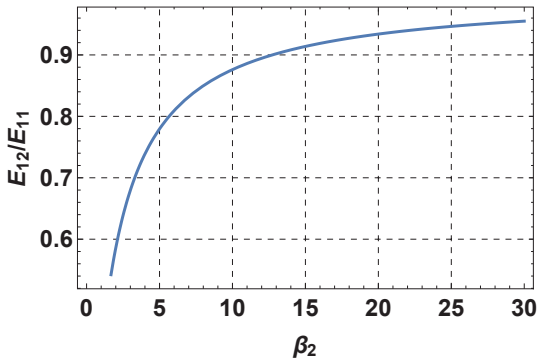

Figure 3.24: Equivalent Poisson ratio in the case of material with reference cell square braced with pivots

In figure 3.24 is plotted the equivalent Poisson ratio for the case $\theta = 0°$, of the network composed by braced cell with pivots, varying the ratio between the thickness of internal and external beams. Recalling expression (3.49) the Poisson ratio is given by:

$$\nu_{eq} = \frac{E_{12}}{E_{11}} = \frac{1}{\frac{\sqrt{2}}{\beta_2} + 1} \tag{3.92}$$

The relation (3.92) is plotted in figure 3.24 as function of β_2, it can be observed that the value are always positive.

Hence, despite having the same geometry as the previous case it isn't possible to design auxetic material.

Chapter 4

Numerical simulations

In this chapter, the models developed in Chapter 3 for fibre networks and woven fabrics are implemented for the numerical simulation of a series of laboratory tests available in the literature.

In particular, bias and extension tests with varying fibres direction will be performed on the following fibre network materials with equal properties of the fibres:

- fibre network material with square cells rigidly connected (bias test in subsection 4.2.1, extension test in subsection 4.3.1);
- fibre network material with square braced cells rigidly connected (bias test in subsection 4.2.2, extension test in subsection 4.3.2);
- fibre network material with square braced cells with pivots (bias test in subsection 4.2.3).

Subsection 4.4.1 presents the results from the simulation of unbalanced fibre materials with varying fibre properties, during bias and extensional tests. The case of a fibre network material with a skew reference cell is analyzed in subsection 4.4.2.

Finally, the case of bias test on a network whose fibres are connected by pivots will be discussed in section 4.5.

4.1 Numerical method employed in the simulation

The numerical experiments have been performed implementing the constitutive relationship of the considered material in a finite elements code (ADINA). In some cases (mainly in the networks material with skew cell), the resulting constitutive equation does not show any particular symmetry, and hence an ad-hoc user model has been implementing in the finite element code.

Simulation have also been carried out for the cell with pivots implementing the strain gradient material resulting from the homogenization. In this case it has been necessary to implement an original code. For strain gradient models C^0 continuity of finite elements is insufficient since the model require at list G^1 continuity.

For the concept of geometric continuity see the work of Greco and Cuomo [56, 95, 96].

Interpolation that guarantees continuity of the slopes in addition to the continuity of the function are used in isogeometric analysis [97–101]. A customer code based on isogeometric interpolation has therefore been used. Open B-splines of third order with internal knots have been adopted for the interpolations.

4.2 Bias test

In this section are presented the results of simulations of a bias test, described in section 1.2, considering the cells analysed in chapter 3.
The scheme of the bias test is represented in figure 4.1. One side of the sheet is fixed, at the opposite side is applied an uniform displacement in the axial direction, while the tangential displacement is constrained, according to the set-up of the test.

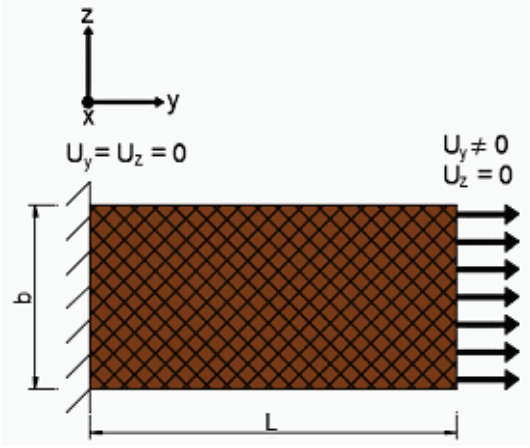

Figure 4.1: Description of the numerical test

In the simulation performed, we considered square cells of different typologies, with the fibres oriented at 45° with respect to the longitudinal axis of the specimen. Initially, balanced network materials will be examined. Next, some simulations of unbalanced cells will be described.

The properties employed for the fibres are:

- $l_1 = l_2 = 5 \quad mm$ the length of the fibres;
- $h_1 = h_2 = 1 \quad mm$ the height of the fibres;
- $s_1 = s_2 = 1 \quad mm$ the thickness of the fibres;
- $E_1 = E_2 = 1600 \quad MPa$.

In the case of networks with braced cell, it will be assumed that the internal fibres will be equal between themselves.

The applied displacement is small enough, so that the hypothesis of small displacements is satisfied.

4.2.1 Fibre network material with square cells rigidly connected

This subsection shows the simulation of network materials with square cells rigidly connected, subjected to bias test. Recall that in this case the homogenized materials is orthotropic, having equal stiffness in the two directions and Poisson's ratio equal to zero.

In figure 4.2 are shown the plots of the stress σ_{yy} and the strain ε_{yy} varying the length ratio L/b of the specimen and keeping constant the properties of the micro-structure of the cell. When the ratio of the length is larger than 2, we can observe three areas with different behaviour in the specimen as we have seen in the section 1.2. In this case the behaviour of the cell is mainly dominant by shear deformation in the central part of the specimen, while in the ends of the specimen the deformation is almost null. In these areas the strain and the stress are constant. From the plot of the stresses it can be observed a concentration near the corners of the specimen, while in the central areas the stress is basically constant.

When the specimen length ratio is smaller than 2, the cell becomes less deformable for shear and the three areas disappear. In this case both the stresses and strains concentrate along diagonal lines. These tests show a transition in the behaviour of the network from a shear dominated to an elongation dominated behaviour, according to the slenderness of the elements, that is caught by the equivalent material obtained by homogenization.

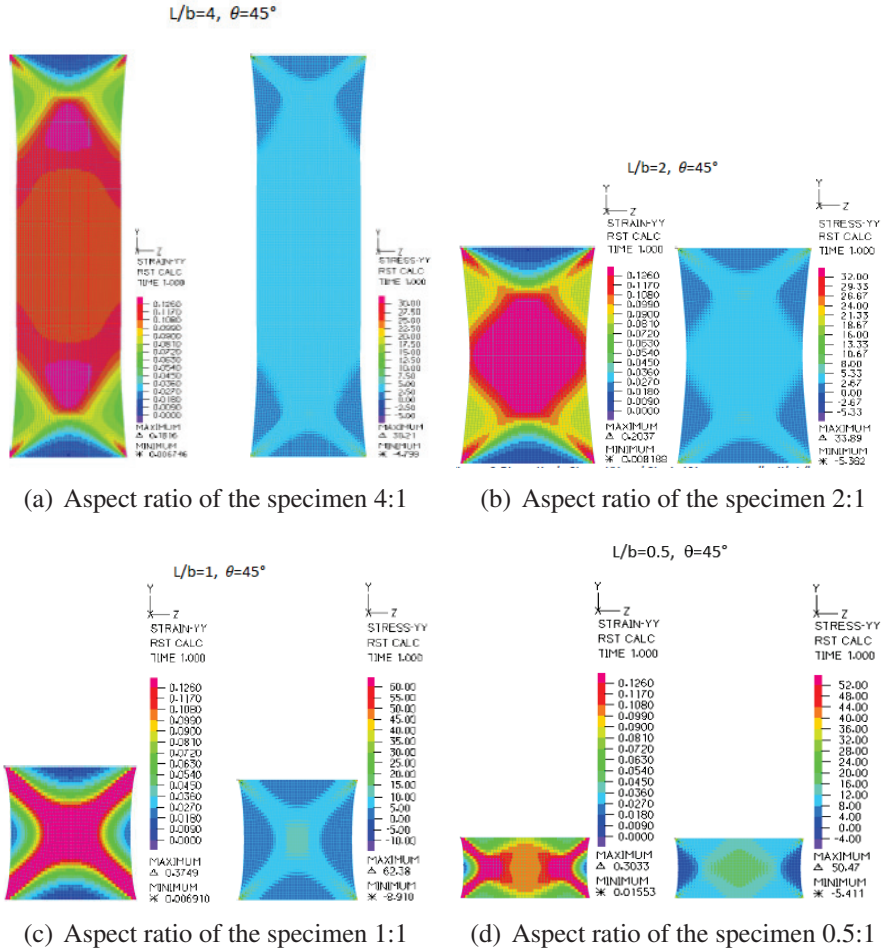

(a) Aspect ratio of the specimen 4:1 (b) Aspect ratio of the specimen 2:1

(c) Aspect ratio of the specimen 1:1 (d) Aspect ratio of the specimen 0.5:1

Figure 4.2: Plot of the strain ε_{yy} and the stress σ_{yy} of a numerical bias test of a network with square reference cell varying the aspect ratio of the specimen.

4.2.2 Fibre network material with square braced cells rigidly connected

A quadriaxial balanced rigid fibre net is consider next. Figure 4.3 summarizes the results from the numerical simulation of the bias test of a network material with square braced cell with fibres rigidly connected, as developed in subsection 3.1. The properties of the fibres of the braces are identical to the ones of the main fibres.

Comparing the plots of the stress and the strain with those obtained in the case without braces, one can easily observe that in the present case the deformation along the specimen is almost uniform independently from the slenderness ratio. Note however that there is a small area near the borders when the strain is almost null. The response in this network is substantially different from the behaviour of a tissue subjected to bias test.

This is due to the rigidity provided by the braces that make the material stiffer along the axis of specimen and the overall deformation dominated by elongation rather than by shear.

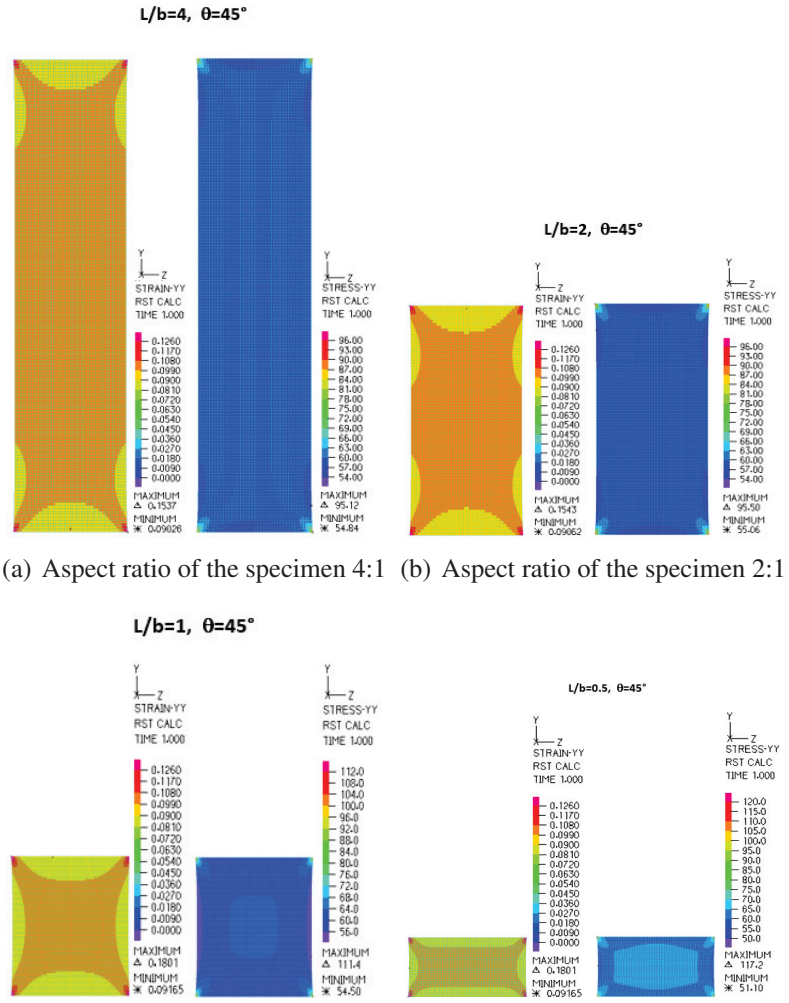

(a) Aspect ratio of the specimen 4:1 (b) Aspect ratio of the specimen 2:1

(c) Aspect ratio of the specimen 1:1 (d) Aspect ratio of the specimen 0.5:1

Figure 4.3: Plot of the strain ε_{yy} and the stress σ_{yy} for bias test of a network with square braced reference cell with rigid connections varying the aspect ratio of the specimen.

In order to highlight the effect of the braces, the case of a network material with less stiff braced cell is examined, see figure 4.4. The Young modulus of the braces is 1/5 of the

Young modulus of the main fibres. In this case the response of the network material lies somewhere in between the two cases previously analysed. Indeed in the longest samples, the strain near the ends shows lines of concentrations starting from the corners and it tends to become uniform in the central region. However, the strain is non zero along the constrained ends, since the braced cell presents a large stiffness in bending. In the shortest samples a response similar to the square cell is obtained, although the strain concentration near the corners is even more evident compared to the case of a square network without braces.

A continuous transition from a shear dominated deformation to an extension dominated one can then be obtained properly modulating the properties of the micro-structure.

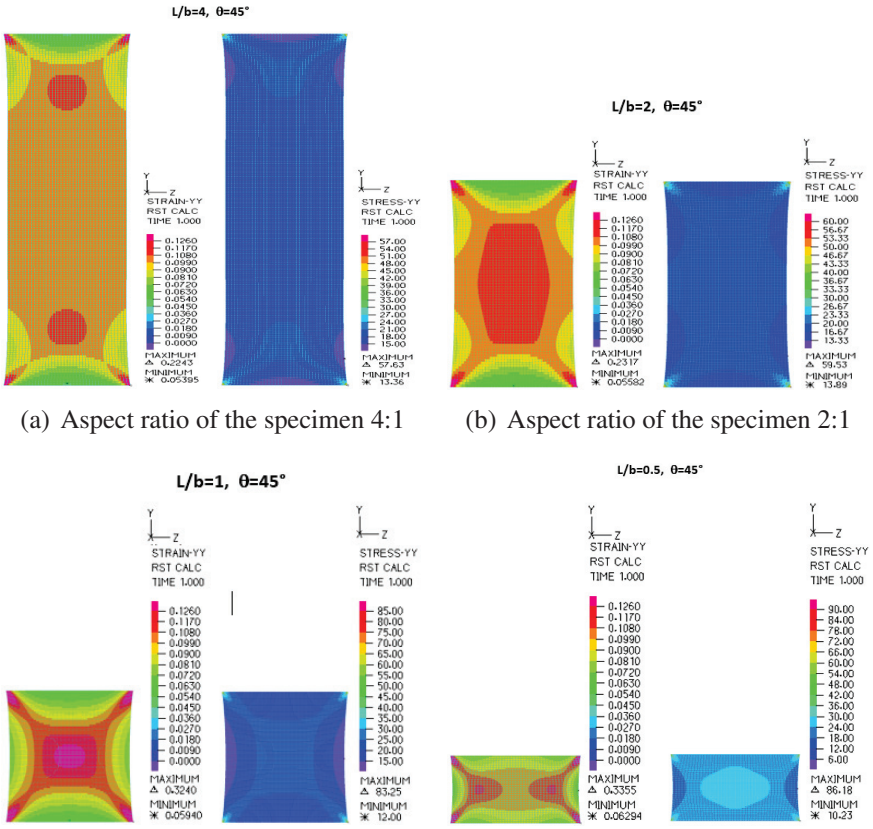

(a) Aspect ratio of the specimen 4:1 (b) Aspect ratio of the specimen 2:1

(c) Aspect ratio of the specimen 1:1 (d) Aspect ratio of the specimen 0.5:1

Figure 4.4: Plot of the strain ε_{yy} and the stress σ_{yy} for bias test of a network with square braced cell with rigid connections. Ratio of the Young modulus of the internal fibres to the Young modulus of the mean fibres, equal to 1/5.

4.2.3 Fibre network material with square braced cells and pivots

This subsection focuses on a material in which the unit cell is square with braces and all the fibres are connected by pivots (see subsection 3.4). The fibres have identical properties. Recall that this cell simulates a quadriaxial fibre tissue, with negligible friction between the fibres.

The response of the material under the bias test is similar to the one of the material with braced cell rigidly connected, since in both cases an extension dominator behaviour of the material is obtained, see figure 4.5.

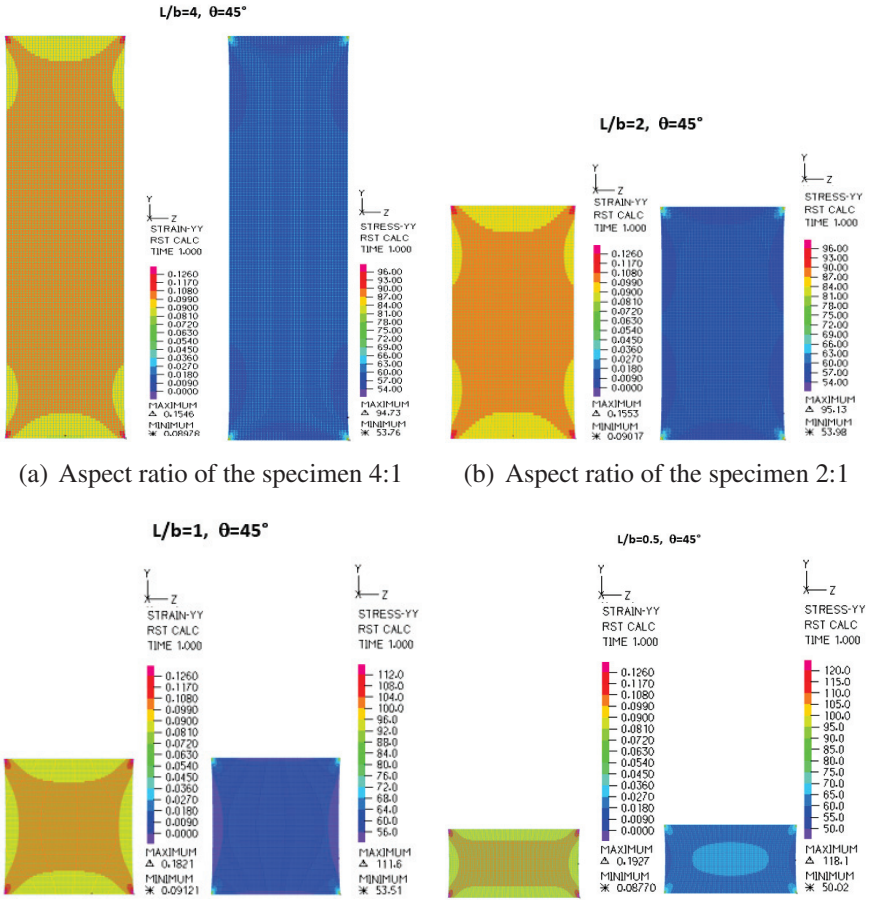

(a) Aspect ratio of the specimen 4:1 (b) Aspect ratio of the specimen 2:1

(c) Aspect ratio of the specimen 1:1 (d) Aspect ratio of the specimen 0.5:1

Figure 4.5: Plot of the strain ε_{yy} and the stress σ_{yy} for bias test of a network with braced cell connected by pivots varying the aspect ratio of the specimen.

4.2.4 Bias test with different boundary condition

Figure 4.6 refers to a test similar to the one described in section 4.2 but with different boundary conditions. In particular, the vertical displacement u_z for the lowest edge is fixed on both sides of the element, while the horizontal displacement is fixed only in one point, to ensure the existence of the solution of the problem. From this simulation it can be observed that this boundary conditions may lead to uniform strain distribution in the sample, but for the fixed point, where concentration of the stresses is present.

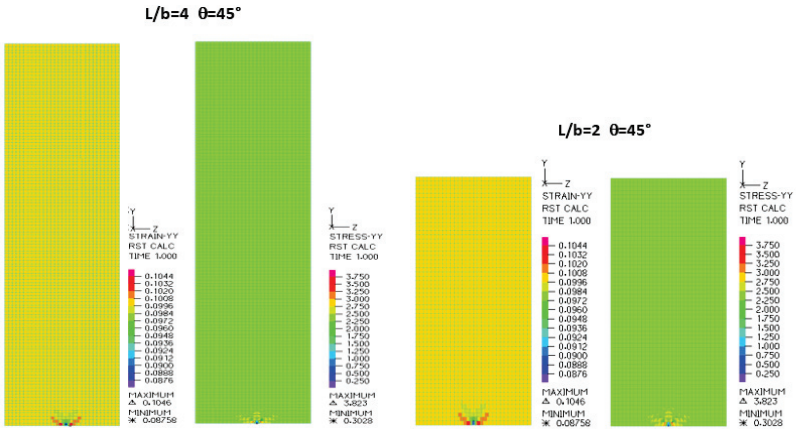

(a) Aspect ratio of the specimen 4:1 (b) Aspect ratio of the specimen 2:1

Figure 4.6: Plot of the strain ε_{yy} and the stress σ_{yy} for bias test of a network with square reference cell. Lateral deformation allowed at the lower edge.

4.3 Extension test for different fibre orientation

The same test as in previous section 4.2 has been simulated for materials composed by square cells with the fibres oriented at angle θ with respect to the specimen axis, where θ varies from 0° to 45°. Three different reference cells have been analysed: square cells rigidly connected, square braced cells rigidly connected and square braced cells connected by pivots.

4.3.1 Fibre network material with square cells rigidly connected

The figure 4.7 shows the extensions test of the network material with square reference cell rigid connected, with fibre's direction coincident with the direction of the load $\theta = 0°$, varying the length ratio L/b of the sample. This case reproduced the standard test performed on tissues for assessing their modulus (see, ISO 13934-1).

In this case the strains and stresses are uniform in the all considered cases, while the response mainly depends on the properties of the fibres in the extension's direction. Furthermore we can easily observe that the behaviour of the material is independent of the length ratio.

Figure 4.8 shows the output of a numerical extension test of the same network material with square reference cell rigidly connected, but with fibres oriented at an angle $\theta = 30°$ with respect the direction of load. The length ratio L/b of the sample varies from 4 to 1/2.

It possible to observe that for the most slender specimen the strain is equal to zero in a small zone near the ends. Two triangle zones of almost uniform strain are present near the lateral borders, and finally, in a diagonal zone, inclined with $\theta = 30°$ like the direction of the fibres, there is strong concentration of strain.

The specimen shows an S-shape deformation. When the length ratio is lower than 2, two diagonal stripes oriented at $\theta = 30°$ form, joined by an orthogonal one (that is oriented as the elementary cell), as in the case of a Ritter-Morsch trellis model.

Figure 4.9(a) shows the apparent elastic modulus in the axial direction as a function of the fibre direction, from 0° to 45° with respect to the load axis.

A balanced network always considered. Different length ratios, varying from 10 to 0.1,

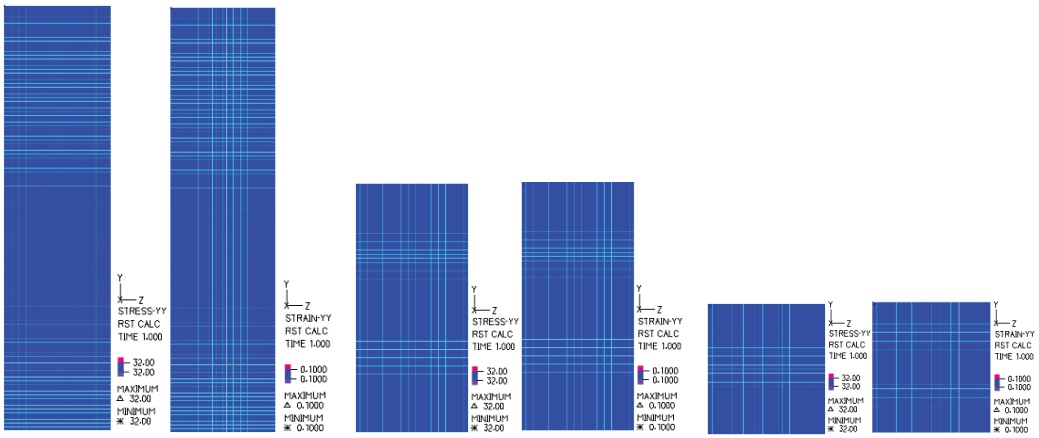

(a) Aspect ratio of the specimen 4:1 (b) Aspect ratio of the specimen 2:1 (c) Aspect ratio of the specimen 1:1

Figure 4.7: Plot of the strain ε_{yy} and the stress σ_{yy} for an extension test of a network with square reference cell. The fibre's axis is coincident with the axis of the specimen.

are examined. From these plots it is possible to observe the influence of the slenderness ratio in the solution. The two upper and lower red curves are analytical result and they are obtained from the constitutive relation of the material.

In particular, the upper curve provides the apparent elastic modulus in the case of a uniaxial deformation state obtained by applying deformation $\varepsilon_{xx} = 0 \quad \varepsilon_{xy} = 0 \quad \varepsilon_{yy} = 0$.

As it is possible observe from figure 4.9(a), this case occurs with the numerical simulation when the length ratio L/b is close to 0.1. Indeed, in this case the lateral deformation is prevented by the boundary conditions, and a uniaxial strain state is obtained.

The lowest curve reefers to the ratio $\dfrac{\sigma_{yy}}{\varepsilon_{yy}}$ for the case of uniaxial stress state, with only the component σ_{yy} is different from zero.

Observing that figure 4.9, this case occurs in the numerical simulation when the length ratios is very large ($L/b = 10$).

In this case, indeed, the hypothesis leading to on more stress state are meet. Other length ratios lie in between the two extreme cases.

The plots 4.9(b), 4.9(c) and 4.9(d) show the apparent elastic modulus as a function of the length ratio for the specimens with fibre directions equal to $\theta = 0°$, $\theta = 30°$ and $\theta = 45°$, respectively. From the same plots we can also see that in order to obtain a response of the material close to the theoretical one without the effect of the boundary condition (red curve), it is necessary to take samples with length ratio greater than 4.

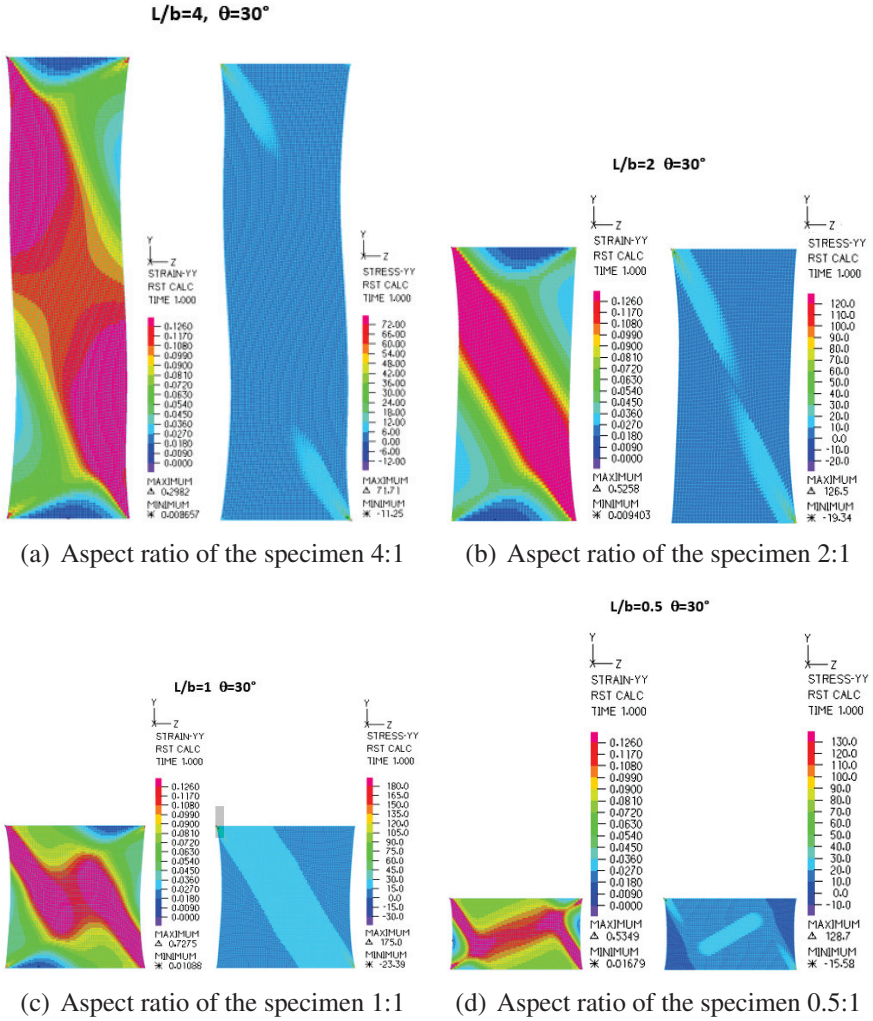

(a) Aspect ratio of the specimen 4:1 (b) Aspect ratio of the specimen 2:1

(c) Aspect ratio of the specimen 1:1 (d) Aspect ratio of the specimen 0.5:1

Figure 4.8: Plot of the strain ε_{yy} and the stress σ_{yy} for an extension test of a network with square reference cell having the fibre's direction rotated by $\theta = 30$ respect the axis of the specimen.

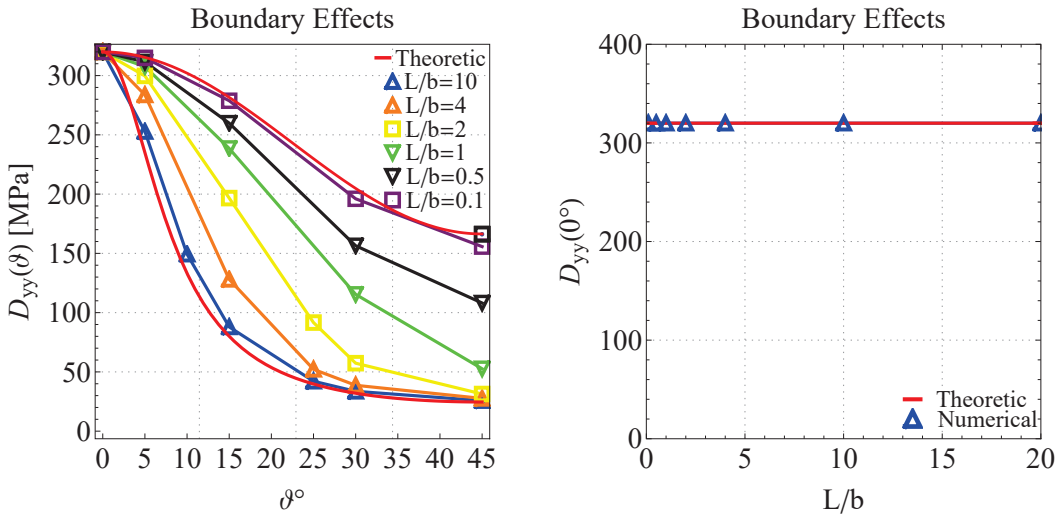

(a) Apparent elastic modulus of the specimen D_{yy} as function of the fibre direction for different aspect ratio of the specimen

(b) Apparent elastic modulus D_{yy} as function of different aspect ratio of the specimen for the fibre direction rotated by 0° respect the specimen axis.

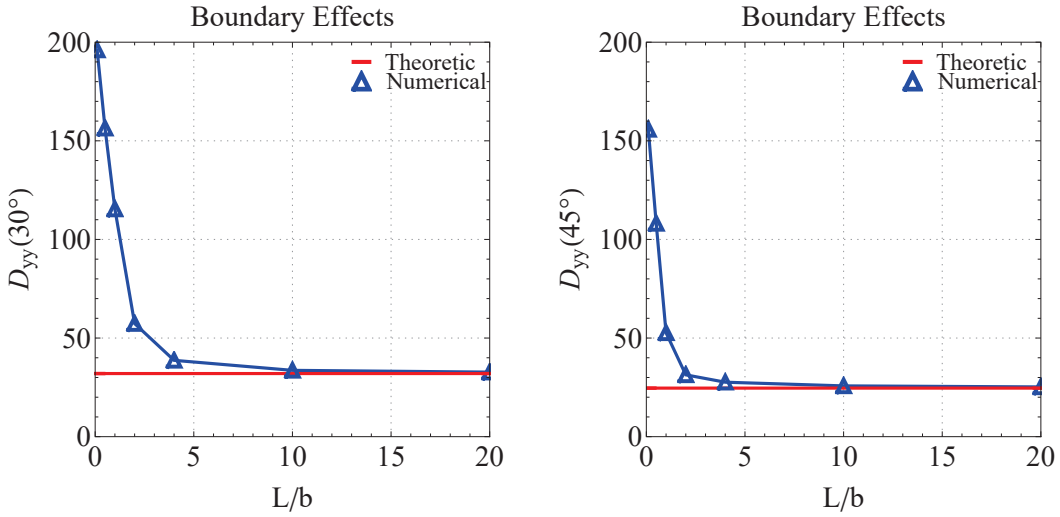

(c) Apparent elastic modulus D_{yy} as function of different aspect ratio of the specimen for the fibre direction rotated by 30° respect the specimen axis.

(d) Apparent elastic modulus D_{yy} as function of different aspect ratio of the specimen for the fibre direction rotated by 45° respect the specimen axis.

Figure 4.9: Extension test simulation: apparent elastic modulus D_{yy} as function of the length ratio of the sample and the direction of the fibers of a network material with square cells rigidly connected.

4.3.2 Fibre network material with square braced cells rigidly connected

The same simulations of the previous cell are made for the fibre network with square cell with braces rigidly connected.

Figure 4.10 shows the results from an extension test where the direction of the fibres coincides with the direction of the load $\theta = 0°$, while the length ratio L/b of the sample varies.

In this case strains and stresses are not uniformly constant like in the case seen in subsection 4.3.1, but a small variation of the strain and the stress in the specimen is observed near the founds, since for the braced cell dos not present Poisson ratio is different from zero.

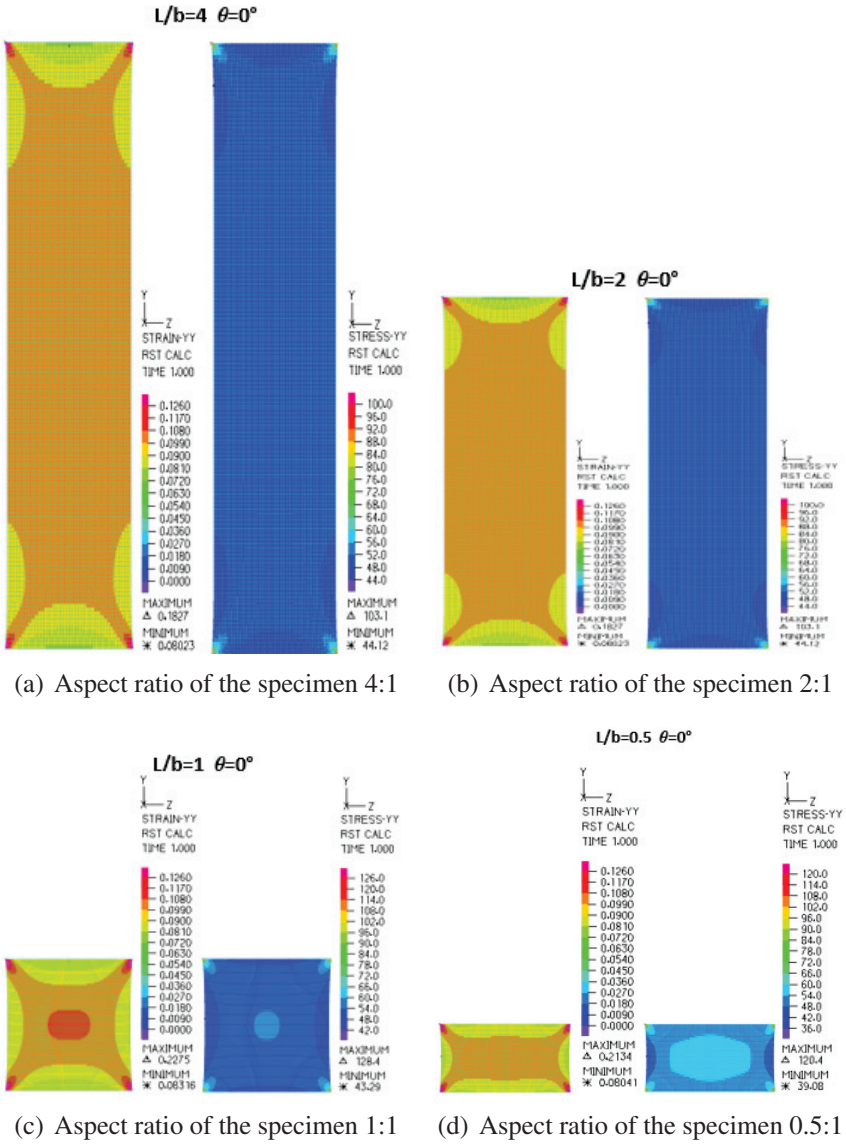

(a) Aspect ratio of the specimen 4:1 (b) Aspect ratio of the specimen 2:1

(c) Aspect ratio of the specimen 1:1 (d) Aspect ratio of the specimen 0.5:1

Figure 4.10: Plot of the strain ε_{yy} and the stress σ_{yy} for an extension test of a network with square braced cells rigidly connected having the main fibre's direction coincident to the axis of the specimen.

When the main fibres form an angle $\theta = 30°$ with the specimen axis, figure 4.11, it is possible to observe a more uniform behaviour of the material respect to the analogous test on a square cell without braces. This is a consequence of the small anisotropy contrast

experienced by this cell. It should be also added that the response of the element is not affected significantly by the length ratio.

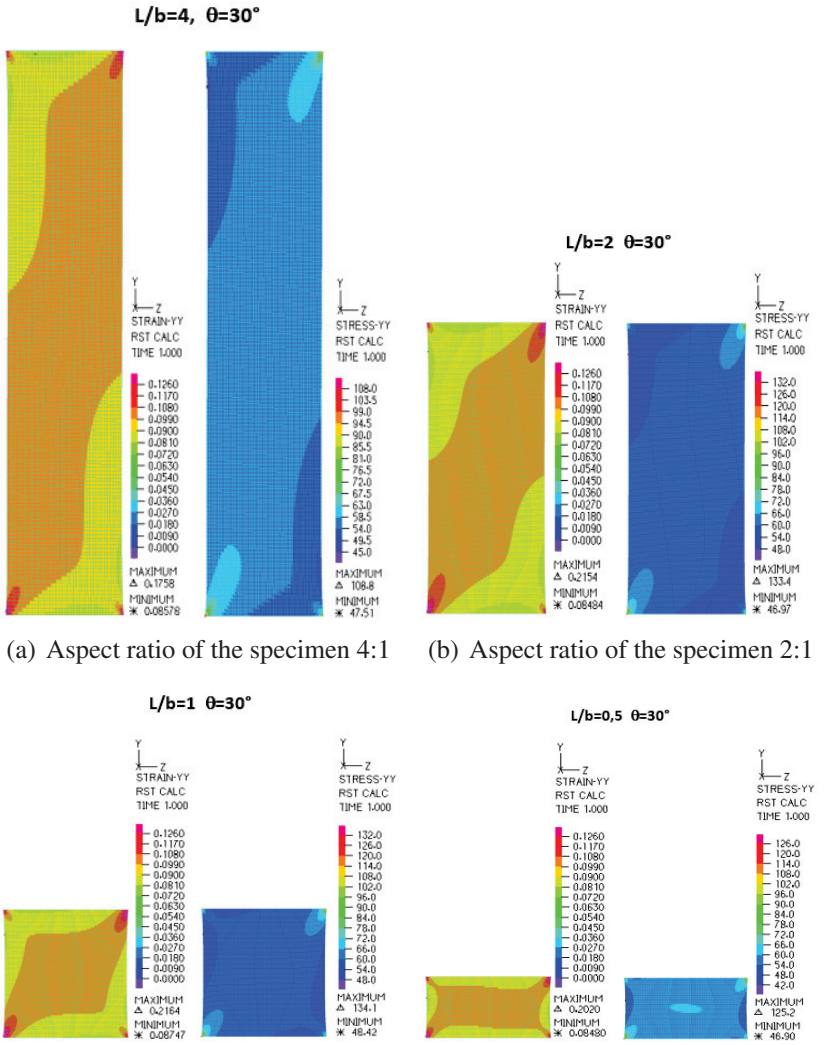

(a) Aspect ratio of the specimen 4:1 (b) Aspect ratio of the specimen 2:1

(c) Aspect ratio of the specimen 1:1 (d) Aspect ratio of the specimen 0.5:1

Figure 4.11: Plot of the strain ε_{yy} and the stress σ_{yy} for an extension test of a network with square braced cells rigidly connected having the main fibre's direction rotated by $\theta = 30$ respect the axis of the specimen.

The plots of figure 4.12 present the apparent elastic modulus as function of the fibre direction θ in the range $(0°, 45°)$, for various length ratios of the sample. Comparing this plot with the one from the previous case, figure 4.9(a), it is possible to observe that in this case the behaviour of the material is almost independent of the fibre direction; moreover, the two limit curves representing the uniaxial strain and uniaxial stress state are very close. This behaviour is due to the stiffness contribution given by the braces in all the specimen directions. The plots 4.9(b), 4.9(c) and 4.9(d) show the apparent elastic modulus vs. the length ratio of the specimen for fibre orientation $\theta = 0°$, $\theta = 30°$ and $\theta = 45°$, respectively. From the latter it is highlighted that for obtaining a response of the material close to the material one without the effect of boundary conditions (red curve), it is sufficient to take samples with length ratio greater than 2.

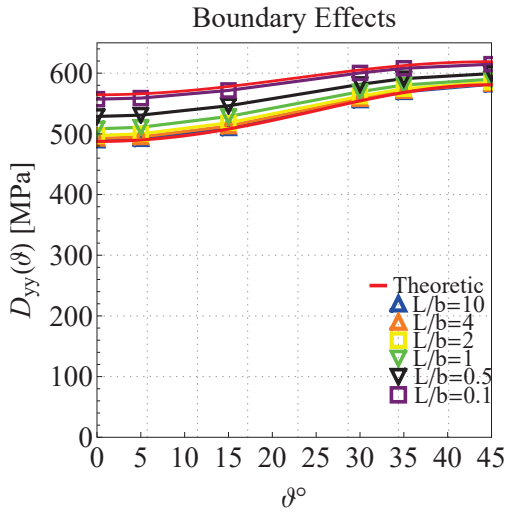

(a) Apparent elastic modulus of the specimen D_{yy} as function of the fibre direction for different aspect ratio of the specimen

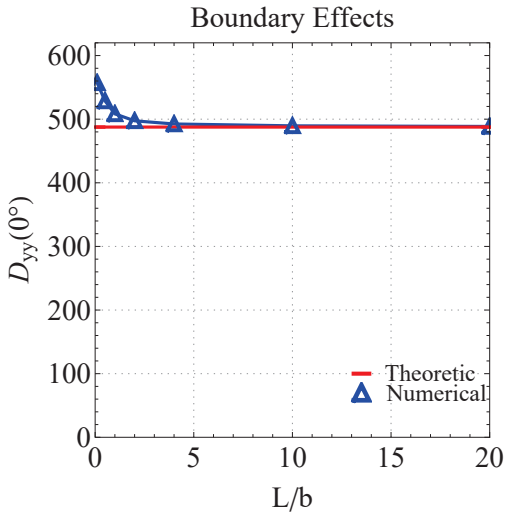

(b) Apparent elastic modulus D_{yy} as function of different aspect ratio of the specimen for the main fibre direction rotated by 0° respect the specimen axis.

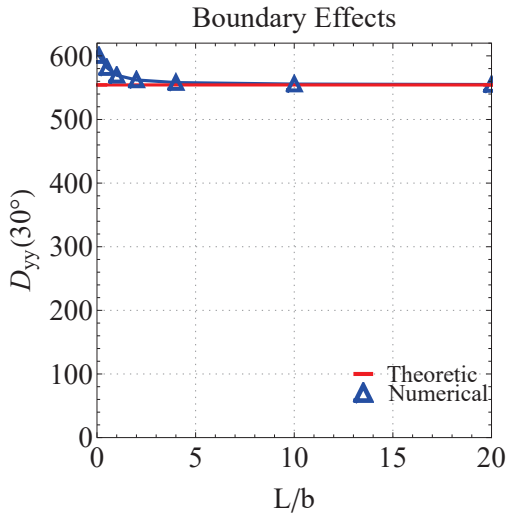

(c) Apparent elastic modulus D_{yy} as function of different aspect ratio of the specimen for the main fibre direction rotated by 30° respect the specimen axis.

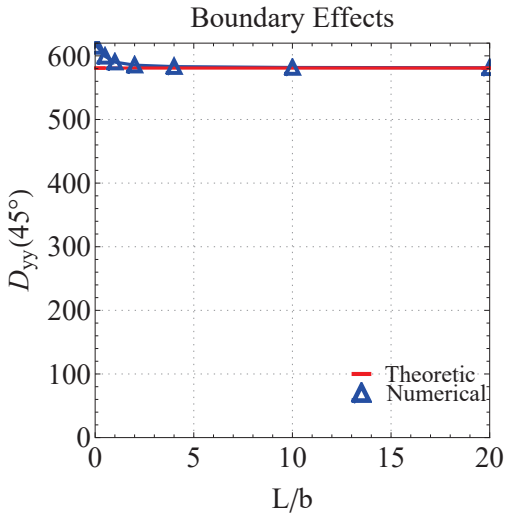

(d) Apparent elastic modulus D_{yy} as function of different aspect ratio of the specimen for the main fibre direction rotated by 45° respect the specimen axis.

Figure 4.12: Extension test simulation: apparent elastic modulus D_{yy} as function of the length ratio of the sample and the direction of the fibers of a network material with braced square cells rigidly connected.

4.4 Unbalanced nets

4.4.1 Square cell with different fibres properties

Up to this point balanced networks were considered, that is networks with equal properties of the fibres in the orthogonal directions. In this section we analyse the behaviour of a square cell characterized by different fibre properties in the two main directions. Extensional tests on a specimen having aspect ratio 4:1 are performed.

The specimen has been subjected to a bias test (elongation test, where the fibres are oriented at 45° with respect to the specimen axis, using the following data:

- $l_1 = l_2 = 5 \quad mm$
- $h_1 = h_2 = 1 \quad mm$
- $E_1 = 1600 \quad MPa$

For the elastic modulus E_2 of the fibres in direction 2 have been considered three different cases:

- $E_2 = 1600 E_1/E_2 = 1$
- $E_2 = 320 E_1/E_2 = 5$
- $E_2 = 80 E_1/E_2 = 20$

For each case in figures 4.13, 4.14 and 4.15 are reported the deformation, the strain ε_{yy} in the axial direction and the shear strain in the material axes γ_{12}. With respect to the balanced case, $E_2 = E_1$, a slight S-shaped deformation is obtained.

Looking at the strains, in the balanced case they are zero near the edges, then two diagonal bands can be detected, next to which the strains reach their maximum value, while in the centre of the specimen the strain is almost uniform, although with smaller values. In the unbalanced cases the distribution of strains is no longer symmetric, and it can be noticed the formation of a band inclined in the direction of the most stiffest fibres. Similarly, a greater concentration of stresses and strains occurs in the corner where converge the fibres disposed in the 1-direction.

It is interesting to compare the previous results with those obtained from an extensional test on a 4:1 specimen composed by unbalanced fibres, where $E_2 = 1/20 E_1$, with in addition the material direction 1 rotated by an angle of 30° with respect to the specimen axis. The results are summarized in figure 4.16. The deformation is similar to the one observed in the previous case, even though the S-shape is more evident (see figure 4.17(a)). However, the strain distribution (figures 4.16(b) and 4.16(c)) is different. In the considered case, a diagonal band having the same direction as the fibres appear, and the largest values of the strain are reached near the border at the ends of this band. For a more convenient examination of the plots, the same colour scales have been used in figure 4.16, as in figures 4.14 and 4.15.

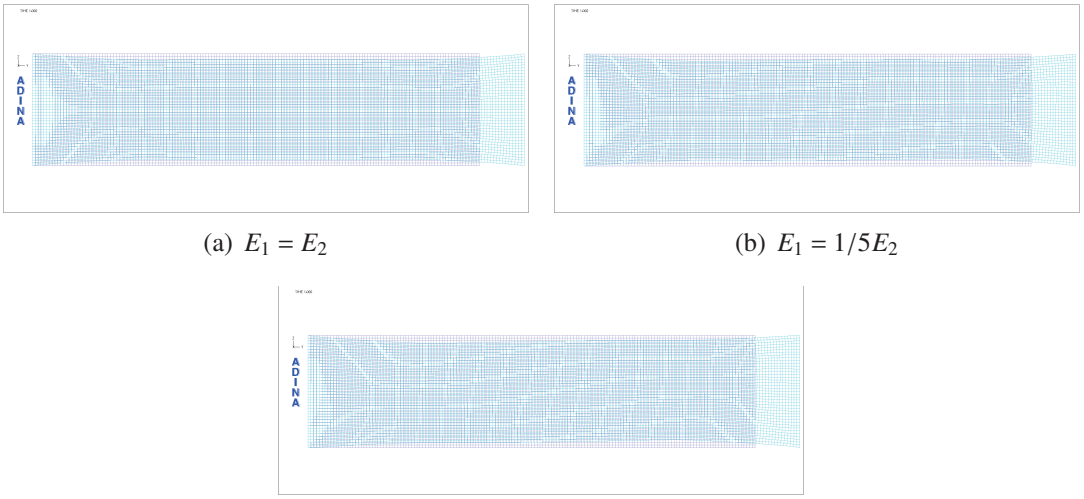

(a) $E_1 = E_2$ (b) $E_1 = 1/5E_2$

(c) $E_1 = 1/20E_2$

Figure 4.13: Bias test in an unbalanced network - Plots of deformed configurations for three values of the Young modulus of the fibers 2

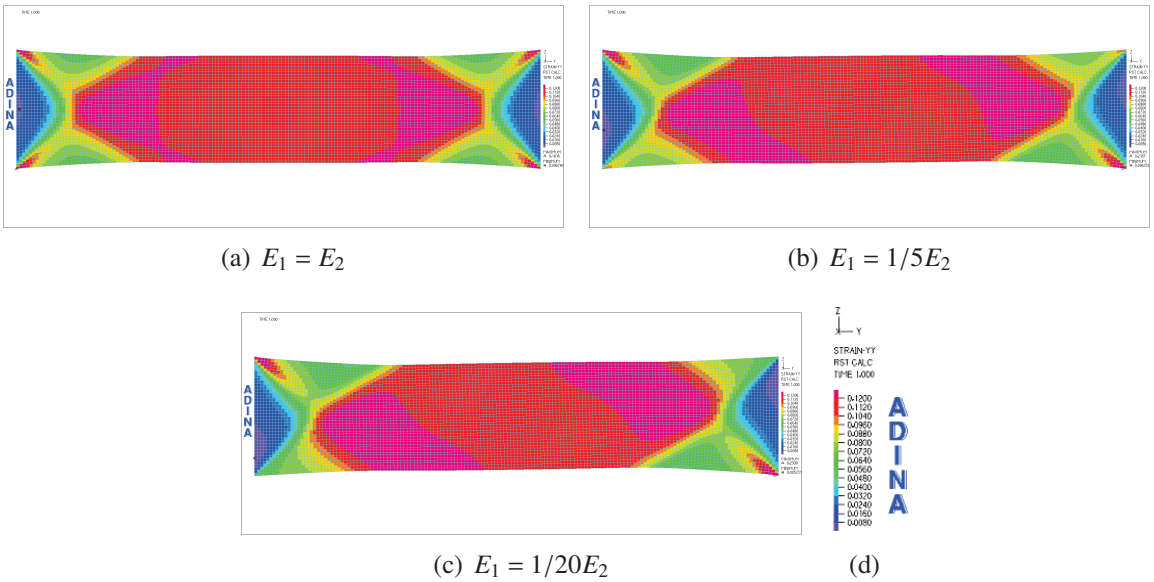

(a) $E_1 = E_2$ (b) $E_1 = 1/5E_2$

(c) $E_1 = 1/20E_2$ (d)

Figure 4.14: Bias test in a unbalanced network - Plots of strain in direction y, ϵ_{yy}, for three values of the Young modulus of the fibers 2

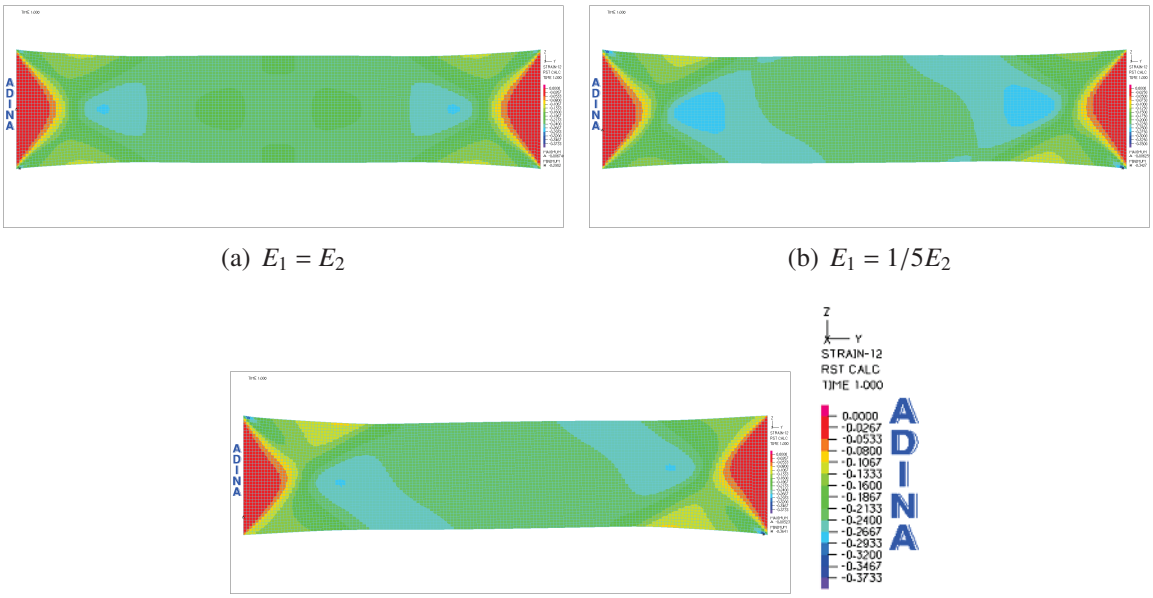

(a) $E_1 = E_2$ (b) $E_1 = 1/5E_2$

(c) $E_1 = 1/20E_2$ (d)

Figure 4.15: Bias test in a unbalanced network - Plots of the shear strain γ_{12} for three values of the Young modulus of the fibers 2

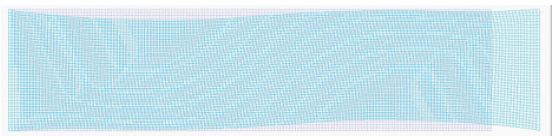

(a) Deformed configurations

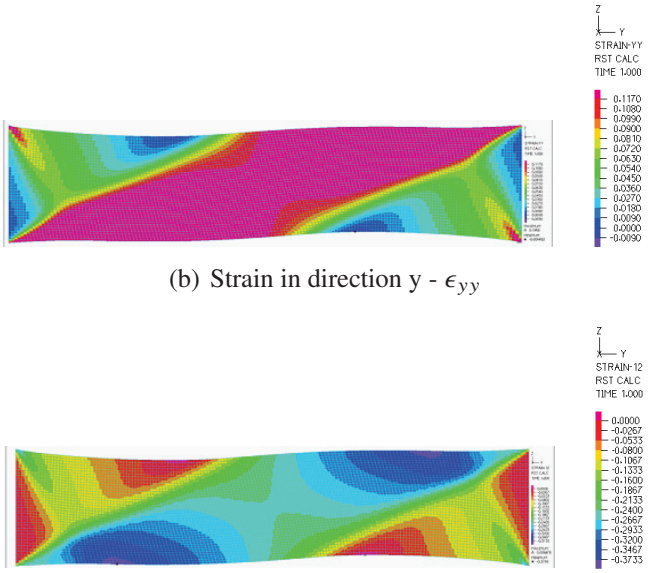

(b) Strain in direction y - ϵ_{yy}

(c) Shear angle γ_{12}

Figure 4.16: Bias test in a unbalanced network material with the direction of the fiber rotated by 30° with $E_2 = 1/20E_1$

4.4.2 Network with skew cell

The following simulation is performed on a 4:1 specimen constituted by a network of two families of fibres forming an angle of 30° among themselves, The 1-axis is coincident with the specimen axis. Equal properties for the fibres and equal length of the sides of the elementary cell have been assumed. The same parameters as those listed in section 4.2 have been used. As it was underlined, in this case an orthotropic material with symmetry axes rotated by 15° is obtained. In figure 4.17 are reported the deformation, and the strain $\varepsilon_{yy}, \gamma_{12}$.

The deformation presents a severe S-shape, due to the fact that the shear strain concentrate along the diagonal of the specimen (figure 4.17(c)). Notice that for the 4:1 specimen the diagonal is inclined of an angle very close to 15°. From these results it can be observed that the response of a fibre network with non orthogonal fibres is quite different from the response of a material with unbalanced orthogonal fibres.

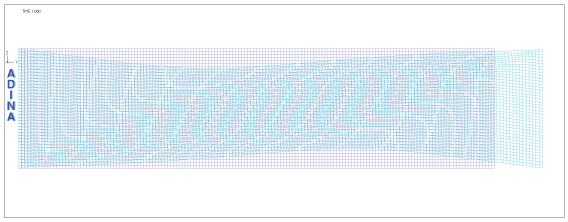

(a) Deformed configurations

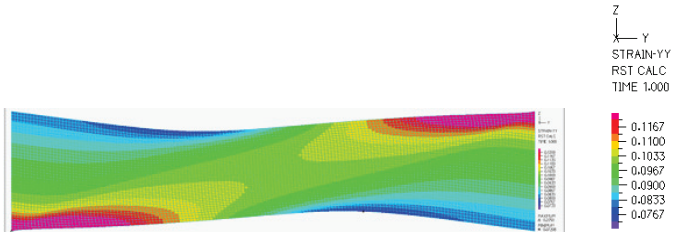

(b) Strain in direction y - ϵ_{yy}

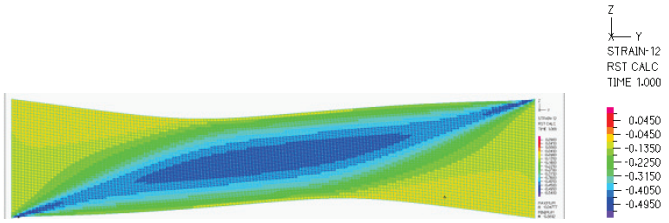

(c) Shear angle respect the material axes - γ_{12}

Figure 4.17: Extension test in network material with skew cell - angle between the fibres is equal to $\alpha = 30$

4.5 Extension of bidirectional tissue

This section concerns bias tests on a tissue composed by two families of fibres, with the same characteristic in the two orthogonal directions. As we said in section 3.5, the repetitive unit of the material can be approximately described by the model of a square cell with a

pivot connecting the two fibres. The properties of the fibres are the same reported in 4.2. A specimen with length/height ratio 2:1 and fibres at an angle of 45° with respect to the longitudinal axis is analysed.

Initially, the tests will be simulated by means of the homogenized first gradient Cauchy model. Since the constitutive relation obtained in equation (3.80) is singular, the properties of the solution will be investigated. The extensional stiffness of the network depends on to the axial stiffness of the fibres and assumes the same values of the extensional stiffness of the case of square cell rigidly connected, as can be observed by the comparison of equations (3.80) and (3.23). The term D_{33} of the constitutive matrix of the square cell rigidly connected, that is the shear modulus, is non-zero and depends on the bending stiffness of the two beams of the cell. The ratio of the shear modulus to the extensional modulus for the square cell with rigid connection is of the order h^2. The terms D_{11} and D_{22}, corresponding to the equivalent stiffness coefficients associated to the extensional deformation modes, are fixed equal to 320 MPa for both the models.

Four numerical experiments have been performed reducing the equivalent shear modulus $G_{12} = D_{33}$ from 10 to 10^{-7}. This numerical experiments are equivalent to analyse a network with square cell rigidly connected having fibres whose bending stiffness becomes smaller and smaller. The case D_{33} equal 10 is appropriate for the networks with rigid connection and slender beams but with a finite bending stiffness. The relevant deformed shapes of the specimen are shown in figure 4.18. In figure 4.19 are represented the contour plots of the shear strain γ_{12}, where 1 and 2 are the fibre axes.

When the shear modulus is one order lower than the extensional modulus (10 vs. 320), a fairly smooth deformed shape is obtained (figure 4.18(a), and correspondingly the distribution of the shear strain shows a smooth transition from the zone of approximately null strain near the edges, to the central zone where the shear strain is constant and approximately equal to 0.3. Notice that the edge red area corresponds to 0.033.

The case $G_{12} = 0.1$, with shear stiffness about 3 orders of magnitude smaller than the extensional stiffness, is illustrated in figures 4.18(b) and 4.19(b). Apparently, this case well reproduces the response typically obtained in a bias test on a bidirectional balanced tissue: the deformation presents sharp discontinuity bands, separating three zones of constant value of the shear strain, clearly shown in the plot of figure 4.19(b). This is the limit solution predicted by Pipkin's model of tissue with inextensible fibres and finite rotational stiffness at the joints [24–26, 64, 78].

However, when the shear modulus is further reduced, the obtained solution departs from Pipkin's result. For $G_{12} = 10^{-3}$ and $G_{12} = 10^{-7}$, that is the shear stiffness is 5 and 9 orders of magnitude lower than the extensional stiffness, a smoother deformation is obtained (figures 4.18(c) and 4.18(d)). It can be seen that when the shear modulus gets smaller, a larger part of the specimen near the ends remains undeformed. This can be also appreciated from the plots of the shear strain, where the red zones (corresponding to nearly zero strain) get larger and extend beyond the corner of the specimen. In addition, a further area of zero shear strain appears near the border at the centre of the specimen. For the smallest value of the shear modulus employed in the simulations, two x-shaped bands where the strain shear ranges between 0.3 and 0.4 are obtained. The transition from the region of these two bands is quite sharp, even if there is not discontinuity line. The concentration of strain may be produced by the fact that the constitutive tensor is singular. Indeed, in this situation it is well known that strain concentration occurs.

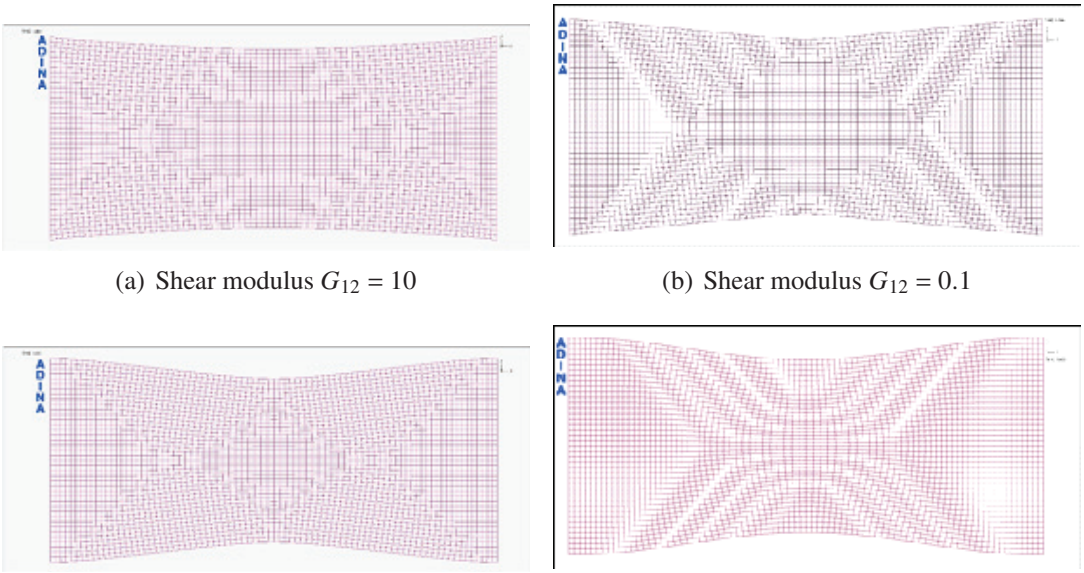

(a) Shear modulus $G_{12} = 10$ (b) Shear modulus $G_{12} = 0.1$

(c) Shear modulus $G_{12} = 0.001$ (d) Shear modulus $G_{12} = 0.0000001$

Figure 4.18: Deformed configurations for four values of the equivalent shear modulus G_{12}

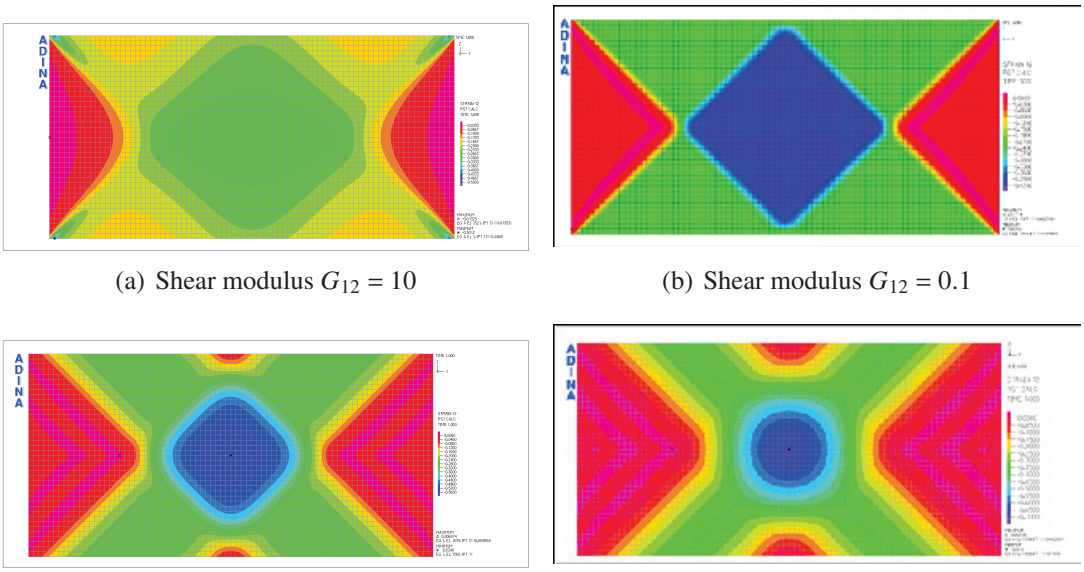

(a) Shear modulus $G_{12} = 10$ (b) Shear modulus $G_{12} = 0.1$

(c) Shear modulus $G_{12} = 0.001$ (d) Shear modulus $G_{12} = 0.0000001$

Figure 4.19: Shear strain γ_{12} for four values of the equivalent shear modulus G_{12}

The case $G_{12} = 0$ has been considered separately, using an original finite element code based on isogeometric interpolation. As said before, a very fine mesh of third order splines was used, shown on the plot of figure 4.21(a) that represents the deformed shape of the sample. The solution is very similar to the one obtained for $G_{12} = 10^{-7}$, with an even sharper definition of the areas of zero strain (red areas in the plot). The transitions from the red zones (zero strain) to the green zone (strain equal to approximately 0.4) and the blue zone (strain equal to about 0.7) are rather sharp.

The result is independent from the aspect ratio of the specimen, as is indicated in figure 4.21, that refers to a specimen with a 3:1 aspect ratio. Also in this case well defined bands of nearly constant strain are obtained, but different from the Pipkin's result where inextensible fibres with finite shear strain are considered. On the contrary, in the case examined here, the fibres have a finite extensional deformation while the shear stiffness of the network is rigorously zero.

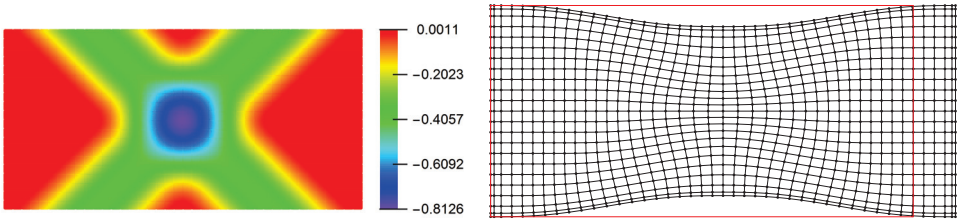

(a) Shear strain γ_{12} (b) Deformed configuration

Figure 4.20: Shear strain γ_{12} and deformed configuration, with the shear modulus $G_{12} = 0$, obtained via isogeometric analysis - Aspect ratio of the specimen 2:1

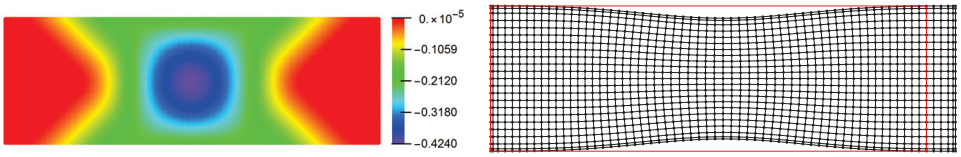

(a) Shear strain γ_{12} (b) Deformed configuration

Figure 4.21: Shear strain γ_{12} and deformed configuration, with the shear modulus $G_{12} = 0$, obtained via isogeometric analysis - Aspect ratio of the specimen 3:1

The presence of jumps in the strain suggests that the first order model employed is not completely adequate, since it disregards the bending stiffness of the fibres, that appears in the coefficients of the second order constitutive relation. Employing the customer IGA code, a simulation of the test using the strain gradient homogenized material model described in section 3.5 has been performed. The constitutive relations are given by equations (3.80) and (3.81). The same boundary conditions as in the bias test for first gradient material have been used. That is, the displacements are fixed on the edges, and the derivatives of the displacement have been left free.

Figure 4.22 shows the deformed shape of the specimen, that appears smooth along the specimen borders.

The shear strain γ_{12} is presented in figure 4.24(c). The zone of zero strain (reproduced in red) is smaller than the one obtained with the first gradient model, and emanates from

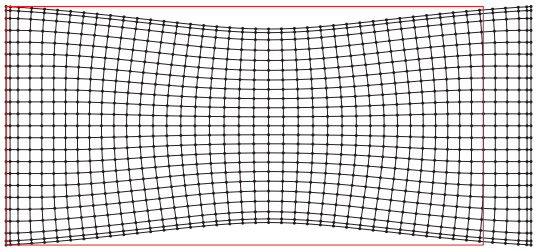

Figure 4.22: Deformed configuration of the bias test on a second gradient material

the corners of the specimen. The zones of zero strain near the borders have disappeared, while the band of constant strain have significantly enlarged. Also the maximum strain at the centre has become smaller than in the first gradient simulation, equal to about 0.4.

The second gradient strain in material coordinates are presented in figure 4.25. The strains $\frac{\partial \varepsilon_{11}}{\partial x_1}$ and $\frac{\partial \varepsilon_{22}}{\partial x_2}$ are almost identically zero, except near the corners, where there is a stress concentration due to the concentrated reaction (figure 4.25(a)). Significant are the strain components $u_{1,22}$ and $u_{2,11}$, representing the bending deformations. Two bands of bending strains appear, corresponding to the position where there is a transition in the first order shear strain. In these bands there is also a non negligible gradient of the shear strain in the direction orthogonal to the band (figure 4.25(c)). Plots of first and second order strains in the global coordinate system are presented in figures 4.26 and 4.27.

From the numerical solution it is easy to evaluate the energy associated to the first gradient strains (E') and the energy associated with the second gradient strains (E''). The two values are plotted in figure 4.23 as a function of the height h of the fibres. The case examined above corresponds to $h = 1$ mm. The plot shows that for $h = 10^{-2}$ there is a transition from first gradient dominated behaviour to second gradient dominated behaviour. The results discussed refer to the latter case. It appears that this dependency of the sensitivity of the solution of the second gradient strain on the details of the micro-structure was not observed before.

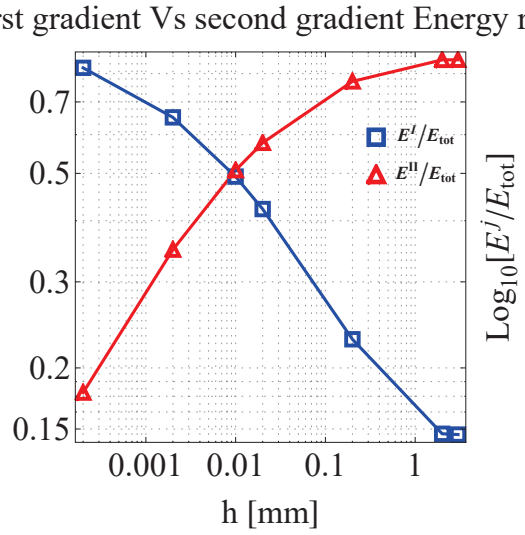

Figure 4.23: Ratio between the first gradient energy and the total energy and ratio between the second gradient energy and the total energy vs. height of the microbeams.

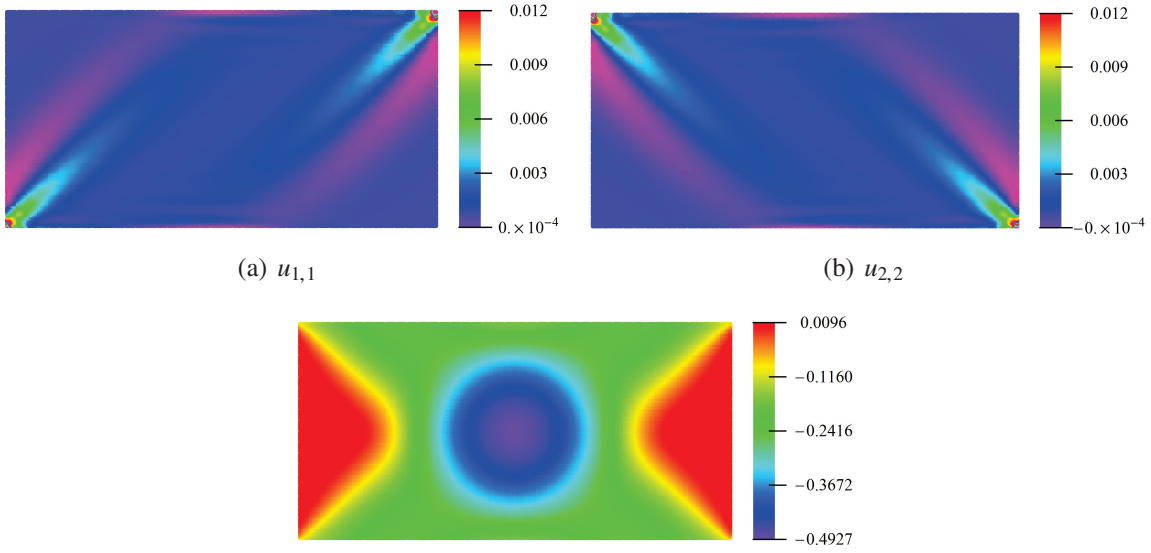

(a) $u_{1,1}$ (b) $u_{2,2}$

(c) $\gamma = u_{1,2} + u_{2,1}$

Figure 4.24: Bias test of a second gradient material: components of the first gradient of the displacement **u** with respect to the material axes.

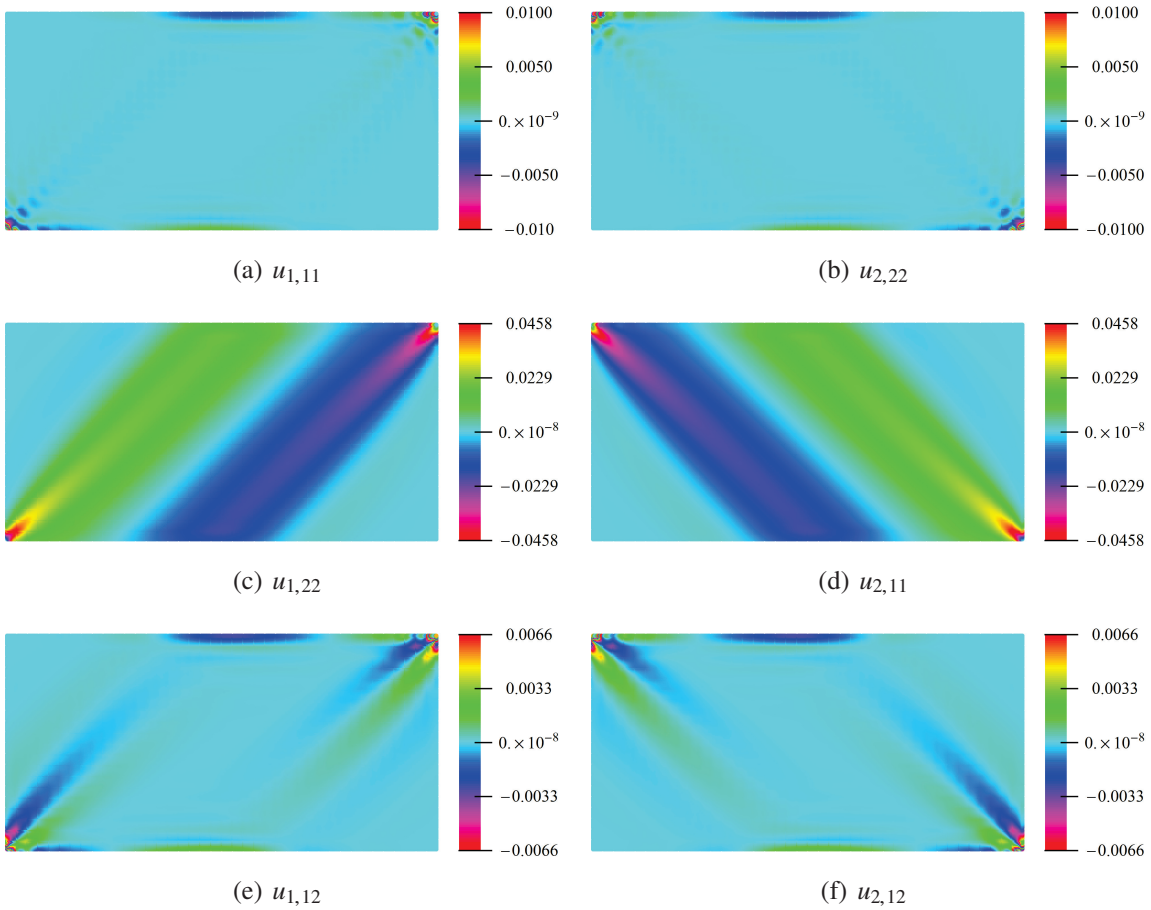

(a) $u_{1,11}$ (b) $u_{2,22}$

(c) $u_{1,22}$ (d) $u_{2,11}$

(e) $u_{1,12}$ (f) $u_{2,12}$

Figure 4.25: Bias test of a second gradient material: components of the second gradient of the displacement **u** with respect to the material axes.

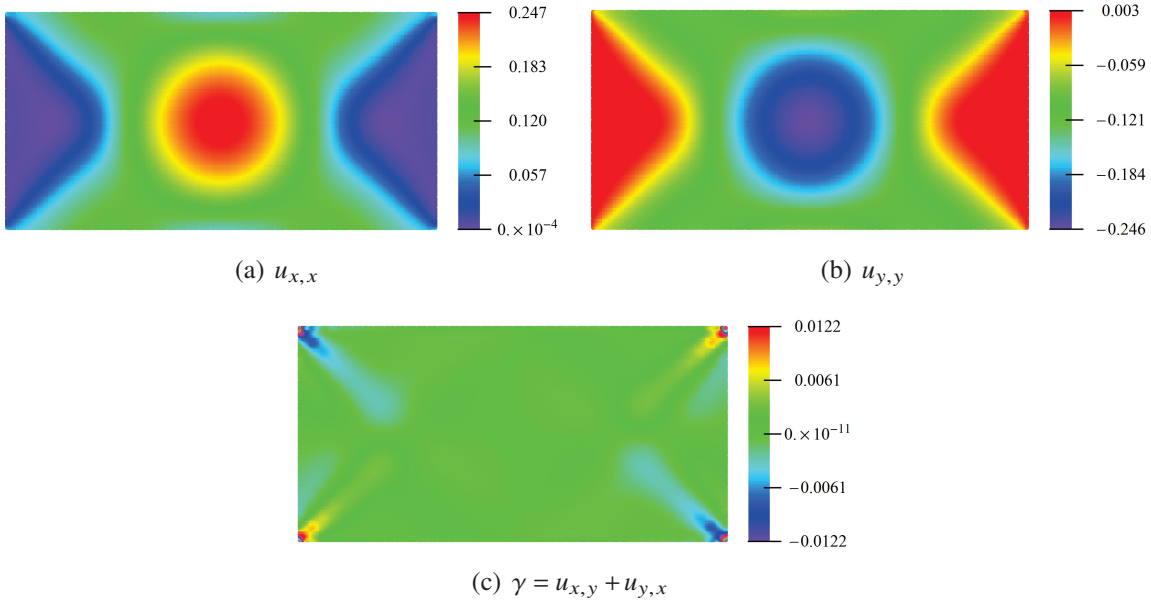

(a) $u_{x,x}$ (b) $u_{y,y}$

(c) $\gamma = u_{x,y} + u_{y,x}$

Figure 4.26: Bias test of a second gradient material: components of the first gradient of the displacement **u** with respect to the global axes (y,z).

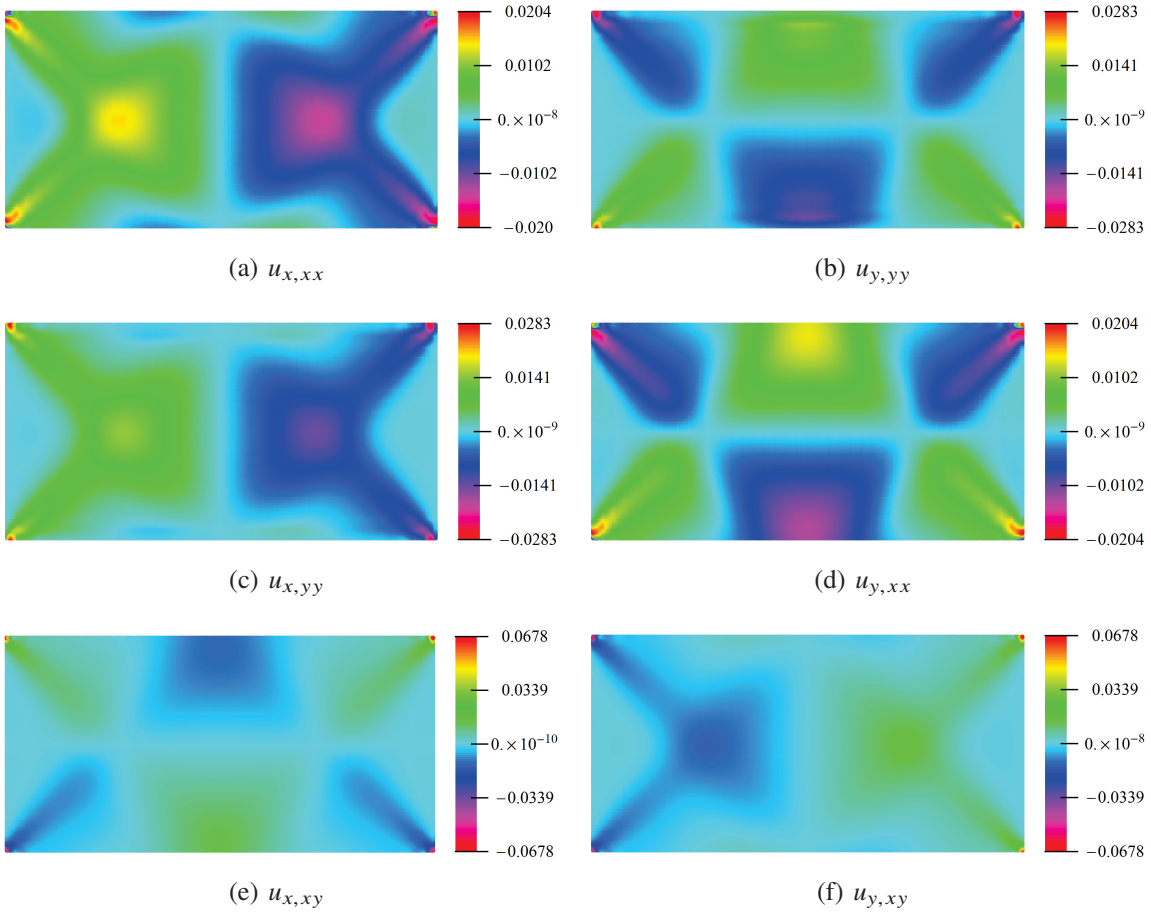

(a) $u_{x,xx}$ (b) $u_{y,yy}$

(c) $u_{x,yy}$ (d) $u_{y,xx}$

(e) $u_{x,xy}$ (f) $u_{y,xy}$

Figure 4.27: Bias test of a second gradient material: components of the second gradient of the displacement **u** with respect to the global axes (y,z).

Conclusions and perspectives

In the thesis the mechanical behaviour of networks of fibres has been studied, with the aim of obtaining a continuum model at the macroscale that could account for the microstructure of the network, which strongly influences the macroscopic response. The fibres in the network have been treated like microbeams, having both extensional and bending stiffness, with different types of connection, according to the pattern and detail of the network.

Since the microelements are beams, asymptotic discrete homogenization has been used. Therefore, in the thesis the discrete homogenization has been applied for obtaining a mechanical model of a network material, in a form convenient for numerical applications. Although the reference model is a network material, it is believed that the results obtained can be applied to other similar kinds of microstructures, like pantographic materials, micro devices composed by microbeams etc.

The results obtained have been limited at the range of linear elasticity, that is small deformation and linear elastic behaviour. While the latter assumption is usually well verified in fibre networks, the former can be a limitation. In the examination of future perspective, however, it will be pointed out that the results obtained can be preparatory to the extension of the model to large deformations.

Nor the method nor application of homogenization procedures to network materials are new, as has been pointed out in Chapter 1, where existing models present in the literature concerning continuum models for network materials have been shortly examined.

The thesis has presented a systematic application of the Homogenization method of Periodic Media (HPDM) to general types of networks. Classical strong formulation and a rigorously developed weak formulation have been compared, and it has been concluded that the weak formulation is more suitable for applications to complex lattices, especially when the repetitive cell presents internal nodes. This case had not been previously systematically presented.

Then, the 2D weak formulation, accounting for the axial and flexural stiffness of the elements of the cell was described. The novelty of the method lies on two aspects. The first regards the definition of a systematic methodology to derive the internal forces in a consistent way based on the asymptotic development of both the displacement and the rotations at the same order of the expansion. The second is the definition of the microrotation as a function of the macroscopic displacement without a-priori assumptions. The same procedure was followed by Caillerie et al. [74], [76] and [75], but only considering the axial deformability, and by Boutin et al. in [82, 83] who developed the procedure only in strong formulation for and considering simple cells, without internal nodes.

The developed procedure was applied for obtaining the homogenized mechanical models for some types of biaxial and quadriaxial networks of fibres, simulating either fibre nets (in this case rigid connection were assumed among the fibres) or tissues with negligible interac-

tion between the fibre bundles, and with relative sliding prevented (in this case the connections were simulated by means of pivots). Different geometries were analysed, including the cases in which the fibres are not orthogonal.

For cells with orthogonal fibres an equivalent Cauchy orthotropic continuum was obtained. When there are only two families of orthogonal fibres, the orthotropic equivalent material has zero Poisson ratio. For all the cases examined the anisotropy contrast was estimated evaluating the apparent stiffness modulus for an uniaxial stress state applied on a direction rotated with respect to the fibre axes. The anisotropy contrast depends on the fibre properties, as it was expected, and also on the structure of the network. Networks with 4 families of fibres, either rigidly connected or connected with pivots, presented a lower degree of contrast between the principal axes of anisotropy. Orthogonal networks of fibres lead to sharply anisotropic materials, difficult to meet in common continua.

Special results were obtained for the case of fibres connected by pivots. In this cases an orthotropic material with zero shear modulus was obtained. Such a material has a not elliptic constitutive tensor, thus it can lead to strain concentrations.

However, it was shown that some considerations about the physical behaviour of such networks indicated that higher order terms had to be included in the expansion of the internal forces and deformations, so that a strain gradient material was obtained. The coefficients of the second gradient strains in the constitutive tensor depend on the bending stiffness of the fibres. The results obtained can be used for the design of specific materials requiring ad-hoc properties.

The numerical simulations were focused on extension tests and bias tests. The obtained deformed configurations are consistent with the literature experimental tests, both for balanced and unbalanced tissues. Moreover, a comparison between first and second gradient numerical predictions was performed. It was observed that second gradient predictions better simulate the experimental evidences, see figure 4.28.

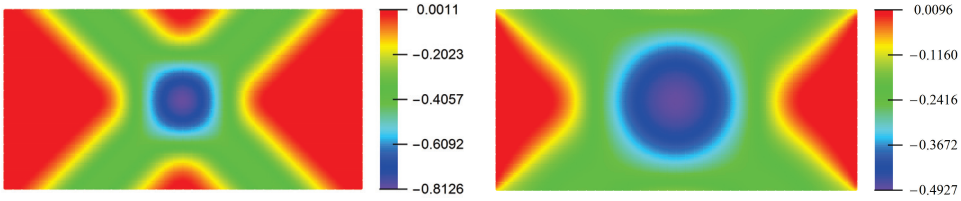

(a) Shear strain γ_{12}, only first gradient is considered

(b) Shear strain γ_{12}, both first gradient and second gradient are considered

Figure 4.28: Shear strain γ_{12}, with the shear modulus $G_{12} = 0$, obtained via isogeometric analysis - Aspect ratio of the specimen 2:1

The comparison between the energy associated to the first gradient strains and the energy associated with the second gradient strains showed the dependency of the sensitivity of the strain gradient solution on the details of the micro-structure (see figure 4.23).

Further developments can regards the 3D formulation, to include out of plane deformation. If the fibres are straight beam the method proposed in this thesis extends without significant modifications. In the case of curved and twisted beams a semi numerical approach will be needed. However, the present method appears to be very easy, much more convenient and useful for the obteining homogenized model than the continuum omogenization tecnique like one used by [72].

Moreover, a possible extension is the geometrical non linearity. When large deformation are involved in the process, the shape of the cells changes. Assuming that the fibres remain substantially straight (bending curvature negligible with the respect to the rotation of the fibre axis) in the deformed configuration the cells with original orthogonal size behaves like the skew cell presented in subsection 3.2.

A non linear procedure based an update Lagrange approach can easily be implemented in a numerical code, using the result derived for the skew cell.

Material non linearity and source of dissipation can be added using for instance the method proposed by Marfia and Sacco in [102, 103].

The application of the obtained results to fibre nets, tissues and pantographic networks can be performed on the base of the numerical method shown in chapter 4.

Bibliography

[1] M.A. Khan, T. Mabrouki, E. Vidal-Salle, and et al. Numerical and experimental analyses of woven composite reinforcement forming using hypoelastic behaviour. application to the double dome benchmark. *J. Mater. Process. Technol*, 210:378–388, 2009.

[2] N. Hamila, , and P. Boisse. A meso-macro three node finite element for draping of textile composite preforms. *Appl. Comp. Mater.*, 14:235–250, 2007.

[3] J. Pora. Composite materials in the airbus a380 from history to future. *In: 13th international conference on composite materials (ICCM-13), Beijing, China, July 2001*.

[4] J. Sinke. Manufacturing of glare parts and structures. *Appl. Comp. Mater.*, 10:293–305, 2003.

[5] A.J.M. Spencer and K.P. Soldatos. Finite deformations of fibre-reinforced elastic solids with fibre bending stiffness. *Int. J. Non-Linear Mech.*, 45(2):355–368, 2007.

[6] H. Nikopour and A. Selvadurai. Torsion of a layered composite strip. *Compos. Struct.*, 95:1–4, 2013.

[7] H. Nikopour and A. Selvadurai. Concentrated loading of a fibre-reinforced composite plate: experimental and computational modeling of boundary fixity. *Compos. B Eng.*, 60:297–305, 2014.

[8] A. Grillo, G. Wittum, A. Tomic, and S. Federico. Remodelling in statistically oriented fibre-reinforced materials and biological tissues. *Math. Mech. Solids*, 20(9):1107–1129, 2015.

[9] S. Federico and A. Grillo. Elasticity and permeability of porous fibre-reinforced materials under large deformations. *Mech. Mater.*, 44:58–71, 2012.

[10] U. Andreaus, I. Giorgio, and T. Lekszycki. A 2-d continuum model of a mixture of bone tissue and bio-resorbable material for simulating mass density redistribution under load slowly variable in time. *ZAMM Z. Angew. Math. Mech.*, 94(12):978–1000, 2014.

[11] I. Giorgio, U. Andreaus, and A. Della Corte T. Lekszycki. The influence of different geometries of matrix/scaffold on the remodeling process of a bone and bioresorbable material mixture with voids. *Math. Mech. Solids*, 2015.

[12] A. Madeo, G. Barbagallo, M.V. DAgostino, and P. Boisse. Continuum and discrete models for unbalanced woven fabrics. *International Journal of Solids and Structures*, 94:263–284, 2016.

[13] A. Misra and V. Singh. Micromechanical model for viscoelastic materials undergoing damage. *Contin. Mech. Thermodyn.*, 25(2-4):343–358, 2013.

[14] P. Boisse, M. Borr, K. Buet, and A. Cherouat. Finite element simulations of textile composite forming including the biaxial fabric behavior. *Compos. B*, 28(41):453–464, 1997.

[15] M. Komeili and A.S. Milani. The effect of meso-level uncertainties on the mechanical response of woven fabric composites under axial loading. *Computers and Structures*, 90:163–171, 2012.

[16] L. Placidi, U. Andreaus, A. Della Corte, and T. Lekszycki. Gedanken experiments for the determination of two-dimensional linear second gradient elasticity coefficients. *Z. Angew. Math. Phys.*, 66(6):3699–3725, 2015.

[17] T. Lekszycki, N. Olhoff, and J.J. Pedersen. Modelling and identification of viscoelastic properties of vibrating sandwich beams. *Compos. Struct.*, 22(1):15–31, 1992.

[18] U. Andreaus, B. Chiaia, and L. Placidi. Soft-impact dynamics of deformable bodies. *Contin. Mech. Thermodyn.*, 25(2-4):375–398, 2013.

[19] L. Placidi. A variational approach for a nonlinear one-dimensional damage-elasto-plastic second-gradient continuum model. *Contin. Mech. Thermodyn.*, 28(1-2):119–137, 2016.

[20] L. Placidi. A variational approach for a nonlinear 1-dimensional damage-elasto-plastic second-gradient continuum model. *Contin. Mech. Thermodyn.*, 27(4-5):623–638, 2015.

[21] N. Roveri and A. Carcaterra. Damage detection in structures under traveling loads by hilbert-huang transform. *Mech. Syst.*, 28:128–144, 2012.

[22] G. Barbagallo, A. Madeo, I. Azehaf, I. Giorgio, F. Morestin, and P. Boisse. Bias extension test on an unbalanced woven composite reinforcement: Experiments and modeling via a second gradient continuum approach. *Journal of Composite Materials*, 51(2):153–170, 2016.

[23] F.dell'Isola M. Ferretti, A. Madeo and P. Boisse. Modeling the onset of shear boundary layers in fibrous composite reinforcements by second-gradient theory. *Z. Angew. Math. Phys.*, 65(2):587–612, 2014.

[24] F. dell'Isola, M. Cuomo, L. Greco, and A. Della Corte. Bias extension test for pantographic sheets: numerical simulations based on second gradient shear energies. *Journal of Engineering Mathematics*, 103(1):127–157, 2017.

[25] A. Pipkin. Some developments in the theory of inextensible networks. *Q. Appl. Math.*, 38(3):343–355, 1980.

[26] A. Pipkin. Plane traction problems for inextensible networks. *Q. Appl. Math.*, 34(4):415–429, 1981.

[27] R. Rivlin. Plane strain of a net formed by inextensible chords. *J. Ration. Mech. Anal.*, 4(6):951–974, 1955.

[28] F. dell'Isola and D. Steigmann. A two-dimensional gradient-elasticity theory for woven fabrics. *J. Elast.*, 118(1):113–125, 2015.

[29] D. Steigmann and F. dell'Isola. Mechanical response of fabric sheets to three-dimensional bending, twisting, and stretching. *Acta Mech. Sin.*, 31(3):373–382, 2015.

[30] D. Steigmann and F. dell'Isola. Pantographic 2d sheets: discussion of some numerical investigations and potential applications. *Int. J. Non-Linear Mech.*, 2015.

[31] F. dell'Isola, P. Seppecher, and A. Della Corte. The postulations á la dalembert and á la cauchy for higher gradient continuum theories are equivalent: a review of existing results. *Proceedings Mathematical Physical Engineering Sciences*, 471, 2015.

[32] Andreaus U. Placidi L. dell'Isola, F. At the origins and in the vanguard of peridynamics, non-local and higher-gradient continuum mechanics: an underestimated and still topical contribution of gabrio piola. *Math. Mech. Solids*, 20(8), 2015.

[33] Giorgio I. Eremeyev V.A. Rosi, G. Propagation of linear compression waves through plane interfacial layers and mass adsorption in second gradient fluids. *ZAMM Z. Angew. Math. Mech.*, 93(12), 2013.

[34] A.C. Eringen. Linear theory of micropolar elasticity. *J. Math. Mech.*, 15:909–923, 1966.

[35] A.C. Eringen. Liebowitz, h. (ed.), fracture, vol. ii. *Academic Press, New York*, pages 621–729, 1968.

[36] A.C. Eringen. Continuum physics - non-local field theories. *Academic Press, New York*, 1976.

[37] A.C. Eringen. Microcontinuum field theories. *Springer*, 1998.

[38] R.D. Mindlin. Micro-structure in linear elasticity. *Archive for Rational Mechanics and Analysis*, 16(1):51–78, 1964.

[39] E. Cosserat and F. Cosserat. Théorie des corps déformables. *A. Hermann et Fils, Paris*, 1909.

[40] R.D. Mindlin and N. N. Eschel. On first strain-gradient theories in linear elasticity. *Int. J. Solids Struct.*, 4:109–124, 1968.

[41] J.L. Bleustein. A note on the boundary conditions of toupins strain-gradient theory. *Int. J. Solids Struct.*, 3(6), 1967.

[42] S. Forest and K. Sab. Cosserat overall modeling of heteregeneous materials. *Mechanics Research Communication*, 25(4):449–454, 1998.

[43] S. Forest. Micromorphic approach for gradient elasticity, viscoplasticity, and damage. *J. Eng. Mech.*, 135:117–131, 2009.

[44] S. Forest, N.M. Cordero, and E.P. Busso. First vs. second gradient of strain theory for capillarity effects in an elastic fluid at small length scales. *Comp. Mater. Sci.*, 50:1299–1304, 2011.

[45] S. Forest and R. Sievert. Nonlinear microstrain theories. *Int. J. Solids Struct.*, 43:7224–7245, 2011.

[46] I. Giorgio D. Del Vescovo. Dynamic problems for metamaterials: review of existing models and ideas for further research. *Int. J. Eng. Sci.*, 80:153–172, 2014.

[47] W.T. Koiter. Couple stresses in the theory of elasticity, i and ii. *Proc. Kon. Ned. Akad. Wet. Ser. B.*, 67(1):17–44, 1964.

[48] V.A. Eremeyev H. Altenbach. On the linear theory of micropolar plates. *ZAMM J. Appl. Math. Mech.*, 89(4):242–256, 2009.

[49] V.A. Eremeyev J. Altenbach, H. Altenbach. On generalized cosserat-type theories of plates and shells: a short review and bibliography. *Arch. Appl. Mech.*, 80(1):73–92, 2010.

[50] W. Pietraszkiewicz V.A. Eremeyev. Material symmetry group of the non-linear polar-elastic continuum. *Int. J. Solids Struct.*, 49(14):1993–2005, 2012.

[51] A. Della Corte D. Scerrato L. Placidi, I. Giorgio. Generalized continua and their applications to the sign of composites and metamaterials: a review of presentations and discussions. *Math. Mech. Solids*, 2015.

[52] A. Della Corte A. Berezovski, I. Giorgio. Interfaces in micromorphic materials: wave transmission and reflection with numerical simulations. *Math. Mech. Solids*, 21(1):37–51, 2015.

[53] P. Boisse, N. Hamila, and A. Madeo. The difficulties in modeling the mechanical behavior of textile composite reinforcements with standard continuum mechanics of cauchy. some possible remedies. *International Journal of Solids and Structures*, 154(55-65):895–898, 2018.

[54] A. Charmetant, J.G. Orliac, E. Vidal-Sallé, and P. Boisse. Hyperelastic model for large deformation analyses of 3d interlock composite preforms. *Compos. Sci. Technol.*, 72(12):1352–1360, 2012.

[55] S. Mathieu, N. Hamila, F. Bouillon, and P. Boisse. Enhanced modeling of 3d composite preform deformations taking into account local fiber bending stiffness. *Compos. Sci. Technol.*, 117:322–333, 2015.

[56] L. Greco and M. Cuomo. An isogeometric implicit g1 mixed finite element for kirchhoff space rods. *Comput. Methods Appl. Mech. Engrg.*, 298:325–349, 2016.

[57] E. Turco A. Cazzani, M. Malagu. Isogeometric analysis of plane-curved beams. *Math. Mech. Solids*, 2014.

[58] E. Turco F. Stochino A. Cazzani, M. Malagu. Constitutive models for strongly curved beams in the frame of isogeometric analysis. *Math. Mech. Solids*, 21:183–209, 2016.

[59] J. Mergheim P. Steinmann R. Müller P. Fischer, M. Klassen. Isogeometric analysis of 2d gradient elasticity. *Comput. Mech.*, 47(3):325–334, 2011.

[60] Battista A. dellIsola F. Della Corte, A. Referential description of the evolution of a 2d swarm of robots interacting with the closer neighbors: perspectives of continuum modeling via higher gradient continua. *Int. J. Non-Linear Mech.*, 79(80):209–220, 2016.

[61] A. Bensoussan, J.L. Lions, and G. Papanicolaou. Asymptotic analysis for periodic structures. *North-Holland Publishing Company*, 1978.

[62] Sanchez-Palencia E. Homogenization method for the study of composite media. asymptotic analysis ii. lecture notes in mathematics. *Berlin Heidelberg: Springer*, 985:192–214, 1983.

[63] J.L. Auriault, C. Boutin, and C. Geindreau. Homogenization of coupled phenomena in heterogenous media. *John Wiley & Sons*, 149, 2010.

[64] P. Harrison. Modelling the forming mechanics of engineering fabrics using a mutually constrained pantographic beam and membrane mesh. *Composites: Part A*, 81:145–157, 2016.

[65] E.M. Parsons, T. Weerasooriya, S. Sarva, and S. Socrate. Macroscopic description of microscopically strongly inhomogenous systems: a mathematical basis for the synthesis of higher gradients metamaterials. *Journal of the Mechanics and Physics of Solids*, 58(11):1995–2021, 2010.

[66] T. Wehrkamp-Richter, N.V. De Carvalho, and S.T. Pinho. A meso-scale simulation framework for predicting the mechanical response of triaxial braided composites. *Composites Part A*, 107:489–506, 2018.

[67] G. Hivet and P. Boisse. Consistent mesoscopic mechanical behaviour model for woven composite reinforcements in biaxial tension. *Composites Part B*, 39:345–361, 2008.

[68] O. Erol, B. Powers, and M. Keefe. Development of a non-orthogonal macroscale material model for advanced woven fabrics based on mesoscale structure. *Composites Part B*, 110:497–510, 2017.

[69] O. Erol, B. Powers, and M. Keefe. Effects of weave architecture and mesoscale material properties on the macroscale mechanical response of advanced woven fabrics. *Composites Part B*, 101:554–566, 2017.

[70] N.V. De Carvalho, S.T. Pinho, and P. Robinson. Numerical modelling of woven composites: Biaxial loading. *Composites Part A*, 43:1326–1337, 2012.

[71] D. Durville. Numerical simulation of entangled materials mechanical properties. *Journal of materials science*, 40:5941–5948, 2005.

[72] D. Durville. Simulation of the mechanical behaviour of woven fabrics at the scale of fibers. *International Journal of Material Forming*, 3:1241–1251, 2010.

[73] G. Haasemann, M. Kastner, and V. Ulbricht. Multi-scale modelling and simulation of textile reinforced materials. *Tech Science*, 3(3):131–145, 2006.

[74] A. Raoult, D. Caillerie, and A. Mourad. Elastic lattices: equilibrium, invariant laws and homogenization. *Ann Univ Ferrara*, 54:297–318, 2008.

[75] A. Mourad. Description topologique de larchitecture fibreuse et modelisation mecanique du myocarde. *Ph.D. thesis, I.N.P.L. Grenoble*, 2003.

[76] H. Tollenaere and D. Caillerie. Continuous modeling of lattice structures by homogenization. *Advances in Engineering Software*, 29:699–705, 1998.

[77] Ivan Giorgio C. Boutin, Francesco dell'Isola and Luca Placidi. Linear pantographic sheets part i. asymptotic micro-macro models identification. *Mathematics and mechanics of complex*, 5(2):127–162, 2017.

[78] F. dell'Isola, I. Giorgio, M. Pawlikowski, and N. L. Rizzi. Large deformations of planar extensible beams and pantographic lattices: heuristic homogenization, experimental and numerical examples of equilibrium. *Proc. R. Soc. A*, 472, 2016.

[79] D. Caillerie, A. Mourad, and A. Raoult. Discrete homogenization in graphene sheet modeling. *Journal of Elasticity*, 84:33–68, 2006.

[80] C. Boutin and J. Soubestre. Generalized inner bending continua for linear ber reinforced materials. *International Journal of Solids and Structures*, 48(3):517–534, 2011.

[81] C. Boutin and S. Hans. Homogenisation of periodic discrete medium: Application to dynamics of framed structures. *Computers and Geotechnics*, 30(4):303–320, 2003.

[82] C. Chesnais, C. Boutin, and S. Hans. Wave propagation and non-local effects in periodic frame materials: Generalized continuum mechanics. *Mathematics and Mechanics of Solids*, 2013.

[83] C. Boutin, S. Hans, and C. Chesnais. Generalized beams and continua. dynamics of reticulated structures. *Mechanics of generalized continua*, pages 131–141, 2010.

[84] C. Pideri and P. Seppecher. A second gradient material resulting from the homogenization of an heterogeneous linear elastic medium. *Continuum Mechanics and Thermodynamics*, 9(5):241–257, 1997.

[85] C. Boutin. Microstructural effects in elastic composites. *Int. J. Solids Struct.*, 33:1023–1051, 1996.

[86] H. Abdoul-Anziz and P. Seppecher. Strain gradient and generalized continua obtained by homogenizing frame lattices. *Mathematics and mechanics of complex*, 6(3):213–250, 2018.

[87] F. Dos Reis and J-F. Ganghoffer. Discrete homogenization of architectured materials: implementation of the method in a simulation tool for the systematic prediction of their effective elastic properties. *Technische Mechanik*, 30:85–109, 2010.

[88] M. Assidi, F. Dos Reis, and J.-F. Ganghoffer. Equivalent mechanical properties of biological membranes from lattice homogenization. *Journal of the mechanical behavior of biomedical materials.*, 4:1833–1845, 2011.

[89] F. Dos Reis and J.F. Ganghoffer. Equivalent mechanical properties of auxetic lattices from discrete homogenization. *Computational Materials Science*, 51(1):314–321, 2012.

[90] F. Dos Reis and J.F. Ganghoffer. Construction of micropolar continua from the asymptotic homogenization of beam lattices. *Computers and Structures*, 112-113:354–363, 2012.

[91] Y. Rahali, F. Dos Reis, and J.F. Ganghoffer. Multiscale homogenization schemes for the construction of second order grade anisotropic continuum media of architectured materials. *Journal for Multiscale Computational Engineering*, 15(1):35–78, 2017.

[92] Y. Rahali, I. Giorgio, and F. dell'Isola J.F. Ganghoffer. Homogenization à la piola produces second gradient continuum models for linear pantographic lattices. *International Journal of Engineering Science*, 97:148–172, 2015.

[93] M. Cuomo and L. Greco F. dell'Isola. Simplified analysis of a generalized bias test for fabrics with two families of inextensible fibres. *L. Z. Angew. Math. Phys.*, pages 61–67, 2016.

[94] F. dell'Isola, M. Cuomo, L. Greco, and A. della Corte. Bias extension test for pantographic sheets: numerical simulations based on second gradient shear energies. *Journal of Engineering Mathematics*, 103(1):127–157, 2017.

[95] L. Greco and M. Cuomo. B-spline interpolation of kirchhoff-love space rods. *Comput. Methods Appl. Mech. Engrg.*, 256:251–269, 2013.

[96] L. Greco, M. Cuomo, L. Contrafatto, and S. Gazzo. An efficient blended mixed b-spline formulation for removing membrane locking in plane curved kirchhoff rods. *Computer Methods in Applied Mechanics and Engineering*, 324:476–511, 2017.

[97] T.J.R. Hughes, A. Cottrell, and Y. Bazilevs. Isogeometric analysis: Cad, finite elements, nurbs, exact geometry and mesh refinement. *Computer Methods in Applied Mechanics and Engineering*, 194:4135–4195, 2005.

[98] A. Cottrell, T.J.R. Hughes, and Y. Bazilevs. *Isogeometric analysis: Toward Integration of CAD and FEA*. Wiley, 2009.

[99] P. Fischer, J. Klassen, M.and Mergheim, P. Steinmann, and R. Müller. Isogeometric analysis of 2d gradient elasticity. *Computational Mechanics*, 47(3):325–334, 2011.

[100] L. Piegl and W. Tiller. *The NURBS Book*. Monographs in Visual Communication. Springer-Verlag Berlin Heidelberg, 2 edition, 1997.

[101] Gerald Farin. *Curves and surfaces for CAGD: A practical guide*. The Morgan Kaufmann Series in Computer Graphics. Morgan Kaufmann, 5 edition, 2001.

[102] V. Sepe, S. Marfia, and E. Sacco. A nonuniform tfa homogenization technique based on piecewise interpolation functions of the inelastic field. *International Journal of Solids and Structures*, 50(5):725–742, 2013.

[103] S. Marfia and E. Sacco. Tfa-based homogenization for composites subjected to coupled damage-friction effects. *Procedia Engineering*, 109:113–120, 2015.

List of Figures